Copper Oxysalts: The Jahn-Teller Effect And Its Structural Implications

by

Raymond K. Eby

A thesis
presented to the University of Manitoba
in fulfillment of the
thesis requirement for the degree of
Masters of Science
in
Department of Geological Sciences

Winnipeg, Manitoba

ISBN 0-315-47941-8

COPPER OXYSALTS: THE JAHN-TELLER EFFECT AND ITS STRUCTURAL IMPLICATIONS

BY

RAYMOND K. EBY

A thesis submitted to the Faculty of Graduate Studies of the University of Manitoba in partial fulfillment of the requirements of the degree of

MASTER OF SCIENCE

I hereby declare that I am the sole author of this thesis.

I authorize the University of Manitoba to lend this thesis to other institutions or individuals for the purpose of scholarly research.

Raymond K. Eby

I further authorize the University of Manitoba to reproduce this thesis by photocopying or by other means, in total or in part, at the request of other institutions or individuals for the purpose of scholarly research.

Raymond K. Eby

The University of Manitoba requires the signatures of all persons using or photocopying this thesis. Please sign below, and give address and date.

ACKNOWLEDGEMENTS

I wish to thank the Natural Sciences and Engineering Research Council for their generosity in supporting my studies financially. I also thank my advisor - Dr. Frank C. Hawthorne - for his inspirational advice involving this thesis. I am also greatful to Dr. Fred Wicks and Dr. Anthony Secco for giving their valuable time and effort to help make this thesis a coherent piece.

ABSTRACT

Copper oxysalts are a common class of minerals that have been considered structurally anamalous. Some copper oxysalt structures have non-Cu analogues, but many do not, and the reasons for this have been unclear. The unique coordination environment of Cu^{2+} is responsible for the anomalous character of Cu oxysalts. A regular octahedral coordination is unstable around Cu^{2+} because of its degenerate d^9 orbital state. Spontaneous electronic relaxation (octahedral distortion) lifts the degeneracy, making distorted Cu-octahedra stable in structures. This is the Jahn-Teller effect. By considering the complete coordination of Cu^{2+}, the topology of Cu^{2+} oxysalt structures is readily interpreted, and similarities to non-Cu oxysalts become evident.

Numerous studies have dealt with only the local coordination environment of Cu^{2+}, but this study also deals with the long range structural effects of octahedral distortions e.g. how distorted octahedra fit into structures, and the geometrical/chemical consequences. Bond-valence analysis and mathematical simulation of crystal structures (using DLS) were used to study the structural effects of octahedral distortions. The Jahn-Teller distortion provides a geometrically flexible coordination environment for Cu^{2+}, resulting in a wide variety of bond-valence distributions. This flexibility creates the potential for polymerization styles not possible with un-distorted M^{2+}-octahedra. Structural analyses show two fundamental structure

types: 1) structures that can be constructed from regular coordination polyhedra, the arrangement of which can distort and accomodate the Jahn-Teller distortion; and 2) structures that can only be constructed from very distorted coordination polyhedra. Isostructuralism is often possible in TYPE I structures, because of their geometrically flexible arrangements. Isostructuralism is not present in TYPE II structures.

Jahn-Teller distortions are often coupled through structural symmetry by polymerization of Cu^{2+}-octahedra. The resulting periodic electronic relaxations (PER) occur as waveforms commensurate with translational symmetry. Polymerization styles control the type of waveform produced. Thus Cu^{2+} oxysalts can be understood by analysis of the local octahedral distortions and their influence on the long-range of structures.

CONTENTS

LIST OF TABLES

LIST OF FIGURES

Chapter I

INTRODUCTION

1.1 Cu^{2+} OXYSALTS

Cu^{2+} oxysalts are a common class of minerals in oxidizing environments associated with Cu-bearing sulfide mineralization. They can occur together with many other oxysalts under similar geochemical conditions. However, Cu^{2+} oxysalts have generally been considered as a class of enigmatic structures that are somehow different from other minerals. Cu^{2+} oxysalt minerals are seldom isostructural with non-Cu^{2+} oxysalts. Synthetically prepared copper oxides with common structure types (spinel,rutile) have structural details that are always somewhat unusual. The static Jahn-Teller effect (described by Jahn & Teller, 1937), related to the local electronic structure of the Cu^{2+} ion, is undoubtedly responsible for the enigmatic structural features of the Cu^{2+} oxysalts. Detailed explanations of the Jahn-Teller effect are provided by Dunitz & Orgel (1957), Opik & Pryce (1956), Orgel & Dunitz (1957), Burdett (1980), Liehr & Ballhausen (1958), and Goodenough (1963). A brief review of the Jahn-Teller effect is presented here, as it applies to Cu^{2+}. A detailed look at the local Cu^{2+} environment will be given in Chapter 4.

1.2 THE JAHN-TELLER EFFECT: INTRODUCTORY REMARKS

The Cu^{2+} ion has a degenerate d^9 orbital ground state when it is surrounded by an octahedral ligand field, because of its half-filled d-orbital (Figure 1.1a). This instability is removed by a spontaneous electronic relaxation that affects the Cu-ligand bond lengths. This relaxation phenomenon is termed the Jahn-Teller effect. The physical expression of the electronic relaxation is usually in the form of an octahedral distortion, with shortening of four equatorial bonds, and lengthening of two co-linear apical bonds (Figure 1.1b; from here on it is assumed that the equatorial bonds refer to the 4 shortened bonds, and the 2 apical bonds are the long co-linear bonds, abbreviated as (4+2)). Ligand-field splitting associated with the distortion shows a net stabilization energy which represents the relaxation phenomenon (Figure 1.1c). Distortions range from trans-elongated octahedra to the more extremely distorted square pyramidal and square planar coordinations (Figure 1.2).

Intuitively, one can understand why the long-range structural properties of Cu^{2+} oxysalts are considered unique. In most structures, the coordination polyhedra are fairly regular, and linkage of the polyhedra into a continuous structure (with translational symmetry) reflects this regularity. Considering the distorted Cu-polyhedra, the topological (and geometrical) details of a structure must be profoundly influenced by Jahn-Teller distortions as the Cu-polyhedra are translated throughout the unit cells of a structure.

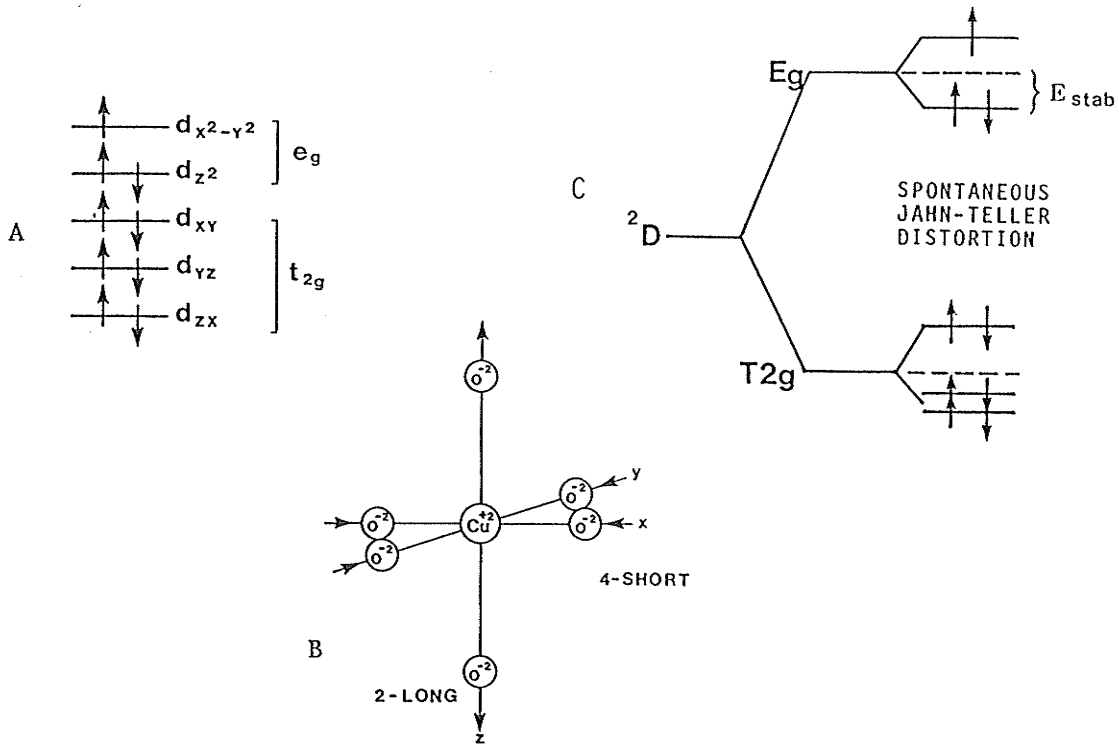

Figure 1.1: Degeneracy and Relaxation of d^9 state in Cu^{2+} a) ground state electron orbital pairs for Cu^{2+}, with one unpaired electron; b) octahedral Jahn-Teller distortion of the Cu-ligand complex; c) energy level splitting of d-orbitals, lifting the unstable degeneracy.

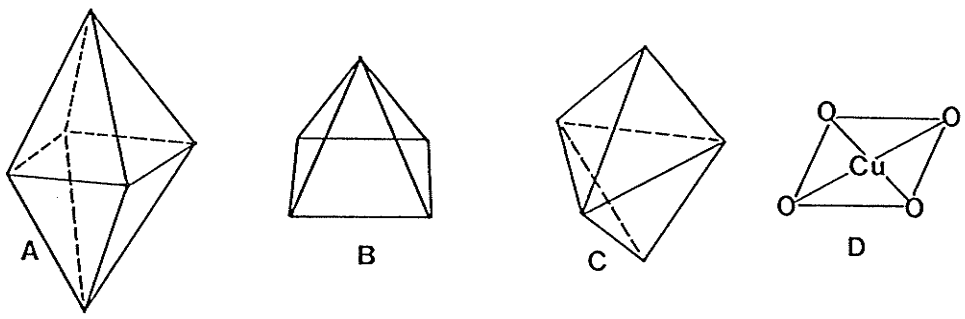

Figure 1.2: Variations of Jahn-Teller Distorted Polyhedra The four most commonly occuring configurations for copper: a) trans-elongated octahedra, designated (4+2); b) square pyramidal; c) trigonal bipyramidal; d) square planar.

1.3 PURPOSE OF THESIS

Despite the large amount of work already done on the details of the local Cu^{2+} environment in crystals, little has been done to answer the questions relating to the long-range structural aspects of Cu^{2+} oxysalts. This thesis will examine the following questions:

1. Why are some Cu^{2+} oxysalts isostructural with non-Cu minerals or synthetic compounds, whereas many others are structurally unique?
2. What are the different fundamental roles of distorted Cu^{2+} polyhedra in oxysalt structures?
3. What are some features of the local Cu^{2+} Jahn-Teller distortion and how do they relate (if at all) to the long-range properties of the structures?
4. What are the characteristic features observed in the long-range aspects of these Cu^{2+} structures?

As a necessary part of this work, a formal structural classification of the Cu^{2+} oxysalts has also been completed.

1.4 DATA BASE

The Cu^{2+} oxysalts considered here represent those structures which are refined sufficiently well to render proper topological information, and give bond lengths accurate to $\leq \pm 0.02$Å. The structures studied are the minerals listed in Table 1.1. These structures will be dealt with in detail because minerals probably represent the most stable structural substances. This study has incorporated as many mineral structures as

possible from previous refinements in the literature and present refinements of the author. Conversely, only a few of the synthetic Cu^{2+}-compounds have been studied for reasons of time.

TABLE 1.1

Cu^{2+} Oxysalt Minerals Studied

Mineral	Formula	Reference
Arsenates:		
Agardite	$(Y,Ca)Cu_6(AsO_4)_3(OH)_6 \cdot 3H_2O$	Aruga & Nakai (1985)
Arthurite	$CuFe_2(AsO_4)_2(OH)_2 \cdot 4H_2O$	Keller & Hess (1978)
Bayldonite	$PbCu_3(AsO_4)_2(OH)_2 \cdot H_2O$	Ghose & Wan (1979)
Clinoclase	$Cu_3(AsO_4)(OH)_3$	This study
Conichalcite	$CaCu(AsO_4)(OH)$	Quarashi & Barnes (1963)
Cornubite	$Cu_5(AsO_4)_2(OH)_4$	Tillmans et al. (1987)
Euchroite	$Cu_2(AsO_4)(OH) \cdot 3H_2O$	This study
Lammerite	$Cu_3(AsO_4)_2$	Hawthorne (1985a)
Liroconite	$Cu_2Al(AsO_4)(OH)_4 \cdot 4H_2O$	This study
Mixite	$BiCu_6(AsO_4)_3(OH)_6 \cdot 3H_2O$	Mereiter & Preissinger(1986)
Olivenite	$Cu_2(AsO_4)(OH)$	Toman (1977)
Stranskiite	$Zn_2Cu(AsO_4)_2$	Keller et al. (1979)
Trippkeite	$CuAs_2^{+3}O_4$	Pertlik (1975)
Borates:		
Bandylite	$CuB(OH)_4Cl$	Collin (1951)
Henmilite	$Ca_2Cu(OH)_4[B(OH)_4]_2$	Nakai et al. (1986)
Carbonates:		
Azurite	$Cu_3(CO_3)_2(OH)_2$	Zigan & Schuster (1972)
Callaghanite	$Cu_2Mg_2(CO_3)(OH)_6 \cdot 2H_2O$	Brunton (1973)
Chalconatronite	$Na_2Cu(CO_3)_2 \cdot 3H_2O$	Mosset et al. (1978)
Malachite	$Cu_2(CO_3)(OH)_2$	Zigan et al. (1977)
Roubaultite	$Cu_2(UO_2)_3(CO_3)_2O_2(OH)_2 \cdot 4H_2O$	Ginderow & Cesbron (1985)
Oxychlorides:		
Atacamite	$Cu_2Cl(OH)_3$	Parise & Hyde (1986)
Botallackite	$Cu_2Cl(OH)_3$	Hawthorne (1985c)
Chloroxiphite	$Pb_3CuCl_2(OH)_2O_2$	Finney et al. (1977)
Eriochalcite	$CuCl_2 \cdot 2H_2O$	Harker (1936)
Paratacamite	$Cu_2(OH)_3Cl$	Fleet (1975)
Iodites:		
Bellingerite	$Cu_3(IO_3)_6 \cdot 2H_2O$	Ghose & Wan (1974)
Salesite	$Cu(IO_3)(OH)$	Ghose & Wan (1978)
Molybdates:		
Lindgrenite	$Cu_3(MoO_4)_2(OH)_2$	Hawthorne & Eby (1985)

TABLE 1.1 - Continued

Mineral	Formula	Reference
Nitrates:		
Buttgenbachite	$Cu_{19}Cl_4(NO_3)_2(OH)_{32}\cdot 2H_2O$	Fanfani et al. (1973)
Likasite	$Cu_3(OH)_5NO_3\cdot 2H_2O$	Effenberger (1986)
Gerhardite	$Cu_2(OH)_3NO_3$	Bovio & Locchi (1982)
Phosphates:		
Cornetite	$Cu_3(PO_4)(OH)_3$	This study
Libethenite	$Cu_2(PO_4)(OH)$	Cordsen (1978)
Metatorbernite	$Cu(UO_2)_2(PO_4)_2\cdot 8H_2O$	Ross et al. (1964)
Pseudomalachite	$Cu_5(PO_4)_2(OH)_4\cdot H_2O$	Shoemaker et al. (1977a)
Reichenbachite(PPM)	" " "	Anderson et al. (1977)
QPM "	" " "	Shoemaker et al. (1981)
Turquoise	$CuAl_6(PO_4)_4(OH)_8\cdot 5H_2O$	Dresdner (1965)
Hentschelite	$CuFe_2(PO_4)_2(OH)_2$	Sieber (1985)
Veszelyite	$(Cu,Zn)_3(PO_4)(OH)_3\cdot 2H_2O$	Ghose et al. (1974)
Selenites:		
Chalcomenite	$CuSeO_3\cdot 2H_2O$	Asai & Kiriyama (1973)
Derriksite	$Cu_4(UO_2)(SeO_3)_2(OH)_6$	Ginderow & Cesbron (1983)
Silicates:		
Cuprorivaite	$CaCuSi_4O_{10}$	Pabst (1959)
Cuprosklodowskite	$Cu(UO_2)_2Si_2O_6(OH)_2\cdot 6H_2O$	Rosenweig & Ryan (1975)
Dioptase	$CuSiO_2(OH)_2$	Ribbe et al. (1977)
Kinoite	$Ca_2Cu_2Si_3O_8(OH)_4$	Laughon (1971)
Litidionite	$KNaCuSi_4O_{10}$	Pozas et al. (1975)
Papagoite	$CaCuAlSi_2O_6(OH)_3$	Groat & Hawthorne (1987)
Plancheite	$Cu_8Si_8O_{22}(OH)_4\cdot H_2O$	Evans & Mrose (1977)
Shattuckite	$Cu_5(SiO_3)_4(OH)_2$	Evans & Mrose (1977)
Stringhamite	$CaCuSiO_4\cdot 2H_2O$	Hawthorne (1984d)
Sulfates:		
Antlerite	$Cu_3(SO_4)(OH)_4$	Hawthorne et al. (1988)
Aubertite	$CuAl(SO_4)_2Cl\cdot 14H_2O$	Ginderow & Cesbron (1979)
Bonattite	$CuSO_4\cdot 3H_2O$	Zahrobsky & Baur (1968)
Boothite	$CuSO_4\cdot 7H_2O$	Schaller (1903)
Campigliaite	$Cu_4Mn(SO_4)_2(OH)_6\cdot 4H_2O$	Menchetti & Sabelli (1982)
Chalcanthite	$CuSO_4\cdot 5H_2O$	Varghese & Maslen (1985)
Chalcocyanite	$CuSO_4$	Kokkoros & Rentzeperis (1958)
Chlorothionite	$K_2Cu(SO_4)Cl_2$	Giachovasso et al. (1976)
Connellite	$Cu_{19}Cl_4(SO_4)(OH)_{32}\cdot 3H_2O$	Maclean & Anthony (1972)
Cuprocopiapite	$CuFe_4^{+3}(SO_4)_6(OH)_2\cdot 20H_2O$	Süsse (1972)

TABLE 1.1 - Continued

Mineral	Formula	Reference
Cyanochroite	$K_2Cu(SO_4)\cdot 6H_2O$	Carapezza & Sanseverino (1968)
Devillite	$CaCu_4(SO_4)_2(OH)_6\cdot 3H_2O$	Sabelli & Zanazzi (1972)
Dolerophanite	$Cu_2(SO_4)O$	Effenberger (1985b)
Guildite	$CuFe^{+3}(SO_4)_2(OH)\cdot 4H_2O$	Ghose & Wan (1978)
Kröhnkite	$Na_2Cu(SO_4)_2\cdot 2H_2O$	Hawthorne & Ferguson (1975)
Ktenasite	$(Cu,Zn)_5(SO_4)_2(OH)_6\cdot 6H_2O$	Mellini & Merlino (1978)
Langite	$Cu_4(SO_4)(OH)_6\cdot 2H_2O$	Gentsch & Weber (1984)
Linarite	$PbCu(SO_4)(OH)_2$	Effenberger (1986)
Mammothite	$Pb_6Cu_4AlSbO_2(OH)_{16}Cl_4(SO_4)_2$	Effenberger (1985a)
Natrochalcite	$NaCu_2(SO_4)_2(OH)\cdot H_2O$	Rumanova & Volodina (1958)
Osarizawaite	$PbCuAl_2(SO_4)_2(OH)_6$	Guiseppetti & Tadini (1980)
Posnjakite	$Cu_4(SO_4)(OH)_6\cdot H_2O$	Mellini & Merlino (1979)
Ransomite	$CuFe_2^{+3}(SO_4)_4\cdot 6H_2O$	Wood (1970)
Serpierite	$Ca(Cu,Zn)_4(SO_4)_2(OH)_6\cdot 3H_2O$	Sabelli & Zanazzi (1968)
Spangolite	$Cu_6Al(SO_4)(OH)_{12}Cl\cdot 3H_2O$	In print (Hawthorne et al.)
Wroewolfeite	$Cu_4(SO_4)(OH)_6\cdot 2H_2O$	Hawthorne & Groat (1985)
Tellurites:		
Balyakinite	$CuTeO_3$	Lindquist (1972)
Teineite	$CuTeO_3\cdot 2H_2O$	Effenberger (1977)
Vanadates:		
Blossite	$\alpha Cu_2V_2O_7$	Calvo & Faggiani (1974)
Fingerite	$Cu_{11}O_2(VO_4)_6$	Finger (1985)
Lyonsite	$Cu_3Fe_4(VO_4)_6$	Hughes et al. (1987)
McBirneyite	$Cu_3V_2O_8$	Shannon & Calvo (1972)
Sengierite	$Cu_2(UO_2)_2V_2O_8\cdot 6H_2O$	Piret et al. (1980)
Stoiberite	$Cu_5V_2^{+5}O_{10}$	Shannon & Calvo (1973)
Volborthite	$Cu_3(VO_4)_2\cdot 3H_2O$	Kashayev & Bakakin (1968)
Ziesite	$\beta Cu_2V_2^{+5}O_7$	Mercurio & Frit (1973)
Mixed Group Oxysalts:		
Caledonite	$Pb_5Cu_2(CO_3)(SO_4)_3(OH)_6$	Giachovazzo et al. (1973)
Chalcophyllite	$Cu_{18}Al_2(AsO_4)_3(SO_4)_3(OH)_{27}\cdot 33H_2O$	Sabelli (1980)
Fornacite	$Pb_2Cu(CrO_4)(PO_4)(OH)$	Cocco et al. (1966)
Schmiederite	$Pb_2Cu_2(SeO_4)(SeO_3)(OH)_4$	Effenberger (1986)
Vauquelinite	$Pb_2Cu(CrO_4)(PO_4)(OH)$	Fanfani & Zanazzi (1968)

1.5 PROCEDURES: EXPERIMENTAL & DESCRIPTIVE

X-ray experimental work is supplemental to the data base of structures examined. Much of this study involves the graphical characterization of previously determined structures, requiring analysis of the structures by manual drawings and computer representation. The Distance Least Squares method (Meier & Villager, 1969) of structural simulation was used to examine the geometrical effects of imposing specific polyhedral distortions on particular structure types.

1.6 BOND-VALENCE THEORY: BACKGROUND

Bond-valence theory is an important part of characterizing the structural properties of oxysalt minerals. It is an expansion of Pauling's (1960) electrostatic valence principle (second rule) and the idea of mean bond strengths. The mean bond strength ($\bar{s}$) is defined as the formal valence of the cation (z) divided by its coordination number (v). Pauling's second rule states that "for the most stable structures, the sum of the mean bond strengths (p) around any anion must be approximately equal to the magnitude of its formal valence, $\Sigma\bar{s}=p=|z|$."

Brown and Shannon (1973) formalized the concept of bond-length bond-strength relations, in which deviations of individual bonds from the average bond length correlate with the deviations from the average bond strengths. More simply, the longer a given bond is, the weaker it is. Brown and Shannon (1973) formulated bond-length bond-strength (BL-BS) curves as the equation:

$$s=s_0(R/R'_0)^{-N}$$

where s=individual bond strengths, R=the observed bond length (Å), s_0=Pauling's mean bond strength ($\bar{s}$), and R'_0 and N are constants derived from fitting the bond-strength bond-length curve to a large number of structures, subject to the constraint that the sums of the bond strengths around both cations and anions are equal to the magnitudes of their formal valences. The resulting bond strengths may then be summed around all ions in a refined crystal structure, and the resulting sums are equal (within a few %) to the magnitude of the formal valences of the ions. Brown & Shannon (1973) also found that a single curve of the form:

$$s=(R/R_0)^{-N}$$

works well for all atoms of an isoelectronic series; again R_0 and N are constants derived from a large number of crystal structures. These curves were of great immediate use in checking the correctness of structures, assignment of hydrogen-bonding arrangements, examining chemical and positional ordering, and examining formal valence states.

Brown (1981) broadened the concept of bond strengths. They realized that the universal curves represent the bridge between ionic and covalent ideas about bonding, because the mean bond strengths of the ions in an isoelectronic series are a function of the valence of the ion. Thus, Brown (1981) renamed individual bond strengths as <u>bond valences</u> (bv), and defined the average bond strengths as <u>Lewis acidities</u> for cations, and <u>Lewis basicities</u> for anions. Lewis base strengths are best considered in terms of the complex oxyanions in oxysalt structures. Resulting from these ideas is the valence-matching principle: "For the most stable structures to exist, the Lewis acid

strengths must nearly equal the Lewis base strengths across the acid-base network of a crystal structure." This rule is closely related to Pauling's valence sum rule, and both ideas work together in considering inorganic structures.

Bond-valence relations have important uses and serious implications for crystal structures. Many common rock-forming mineral structures significantly deviate from Pauling's simple model using mean bond strengths and the second rule. However, considering these minerals in terms of bond-valence theory, we can understand the bonding relationships in these structures. Distortions in cation polyhedra help satisfy the valence sum rule by providing variations in bond-valences with the varying bond lengths.

It is obvious then, that bond-valence theory and the valence sum rule are critical in understanding the structures of the Cu^{2+} oxysalts, because of the characteristic bond length variations in Jahn-Teller (J-T) distorted polyhedra. The considerable variation in bond-valences resulting from J-T distortions must have a profound influence on the connectivity of Cu^{2+} oxysalts. One must consider the topological combinations that are compatible with the bond-valence distributions of distorted Cu-polyhedra. The J-T distortions should give rise to unique bond-valence distributions in some structures, limiting the possibility of only Cu^{2+} occurring in particular topological arrangements. For example:

1. an oxygen bonded to three edge-sharing octahedra of regular geometry cannot bond to a tetrahedrally coordinated cation with

a formal valence >4 (bond valence sum on the oxygen would be >>2). However, this situation is common in Cu^{2+} sheet structures, in which the apices of the longest (and weakest) bonds in the J-T distorted Cu-octahedra are linked to sulfate groups.

2. because bond-valence relations impose bond length restrictions on specific topological arrangements of bonds, some structures require severe polyhedral distortions. These distortions are only possible with cations that undergo J-T effects.

This suggests why some Cu^{2+} oxysalts have no non-Cu analogues, and why other structures can take in both Cu^{2+} and non J-T elements. Cu^{2+} oxysalts without structural analoques may have a bond topology that is compatible only with the extreme bond-valence distributions possible in J-T distorted polyhedra. Conversely, Cu^{2+} oxysalt structures with non J-T analogues should have a bond topology that allows a more moderate dispersion of bond-valences, possible with both J-T and non-J-T cations. The principal theme of this thesis is to examine this hypothesis.

Chapter II

X-RAY STRUCTURE REFINEMENTS

This chapter provides structural data that is supplementary to the main body of the thesis. The resulting improvement in bond lengths and polyhedral geometry will enhance the data base for detailed analysis of Jahn-Teller effects on Cu^{2+} polyhedra. The experimental procedures and data generated by the experiments are given here; descriptions of the structures are in Chapter 3.

2.1 EXPERIMENTAL METHODS

The methods used for data collection and reduction are the same for all refinements, so the general procedure explained applies to all minerals examined. Pertinent data for each mineral is tabulated and discussed following the explanation of experimental methods.

2.1.1 Data Collection

The crystals were mounted on a Nicolet R3m automated 4-circle diffractometer, equipped with a Mo-target X-ray tube and a graphite crystal monochromator. Unit cell data were obtained by choosing approximately 25 reflections from a random-orientation phi-axis rotation photograph. These reflections were automatically centred, and real-space vectors corresponding to possible unit-cell axes were derived from the centred reflections. Least-squares refinement of the reflections produced the unit cell dimensions. An orientation matrix

also resulted from the centring procedure, relating the crystal axes to the diffractometer axes, and providing a reference frame for automatic data collection.

Intensity data were collected using a θ-2θ scan in 96 steps, with a scan range of 3°-60° 2θ. X-rays were generated at 50kV/30mA, and were measured at a variable scan-rate between 4.0° and 29.3°/min, depending on an initial one second intensity count at peak centre. Backgrounds were measured for half the scantime, before and after each peak scan. Two check reflections were monitored after every 46 measurements to verify consistency in crystal alignment and x-ray source.

Empirical absorption corrections were done after each data collection. Approximately 10 strong reflections, uniformly distributed over the range 3°-60° 2θ, were measured on psi-axis rotations at 10° intervals for a full psi-axis cycle (termed a psi-scan). Crystal shapes were modelled as an ellipsoid. The lengths of the principal axes of the ellipsoid were refined to minimize the merging R-index of the psi-scan data. The intensity data were then corrected for absorption effects using the refined shape of the crystal, resulting in a minimum-maximum transmission value (min-max).

The merged data were corrected for Lorentz, polarization and background effects, and then reduced to structure factors ($|F_o|$). Reflections with $I>3.0\sigma(I)$ were classified as observed. A calculated density is produced by specifying the cell contents, giving an absorption coefficient for the absorption correction.

2.1.2 Structure Refinement

Scattering curves for neutral atoms together with anomalous dispersion coefficients were taken from Cromer and Mann (1968) and Cromer and Libermann (1970).

The sequence of refinement was as follows:

1. Input the heavy-atom positions, using coordinates of the previous authors. Fix occupancies and isotropic temperature factors (U=0.010). Use 3 or 4 least-squares cycles, which converge rapidly (expected R, 20-25%).
2. The resulting difference-Fourier densities are assigned to oxygen positions (which should correspond to those of previous authors).
3. Fix the anion occupancies and isotropic temperature factors (U=0.015), and refine with 3-4 more cycles (expected R, 10%). A secondary extinction correction is also applied at this stage.
4. Refine 3-4 more cycles, using free-variable isotropic temperature factors.
5. Change to anisotropic temperature factors, and refine 5 more cycles (R should be below 4.5%).
6. If the R-index is low enough, residual electron density on the difference map may represent hydrogen positions. Check the geometry, and if plausible bonding conditions exist, refine the hydrogen(s) with fixed isotropic temperature factors (U=0.015-0.020). If the position(s) of the hydrogen(s) does not converge, then fix the positional parameters and refine to see if donor-acceptor H-bonding conditions remain acceptible, and if the R-index drops.

After stage 5, approximately 15 least-squares cycles have been used, and the structure will be refined to convergence. Stage 6 is supplementary, as the intention of these experiments is to improve cation polyhedral geometries.

The R-indices reported have the following definitions:

$$R(obs) = \Sigma(|F_o|-|F_c|)/\Sigma|F_o| \qquad (2.1)$$

and

$$Rw(obs) = [\Sigma w(|F_o|-|F_c|)^2/\Sigma wF_o^2]^{1/2},\ w=1 \qquad (2.2)$$

Bond length/angle data are used to assign cation coordination numbers and to confirm O-O and O-H···O geometries for hydrogen-bonding. Empirical bond-valence calculations, using the parameters of Brown (1981), were used to determine anion type (O,OH,H_2O) and to confirm that the refined structures have acceptable structural arrangements. Structure factor tables for each refinement are in Appendix A.

2.2 MINERAL STRUCTURE REFINEMENTS

2.2.1 Cornetite

Cornetite crystals from Mine de L'etoile, Katanga, are subhedral prisms, sky blue, and 0.3-1.0mm in size. A crystal fragment was cut and shaped (by shaving the edges with a razor) to an ellipsoid 0.16x0.20x0.24mm in size. The experimental data for cornetite is listed in Table 2.1. Unit cell errors are of reasonable magnitude, and the cell obtained matches that of Fehlmann et al. (1964). The psi-scan gave a good absorption correction, and only 3 reflections were rejected during reduction of the raw data (Note: reflections in all refinements are rejected only during the initial data reduction process, and are eliminated due to bad

backgrounds or asymmetric peak shapes). Systematic absences are compatible with the space group assignment (Pbca) of Fehlmann et al.

TABLE 2.1

Pertinent Data for Cornetite

Unit Cell: a = 10.854(1)Å	Number of reflections used
b = 14.053(3)	in cell determination : 25
c = 7.086(2)	No. Reflections Collected : 1882
V = 1080.8(3)Å^3	No. Reflections Rejected : 3
	Total Observed $\|F_o\|$ I>3.0σI: 1572
Space Group : Pbca	Total Unique Observed $\|F_o\|$: 1231
Part of Sphere	No. of psi-scan reflections : 10
Collected : 1 octant	No. of psi-scan measurements : 360
	Absorption corr. R-merge : 1.43%
dens.(calc) = 4.14g/cm^3	min-max : 0.058 - 0.097
dens.(meas) = 4.10g/cm^3	Cell contents : 8[$Cu_3(PO_4)(OH)_3$]

R(obs) = 3.93% ; Rw(obs) = 2.97%

(1964).

The refinement procedure converged smoothly to an R-index of 5.56% with an isotropic model, and all atom positions of Fehlmann et al. (1964) are confirmed. Anisotropic temperature variables brought the R-index down to 3.93%. No significant electron density remained in the difference-Fourier map; thus no hydrogen positions were located. The refined atomic coordinates and anisotropic thermal parameters are listed in Table 2.2. The resulting bond lengths and bond angles are given in Tables 2.3 and 2.4, respectively. There are no major structural changes

TABLE 2.2

Atomic (fractional) & Thermal Parameters for Cornetite

	x	y	z	U(equiv)
Cu(1)	0.48100(6)	0.62739(5)	0.1876(1)	0.0127(2)
Cu(2)	0.19409(6)	0.25355(6)	-0.09707(9)	0.0128(2)
Cu(3)	0.60041(6)	0.45217(5)	0.3908(1)	0.0121(2)
P	0.3800(1)	0.3864(1)	0.2070(2)	0.0114(4)
O(1)	0.2690(3)	0.4101(3)	0.0857(6)	0.016(1)
O(2)	0.4211(4)	0.4726(3)	0.3246(6)	0.013(1)
O(3)	0.4896(4)	0.3596(3)	0.0812(5)	0.016(1)
O(4)	0.3499(4)	0.3034(3)	0.3415(6)	0.015(1)
OH(1)	0.5564(4)	0.3390(3)	0.5449(5)	0.011(1)
OH(2)	0.1822(4)	0.3124(3)	0.6470(5)	0.013(1)
OH(3)	0.6343(4)	0.5679(3)	0.2550(6)	0.013(1)

Anisotropic Temperature Factors

	*U(11)	U(22)	U(33)	U(23)	U(13)	U(12)
Cu(1)	102(3)	166(4)	112(3)	10(3)	-7(3)	-29(2)
Cu(2)	115(3)	158(3)	110(3)	-8(4)	14(3)	-38(3)
Cu(3)	95(3)	128(3)	140(3)	-22(3)	0(3)	8(3)
P	95(7)	149(7)	98(7)	-9(6)	6(5)	-8(6)
O(1)	79(17)	243(22)	165(20)	-11(19)	-10(16)	17(17)
O(2)	121(18)	127(19)	152(19)	33(17)	-6(17)	8(15)
O(3)	103(18)	249(22)	131(19)	13(18)	27(16)	19(17)
O(4)	157(19)	173(20)	115(20)	13(17)	-5(17)	-52(17)
OH(1)	110(18)	110(18)	100(20)	-22(15)	4(15)	17(16)
OH(2)	139(18)	145(19)	95(19)	5(16)	-23(16)	-21(16)
OH(3)	118(18)	131(19)	148(19)	-35(18)	10(16)	20(16)

*U(ij) = U(ij) x 10^4 ($Å^2$)

from the structure determination of Fehlmann et al. (1964), although interpretation of the structure is significantly different.

The bond-valence scheme for cornetite (Table 2.5) shows an acceptable distribution of bond-valences. From the observed O-O distances (in

TABLE 2.3

Selected Bond Lengths (Å) of Cornetite

Cu(1)- OH(3)	1.923(4)	Cu(2)- O(4)	1.921(4)	Cu(3)- OH(3)	1.925(4)
" - O(3)	1.940	" - OH(1)	1.952	" - O(1)	1.930
" - OH(2)	1.984	" - OH(2)	1.966	" - OH(1)	1.988
" - OH(1)	1.996	" - OH(2)	1.988	" - O(2)	2.023
" - O(2)	2.470	" - O(1)	2.679	" - O(2)	2.280
" - O(4)	3.087	" - O(3)	2.734	" - O(3)	2.821
<Cu(1)-O> =	2.233	<Cu(2)-O> =	2.207	<Cu(3)-O> =	2.163
OH(3)- O(3)	2.919(6)	O(4) - OH(2)	2.831(6)	OH(3)- O(1)	2.886(6)
" - OH(2)	3.901	" - OH(2)	2.804	" - O(2)	2.719
" - OH(1)	2.830	" - O(1)	3.573	" - O(2)	3.092
" - O(2)	2.719	" - O(3)	4.028	" - O(3)	3.543
O(3) - OH(2)	2.726	OH(1)- OH(2)	2.871	O(1) - OH(1)	2.679
" - O(2)	3.843	" - OH(2)	2.602	" - O(2)	3.225
" - O(4)	3.229	" - O(1)	2.679	" - O(3)	3.908
OH(2)- OH(1)	2.602	" - O(3)	2.895	OH(1)- O(2)	2.849
" - O(2)	3.460	OH(2)- O(1)	3.294	" - O(2)	2.815
" - O(4)	3.960	" - O(3)	2.726	" - O(3)	3.378
OH(1)- O(2)	2.815	OH(2)- O(1)	3.527	O(2) - O(2)	3.116
" - O(4)	3.667	" - O(3)	3.732	" - O(3)	2.459
<O-O>Cu(1) =	3.223	<O-O>Cu(2) =	3.130	<O-O>Cu(3) =	3.056

P - O(1)	1.518(4)	O(1) - O(3)	2.497(6)
P - O(3)	1.532	O(1) - O(2)	2.522
P - O(2)	1.536	O(1) - O(2)	2.522
P - O(4)	1.541	O(3) - O(2)	2.459
<P-O> =	1.532	O(3) - O(4)	2.514
		O(2) - O(4)	2.503
		<O-O>P =	2.501

H-bonding distances

OH(1) - O(4)	2.712
OH(2) - O(3)	2.727
OH(3) - O(1)	2.651

Table 2.3), the proposed scheme of hydrogen-bonding in Table 2.5 seems valid. Coordination assignments of copper are based on topological considerations, and differ from Fehlmann et al. (1964). With copper in [6]-coordination, the structure is more amenable to interpretation than if copper is considered as [5]-coordinate (see Chapter 3 for structural

TABLE 2.4

Selected Bond Angles (°) for Cornetite

(O- Cu(1) -O)°		(O- Cu(2) -O)°		(O- Cu(3) -O)°	
OH(3)-O(3)	98.2(2)	O(4) -O(3)	118.8(2)	OH(3)-O(1)	96.9(2)
" -O(4)	81.4	" -OH(2)	93.5	" -O(3)	94.7
" -OH(1)	92.5	" -OH(2)	91.4	" -O(2)	87.0
" -O(2)	75.4	" -O(1)	100.6	" -O(2)	94.0
O(3) -OH(2)	88.0	OH(1)-OH(2)	94.2	O(1) -OH(1)	86.3
" -O(4)	76.2	" -OH(2)	82.4	" -O(3)	109.3
" -O(2)	120.8	" -O(1)	68.6	" -O(2)	99.3
OH(2)-O(4)	100.3	" -O(3)	74.2	OH(1)-O(3)	87.5
" -OH(1)	81.7	OH(2)-O(3)	68.7	OH(1)-O(2)	90.6
" -O(2)	101.4	" -O(1)	88.9	" -O(2)	82.0
OH(1)-O(2)	77.4	OH(2)-O(1)	96.8	O(2) -O(2)	92.3
" -O(4)	89.7	" -O(3)	103.0	" -O(3)	58.3
	====		====		====
<O-Cu(1)-O>=	90.2	<O-Cu(2)-O>=	90.1	<O-Cu(3)-O>=	89.9
O(2) -O(4)	152.7(2)	O(1) -O(3)	134.8(2)	O(2) -O(3)	148.7(2)
OH(3)-OH(2)	173.8	O(4) -OH(1)	166.7	OH(3)-OH(1)	175.3
O(3) -OH(1)	160.7	OH(2)-OH(2)	171.7	O(1) -O(2)	167.4

(O - P - O)°

O(1) - O(3)	109.9(2)	O(3) - O(2)	106.6
O(1) - O(2)	111.4	O(3) - O(4)	109.8
O(1) - O(4)	110.3	O(2) - O(4)	108.8
			=====
		<O-P-O> =	109.5

description). The resulting octahedral geometries are very distorted, with an extreme degree of Jahn-Teller distortion. Bond-valence criteria neither negate nor support these coordination assignments.

TABLE 2.5

Bond-Valences for Cornetite

	Cu(1)	Cu(2)	Cu(3)	P	H(1)	H(2)	H(3)	ΣO^{-2}
O(1)		0.070	0.498	1.328			0.20	= 2.096
O(2)	0.113		0.179,0.375	1.263				= 1.930
O(3)	0.482	0.062	0.051	1.277		0.20		= 2.072
O(4)	0.030	0.512		1.249	0.20			= 1.991
OH(1)	0.407	0.465	0.417		0.80			= 2.089
OH(2)	0.422	0.404,0.445				0.80		= 2.071
OH(3)	0.508		0.505				0.80	= 1.813
ΣM^{+}	1.962	1.958	2.025	5.117	1.00	1.00	1.00	

Bond-valence values for hydrogens are ideal contributions

2.2.2 Clinoclase

Clinoclase crystals from the Roughton Gill locality, England, were provided by the Geological Survey of Canada, National Mineral Collection, cataloque number - 18291. Crystals are prismatic, 0.5-1.0mm in size, and dark greenish-blue. A shaped crystal fragment, 0.18x0.24x0.28mm in size, was used for x-ray analysis. Experimental data for clinoclase are listed in Table 2.6. The unit cell reported by Ghose et al. (1965) was confirmed by the automatic cell determination procedure. The psi-scan gave a merging R of 5.34%, and a spherical correction of the raw data gave transmission values of min=0.020 and max=0.042. The calculated cell density closely matches the previously determined value. Systematic absences confirm the space group ($P2_1/c$) assigned by Ghose et al. (1965).

TABLE 2.6

Pertinent Data for Clinoclase

Unit Cell: a = 7.260(1)Å	Number of reflections used
b = 6.4576(7)	in cell determination : 23
c = 12.386(2)	
ß = 99.50(1)°	No. Reflections Collected: 1979
V = 572.8(1)Å^3	No. Reflections Rejected : 13
	Total Observed $\|F_o\|$ I>3.0σI: 1742
Space Group : $P2_1/c$	Total Unique Observed $\|F_o\|$: 1404
Part of Sphere	No. of psi-scan reflections : 10
Collected : 1 quadrant	No. of psi-scan measurements : 332
	Absorption corr. R-merge : 5.34
dens.(calc) = 4.41g/cm^3	min-max : 0.020 - 0.042
dens.(meas) = 4.33g/cm^3	Cell contents : $4[Cu_3(AsO_4)(OH)_3]$

R(obs) = 4.45% ; Rw(obs) = 3.81%

All atom positions of Ghose et al. (1965) are confirmed. The refinement procedure converged smoothly to a final R-index of 4.45% with anisotropic temperature factors. Hydrogen atoms were not located because of the large final R-index.

Refined atomic and thermal parameters are listed in Table 2.7. The bond lengths and angles do not differ significantly from Ghose et al. (1965), (Tables 2.8 and 2.9). However, an interpretation of the bonding does differ. Oxygen-oxygen distances involved in donor-acceptor hydrogen-bonding (listed in Table 2.8) seem valid choices when considering the bond-valence distributions that result. The OH(1)-O(4) distance is not listed by Ghose et al. (1965), and instead a OH(1)-O(1) distance is proposed for H-bonding which does not comply with the bond-valence scheme.

TABLE 2.7

Atomic (fractional) & Thermal Parameters for Clinoclase

	x	y	z	U(equiv)
Cu(1)	0.2123(1)	0.6400(2)	0.17059(8)	0.0177(3)
Cu(2)	0.8163(1)	0.3813(2)	0.12742(8)	0.0169(3)
Cu(3)	0.3869(1)	0.3531(2)	0.41260(8)	0.0183(3)
As	0.3087(1)	0.1499(1)	0.17955(6)	0.0142(2)
O(1)	0.4149(8)	0.0710(9)	0.0738(5)	0.018(2)
O(2)	0.1623(8)	0.3423(9)	0.1348(4)	0.018(2)
O(3)	0.1798(8)	-0.0531(9)	0.2130(4)	0.016(2)
O(4)	0.4711(8)	0.221(1)	0.2854(5)	0.019(2)
OH(1)	0.780(1)	0.2034(9)	0.4780(5)	0.025(2)
OH(2)	0.1912(8)	0.5943(9)	0.3227(4)	0.017(2)
OH(3)	0.1808(8)	0.1670(9)	0.4106(5)	0.021(2)

Anisotropic Temperature Factors

	*U(11)	U(22)	U(33)	U(23)	U(13)	U(12)
Cu(1)	246(5)	157(5)	133(4)	7(4)	50(3)	10(5)
Cu(2)	227(5)	151(5)	132(4)	-2(2)	40(3)	0(4)
Cu(3)	227(5)	183(5)	149(4)	-28(4)	64(4)	-42(5)
As	165(4)	146(4)	120(3)	-5(3)	35(3)	0(3)
O(1)	177(27)	193(28)	171(26)	19(23)	62(21)	49(23)
O(2)	201(27)	167(27)	183(26)	-11(24)	41(21)	-10(24)
O(3)	195(28)	130(26)	172(27)	0(22)	53(22)	-25(22)
O(4)	179(28)	251(31)	158(26)	-39(23)	47(22)	35(24)
OH(1)	423(38)	181(30)	155(27)	5(23)	94(26)	54(27)
OH(2)	225(28)	181(28)	123(23)	-20(22	47(21)	-5(23)
OH(3)	252(30)	199(30)	188(27)	-20(24)	57(23)	-36(25)

*U(ij) = U(ij) x 10^4 ($Å^2$)

Copper coordination geometries are very similar to Ghose et al. (1965), and the interpretation of Cu(2) and Cu(3) in square pyramidal coordination remains. However, Cu(1) has an acceptable octahedral geometry, rather than square pyramidal. A topological description of clinoclase (see Chapter 3) does not favour the assignment of Cu(2) or

TABLE 2.8

Selected Bond Lengths (Å) of Clinoclase

Cu(1)- OH(1)	1.895(6)	Cu(2)- OH(3)	1.905(6)	Cu(3)- OH(3)	1.916(6)
" - OH(2)	1.938	" - OH(1)	1.906	" - O(4)	1.977
" - O(2)	1.993	" - OH(2)	1.957	" - O(1)	2.000
" - O(3)	2.074	" - O(3)	2.016	" - O(1)	2.033
" - O(4)	2.332	" - O(2)	2.518	" - OH(2)	2.272
" - OH(3)	2.871		=====		=====
	=====	<Cu(2)-O> =	2.060	<Cu(3)-O> =	2.040
<Cu(1)-O> =	2.233				
OH(1)- O(2)	2.786(8)	OH(3)- OH(1)	2.752(8)	OH(3)- O(4)	2.836(8)
" - O(3)	2.895	" - O(3)	2.829	" - O(1)	2.950
" - O(4)	2.994	" - O(2)	3.233	" - OH(2)	2.972
" - OH(3)	3.166	OH(1)- OH(2)	2.770	O(4) - O(1)	2.894
OH(2)- O(2)	2.819	" - O(2)	3.129	O(4) - OH(2)	3.237
" - O(3)	2.646	OH(2)- O(3)	2.646	O(1) - O(1)	2.541
" - O(4)	3.090	" - O(2)	3.142	" - OH(2)	3.433
" - OH(3)	3.646		=====		=====
O(2) - O(4)	3.627	<O-O>Cu(2) =	2.991	<O-O>Cu(3) =	2.975
" - OH(3)	3.233				
O(3) - O(4)	2.923	As - O(2)	1.669(5)	O(2) - O(4)	2.783(8)
" - OH(3)	3.338	" - O(4)	1.676	" - O(3)	2.726
	=====	" - O(3)	1.701	" - O(1)	2.731
<O-O>Cu(1) =	3.097	" - O(1)	1.704	O(4) - O(3)	2.788
			=====	" - O(1)	2.760
H-Bonding O-O Distances		<As-O> =	1.688	O(3) - O(1)	2.739
----------					=====
OH(1) - O(4)	2.944			<O-O>As =	2.755
OH(2) - O(3)	2.822				
OH(3) - O(2)	2.803				

Cu(3) as octahedral. Also, the sixth closest ligands would produce distortions much greater than other observed octahedral coordinations.

TABLE 2.9

Selected Bond Angles (°) for Clinoclase

(O- Cu(1) -O)°		(O- Cu(2) -O)°		(O- Cu(3) -O)°	
OH(1)-OH(2)	175.4(2)	OH(3)-OH(1)	92.5(2)	OH(3)-O(4)	93.5(2)
" -O(2)	91.5	" -OH(2)	175.8	" -O(1)	172.7
" -O(3)	93.6	" -O(3)	92.3	" -O(1)	96.6
" -O(4)	89.6	" -O(2)	92.9	" -OH(2)	90.0
" -OH(3)	80.4	OH(1)-OH(2)	91.6	O(4) -O(1)	93.4
OH(2)-O(2)	91.6	" -O(3)	171.9	" -O(1)	153.3
" -O(3)	82.5	" -O(2)	88.9	" -OH(2)	99.0
" -O(4)	92.3	OH(2)-O(3)	83.5	O(1) -O(1)	78.1
" -OH(3)	96.7	" -O(2)	88.3	" -OH(2)	86.7
O(2) -O(3)	162.6	O(3) -O(2)	97.4	O(1) -OH(2)	105.6
" -O(4)	113.8				
" -OH(3)	81.2		(O - As - O)°		
O(3) -O(4)	82.9				
" -OH(3)	83.3	O(2) - O(4)	112.6(3)	O(4) - O(3)	111.3
O(4) -OH(3)	162.4	" - O(3)	108.0	" - O(1)	109.5
		" - O(1)	108.1	O(3) - O(1)	107.1
					=====
				<O-As-O> =	109.4

TABLE 2.10

Bond-Valences for Clinoclase

	Cu(1)	Cu(2)	Cu(3)	As	H(1)	H(2)	H(3)	ΣO^{-2}
O(1)			0.364,0.402	1.175				= 1.941
O(2)	0.412	0.101		1.279			0.15	= 1.942
O(3)	0.323	0.383		1.183		0.14		= 2.029
O(4)	0.160		0.432	1.258	0.10			= 1.950
OH(1)	0.555	0.535			0.90			= 1.990
OH(2)	0.485	0.459	0.187			0.86		= 1.991
OH(3)	0.050	0.538	0.520				0.85	= 1.998
ΣM^{+}	1.981	2.015	1.905	4.895	1.0	1.0	1.0	

Bond-valence values for hydrogens from curves of Brown (1976)

2.2.3 Euchroite

Euchroite from Copper Cliff, Montana, was provided by the Geological Survey of Canada, National Mineral Collection, catalogue number - 65222. Stubby prismatic crystals, 1-5mm in size, are emerald green. A crystal fragment was shaped to a form intermediate between a cube and a sphere, with a size of 0.28mm diameter. Experimental data for euchroite are listed in Table 2.11. The unit cell data agrees with that of Finney (1966). Data collection proceeded smoothly with a good absorption correction, and only 3 reflections were rejected. Although this mineral structure is non-centrosymmetric, only an octant of the reciprocal sphere was collected, because it was felt that no additional resolution was obtainable with a quarter sphere. Systematic absences confirm the

TABLE 2.11

Pertinent Data for Euchroite

Unit Cell: a = 10.056(2)Å	Number of reflections used
b = 10.506(2)	in cell determination : 25
c = 6.103(2)	No. Reflections Collected : 1187
V = 644.8(3)Å^3	No. Reflections Rejected : 3
	Total Observed $\|F_o\|$ I>3.0σI: 1118
Space Group : $P2_12_12_1$	Total Unique Observed $\|F_o\|$: 1061
Part of Sphere	No. of psi-scan reflections : 11
Collected : 1 octant	No. of psi-scan measurements : 396
	Absorption corr. R-merge : 2.96%
dens.(calc) = 3.47g/cm^3	min-max : 0.017 - 0.044
dens.(meas) = 3.44g/cm^3	Cell contents : 4[$Cu_2AsO_4(OH)\cdot 3H_2O$]
R(obs) = 3.73% ;	Rw(obs) = 3.57%

space group ($P2_12_12_1$) assigned by Finney (1966).

Structural refinement converged rapidly below 8% upon refining all atom positions corresponding to those of Finney (1966). The free isotropic model refined to an R-index of 4.6%. Anisotropic refinement yielded one plausible hydrogen position at an R-index of 3.79%. Free positional refinement of the hydrogen failed. The hydrogen position was fixed and two cycles of refinement were then done. Refinement gave a good H-bonding geometry with a final R(obs) of 3.73%. The refined atomic coordinates and thermal parameters of euchroite are listed in Table 2.12.

Bond lengths and bond angles of euchroite are listed in Tables 2.13 and 2.14. The bond lengths of Cu(1) and Cu(2) show little change from Finney (1966), but the AsO4 geometry is significantly different. The mean <As-O> distance is greater than Finney's, and his bond lengths deviate more from the mean. The bond-valence sum on As (Table 2.15) is slightly low, but the overall bonding arrangement proposed is good. The O-O distances relevant to H-bonding differ from Finney (1966), and they are supported by the bond-valence distributions in Table 2.15.

The coordination number of Cu(2) was originally considered to be [5], but requires a new interpretation. Cu(2) is clearly in very distorted octahedral coordination, rather than square pyramidal coordination (Finney, 1966). The resulting topology is different (discussed in Chapter 3), and establishes new structural relationships with several other mineral structures.

TABLE 2.12

Atomic (fractional) & Thermal Parameters for Euchroite

	x	y	z	U(equiv)
Cu(1)	0.2562(1)	-0.0087(1)	0.4686(2)	0.0174(3)
Cu(2)	0.1995(1)	0.2492(1)	0.6667(2)	0.0184(3)
As	0.39064(9)	0.23582(8)	0.2176(2)	0.0159(2)
O(1)	0.3270(7)	0.1686(6)	0.456(6)	0.019(2)
O(2)	0.3028(7)	0.1846(6)	0.0032(1)	0.021(2)
O(3)	0.5478(6)	0.1815(6)	0.185(1)	0.019(2)
O(4)	0.3885(7)	0.3936(5)	0.248(1)	0.020(2)
OH	0.1529(6)	0.0663(6)	0.709(5)	0.019(2)
OW(1)	0.2789(7)	0.4188(6)	0.639(1)	0.021(2)
OW(2)	0.0703(7)	0.0550(7)	0.222(1)	0.029(2)
OW(3)	0.0668(8)	0.3110(7)	0.276(1)	0.031(2)
H	0.058	0.069	0.691	0.020

Anisotropic Temperature Factors

	*U(11)	U(22)	U(33)	U(23)	U(13)	U(12)
Cu(1)	200(5)	159(5)	162(4)	6(4)	-22(4)	-8(3)
Cu(2)	185(5)	151(5)	218(5)	-10(5)	32(4)	0(4)
As	159(4)	153(4)	165(4)	3(4)	5(3)	-10(3)
O(1)	219(31)	160(30)	186(32)	-26(27)	-53(27)	-15(26)
O(2)	224(31)	175(30)	219(34)	0(27)	-43(31)	-32(27)
O(3)	164(29)	197(28)	209(36)	18(29)	-19(25)	17(24)
O(4)	212(30)	138(24)	257(37)	-14(25)	-43(30)	-20(25)
OH	173(29)	195(28)	201(30)	17(29)	-4(28)	6(23)
OW(1)	217(35)	183(30)	235(34)	8(27)	-46(28)	-31(24)
OW(2)	258(34)	270(33)	353(41)	-40(36)	42(36)	-46(28)
OW(3)	281(35)	335(37)	300(39)	38(38)	-38(36)	-62(31)

*U(ij) = U(ij) x 10^4 ($Å^2$)

2.2.4 Liroconite

Liroconite from Cornwall, England, was provided by the Mineral Sciences Division, National Museum of Natural Sciences, Ottawa, catalogue number - 39859. Subhedral crystals, 0.5-2.0mm in size, are

TABLE 2.13

Selected Bond Lengths (Å) of Euchroite

Cu(1)-	OH	1.928(7)	Cu(2)-	O(3)	1.918(7)	As -	O(2)	1.668(7)
"	O(2)	1.952(7)	"	OW(1)	1.960(7)	"	O(4)	1.668(6)
"	OH	1.962(7)	"	OH	1.994(6)	"	O(3)	1.692(6)
"	O(1)	1.996(7)	"	O(1)	2.004(7)	"	O(1)	1.738(7)
"	OW(2)	2.381(8)	"	O(2)	2.399(7)			=====
"	OW(2)	2.491(8)	"	OW(3)	2.806(8)	<As-O> =		1.692
		=====			=====			
<Cu(1)-O> =		2.118	<Cu(2)-O> =		2.180			
OH	O(2)	2.653(11)	O(3)	OW(1)	2.768(11)	O(2)-	O(4)	2.791(9)
"	O(1)	2.898	"	OH(1)	2.926	"	O(3)	2.702(9)
"	OW(2)	3.241	"	O(2)	3.142	"	O(1)	2.778(10)
"	OW(2)	3.062	"	OW(3)	3.297	O(4)-	O(3)	2.771(9)
O(2)	OH	2.954	OW(1)-	O(1)	2.897	"	O(1)	2.754(9)
"	OW(2)	3.017	"	O(2)	3.325	O(3)-	O(1)	2.772(10)
"	OW(2)	3.303	"	OW(3)	3.277			=====
OH	O(1)	2.571	OH	O(1)	2.571	<O-O>As =		2.761
"	OW(2)	3.062	"	O(2)	2.653			
"	OW(2)	3.088	"	OW(3)	3.787	H-Bonding Distances		
O(1)	OW(2)	3.037	O(1)	O(2)	3.354	---		
"	OW(2)	3.182	OW(3)-	O(1)	3.208	OW(1)-	O(4)	2.643(11)
		=====			=====	OW(1)-	O(4)	2.676
<O-O>Cu(1) =		3.005	<O-O>Cu(2) =		3.100	OW(2)-	OW(3)	2.708
						OW(3)-	O(3)	2.825
						H -	OH	0.96
						H···O(4)		1.79

bluish-green. A crystal fragment was ground into a sphere 0.32mm in diameter. Experimental data for liroconite are listed in Table 2.16. The unit cell obtained agrees with that of Kolesova & Fesenko (1968). A quadrant of the reflection sphere was collected, and the psi-scan data yielded a very good spherical absorption correction (R-merge=1.53%). Only five reflections were rejected during data reduction. Systematic reflections indicate that the a-glide may not be present because a significant number of h0l-reflections exist (18 reflections with $I>3\sigma I$;

TABLE 2.14

Selected Bond Angles (°) for Euchroite

(O- Cu(1) -O)°			(O- Cu(2) -O)°			(O- As -O)°	
OH	-O(2)	86.3(3)	O(3)	-OW(1)	91.1(3)	O(2) - O(4)	113.6(3)
"	-OW(2)	86.7	"	-OH	96.8	" - O(3)	107.1
"	-O(1)	95.2	"	-OW(3)	86.2	" - O(1)	109.3
"	-OW(2)	97.0	"	-O(2)	92.7	O(4) - O(3)	111.1
O(2)	-OH	98.0	OW(1)	-OW(3)	84.9	" - O(1)	107.9
"	-OW(2)	95.3	"	-O(1)	93.9	O(3) - O(1)	107.8
"	-OW(2)	87.7	"	-O(2)	98.9		=====
OH	-O(1)	81.0	OH	-O(1)	80.0	<O-As-O> =	109.5
"	-OW(2)	89.1	"	-O(2)	73.7		
"	-OW(2)	86.9	"	-OW(3)	102.7	OH - H···O(4)	158
O(1)	-OW(2)	87.4	O(1)	-O(2)	98.8		
"	-OW(2)	89.6	"	-OW(3)	81.8		
		====			====		
<O-Cu-O> =		90.0	<O-Cu-O> =		90.1		
OW(2)	-OW(2)	175.4	O(2)	-OW(3)	176.2		
OH	-OH	172.6	O(3)	-O(1)	166.5		
O(2)	-O(1)	174.9	OW(1)	-OH	169.2		

and 3 reflections with I>10σI). The violations are a "borderline case" for the need to change the symmetry.

The original space group assignment was used in this refinement to see if the structure could be refined without changes. The R-indices dropped quite low using the starting model of Kolesova & Fesenko (1968), and an anisotropic model gave a final R(obs)=4.20%. This model is quite sufficient for the purposes of this study, and further refinement of the structure shall be left to publication outside the bounds of this thesis. With these factors in mind, the atomic coordinates and thermal parameters are listed in Table 2.17.

TABLE 2.15

Bond-Valences for Euchroite

	Cu(1)	Cu(2)	As	H1	HW1	HW1'	HW2	HW2'	HW3	HW3'	ΣO^{-2}
O1	0.407	0.397	1.081								= 1.885
O2	0.462	0.135	1.282								= 1.879
O3		0.516	1.212						0.15		= 1.878
O4			1.282	0.20	0.25	0.23					= 1.972
OH	0.455,0.498	0.415		0.79							= 2.158
OW1		0.454			0.75	0.77					= 1.974
OW2	0.140,0.101						1.00	0.80			= 1.941
OW3		0.053						0.20	1.00	0.85	= 2.103
ΣM^{+}=	2.068	1.970	4.857	0.99	1.00	1.0	1.00	1.00	1.00	1.00	

Bond-valence values for hydrogens are from curves of Brown (1976)

Bond lengths and bond angles of liroconite are listed in Tables 2.18 and 2.19. The bonding geometry of the polyhedra are all slightly modified from previous work. The As-O distances were quite low in the report of Kolesova & Fesenko (1968), with <As-O> less than 1.62Å. Thus the bond-valence conditions of such a model were unrealistic, unless significant substitution by P is present. The bond-valence scheme proposed (Table 2.20) includes hydrogen-bonding that is based on the O-O distances in Table 2.18. The bond-valence sums satisfy the bonding requirements of all the atoms except OW(1), which is slightly underbonded. The interpretation of coordination number for Cu remains the same as the previous authors, and the topological interpretation is also unchanged (see Chapter 3).

TABLE 2.16

Pertinent Data for Liroconite

Unit Cell: a = 12.655(3)Å	Number of reflections used
b = 7.562(2)	in cell determination : 25
c = 9.877(2)	No. Reflections Collected : 3313
ß = 91.28(2)	No. Reflections Rejected : 5
V = 944.9(4)Å^3	
	Total Observed $\|F_o\|$ I>3.0σI: 3208
Space Group : $I2_1/a$	Total Unique Observed $\|F_o\|$: 1314
Part of Sphere	No. of psi-scan reflections : 8
Collected : 1 quadrant	No. of psi-scan measurements : 288
	Absorption corr. R-merge : 1.53%
dens.(calc) = 3.05g/cm^3	min-max : 0.033 - 0.065
dens.(meas) = 2.93g/cm^3	Cell contents:4$[Cu_2Al(AsO_4)(OH)_4 \cdot 4H_2O]$

R(obs) = 4.20% ; Rw(obs) = 4.17%

TABLE 2.17

Atomic (fractional) & Thermal Parameters for Liroconite

	x	y	z	U(equiv)
Cu(1)	0.63091(5)	0.7218(1)	0.77032(6)	0.0150(2)
As	0.7500(0)	0.5459(1)	0.5000(0)	0.0157(2)
Al	0.5000(0)	0.5000(0)	0.5000(0)	0.0104(5)
O(1)	0.6436(3)	0.4195(6)	0.4938(4)	0.011(1)
O(2)	0.7455(3)	0.6743(6)	0.6387(4)	0.017(1)
OH(1)	0.5245(3)	0.5947(6)	0.6740(4)	0.020(1)
OH(2)	0.5412(3)	0.7759(6)	0.9227(4)	0.017(1)
OW(1)	0.6843(4)	0.3792(8)	0.8394(6)	0.042(2)
OW(2)	0.6109(4)	0.9929(7)	0.6210(4)	0.030(1)

Anisotropic Temperature Factors

	*U(11)	U(22)	U(33)	U(23)	U(13)	U(12)
Cu(1)	123(3)	220(4)	107(3)	-46(2)	7(2)	-20(2)
As	151(4)	195(4)	125(4)	0(0)	-3(3)	0(0)
Al	97(9)	144(10)	71(8)	-4(8)	-6(7)	-6(8)
O(1)	127(17)	194(19)	189(18)	-11(15)	-2(14)	-11(15)
O(2)	124(17)	253(21)	125(17)	-81(15)	13(13)	-29(16)
OH(1)	189(19)	296(22)	113(17)	-42(16)	-4(14)	-63(17)
OH(2)	145(18)	199(20)	167(18)	37(15)	25(14)	18(15)
OW(1)	418(31)	460(34)	393(30)	-217(27)	21(24)	48(27)
OW(2)	349(26)	339(26)	223(21)	2(20)	70(19)	100(22)

*U(ij) = U(ij) x 10^4 ($Å^2$)

TABLE 2.18

Selected Bond Lengths (Å) of Liroconite

Cu - OH(1)	1.894(7)	Al - OH(1)x2	1.881(7)	As - O(1)x2	1.651(7)
" - OH(2)	1.948(7)	" - O(1) x2	1.960(7)	" - O(2)x2	1.681(7)
" - O(2)	1.951(7)	" - OH(2)x2	1.919(7)		=====
" - O(2)	2.001(7)		=====	<As-O> =	1.666
" - OW(2)	2.535(8)	<Al-O> =	1.912		
" - OW(1)	2.759(8)				
	=====				
<Cu-O> =	2.181				

OH(1)- OH(2)	2.817(11)	OH(1)-O(1)x2	2.705(10)		
" - O(2)	2.890	" -O(1)x2	2.670		
" - OW(2)	3.350	" -OH(2)x2	2.681	O(1)-O(2)x2	2.709(9)
" - OW(1)	3.044	" -OH(2)x2	2.717	O(2)-O(2)	2.745
OH(2)- O(2)	2.805	O(1) -OH(2)x2	2.727	O(1)-O(1)	2.693
" - OW(2)	3.531	" -OH(2)x2	2.723	O(1)-O(2)x2	2.734
" - OW(1)	3.609		=====		=====
O(2) - O(2)	2.479	<O-O>Al =	2.704	<O-O>As =	2.712
" - OW(2)	3.216				
" - OW(1)	3.497				
O(2) - OW(2)	2.954				
" - OW(1)	3.095				
	=====				
<O-O>Cu =	3.099				

Donor-Acceptor H-Bonding Distances

OW(1) - O(1)	2.780(7)
OW(2) - OH(1)	2.790(6)
OW(2) - OH(2)	2.904(6)
OW(1) - OW(2)	2.786(7)

TABLE 2.19

Selected Bond Angles (°) for Liroconite

(O- Cu -O)°		(O- Al -O)°		(O- As -O)°	
OH(1)-OH(2)	94.3(3)	OH(1)-O(1) x2	90.7(3)	O(1)- O(1)	109.3(3)
" -OW(1)	79.3	" -O(1) x2	89.3(3)	" - O(2)x2	110.3
" -O(2)	95.7	" -OH(2)x2	89.2(3)	" - O(2)x2	108.8
" -OW(2)	93.3	" -OH(2)x2	90.7(3)	O(2)- O(2)	109.4
OH(2)-OW(1)	98.6	O(1) -OH(1)x2	89.9(0)		=====
" -O(2)	92.0	" -OH(2)x2	90.1(3)	<O-As-O> =	109.5
" -OW(2)	103.1		====		
O(2) -O(2)	77.7				
" -OW(2)	90.6	<O-Al-O>apical=	90.0		
" -OW(1)	94.3				
O(2) -OW(2)	80.3	OH(1)-OH(1)	180.0		
" -OW(1)	79.3	OH(2)-OH(2)	180.0		
	====	O(1) -O(1)	180.0		
<O-Cu-O>apical=	89.9				
OH(1)-O(2)	171.7				
OH(2)-O(2)	169.2				
OW(1)-OW(2)	157.5				

TABLE 2.20

Bond-Valences for Liroconite

	Cu	Al	As	H1	H2	HW1	HW1'	HW2	HW2'	ΣO^{2-}
O1		0.485(x2)↓	1.337(x2)↓			0.16				= 1.982
O2	0.401,0.466		1.242(x2)↓							= 2.109
OH1	0.557	0.536(x2)↓		1.00					0.15	= 2.093
OH2	0.471	0.456(x2)↓			1.00		0.09			= 2.026
OW1	0.058					0.84	0.85			= 1.748
OW2	0.097						0.15	0.91	0.85	= 2.007
ΣM^{+}=	2.050	2.972	5.158	1.0	1.0	1.0	1.0	1.0	1.0	

Chapter III

A STRUCTURAL CLASSIFICATION OF Cu^{2+} OXYSALT MINERALS

The structures of the Cu^{2+} oxysalt minerals are described and classified in this chapter using the method of Hawthorne (1983). This approach illustrates the structural similarities and differences between the Cu oxysalts and other oxysalts, regardless of the Jahn-Teller effect.

3.1 CLASSIFICATION CRITERIA

Using the ideas of bond-valence theory (Brown, 1981), Hawthorne (1983) has devised a scheme for the structural classification of all oxysalt minerals, based on the polymerization of those coordination polyhedra with higher bond-valences. This method of classification is hierarchical, incorporating all the different chemical groups of oxysalt minerals (as listed in Table 1.1) and reorganizing them into a sensible structural format.

Structural categories are arranged according to the increased dimensionality of polymerization of the more tightly-bonded cation polyhedra. In general, cations with Lewis acidities greater than 0.3 valence units (v.u.) (coordinations ≤ 6 and charges $\geq +2$) form tightly-bonded units. The categories of classification are:

1. Isolated Polyhedra - structures involving no polymerization of the cation polyhedra; hydrogen-bonds and weakly bonded high-coordination cations hold the strongly bonded polyhedra together.

2. Finite Clusters - polymerization of strongly bonded polyhedra to form finite clusters which are interconnected in the same way as the isolated polyhedra.
3. Infinite Chains of Polyhedra - one dimensional polymerization of strongly bonded polyhedra, linked together by hydrogen-bonding and interchain higher-coordination cations to form a three-dimensional structure.
4. Infinite Sheets of Polyhedra - polymerization of strongly bonded polyhedra in two dimensions, the third dimension of bonding consisting of hydrogen-bonding and weakly bonding interlayer cations.
5. Frameworks of Polyhedra - polyhedral connectivity of strong bonds in three dimensions, with void space possibly occupied by more weakly bonded chemical units.

Structures within the 5 main categories are arranged according to the degree of connectivity of their polyhedral units, and by increasing structural complexity: eg. (1) groups of corner-sharing chains followed by edge-sharing chains; (2) simple Cu-octahedral sheets, followed by complex mixed polyhedral sheets. These latter subcategories are not made by Hawthorne (1985a, 1986), but they are convenient for the description of this large family of inter-related Cu^{2+} oxysalt structures. The framework structures have been arranged into three subgroups with polymerized structural components that resemble the other structural categories. These subgroups allow for structural comparisons with the other major categories.

Many of the structural drawings presented in this classification were done with the aid of STRUPLO, a plot program by Fischer (1984). Table 3.1 shows the scheme of polyhedral shading used in the drawings throughout this thesis. Coordinations of cations are given as

TABLE 3.1

Shading Scheme For Polyhedral Drawings

There are two schemes of shading: 1) STRUPLO, with lines; 2) patterned sketches. These two styles are used together.

I. STRUPLO Shaded Polyhedra

1. tetrahedra 

2. octahedra 

II. Other Types of Shading

1. tetrahedra and trigonal pyramids 

2. planar groups - square and triangular 

3. octahedra and other coordinations > [4] 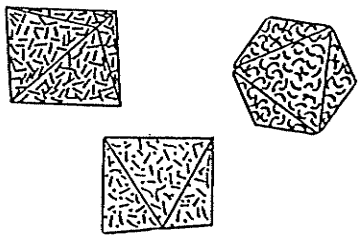

superscripts to the left of M, A or T cations, or in square brackets.

3.2 ISOLATED POLYHEDRA AND FINITE CLUSTERS

This is the smallest structural group in the Cu^{2+} oxysalt family; Table 3.2 lists the minerals involved. The structural determination of Aubertite (Ginderow and Cesbron, 1979) shows Cu^{2+} in typical J-T type coordination with 2 long and 4 short Cu-O bonds. The isolated polyhedra are all linked by hydrogen-bonding from H_2O groups (Figure 3.1). Interestingly, the chlorine ion is not part of any coordination polyhedron.

TABLE 3.2

Isolated Polyhedra and Finite Clusters

Aubertite	$CuAl(SO_4)_2Cl \cdot 14H_2O$
Boothite	$CuSO_4 \cdot 7H_2O$
Cyanochroite	$K_2Cu(SO_4) \cdot 6H_2O$
Henmilite	$Ca_2Cu(OH)_4[B(OH)_4]_2$

Boothite is an end-member of the $M^{2+}SO_4 \cdot 7H_2O$ series. The boothite structure itself has not been solved, but axial ratios and optical data (Palache et al., 1951) show it to be isostructural with the Fe-member, mellanterite (Baur, 1964). The structure (Figure 3.2) is a simple arrangement of layers of isolated tetrahedra and octahedra, all hydrogen bonded into a low-density, layered packing scheme. The substitution of Cu for Fe and Co, without the first order J-T effect, is possible because of the flexibility of the hydrogen-bonding scheme (Fe^{2+} does possess the weak second order J-T effect, but it is small; discussed in Chapter 4).

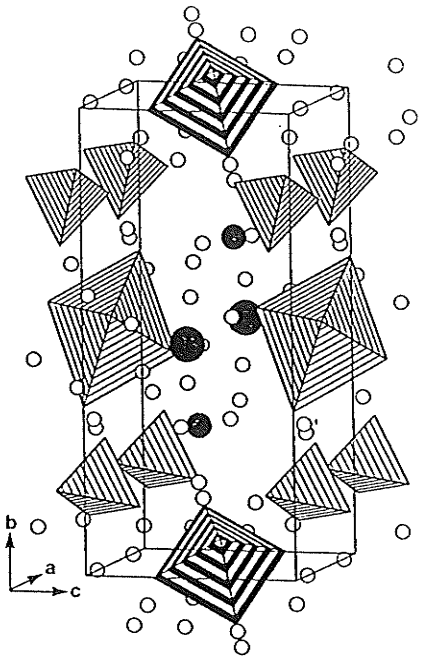

An oblique view down the a-axis;
large solid circles - chlorine;
medium solid circles - oxygen;
small open circles - hydrogen
banded octahedra - Al^{3+}
open shaded octahedra - Cu^{2+}
shaded tetrahedra - S^{6+}

Figure 3.1: Structure of Aubertite.

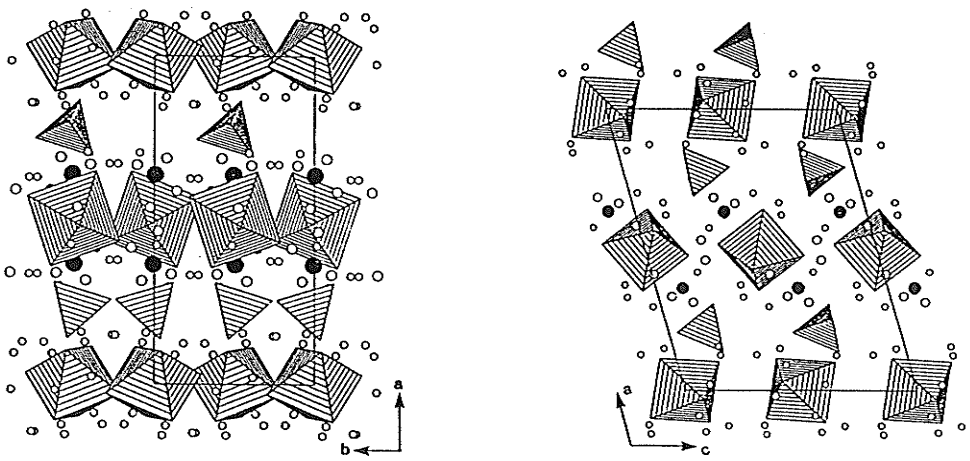

A B

Figure 3.2: $M^{2+}SO_4 \cdot 7H_2O$ Structure. (a) down the c-axis; (b) down the b-axis; oxygens are solid circles, hydrogens are small open circles. Notice the tetrahedral-octahedral layering on (100), and the complex network of H_2O and hydrogen-bonding

Cyanochroite is a natural analogue of the common Tutton Salt series: $A^{+}_{2}M^{2+}(X^{6+}O_4)\cdot 6H_2O$. The M^{2+} and X^{6+} polyhedra are bonded by high coordinated A^{+} and H_2O groups into a low-density, loosely packed structure (Figure 3.3). As in boothite, the geometry of the M^{2+} polyhedron is very flexible, and allows the substitution of Mg,Zn,Ni,Cu,Cd,Mn,V,Fe and Co (Brown and Chidambram, 1969). Bond lengths of the weakly bonded A^{+} ions and hydrogen-bonds (from the H_2O molecules) are flexible enough to allow the M-site substitutions. The A^{+} site is [8]-coordinate in cyanochroite, but varies from [5] to [11] in other Tutton Salts (Baur, 1973), further attesting to the flexibility of the structure.

Henmilite is the only member of the finite cluster category. It is an unusual borate compound, because the borate tetrahedra are not polymerized to one another. Hydrogen ions give large bond-valence contributions to the tetrahedra and prohibit polymerization. Figure 3.4 shows the loosely packed arrangement of isolated corner-sharing tetrahedral-octahedral-tetrahedral trimeric clusters, held weakly together by [8]-coordinate Ca^{2+}. In fact, this structure is so loosely packed together and fragile that it decomposes under an electron beam analysis (Nakai, 1985). Nakai (1985) reports the Cu as square planar coordinated. However, the bond-valence sum on copper indicates a value of 2.00v.u. when in very distorted six coordination, and this interpretation shows that some polymerization is present. Considering the Cu in six coordination also reveals the similarity to the bloedite group of structures (Hawthorne, 1985b), which consist of trimeric clusters held together by large highly-coordinated cations.

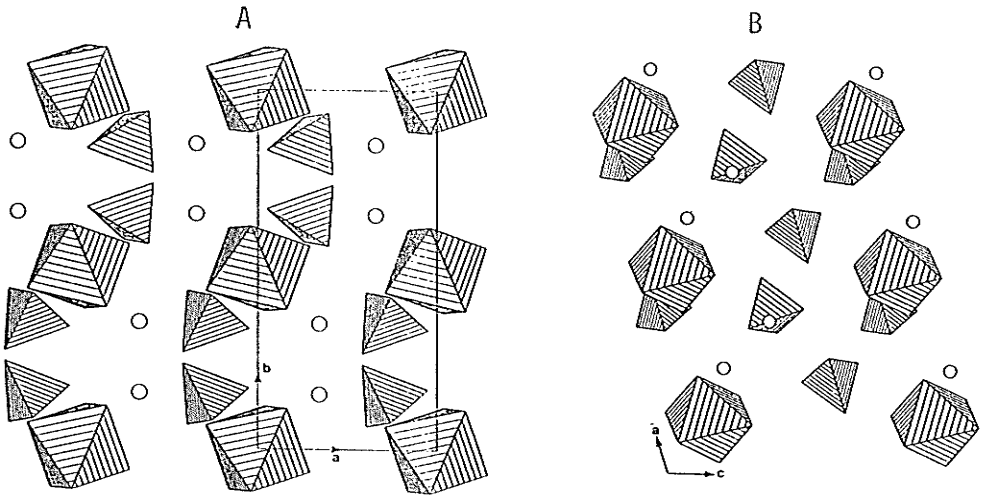

Figure 3.3: Structure of Cyanochroite. (a) a view down the c-axis; (b) viewed down the b-axis. Circles are K^+ ions; H_2O groups and hydrogens are not shown.

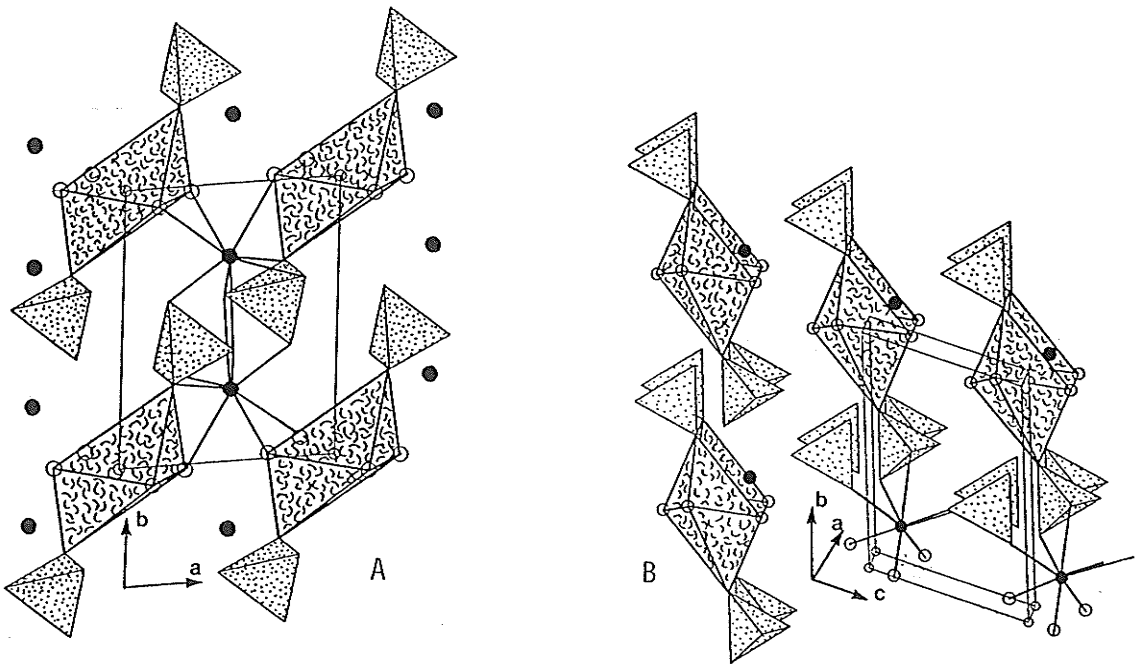

Figure 3.4: Structure of Henmilite. (a) viewed down the c-axis, the highly coordinated Ca cations (solid circles) weakly hold the trimeric clusters together; (b) an oblique view down the a-axis, showing the loosely bound arrangement.

It is interesting to note that the tetrahedral cations found in this group are usually hexavalent. Hawthorne (1985a) noted that there are no pentavalent or quadrivalent cations in the isolated or cluster type polyhedral structures of his classification. Weak interpolyhedral bonding can usually only satisfy the bond-valence requirements of the hexavalent cation tetrahedra, whereas, lower charged tetrahedral cations require polymerization. Henmilite is the obvious exception to this trend, and is also unique for borate compounds, which are usually polymerized.

3.3 INFINITE POLYHEDRAL CHAINS

3.3.1 Corner-Sharing Chains

The most loosely linked chain structure is chalcanthite (Figure 3.5). Octahedra and tetrahedra share only two corners each to form wavy chains along the b-axis; H_2O groups link these chains together by hydrogen-bonding. Because of the low connectivity of the octahedra, the $M^{2+}X^{6+}O_4 \cdot 2H_2O$ series can accept Mg^{2+} and Cr^{6+} into its structure as well as Cu^{2+} and S^{6+} (Baur & Rolin, 1972). The Jahn-Teller effect does not limit substitution in this case.

The kröhnkite structure (Figure 3.6) was refined by Hawthorne and Ferguson (1975). Hawthorne and Ferguson (1977) then refined roselite $[Ca(Mg,Co)AsO_4{}_2 \cdot 2H_2O]$ and brandtite (the Mn-analogue), and found all three minerals to be isostructural. The $M^{2+}T_2O_4$-chain (Figure 3.6) is apparently structurally convenient for $AM^{2+}(TO_4)_2 \cdot H_2O$ minerals, and also occurs in the fairfieldite and messelite series of structures

TABLE 3.3

Infinite Polyhedral Chains

A. Corner-sharing (^{6}M & ^{4}T) chains:

Chalcanthite	$CuSO_4 \cdot 5H_2O$
Kröhnkite	$Na_2Cu(SO_4)_2 \cdot 2H_2O$
Cuprocopiapite	$CuFe_4^{+3}(SO_4)_6(OH)_2 \cdot 20H_2O$

B. ^{6}M-chains sharing edges with ^{3+4}T:

Chalconatronite	$Na_2Cu(CO_3)_2 \cdot 3H_2O$
Chlorothionite	$K_2Cu(SO_4)Cl_2$

C. Edge-sharing ^{6}M chains:

i. Without tetrahedra -

Eriochalcite	$CuCl_2 \cdot 2H_2O$
Chloroxiphite	$Pb_3CuCl_2(OH)_2O_2$

ii. With tetrahedra -

Caledonite	$Pb_5Cu_2(CO_3)(SO_4)_3(OH)_6$
Linarite	$PbCu(SO_4)(OH)_2$
Schmiederite	$Pb_2Cu_2(SeO_4)(SeO_3)(OH)_4$
Fornacite	$Pb_2Cu(CrO_4)AsO_4(OH)$
Vauquelinite	$Pb_2Cu(CrO_4)(PO_4)(OH)$

(Hawthorne, 1985a). The octahedral distortion found in kröhnkite is repeated in the octahedra of the roselite and brandtite structures, although Mg and Co do not exhibit the J-T effect. This interesting feature will be dealt with in Chapter 5. Large interchain cations provide structural support and linkage for the $M^{2+}T_2O_4$-chains.

The structure of cuprocopiapite has not been solved, but the cell dimensions, symmetry, and composition (Berry, 1947) indicate that it is isostructural with copiapite, Cu replacing Mg. The structure (Figure 3.7) shows Fe^{3+}-octahedral and SO_4-tetrahedral corner-sharing chains

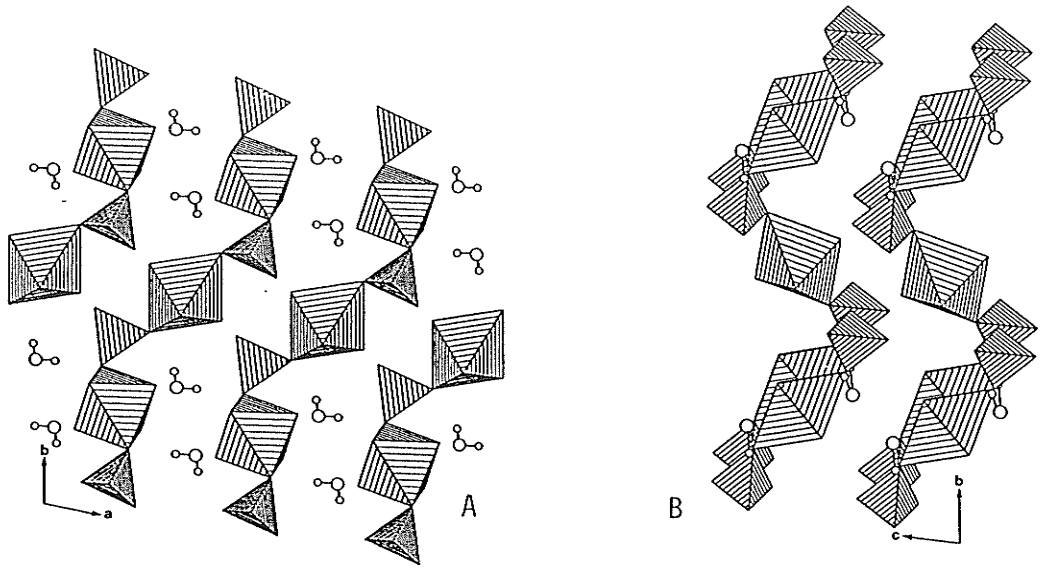

Figure 3.5: Chalcanthite Structure. (a) down [001]; (b) down [100]; H_2O hold together the wavy corner-sharing tetrahedral-octahedral chains along b-axis.

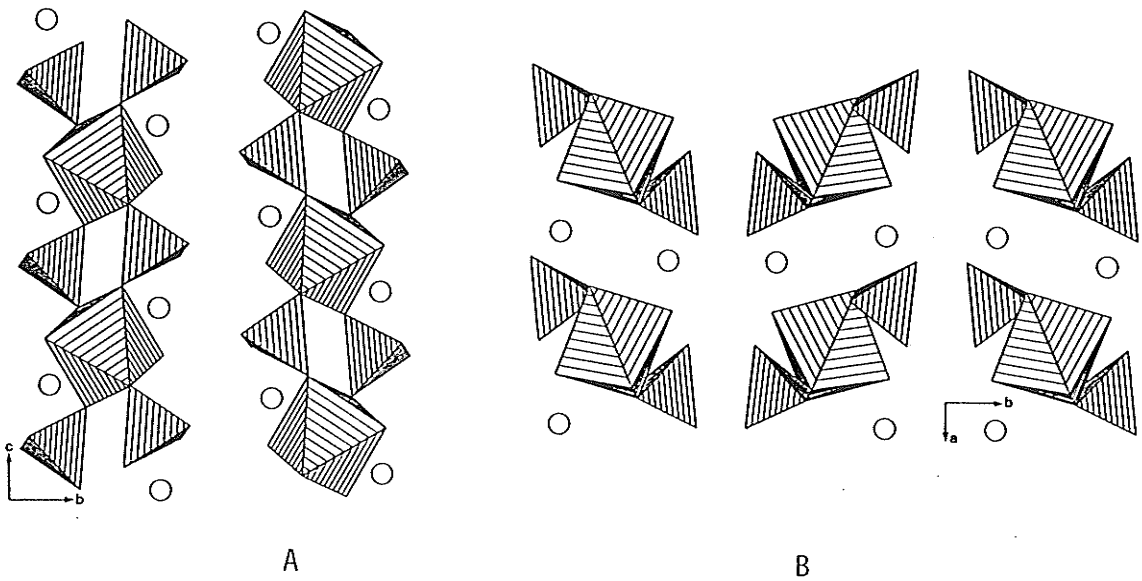

Figure 3.6: Kröhnkite Structure. (a) the $M^{2+}T_2O_4$ chain viewed down the a-axis; (b) the chains and linking interlayer cations, viewed down [001], to illustrate the packing.

hydrogen-bonded to isolated Cu-octahedra by H_2O groups. Clearly, bond length requirements at the copper site are flexible, as the H-bonding network can buffer bond length variations from Mg->Cu.

3.3.2 Octahedral Chains Edge-Sharing With $^{3+4}$T-groups

This small group is based on unique edge-sharing by J-T distorted Cu-octahedra with complex oxy-anions. Chalconatronite (Figure 3.8) could be categorized with corner-sharing chains, and chlorothionite (Figure 3.9) with the edge-sharing chains. The connectivity of Group B, in Table 3.2, is therefore transitional between groups A and C.

Chalconatronite was originally described by Mosset et al.(1978) as having Cu in square pyramidal coordination, and this presented problems in classifying the structure. Hawthorne (1986b) described the Cu with a very distorted [6]-coordination, which conveniently places the structure into the octahedral chain category. Chains of Na-octahedra weakly bond the Cu-chains together.

Chlorothionite is an interesting structure. The Cu^{2+} environment has 2 long and 2 short Cu-Cl bonds, and two short Cu-O bonds (Giachovazzo et al. 1976), and the oxygen edge shares an edge with the sulfate tetrahedron. Figure 3.10 shows the edge-sharing tetrahedral-octahedral group, and as suggested by the geometry, there is cation-repulsion perpendicular to the shortened shared edge. The Cu-octahedra share edges to form chains, and K^+ ions bond together the chains.

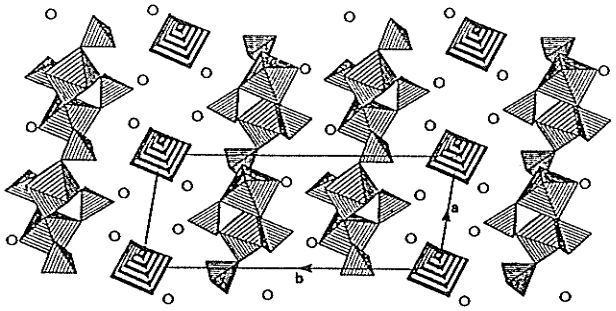

$Fe-SO_4$ polyhedral chains and isolated Mg octahedra H-bonded together. Cu can replace Mg, forming cuprocopiapite.

Figure 3.7: Copiapite Structure

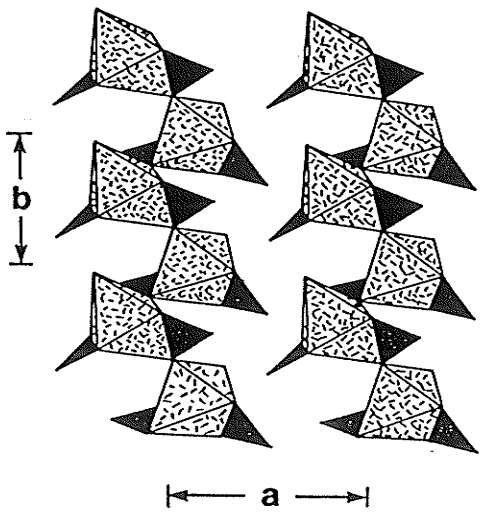

Figure 3.8: Chalconatronite Structure. Edge-sharing chains viewed down the c-axis; note the extreme octahedral distortion and shorter shared edges; from Hawthorne 1986b.

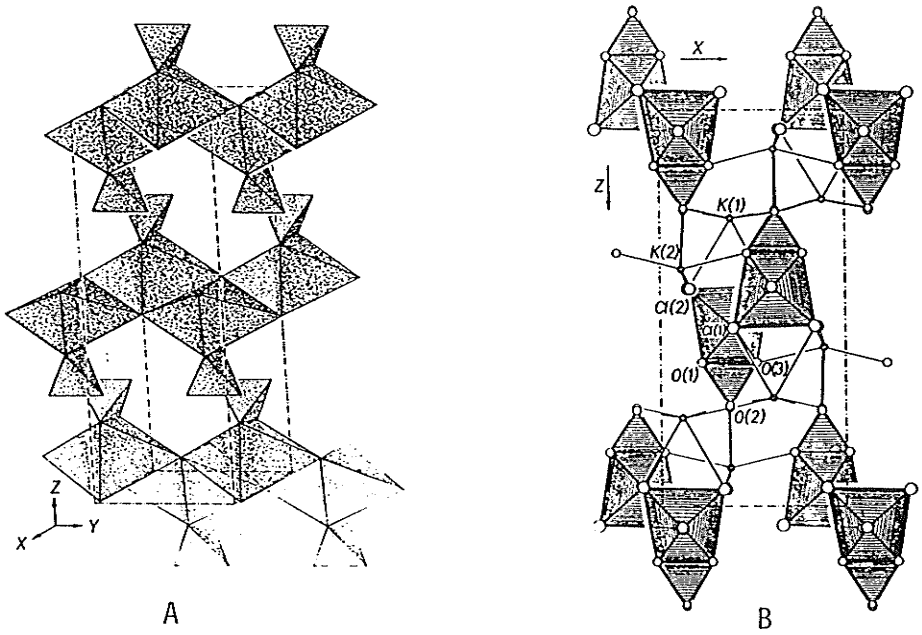

Figure 3.9: Chlorothionite Structure. (a) edge-sharing chains viewed obliquely down a-axis; (b) chains are viewed down the b-axis; K^+ cations weakly bond together the chains, from Giachovazzo et al. (1977)

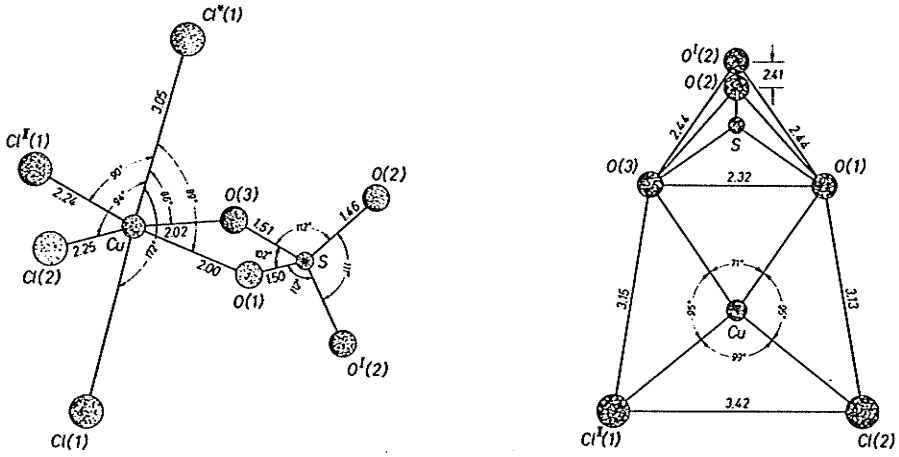

Figure 3.10: Geometry of Edge-sharing Tetrahedral-Octahedral Group diagrams from Giachovazzo et al. (1977)

3.3.3 Edge-Sharing Chains

CuO_6-chains Without Tetrahedra:

Eriochalcite, solved by Harker (1939), is a simple structure of $CuCl_4O_2$ chains, held together by hydrogen-bonding from the apical H_2O groups of the octahedra. Figure 3.11 shows the chains and H_2O groups. The octahedral connectivity is very similar to that of the chlorothionite chains (without tetrahedra, refer to Figure 1.8).

Chloroxiphite was determined by Finney et al. (1977) to consist of simple CuO_4Cl_2 chains in a complex network of Pb-polyhedra. Unlike eriochalcite, the shared edges are along four short equatorial oxygen-bonds, and two Cl form the long apical bonds. Finney et al. (1977) described the structure as sheets of PbO_7 and CuO_4 polyhedra parallel to $(\bar{1}01)$, but the complexity and irregular polymerization of these "sheets" makes this description inconvenient. The description of this structure, with simply Cu-octahedral chains (Figure 3.12), is in accordance with Hawthorne's (1985a) classification, and gives a better understanding of the structure.

CuO_6-chains Flanked by Corner-Sharing Tetrahedra:

This group of minerals is dominated by single edge-sharing chains of CuO_6 octahedra flanked by corner-sharing tetrahedra (all shown in Figure 3.13). The chains are all held together by Pb^{2+} ions of [8] to [10] coordination. The type of connectivity between the tetrahedra and octahedra, and the proportions of $Pb:Cu:TO_4$, determine the type of

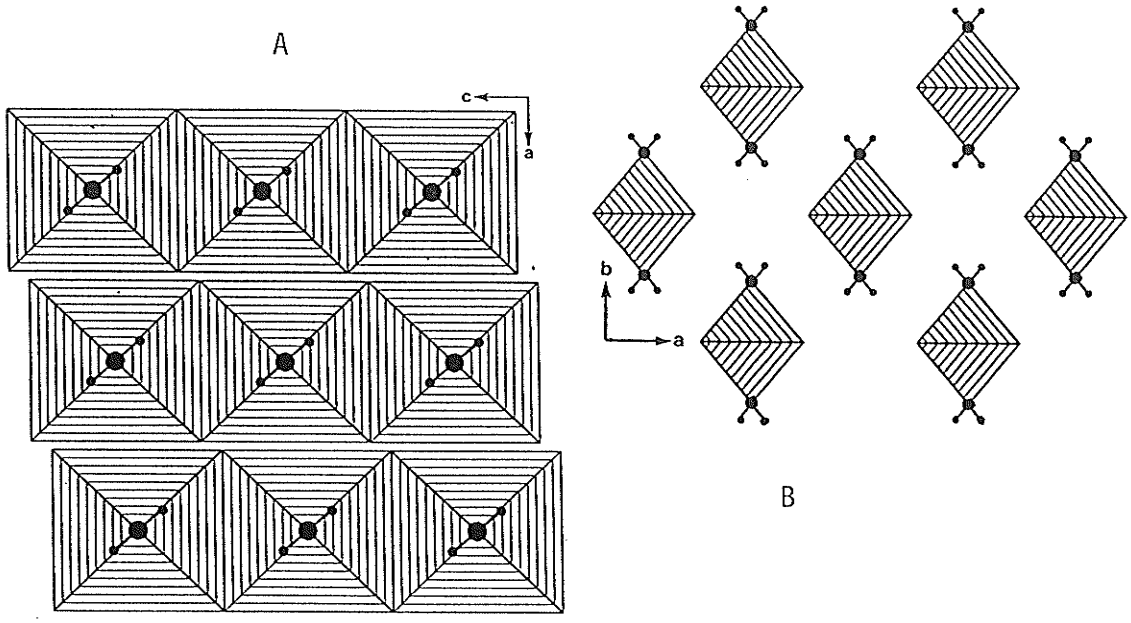

Figure 3.11: Eriochalcite Structure. (a) simple edge-sharing chains, down [010], and apical H_2O groups; (b) face-centred packing of the chains down [001], held together by H_2O.

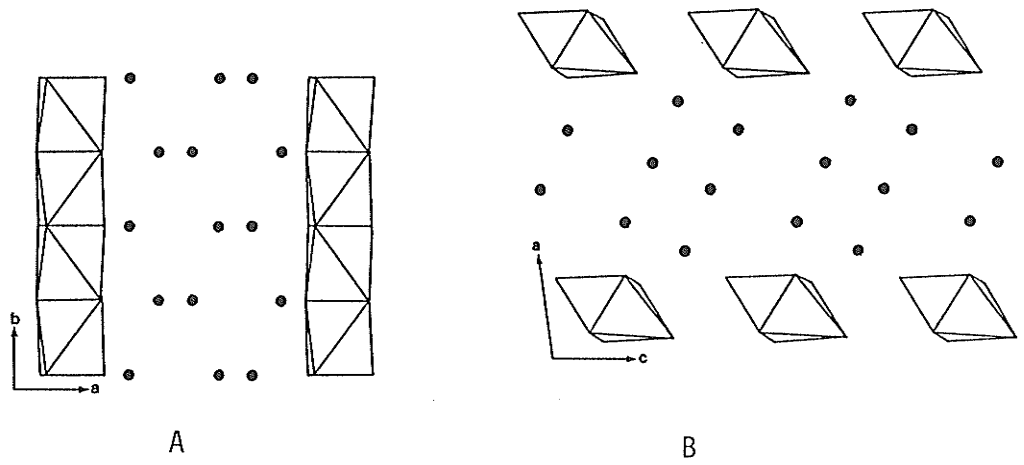

Figure 3.12: Chloroxiphite Structure. (a) simple edge-sharing octahedral chains and Pb atoms (circles), down [001]; (b) simple packing scheme, with interchain Pb atoms, down [010].

chains and the way they are arranged in the structures. Figure 3.13a shows the caledonite chain, with SO_4 tetrahedra corner-sharing to two apical bonds on the shared-edge of the (4+2) octahedra. The caledonite chain has the lowest connectivity, and the packing scheme of caledonite (Figure 3.13b) is the least dense of this group of structures.

Linarite and schmeiderite (Effenberger 1987) are nearly isostructural, and have their apical octahedral bonds non-edge-sharing, and bonded to TO_4 groups. The connectivity and structural rigidity of the edge-sharing chain is increased from that of caledonite, because now both the tetrahedral and octahedral groups share two corners (Figure 3.13c). Notice that the octahedra are canted along the chains to accomodate linkage of the smaller TO_3 and TO_4 groups. The packing of this chain type (Figure 3.13d,e) is different from caledonite. The chains are more loosely packed than in caledonite so that fewer Pb-atoms, relative to Cu, can be accomodated.

Fornacite and vauquelenite are isostructural (Fanfani and Zanazzi 1968) and have the most complex chains in this group. The chain type (Figure 3.13f) is a combination of the two previous chain types. The $T^{6+}O_4$ group shares a corner with the edge-sharing octahedra, as in caledonite (Figure 3.13a). The $T^{5+}O_4$ group shares two corners with the non-edge-sharing octahedral vertices, as in linarite. The bond-valence requirements of the CuO_6 oxygens are complex because of the mixed charges of the tetrahedral groups. The J-T distortion on the CuO_6 polyhedra is unusual: a (2+2+2) arrangement occurs, rather than the

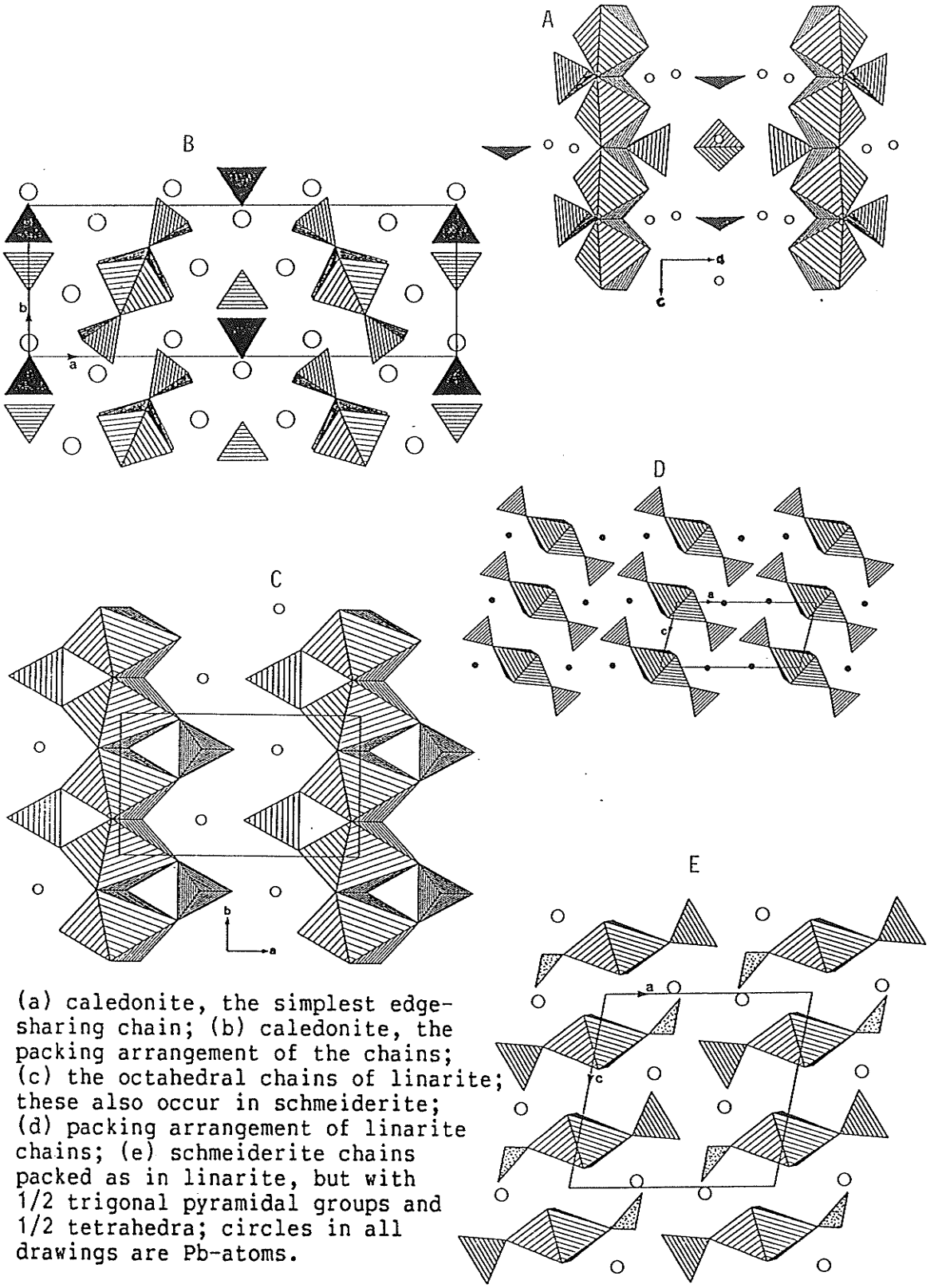

(a) caledonite, the simplest edge-sharing chain; (b) caledonite, the packing arrangement of the chains; (c) the octahedral chains of linarite; these also occur in schmeiderite; (d) packing arrangement of linarite chains; (e) schmeiderite chains packed as in linarite, but with 1/2 trigonal pyramidal groups and 1/2 tetrahedra; circles in all drawings are Pb-atoms.

Figure 3.13 - Edge-Sharing CuO_6 Chains with Tetrahedra.

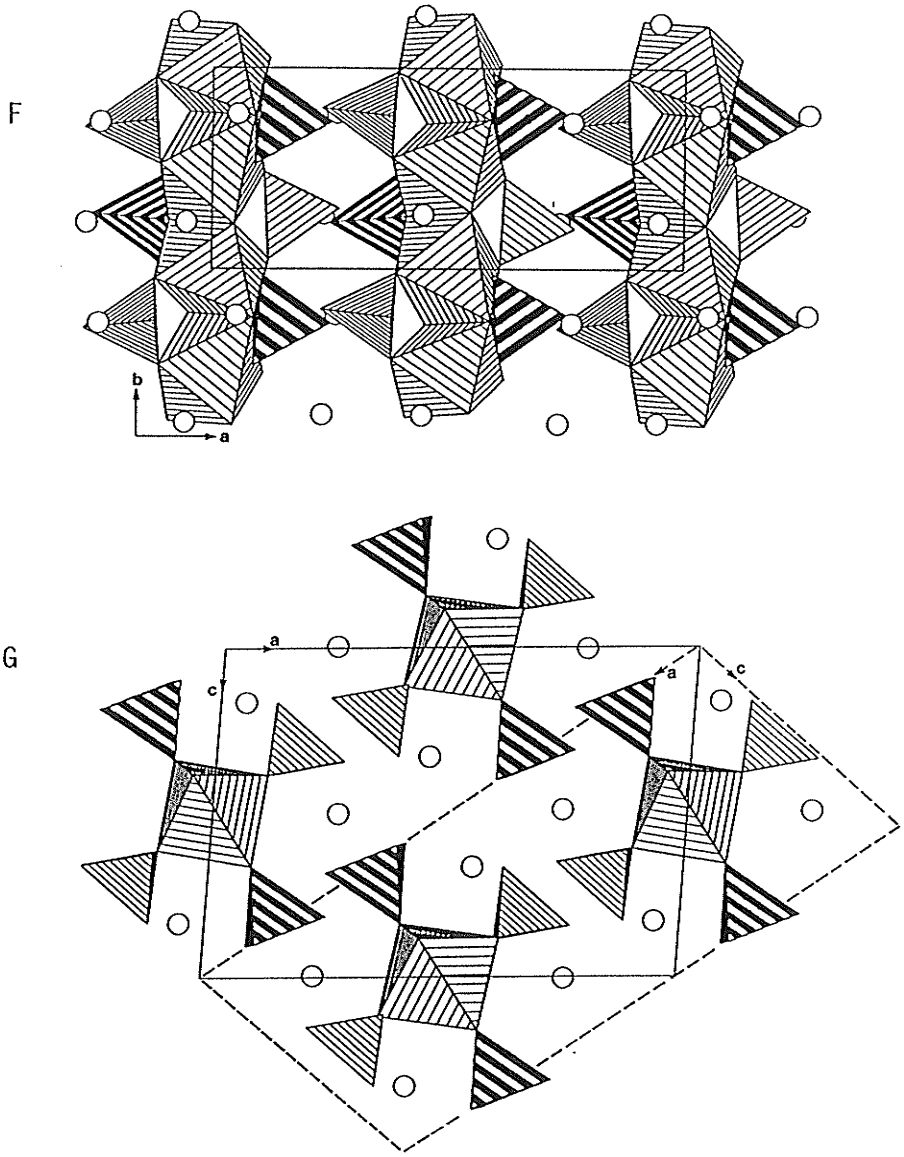

Figure 3.13: Edge-Sharing CuO_6 Chains with Tetrahedra. (continued) (f) complex corner-sharing arrangement of tetrahedra and edge-sharing octahedral chains, seen in vauquelenite and fornacite; (g) packing scheme of the complex tetrahedral-octahedral chains and Pb atoms; Cr tetrahedra are banded and open shaded tetrahedra are P; Unit cell of vauquelenite is the solid line, and cell of fornacite is dashed, Fanfani & Zanazzi (1968) and Cocco et al. (1966) respectively.

standard (4+2) distortion, and is probably a result of more complex bond-valence requirements. The packing of the octahedral chains is less dense than in linarite and greater than in caledonite as a result of the proportion of Pb:Cu (caledonite->5:2; fornacite/vauquelenite->2:1; linarite/schmeiderite->1:1). Figure 3.13g shows the arrangement of the chains.

3.4 INFINITE POLYHEDRAL SHEETS

The minerals of this category are listed in Table 3.4. These structures are built from two-dimensional polymerizations, weakly bonded together in the third dimension.

3.4.1 Edge-Sharing Cu-Octahedral Sheets

Fully Occupied Sheets:

This group of minerals is based upon edge-sharing sheets of copper octahedra made with the structural building block: $[M_4X_n\,\emptyset_{8-n}]$; with M=octahedrally coordinated cation; X=complex anion; $\emptyset$=simple anion (O^{-2},$(OH)^-$,H_2O), as outlined by Hawthorne (1985). The octahedral sites are fully occupied. The series is built up by addition of SO_4 tetrahedra corner-sharing to the sheets. Adjacent sheets are bonded together by weak hydrogen-bonds and interlayer cations. All octahedral sheets show the same corrugation pattern, illustrated in Figure 3.14. The corrugation results from the requirement of J-T distorted octahedra fitting into the ideal hexagonal close-packing layers of oxygen ions (HCP). This will be discussed further in Chapter 7.

TABLE 3.4

Infinite Polyhedral Sheets

A. Edge-sharing Cu-sheets With ($^{6}M_4X_n\emptyset_{8-n}$) Building Block:
(Cu-sheets in i-iii fully occupied)

i. n=0; no tetrahedra -

Botallackite	$Cu_2Cl(OH)_3$

ii. n=1; tetrahedra on one side of sheets -

Wroewolfeite	$Cu_4(SO_4)(OH)_6 \cdot 2H_2O$
Langite	$Cu_4(SO_4)(OH)_6 \cdot 2H_2O$
Posnjakite	$Cu_4(SO_4)(OH)_6 \cdot H_2O$
Spangolite	$Cu_6Al(SO_4)(OH)_{12}Cl \cdot 3H_2O$

iii. n=2; tetrahedra on both sides of sheets -

Gerhardite	$Cu_2(OH)_3NO_3$
Campigliaite	$Cu_4Mn(SO_4)_2(OH)_6 \cdot 4H_2O$
Ktenasite	$(Cu,Zn)_5(SO_4)_2(OH)_6 \cdot 6H_2O$
Devillite	$CaCu_4(SO_4)_2(OH)_6 \cdot 3H_2O$
Serpierite	$Ca(Cu,Zn)_4(SO_4)_2(OH)_6 \cdot 3H_2O$

iv. n=2; sheets are partially occupied -

Bayldonite	$PbCu_3(AsO_4)_2(OH)_2 \cdot H_2O$
Chalcophyllite	$Cu_{18}Al_2(AsO_4)_3(SO_4)_3(OH)_{27} \cdot 33H_2O$

B. Mixed Polyhedral Sheets:

i. tetrahedral-octahedral corner-sharing sheets -

Cuprorivaite	$CaCuSi_4O_{10}$
Osarizawaite	$PbCuAl_2(SO_4)_2(OH)_6$
Guildite	$CuFe^{+3}(SO_4)_2(OH) \cdot 4H_2O$
Ransomite	$CuFe_2^{+3}(SO_4)_4 \cdot 6H_2O$
Metatorbernite	$Cu(UO_2)_2(PO_4)_2 \cdot 8H_2O$

ii. Edge-sharing polyhedral sheets -

Sengierite	$Cu_2(UO_2)_2V_2O_8 \cdot 6H_2O$
Cuprosklodowskite	$Cu(UO_2)_2Si_2O_6(OH)_2 \cdot 6H_2O$
Roubaultite	$Cu_2(UO_2)_3(CO_3)(OH)_{10} \cdot 5H_2O$
Turquoise	$CuAl_6(PO_4)_4(OH)_8 \cdot 5H_2O$
Stringhamite	$CaCuSiO_4 \cdot 2H_2O$
Likasite	$Cu_3(OH)_5NO_3 \cdot 2H_2O$

Botallackite, an oxychloride, is the only structure of the series without tetrahedral "appendages" to the sheets (n=0). Stacking of the simple octahedral sheets is illustrated in Figure 3.15. The chlorine ions form 3 of the 4 apical bonds to the Cu(1) and Cu(2) sites (Hawthorne, 1985c), and are acceptors of hydrogen-bonding from adjacent sheets, holding the sheets together.

Wroewolfeite, langite, and posnajakite all have SO_4 tetrahedra on one side of their octahedral sheets (n=1). Figure 3.16a-c shows the subtle structural differences of their sheet stacking arrangements. Langite and wroewolfeite are true polymorphs. Posnajakite has no interlayer H_2O, but is otherwise polymorphic with langite and posnajakite. All of their octahedral sheets have 4 crystallographically distinct Cu-octahedra, with only 3 sites corner-linked to SO_4 tetrahedra.

Spangolite is a more complex derivative of the $M_4X\emptyset_7$ structure. It is is hexagonal, owing to the arrangement of $Al\emptyset_6$ and chlorine positions in the sheets, Figure 3.17a. Three Cu(1) octahedra link to the SO_4 tetrahedra, but the $Al\emptyset_6$ do not. Cu(2) has an octahedral coordination with five $\emptyset$-groups and one chlorine atom. Figure 3.17b shows that with mixed polyhedral types in the sheet, a corrugation is still present.

Gerhardite is the only non-sulphate which falls into the $[M_4X_2\emptyset_6]$ building block series. It is the simplest structure of the n=2 group. Nitrate planar triangles flank both sides of the octahedral sheets. The sheets are cross-linked by hydrogen-bonds from the octahedra to the NO_3 corners, Figure 3.18. A synthetic polymorph has topologically identical sheets, but which pack differently to change the symmetry (Effenberger, 1983).

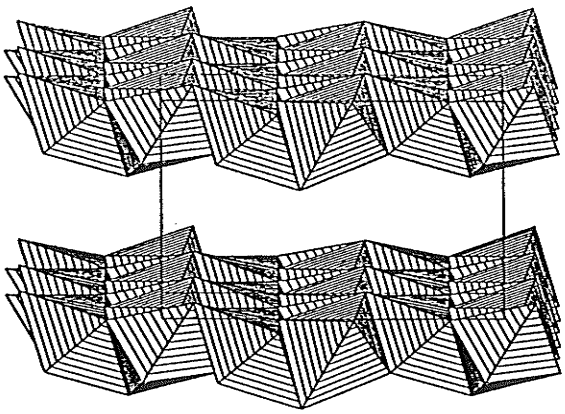

Figure 3.14: Corrugated Cu-Octahedral Sheet
Corrugated octahedral sheets as a result of Jahn-Teller distortions around copper imposing themselves upon HCP layers of anions

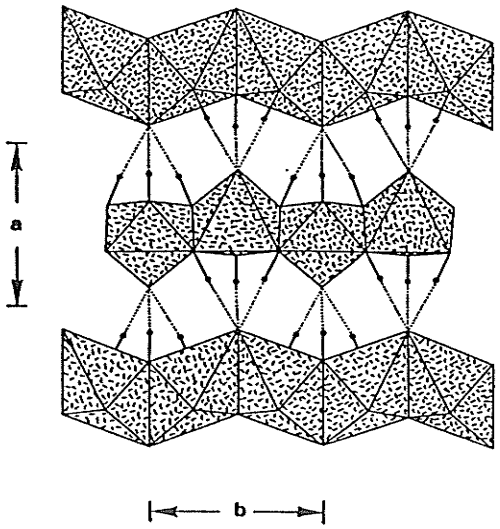

Figure 3.15: The Botallackite Structure. Simple packing of the oxychloride-copper sheets, and hydrogen bonding to chloride ions holding the sheets together (dashed lines); from Hawthorne, 1985c.

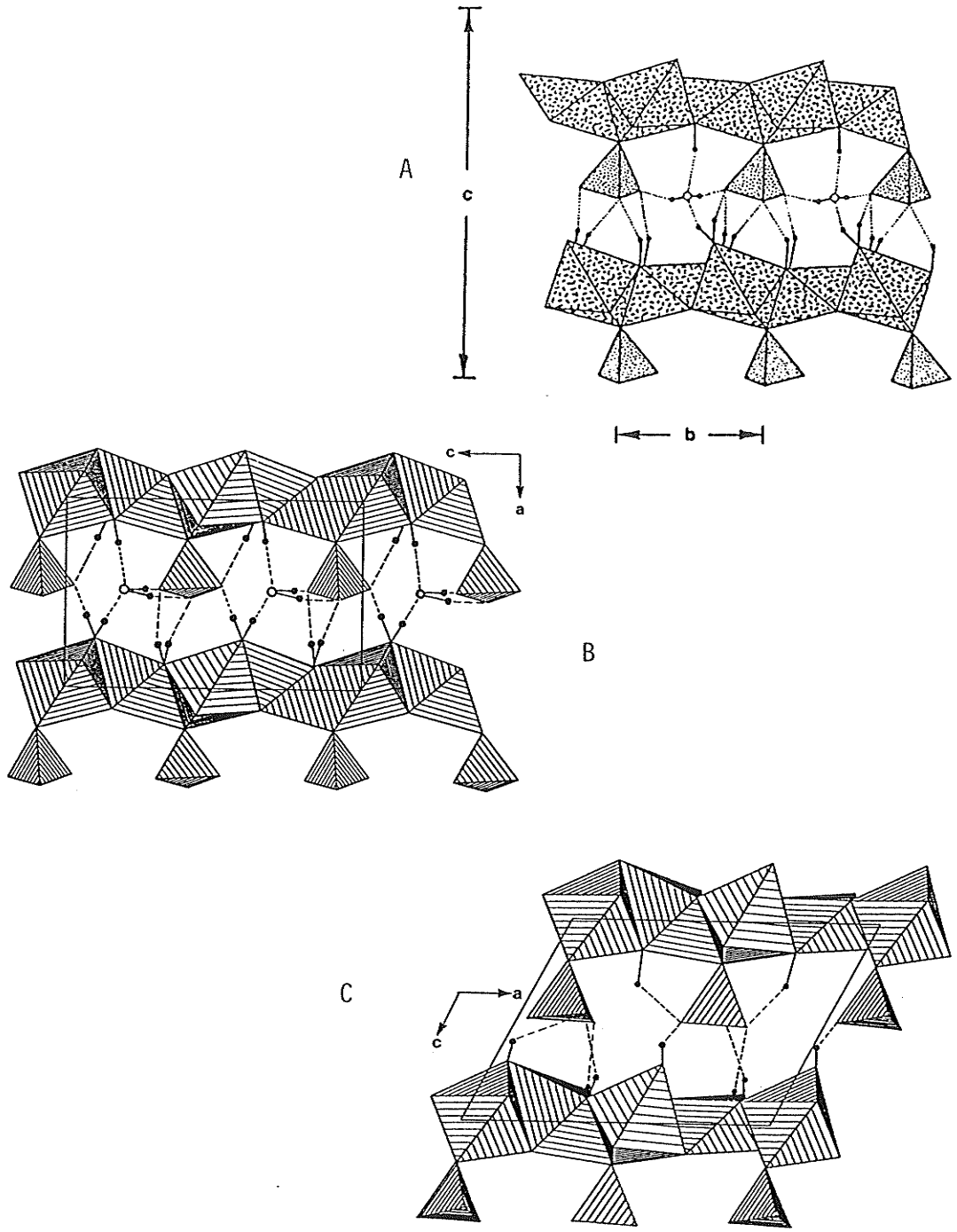

Figure 3.16: Octahedral Sheets of $M_4X\emptyset_7$ structures. The stacking of $Cu_4SO_4(OH)_6 \cdot nH_2O$ polymorphs: (a) wroewolfeite, from Hawthorne & Groat 1985; (b)langite; (c) posnajakite. Hydrogen-bonding schemes proposed by the authors are included (by dashed lines).

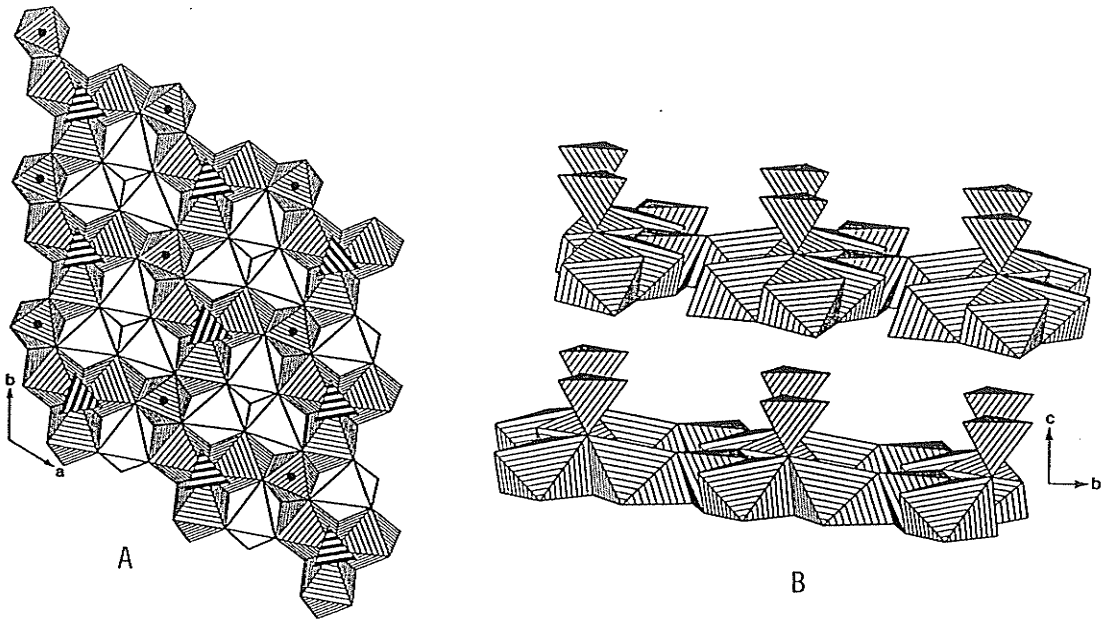

Figure 3.17: The Spangolite Structure. (a) viewed down the sheet, the AlO_6 octahedra (with small circles) and $Cu\emptyset_5Cl$-octahedra (unshaded) control the symmetry of tetrahedral linkage to the sheet; (b) corrugation of CuO_6 octahedra in sheets.

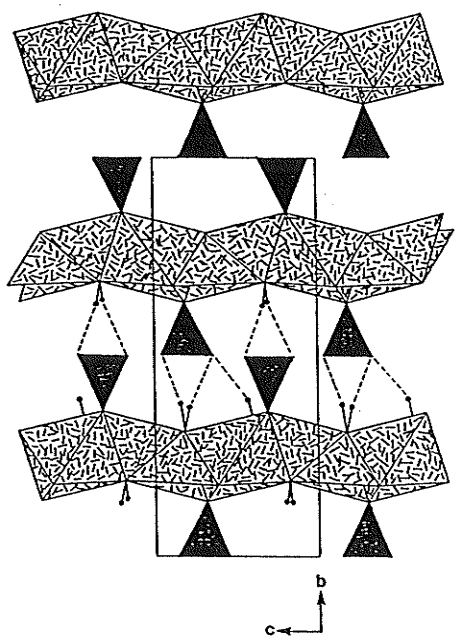

Figure 3.18: The Gerhardite Structure. NO_3 triangles flank corrugated octahedral sheets on both sides. H-bonds from hydroxyl anions bond to NO_3 groups of adjacent sheets.

Serpierite, devillite, campigliaite and ktenasite are subtle structural variations with the $[Cu_4SO_4{}_2\emptyset_6]$ building block. Sulphate tetrahedra corner-link to both sides of the octahedral sheets. These structures are more loosely packed than gerhardite or the n=1 group, because H_2O groups and interlayer cations are present between the octahedral sheets. Structural differences between these copper sulphates are compositionally dependent. Devillite and serpierite are evidently a limited solid solution series. In serpierite, Zn substitutes at the Cu(1) and Cu(4) sites which do not link to SO_4. This is evident by the bond lengths around these sites, which deviate significantly from characteristic J-T distortions (Sabelli & Zannazzi, 1968). The substitution of Zn changes the geometry of the octahedral sheet relative to devillite (nearly pure Cu). The two topologically identical sheets must therefore pack differently (Figures 3.19a,b). Calcium ions cross-link the sheets by bonding to oxygens of the SO_4 tetrahedra of adjacent sheets.

Campigliaite is a more loosely packed structure than devillite and serpierite. There are more H_2O groups between the sheets. The Mn polyhedra corner-link to SO_4 groups of only one sheet, and H-bond to (SO_4) tetrahedra of the other (Figure 3.19c). More H_2O groups and lower interlayer connectivity results in a wider separation of the sheets, relative to Figures 3.19 a,b.

Ktenasite is the most loosely packed of the n=2 copper sulphates. Isolated $Zn(H_2O)_6$ octahedra are packed in between the sheets, and H-bond

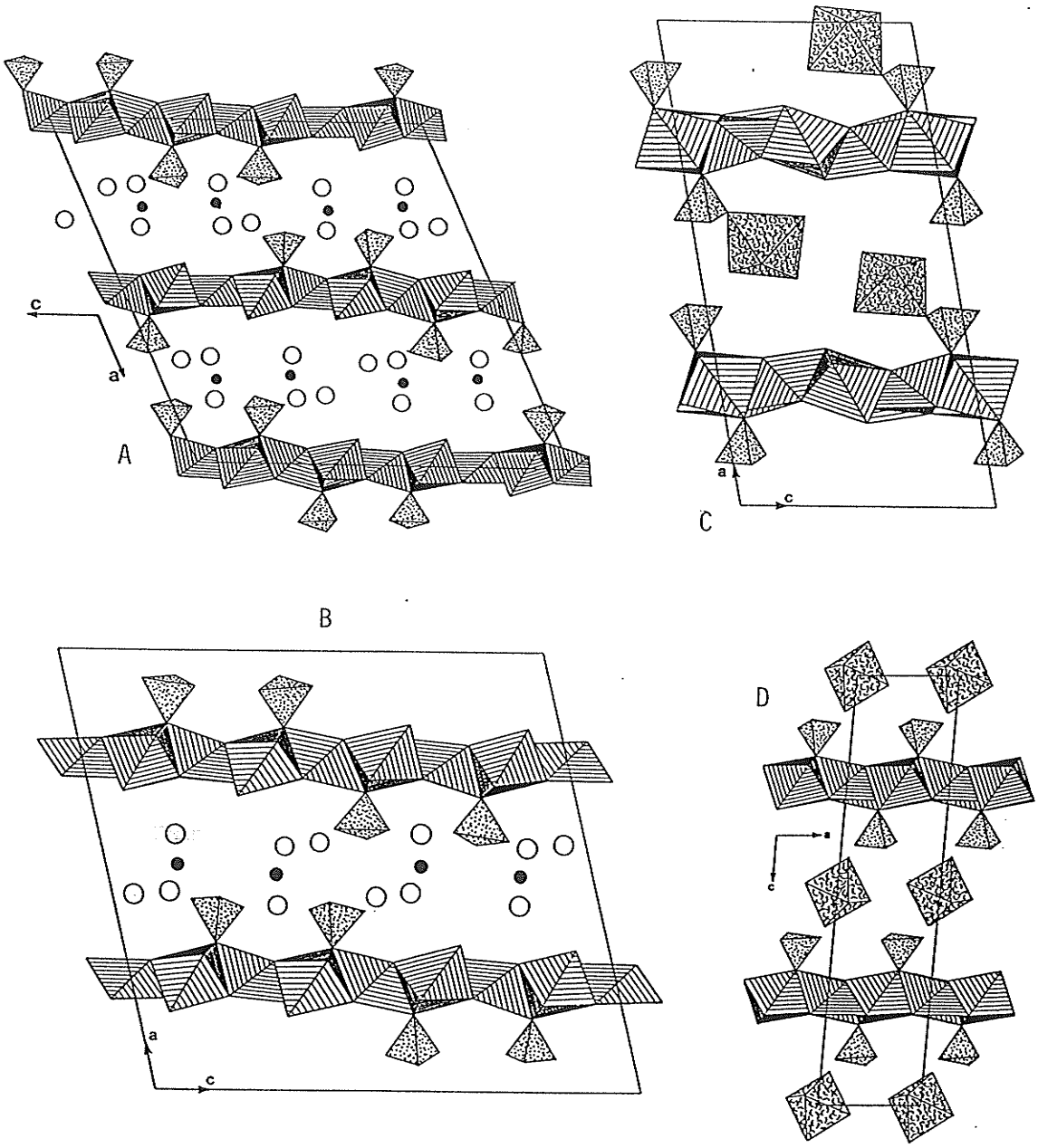

Figure 3.19: Copper-Sulphate Sheets of n=2 Group. The arrangements of copper-sulphate sheets with respect to stacking styles and tetrahedra positioning on the sheets. (a) serpierite; (b) devillite; both have identical sheets, but are packed differently, with Ca interlayer cations (solid circles) and H_2O groups (open circles) between the sheets. (c) campigliaite, a wider sheet separation because of lower connectivity of Mn interlayer cations (curled dashes); (d) ktenasite, loosely packed sheets with isolated interlayer Zn-octahedra.

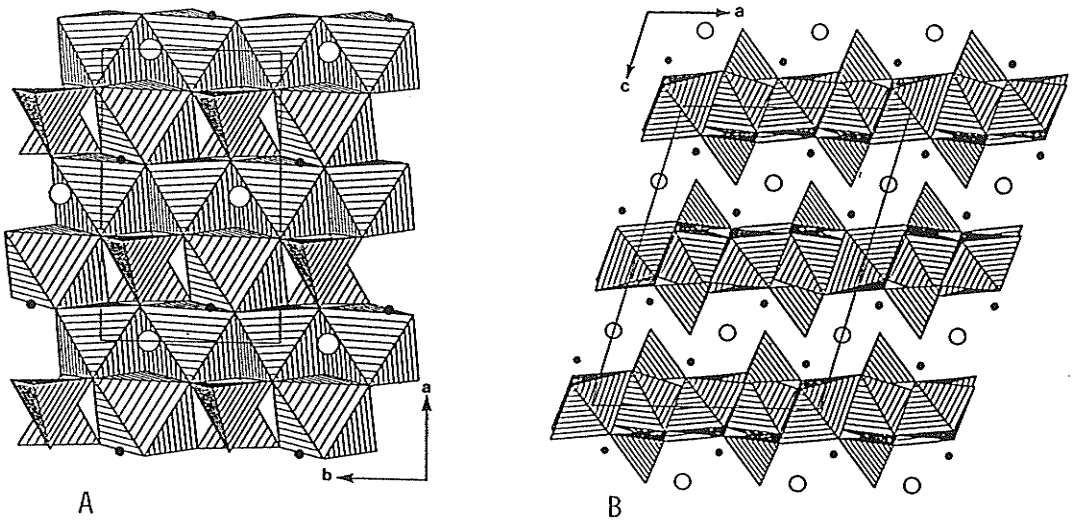

Figure 3.20: The Bayldonite Structure. (a) 3/4 occupancy of Cu-octahedral sites; (b) looking obliquely down the sheets, layer corrugation is evident, large circles - Pb^{2+}, small - H^{+}

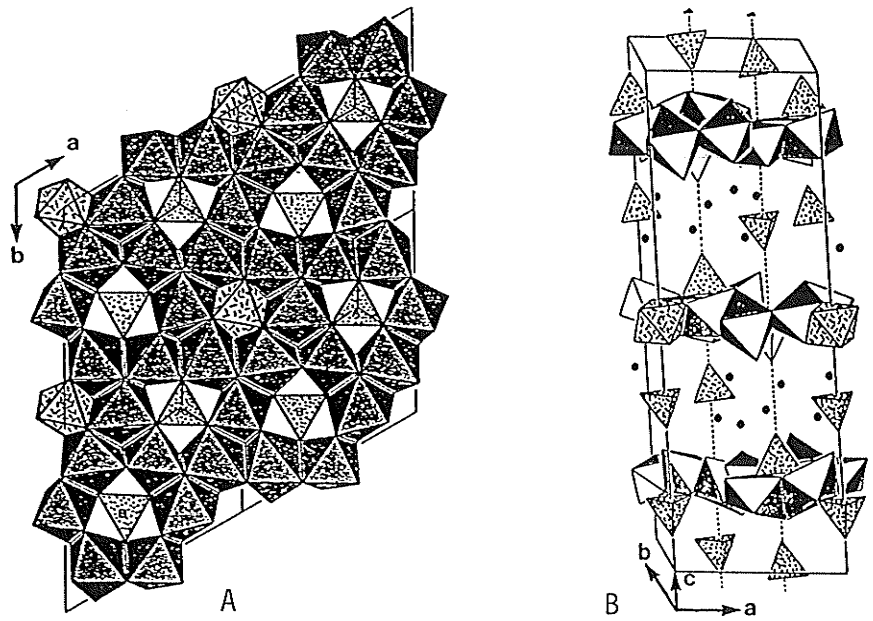

Figure 3.21: Structure of Chalcophyllite. (a) Cu-Al octahedral sheet, 9/12 Cu occupancy, 1/12 Al occupancy at the cell origins, AsO_4 linked on top of sheets in A sites, and on the bottom in B sites; (b) cross section of sheets, with SO_4 tetrahedra suspended in an H-bonding network between the corrugated complex octahedral sheets.

the sheets together. The separation of the sheets is the largest in the n=2 series, Figure 3.19d. Partial Zn substitution for Cu is suggested by Mellini & Merlino (1978), because of bond lengths differing from the usual J-T distortion arrangement.

The arrangement of tetrahedral linkage to the octahedral sheets is different for devillite & serpierite, ktenasite and campigliaite. This is presumably a result of stacking requirements of the sheets, which is in turn controlled by the arrangement of the interlayer cations and H_2O groups. Bond-valence requirements are a controlling factor in the arrangement of interlayer cations, H_2O groups and linking tetrahedra. Variation in the amount of H_2O between the sheets also affects the tetrahedral arrangement and stacking style.

Bayldonite is related to the $[M_4X_2\phi_6]$ building block, see Figure 3.20a. It has octahedral sheets with 3/4 cation occupancy, making $M_4 \rightarrow M_3$ and $\phi_6 \rightarrow \phi_4$. The tetrahedral position is occupied by AsO_4 rather than SO_4. In Figure 3.20b, one can see that Pb^{2+} ions are positioned between the octahedral sheets in the same way as Ca in devillite (both Ca and Pb are in [8] coordination). H_2O groups also link the sheets by hydrogen-bonding.

Chalcophyllite is a complex octahedral sheet structure, further removed from the n=2 structures than bayldonite. The octahedral sites are 9/12 occupied by Cu, and 1/12 by Al (at the cell origin; Figure 3.21a). AsO_4 tetrahedra link to both sides of the sheets by sharing 3 corners face down over the cation vacancies (A sites on the top, B sites

on the bottom). Figure 3.21b shows loose packing of the sheets, with (SO_4) tetrahedra resting in an H-bonding network of H_2O groups between the sheets. Corrugation is present in this highly diversified type of octahedral-tetrahedral sheet.

3.4.2 Mixed Polyhedral Sheets

This category of two dimensional polymerizations is more structurally and chemically diverse. Polyhedra of various coordinations are incorporated into the sheets, with a variety of polymerization styles.

Corner Sharing Sheets:

Egyptian blue, synthesized by Pabst (1959), is synonymous with natural cuprorivaite. It has an elegant structure made from groups of four corner-linked silicate tetrahedra, further corner-linked to each other into a double tiered sheet, and yet further linked to CuO_4 square-planar groups (Figure 3.22). The bonding within such a sheet is quite strong. Calcium is the interlayer cation which bonds the sheets together. Gillespite, $BaFeSi_4O_{10}$, is isostructural with cuprorivaite, and has Fe in square planar coordination. Copper is much more stable in this coordination than Fe, because the driving force for deviation from holosymmetric octahedral coordination is stronger in Cu^{2+} than in Fe^{2+}. Consequently, cuprorivaite is more stable than gillespite (Pabst, 1959).

Osarizawaite is a structural member of the alunite group, and is illustrated in Figure 3.23a,b. Corner-sharing trimers of octahedra corner share into sheets, and are further linked to triple corner-sharing SO_4 tetrahedra. The octahedral bond lengths listed by

Guisepetti & Tadini (1980) do not differentiate between the Cu and $(Al,Fe)^{3+}$ cations. Therefore the copper is either disordered throughout the octahedral sites, making local distortions in the crystal structure (with J-T distortions), or the symmetry of this structure is actually lower with ordering of Cu.

Guildite and ransomite are two fundamentally related structures with similar compositions, and occur together as products of a mine fire in Jerome, Arizona (Lausen, 1929). The main components of their structures are corner-sharing Fe^{3+}-octahedral and SO_4-tetrahedral chains, with building blocks: $M(TO_4)_2O_2$ and $M_2(TO_4)_4O_3$ for guildite and ransomite respectively (Figures 3.24a,b). The chains are cross-linked by corner-sharing of Cu-octahedra and SO_4-tetrahedra, forming layers. The style of linkage by Cu differs in the two sheet types, and is illustrated in Figures 3.24c,d. As in cuprorivaite, the Cu-octahedra play a supportive role in the mixed polyhedral sheets, crosslinking the more dominant structural subunits.

The last of the corner-sharing sheets is the first of the uranyl-layer series of minerals. Metatorbernite consists of corner-sharing PO_4-tetrahedra and UO_6 octahedra, forming the tightly bonded polyhedral layers seen in Figure 3.25a. The long and weak apical bonds of copper octahedra corner-link the uranyl-phosphate layers together, playing the role of a weakly bonding interlayer cation. It is for this reason that the Cu-uranyl layer minerals are not considered as framework structures.

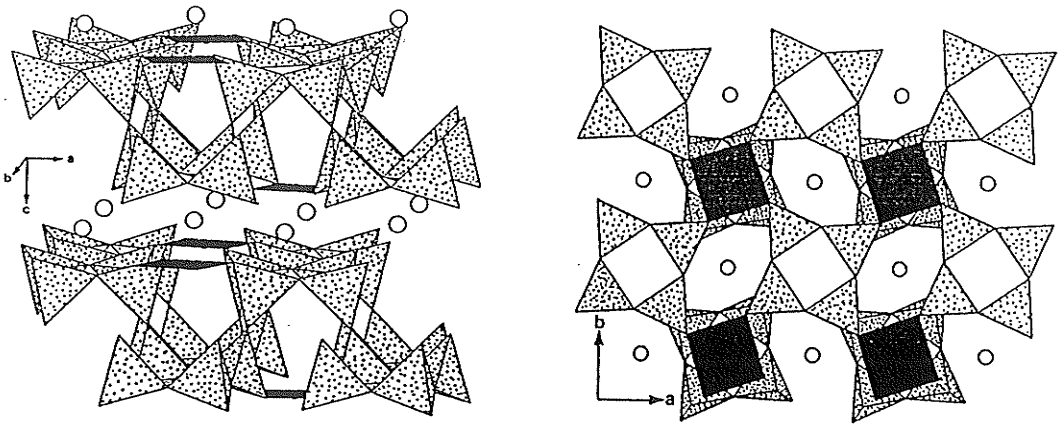

A B

Figure 3.22: Structure of Cuprorivaite. (a) double tiered silicate sheets, with added structural rigidity from the CuO_4 square planes; Ca is the interlayer cation. (b) corner-sharing between 4 tetrahedra and CuO_4 square planes.

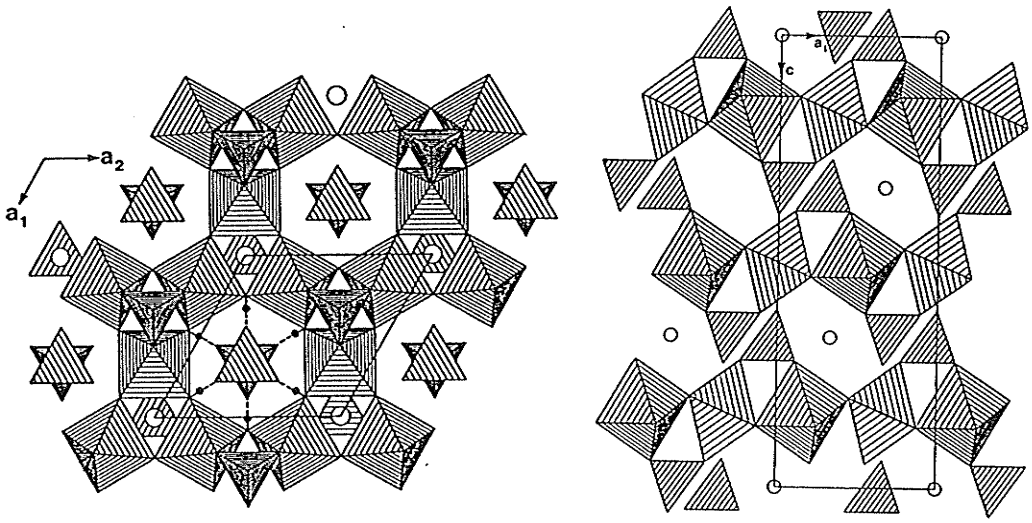

A B

Figure 3.23: Structure of Osarizawaite. (a) viewed down the sheets, corner-sharing polyhedra; (b) a cross sectional view of the complex sheets; (large circles - Pb, small - H+).

Edge-Sharing Sheets:

The structures of sengierite and cuprosklodowskite are fundamentally similar. Edge-sharing is the type of connectivity within their uranyl-layer sheets, and Cu-octahedra play the role of interlayer cations corner-linking the sheets together. Figure 3.25b shows the uranyl-silicate layer of cuprosklodowskite with predominant edge-sharing. Figure 3.25c shows how Cu-octahedral dimers corner-share their apical ligands with VO_5 polyhedra in the schematically drawn uranyl-vanadate layers of sengierite. Sengierite belongs to the carnotite group of minerals. In other carnotite-group structures, Cu-dimers are replaced by larger interlayer cations (Ca and Ba). Cuprosklodowskite is related to the sklodowskite group, and Cu is replaced by similar sized M^{2+} cations in the other structures of this group. Clearly, copper is playing a supportive role in these structures, and can be substituted by other cations which do not show the J-T effect. This structural role is apparently quite flexible with respect to bond lengths.

Roubaultite is somewhat different than the other uranyl-layer structures because Cu-octahedra are part of the layers. In Figure 3.25d, we see rutile-type chains corner-linked to UO_6 and UO_8 polyhedral double-chains with edge-sharing carbonate groups. These complex layers are linked together by H-bonds from Cu-octahedra to U-polyhedra from adjacent sheets (above and below).

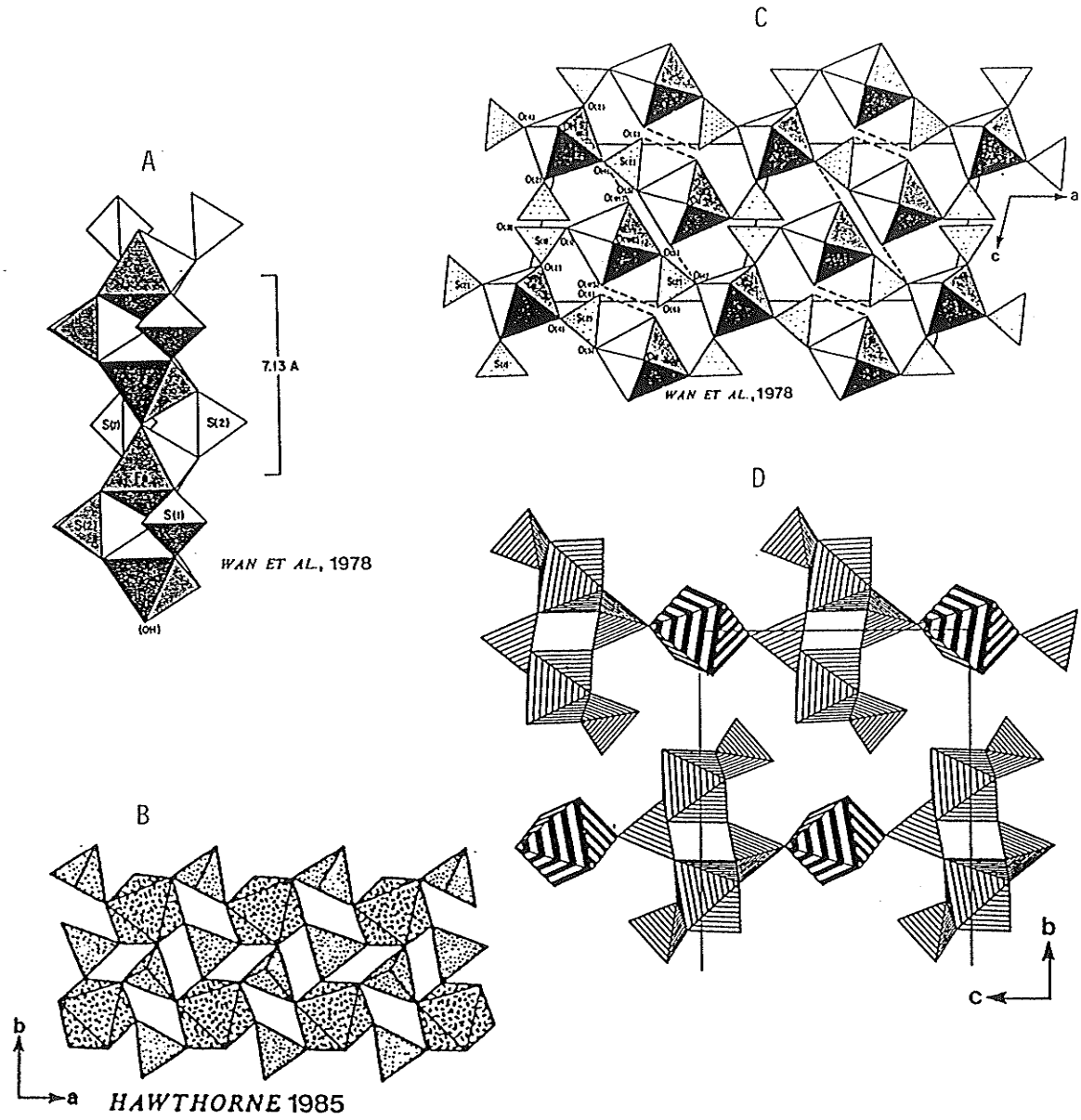

Figure 3.24: Structures of Guildite and Ransomite. (a) Fe-octahedral-SO_4-tetrahedral chain of guildite; (b) Fe-octahedralSO_4-tetrahedral chain of ransomite; (c) copper octahedra crosslink the Fe-sulphate chains into sheets along [010], in guildite; (d) the linkage of Fe-sulphate chains into sheets along [010], is different in ransomite.

Turquoise is another complicated structure. Close-packed oxygen layers are parallel to (001), Figure 3.26a. Cu-octahedra with PO_4 tetrahedra, and Al-octahedra are found in alternating close-packed layers. Edge-sharing Al-Cu-Al octahedral trimers are cross-linked into a complex sheet by corner-sharing with Al-octahedra and PO_4 tetrahedra (Figure 3.26). Fe substituting for Al forms a solid solution series to chalcosiderite, Dresdner (1964). Replacement of Cu by Zn gives faustite, but there is not a solid solution series between these minerals.

Stringhamite is a very complex structure. Figure 3.27a shows open sheets of edge-sharing very distorted Cu-octahedra and SiO_4 tetrahedra, cross-linked by square planar CuO_4. These sheets are linked across by CaO_7 polyhedra, illustrated in Figure 3.27b. The validity of considering Cu(2) as a very distorted octahedron was suggested by Hawthorne (1985d) from bond-valence analysis. Neither an octahedral or square-planar coordination for Cu(2) simplifies the structure of stringhamite.

Likasite, illustrated in Figures 3.28a,b, is an elegant structure consisting of interlocking Cu-octahedral chains forming a triple-layered sheet, flanked by corner-sharing NO_3 planar triangles. These intricately connected sheets are bonded together by the H-bonds of hydroxyls in octahedra to NO_3 triangles of adjacent sheets.

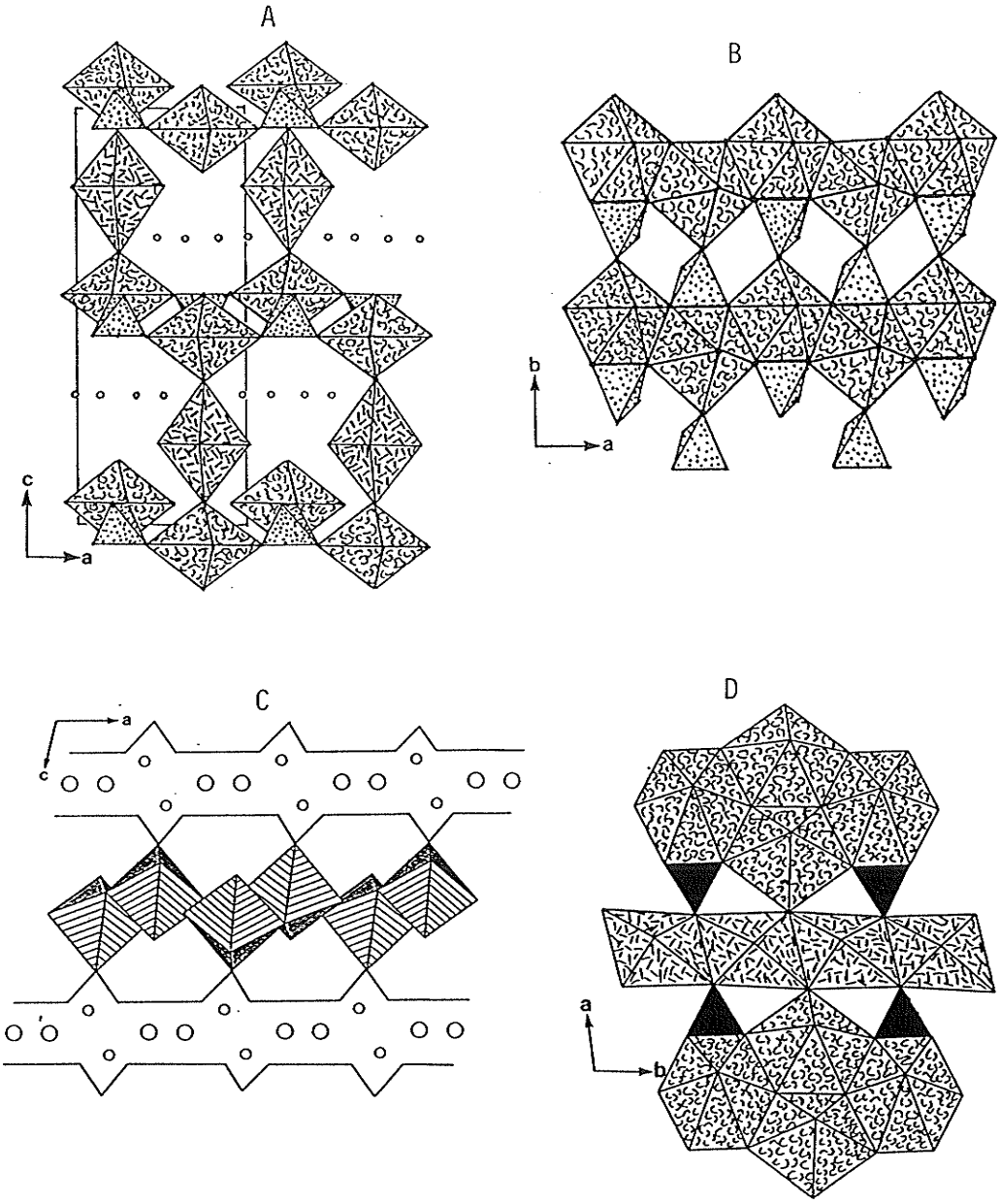

Figure 3.25: Uranyl-layer Structures (a) Metatorbernite, mixed uranyl-phosphate layers (curl-dashed & dotted) bonded together by Cu-octahedra (straight-dashed) and H_2O groups (circles); (b) edge-sharing uranium polyhedra (dashed) and silicate tetrahedra forming a tightly bonded sheet in cuprosklodowskite. (c) schematic uranyl-vanadate layers, corner-linked together by edgesharing dimers of Cu-octahedra in sengierite. (d) edge-sharing Cu-octahedral chains (straight-dashed), corner-linked to edge-sharing uranyl-carbonate chains, in sheets of roubaultite; U-polyhedra curled dashes

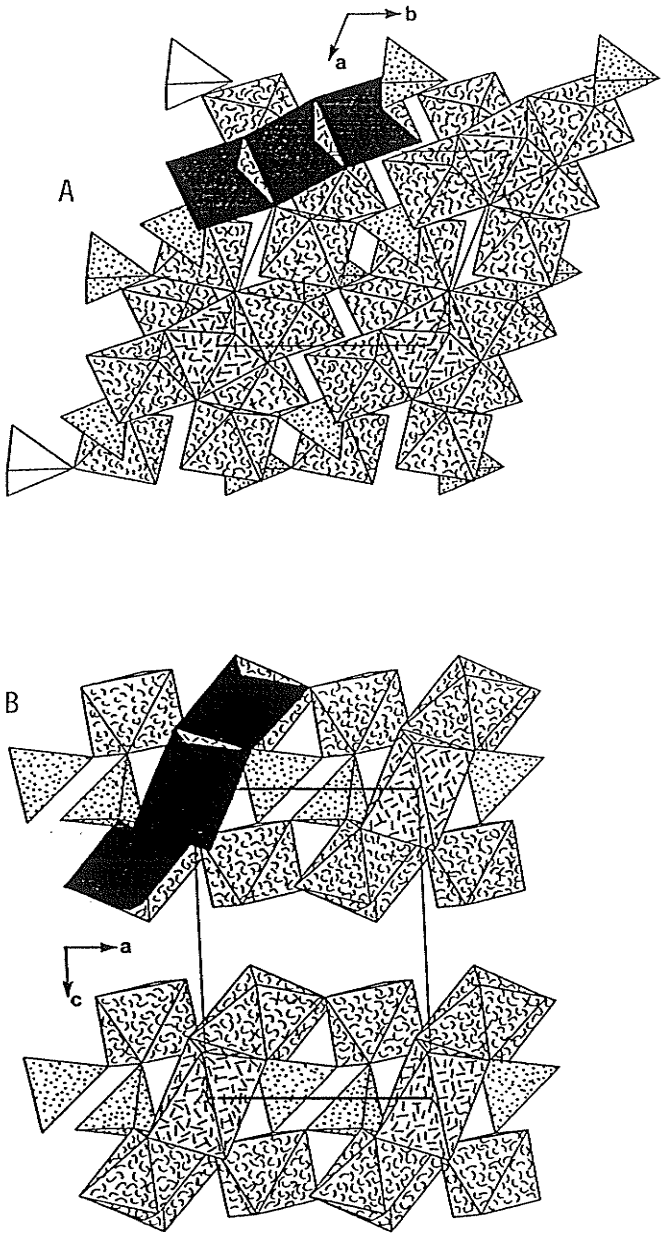

Figure 3.26: Structure of Turquoise. (a) AlO_6 and CuO_6/PO_4 polyhedral layers in a CCP array; notice the Al-Cu-Al trimers; (b) trimers are linked into a complex sheet by PO_4 and AlO_6; straight-dashed octahedra are Cu, curled dashes are Al; a single trimer is shaded for clarity.

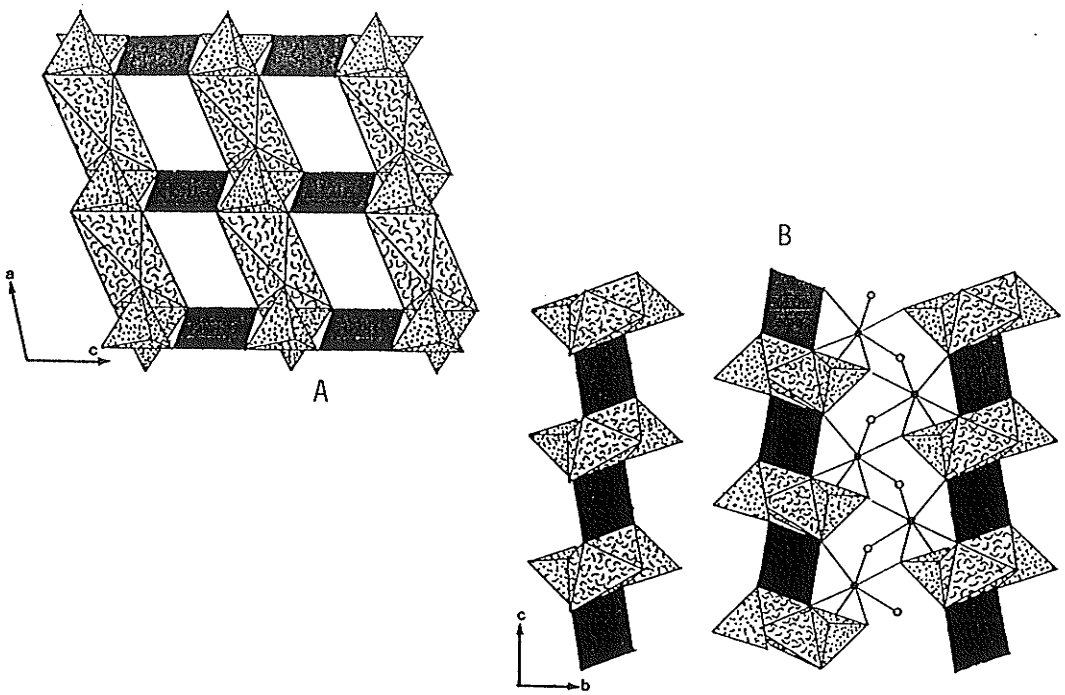

Figure 3.27: Structure of Stringhamite. (a) edge-sharing Cu(2) octahedra and SiO_4 tetrahedra, and corner-sharing square planar CuO_4, forming a complex sheet; (b) Complex sheets are linked by Ca interlayer cations.

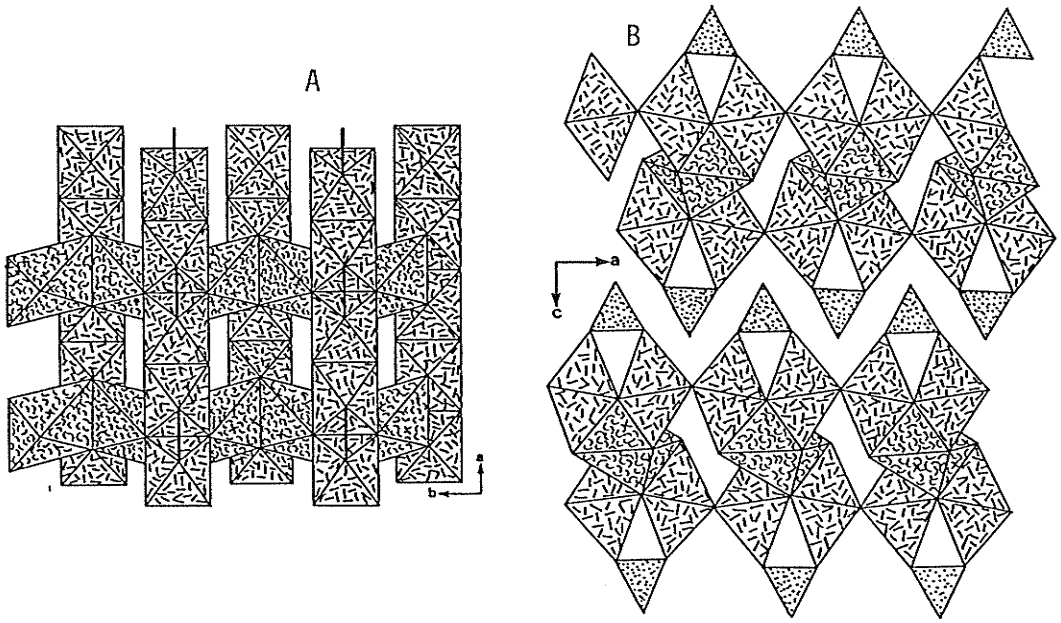

Figure 3.28: Structure of Likasite. (a) looking onto the interconnected octahedral chains, NO_3 triangles are viewed on edge; (b) triple-layered sheets are cross-linked only by H-bonds to NO_3 triangles.

3.5 STRUCTURES OF POLYHEDRAL FRAMEWORKS

This structure type consists of three-dimensional polymerizations, and can be classified into three categories, based on structural units (within the frameworks) which are recognizably homogenous in their style of connectivity. Table 3.5 lists these categories, which essentially

TABLE 3.5

Polyhedral Framework Categories

A. Frameworks of Chains

B. Frameworks of Sheets

C. Complex Octahedral Frameworks

reflect the degree of anisodesmicity in the bonding networks.

3.5.1 Category A: Frameworks of Chains

These framework structures have one-dimensional polymerized subunits as their main structural components. They are listed in Table 3.6. Many of the chain subunits are related to each other, and some are identical to the chains found in minerals of the infinite chain structures (Part 3.3).

TABLE 3.6

Category A: Polyhedral Frameworks of Chains

i. corner-sharing octahedra and ^{3+4}T –

Bonattite	$CuSO_4 \cdot 3H_2O$
Liroconite	$Cu_2Al(AsO_4)(OH)_4 \cdot 4H_2O$
Chalcomenite	$CuSeO_3 \cdot 2H_2O$
Teineite	$CuTeO_3 \cdot 2H_2O$
Poitevinite	$(Cu,Fe^{+2},Zn)SO_4 \cdot H_2O$
Bandylite	$CuB(OH)_4Cl$

ii. edge-sharing ^5M linked to polymerized TO_4 –

Litidionite	$KNaCuSi_4O_{10}$
Ziesite	$\beta Cu_2V_2O_7$
Blossite	$\alpha Cu_2V_2O_7$
Kinoite	$Ca_2Cu_2Si_3O_8(OH)_4$

iii. edge-sharing ^{5+6}M linked to single ^{3+4}T –

Callaghanite	$Cu_2Mg_2(CO_3)(OH)_6 \cdot 2H_2O$
Stranskiite	$Zn_2Cu(AsO_4)_2$
Stoiberite	$Cu_5V_2^{+5}O_{10}$

iv. edge-sharing ^6M chains linked to ^{3+4}T –

a. wallpaper family

Mixite Group	$ACu_6(XO_4)_3(OH)_6 \cdot 3H_2O$
Mixite,	A=Bi; X=As
Agardite,	A=Y,REE,Ca; X=As
Goudeyite,	A=Y,Al; X=As
Petersite,	A=Y,REE; X=P
Euchroite	$Cu_2(AsO_4)(OH) \cdot 3H_2O$
Olivenite	$Cu_2AsO_4(OH)$
Libethenite	$Cu_2(PO_4)(OH)$
Conichalcite	$CaCu(AsO_4)(OH)$
Papagoite	$CaCuAlSi_2O_6(OH)_3$
Malachite	$Cu_2(CO_3)(OH)_2$
Antlerite	$Cu_3(SO_4)(OH)_4$

b. non-wallpaper minerals

Mammothite	$Pb_6Cu_4AlSbO_2(OH)_{16}Cl_4(SO_4)_2$
Chalcocyanite	$CuSO_4$
Trippkeite	$CuAs_2^{+3}O_4$
Lindgrenite	$Cu_3(MoO_4)_2(OH)_2$

c. αPbO_2-chains

Lammerite	$Cu_3(AsO_4)_2$
Azurite	$Cu_3(CO_3)_2(OH)_2$

Corner-Sharing Chains:

Bonattite consists of chalcanthite-type tetrahedral-octahedral chains which are further polymerized by SO_4 tetrahedra sharing a third corner with the octahedra of adjacent chains (Figure 3.29). Bonattite and chalcanthite belong to the series: $CuSO_4 \cdot nH_2O$. These structures are related by hydration-dehydration processes, which vary the connectivity of the structures, and are described by Baur (1964,1968).

The solution of liroconite by Kolesova & Fesenko (1968) is topologically correct, although some of the bond lengths were inaccurate (see Chapter 2). The structure consists of chalcanthite-type chains, linked together by edge-sharing dimers of Cu-octahedra. The dimers corner-link to Al-octahedra and AsO_4 tetrahedra (Figures 3.30a,b). Although there is a component of edge-sharing, the main form of connectivity is corner-sharing. The dimers can be considered as a single corner-sharing structural unit. Only the long apical vertices of the Cu-dimers remain unshared, and the connectivity of liroconite is greater than bonattite.

Chalcomenite, refined by Asai & Kiriyama (1973), was described with square-pyramidal Cu-sites (the longest apical Cu-O=3.14Å). Considering the connectivity of the structure (in line with the classification scheme proposed), Cu^{2+} is more conveniently described as [6]-coordinate, although bond-valence features for this structure do not favor either coordination for Cu^{2+}. Figure 3.31a,b illustrates the chalcomenite structure with [6]-coordinate Cu. It consists of corner-sharing Cu-octahedral and SeO_3-pyramidal chains (Cu-Se polyhedral ratio 1:1),

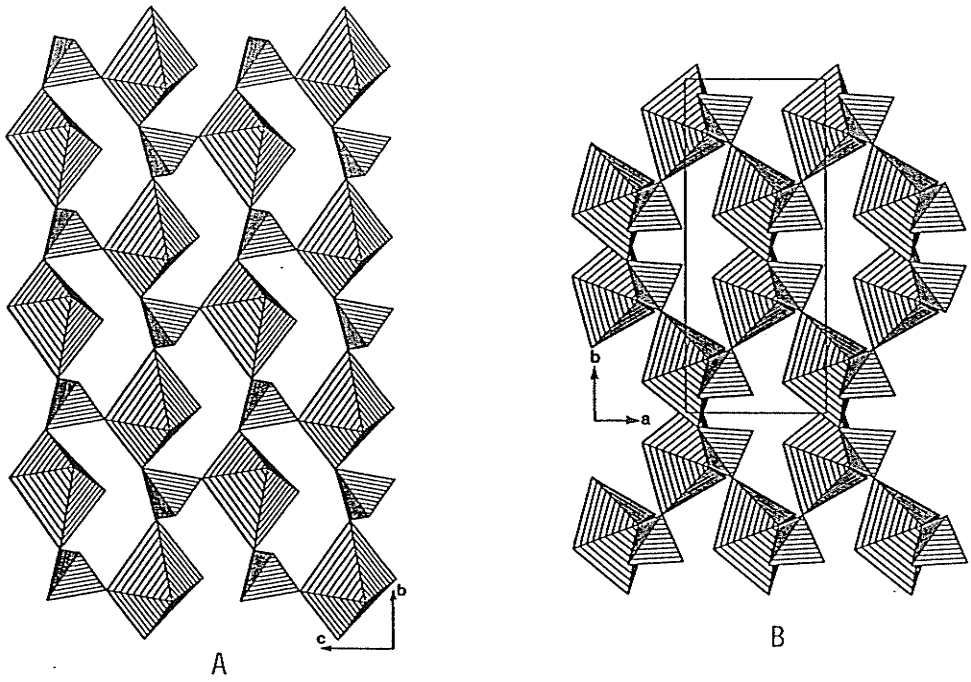

Figure 3.29: Structure of Bonattite.
(a) corner-sharing tetrahedral-octahedral chains along [100];
(b) further corner-linked along [001] into a network.

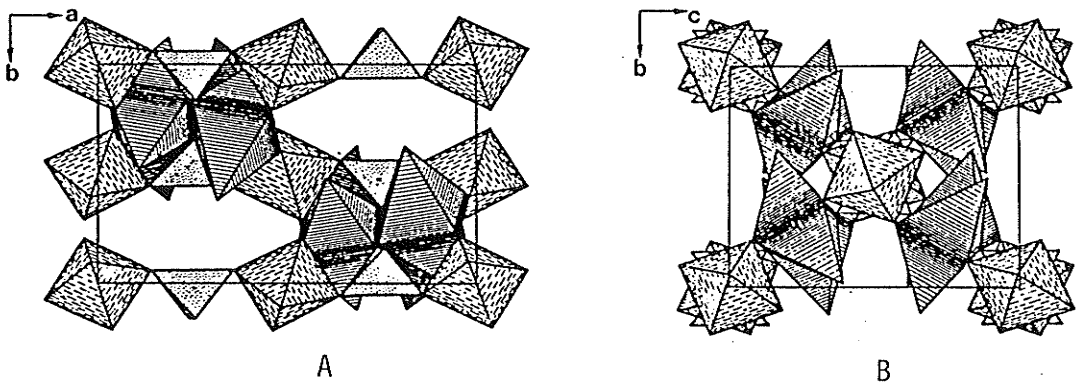

Figure 3.30: Structure of Liroconite. (a) chalcanthite-type chains, corner-linked to Cu-octahedral dimers (ruled shading); (b) viewed down the tetrahedral-octahedral chains; from Kolesova & Fesenko (1968).

which further corner-share between octahedra and SeO_3 pyramids of adjacent chains in the third dimension.

Teinite (Effenberger, 1977) has copper in square pyramidal coordination, but for practical purposes is otherwise isostructural with chalcomenite. A sixth Cu-O distance of 3.37Å, giving a bond-valence strength of 0.018vu, is too weak to be considered significant. However, to keep the relationship between chalcomenite and teinite clear, teinite can be described with the same topology as the former structure (Figures 3.31a,b), with Cu in [6]-coordination. The difference between the sixth Cu-O distances of the two structures represent variations in the amount of Jahn-Teller distortion, presumeably due to the influence of different cation sizes in SeO_3 and TeO_3.

The poitenvenite structure has not been solved, but it is apparently isostructural with the kieserite group of structures, according to Hawthorne et al. (1987). The structure of kieserite consists of $M\emptyset_6$ vertex-linked chains which further polymerize in the third dimension using all available vertices of the tetrahedra and octahedra (Figure 3.31c). This is essentially the same style of interchain linkage as chalcomenite (Figure 3.31a) except that (SeO_3) has one less vertex to share, and therefore the octahedra of chalcomenite have one unshared corner. We now realize the importance of considering Cu as [6]-coordinate whenever possible. If copper in chalcomenite/teinite is considered [5]-coordinate, the relationship to the kieserite group is lost. The poitenvenite/keiserite structure represents the maximum

extent of connectivity for corner-sharing topologies, and is apparently comfortable with the J-T distortion in Cu-octahedra (assumed present).

Bandylite is a very interesting structure. It is tetragonal, which is high symmetry for a Cu^{2+} oxysalt, because the J-T distortion tends to reduce the symmetry of polyhedral assemblages. Bandylite was described by Collin (1951) as a Cu-octahedral & boron-tetrahedral layer structure, because of cleavage by the mineral into sheets on (001). However, regardless of physical properties, bandylite is not a layer structure. It consists of octahedral chains which are linked laterally by borate tetrahedra into a network of parallel chains perpendicular to (001) (Figures 3.33a,b). This framework is one of maximum connectivity. The good cleavage on (001) is caused by the breakage of weaker Cu-Cl bonds (apical), which are aligned perpendicular to the cleavage direction of the sheets.

Edge-Sharing Square Pyramidal Cu^{2+}:

Litidionite is isostructural with fenaksite, $KNaFeSi_4O_{10}$ (Pozas et al., 1975). The structure (Figure 3.34a) is made of tubular chains of SiO_4 tetrahedra, crosslinked by square pyramidal CuO_5-dimers and NaO_7 polyhedra into a network. Potassium ions are in the large cavities of the SiO_4 tubular chains.

Synthetic $\beta Cu_2V_2O_7$, prepared by Mercurio-Lavaud & Frit (1973), is the mineral ziesite; synthetic $\alpha Zn_2V_2O_7$ (Gopal & Calvo, 1972), and $\alpha Cu_2P_2O_7$ (Robertson & Calvo, 1967), are isostructural with ziesite. The structure has edge-sharing and corner-sharing chains of CuO_5 square

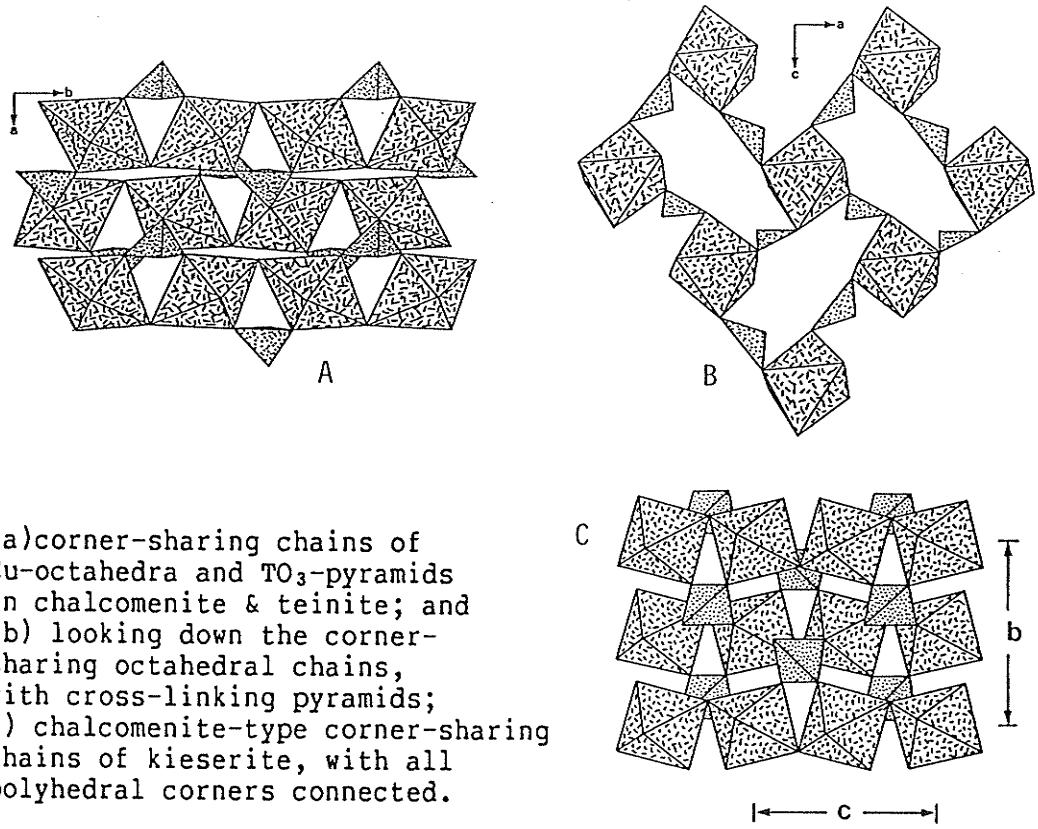

(a)corner-sharing chains of Cu-octahedra and TO_3-pyramids in chalcomenite & teinite; and (b) looking down the corner-sharing octahedral chains, with cross-linking pyramids; c) chalcomenite-type corner-sharing chains of kieserite, with all polyhedral corners connected.

Figure 3.31: The Chalcomenite & Kieserite Type Structures.

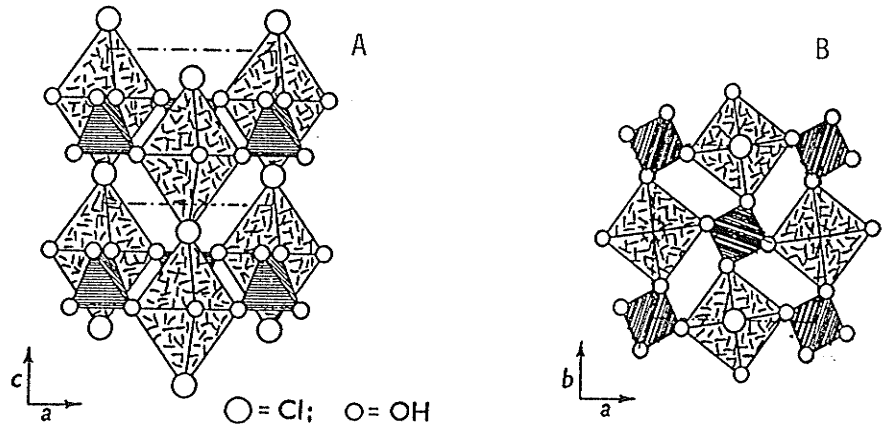

Figure 3.33: Structure of Bandylite. (a) corner-sharing octahedral chains, cross linked by borate tetrahedra; (b) looking down the axes of the chains, we see the highly symmetrical arrangement with a high degree of connectivity.

pyramids linked together by corner-sharing V_2O_7 dimers (Figure 3.34b). This structure is based upon a distorted HCP arrangement, with the stacking direction down [001] (Gopal & Calvo, 1972). As a result of HCP, the structure is more densely packed and the connectivity of ziesite is higher than litidionite.

At 712°, ziesite reverts to blossite ($\alpha Cu_2V_2O_7$), a thortvietite-type structure. This transformation involves rotation of the V_2O_7 tetrahedral pairs by 25°. Consequently, the geometry of the square pyramids is changed. Calvo & Faggiani (1975) report that changes at the copper site involve significant reconstruction of the bonds. However, Cu remains in five coordination.

Kinoite is an elaborate structure, with edge-sharing CuO_5-chains, edge-sharing CaO_6-dimers, and corner-sharing SiO_4-trimers (Figures 3.35a,b). The CuO_5-chains form the basic skeleton of the structure, and the other polymerized units link them together into a framework. The degree of polymerization is increased from litidionite and ziesite due to a large number of shared edges. Unlike the previous two minerals, kinoite has no other structural analogue.

Complex Edge-Sharing $^{5+6}$M Linked to Single $^{3+4}$T:

These structures have more complexity in their arrangements than the previous group, although their degree of connectivity does not differ greatly.

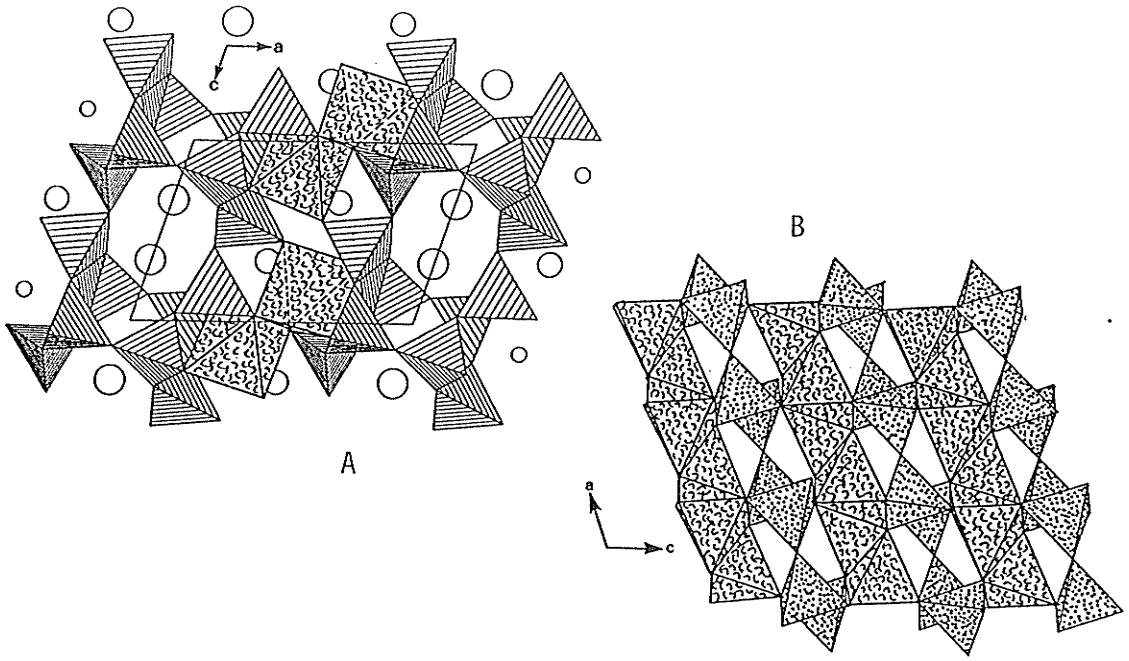

Figure 3.34: Structures of Litidionite and Ziesite. (a) tubular SiO_4 chains, crosslinked by CuO_5-dimers, with Na ions (smaller circles) and K ions (larger circles), in litidionite; (b) CuO_5-chains, crosslinked by V_2O_7 groups, in ziesite.

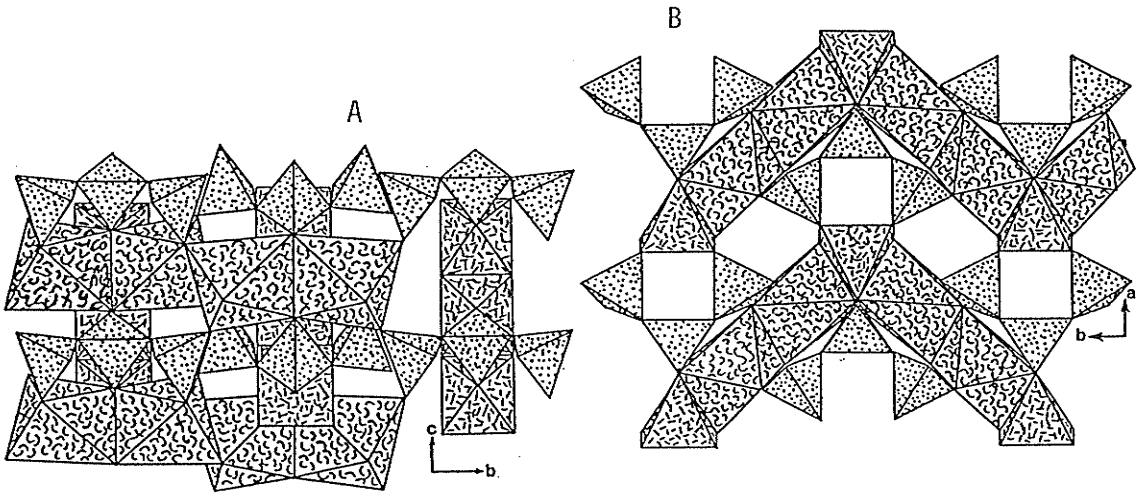

Figure 3.35: Structure of Kinoite. (a) looking across the CuO_5-chains of square pyramids (straight dashes), crosslinked by Ca_2O_{10} octahedral dimers (curled dashes); (b) viewed down the axes of CuO_5-chains, crosslinked by corner-sharing SiO_4-trimers.

Callaghanite is made of contorted edge-sharing Mg-octahedral chains, linked together by edges to edge-sharing CuO_5-square pyramidal dimers (Figure 3.36a). Carbonate triangles corner-share with adjacent octahedral chains. The face-centred packing arrangement (FCP) of the spiralling octahedral chains, emphasized in Figure 3.36b, is common in the network chain structures (because it is a convenient way to pack rod-shaped chains).

Stranskiite consists of very distorted Cu-octahedra, sharing edges with ZnO_5-trigonal bipyramidal dimers, making staggered chains parallel to [010]. These complex chains are corner-linked by AsO_4 tetrahedra (Figure 3.37a). Alternatively, this structure may be classified as a framework of ZnO_5-AsO_4 rings (Zn-dimers and As-tetrahedra alternating), illustrated in Figure 3.37b. Stranskiite is isostructural with $Cu_3(PO_4)_2$ (Shoemaker et al., 1977). In this synthetic isomorph, Cu assumes both octahedral and trigonal bipyramidal coordinations.

$Cu_5V_2O_{10}$, synthesized by Shannon and Calvo (1973), is also the new mineral stoiberite (Birnie & Hughes, 1979). Its structure is a complex arrangement of double octahedral chains parallel to (010), and chains of Cu-octahedra and CuO_5-trigonal bipyramidal dimers parallel to (001). (VO_4) tetrahedra corner-link these edge-sharing chains together into a densely packed network (Figures 3.38a,b). Cu(4) has an unusual (4+2) coordination because the two longest bonds are <u>cis</u> to each other.

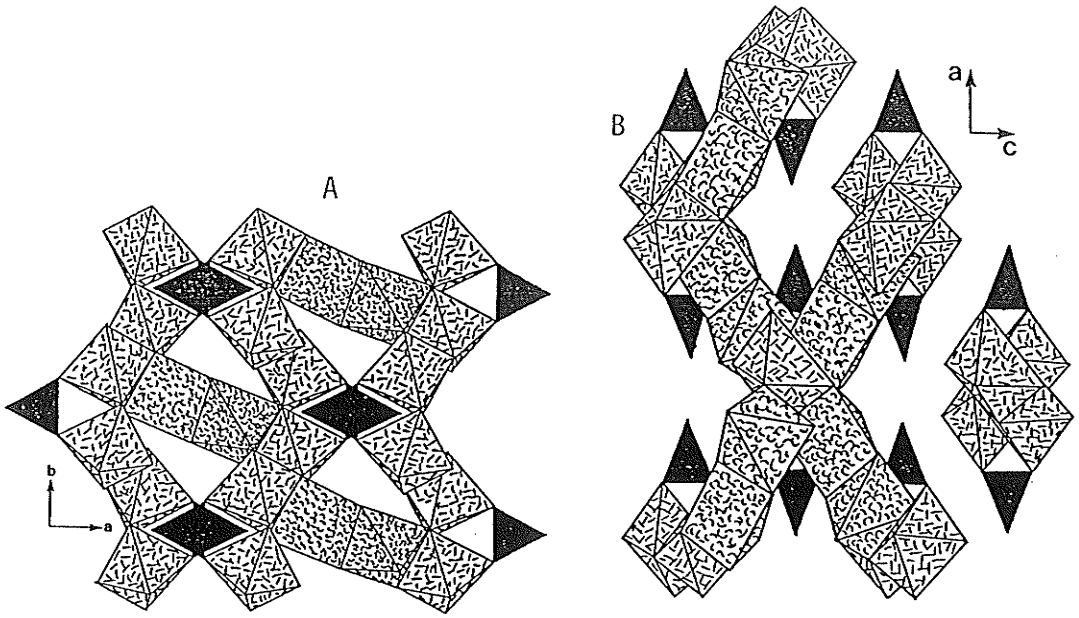

Figure 3.36: Structure of Callaghanite. (a) staggered chains of Mg-octahedra (straight dashes), corner-linked to CO_3 triangles and edge-sharing to Cu_2O_8-dimers (curled dashes); (b) viewed down the spiralling Mg-octahedral chains, with a face-centred packing arrangement (rod packing).

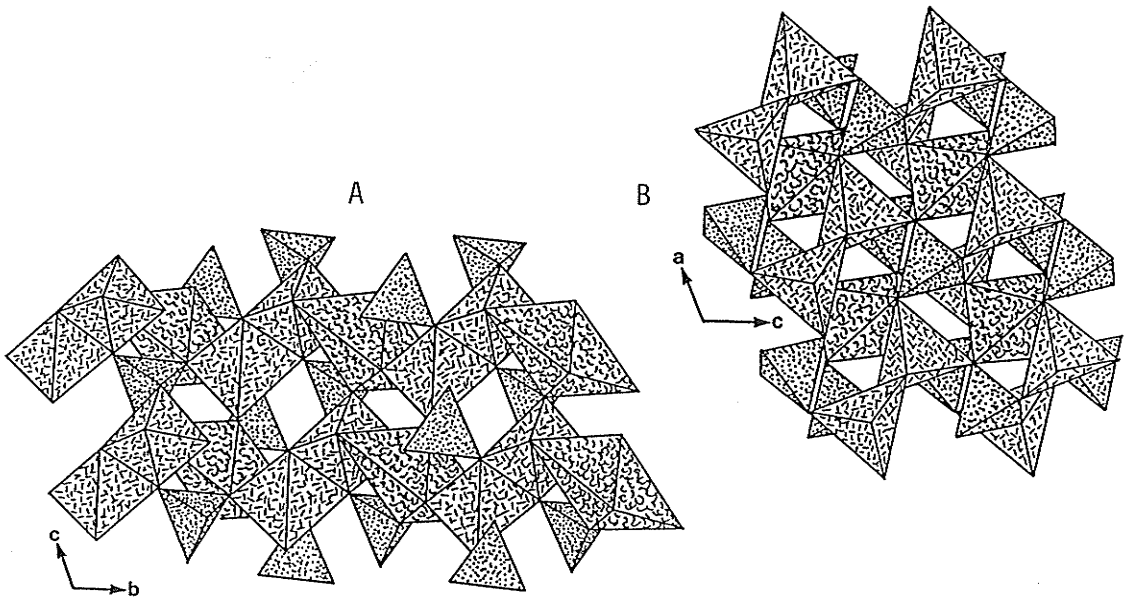

Figure 3.37: Structure of Stranskiite. (a) zig-zagging chains of Zn_2O_8-dimers (straight dashes) and Cu-octahedra (curled dashes) along the b-axis, linked by AsO_4 tetrahedra; (b) six-membered rings of Zn and As polyhedra, crosslinked by Cu-octahedra.

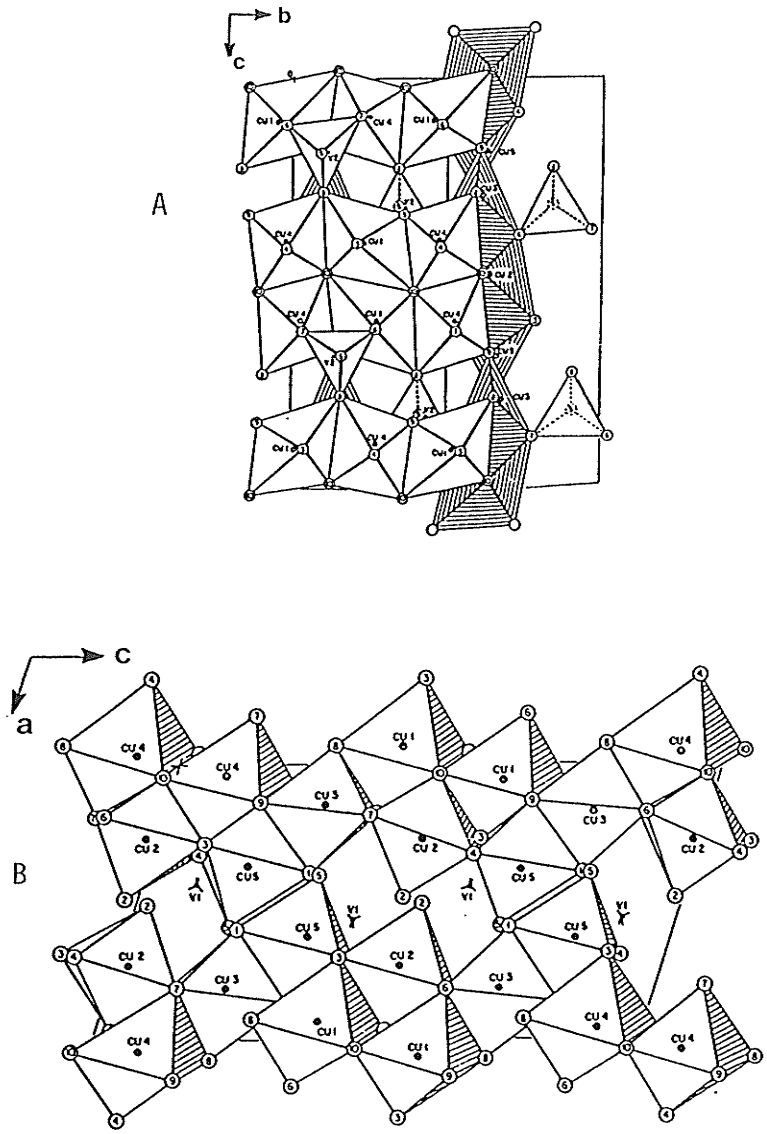

Figure 3.38: Structure of Stoiberite. (a) looking across double octahedral chains perpendicular to chains of trigonal bipyramidal dimers and octahedra, with crosslinking VO_4 tetrahedra; (b) a close packed array of oxygens stacked on [101]; from Shannon & Calvo (1973).

Edge-Sharing ^{6}M-chains:

A large number of Cu^{2+} oxysalts in this structural group fall into the category of wallpaper structures (refer to Table 3.6). The term "wallpaper structures" was originally used by Moore & Araki (1974) to describe several oxysalt minerals made of edge-sharing octahedral chains linked by triangular borate groups into polyhedral networks. Wallpaper structures may be drawn as idealized monomers (TO_3 or TO_4) and dimers (octahedra) on to a 3^6 net, with the octahedral chains perpendicular to the net. Wallpaper structures have a unit cell repeat distance of 3Å down their chains. The original definition has been generalized to include framework chain structures that have unit cell repeats of an integral multiple of 3Å. Figures 3.39a-g show the framework Cu^{2+} oxysalt minerals which can be drawn as wallpaper structures. Figures 3.40a-g show the chain components which make up these structures.

The mixite group of minerals has the formula: $A^{2+3+}Cu_6(HXO_4)_3(OH)_6 \cdot H_2O$; where A=Bi, X=As in mixite; A=Y,Ca,REE, X=As in agardite; A=Al,Y, X=As in goudeyite; and A=Y,REE,Ca, X=P in petersite. According to Aruga and Nakai (1985), the charge imbalance created by substitution of A^{2+} for A^{3+} is balanced by $(OH)^-$ for O^{-2} substitution at the tetrahedral ligands in agardite. Also, they report that the H_2O statistically occupies the apical octahedral positions in the large open channels (Figure 3.39a). Without the H_2O, Cu would be in square pyramidal coordination, though strangely enough, the structure could still be drawn as a tiling. These features are assumed to hold

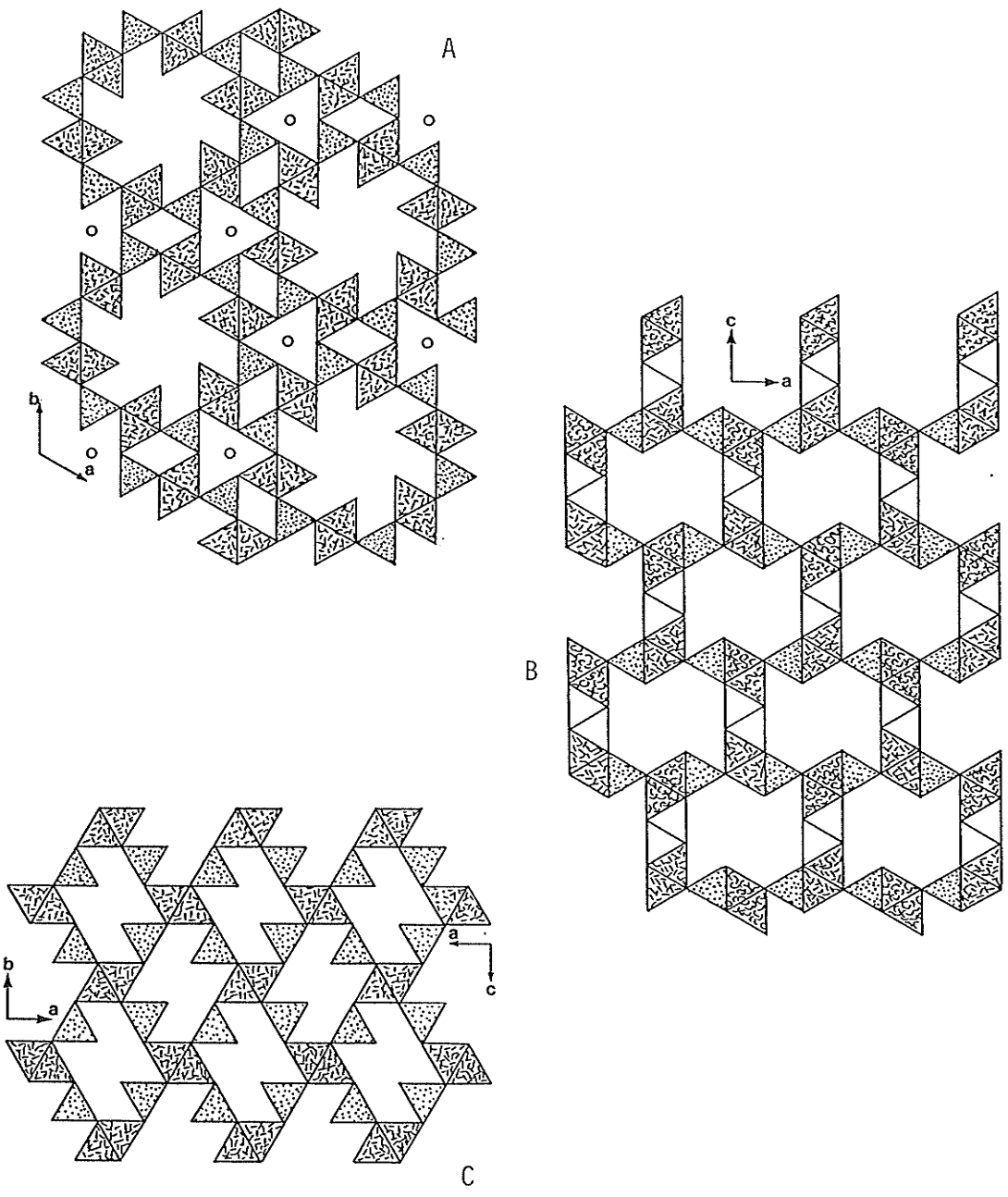

Figure 3.39: Cu Oxysalt Wallpaper Structures.
(a) mixite group, circles are AO_9 polyhedra; (b) euchroite, curl-dashed octahedra at 1/4, straight-dashed at 3/4, unshaded octahedra at 1/2 and 0 heights, tetrahedra dotted, there is no edge sharing of tetrahedra and octahedra; c) the wallpaper framework for olivenite and conichalcite, [8]-coordinate units not included; axes for olivenite on the left, for conichalcite on the right.

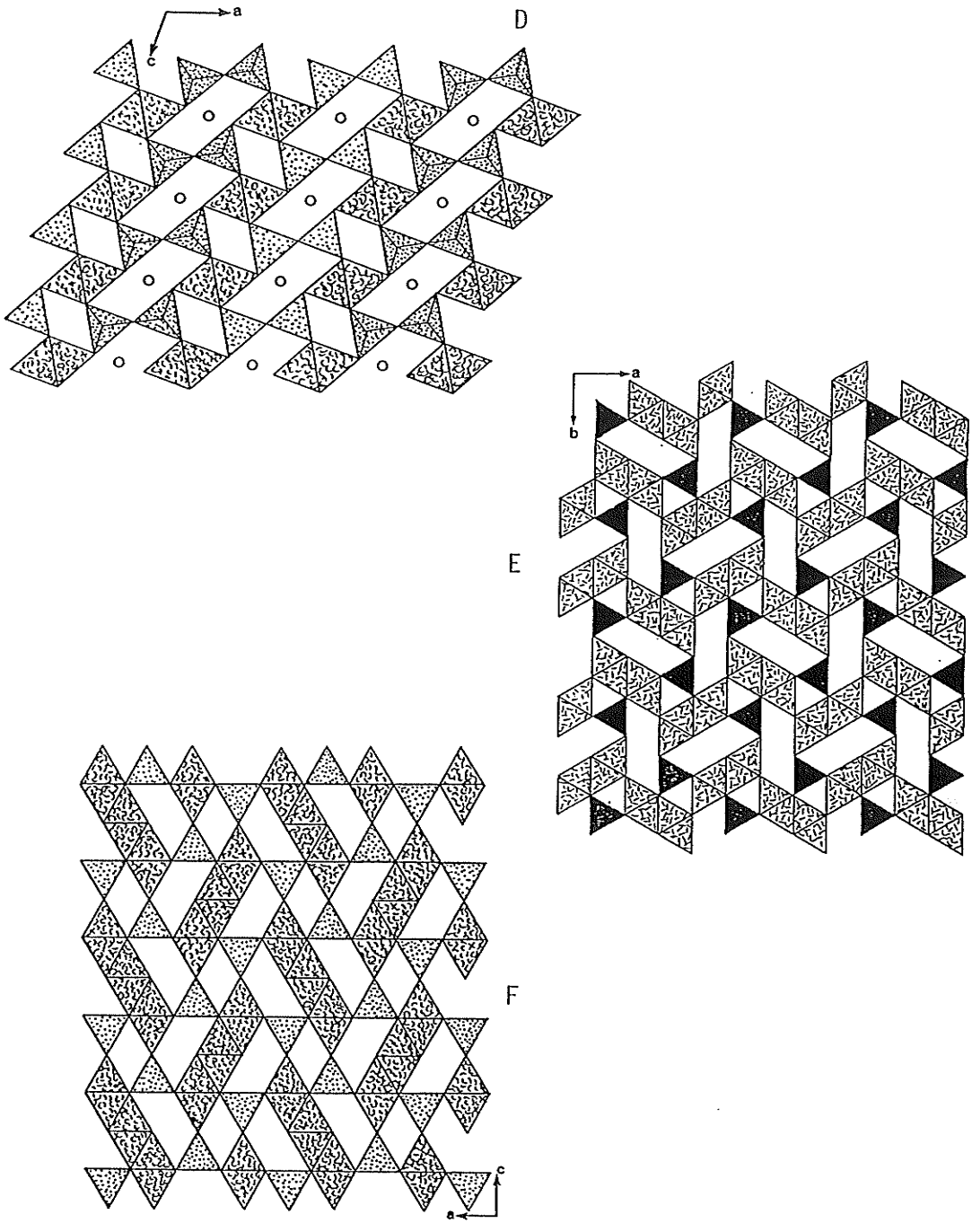

Figure 3.39: Cu^{2+} oxysalt Wallpaper Structures. (d) papagoite, circles are CaO_6 polyhedra (e) malachite (f) antlerite

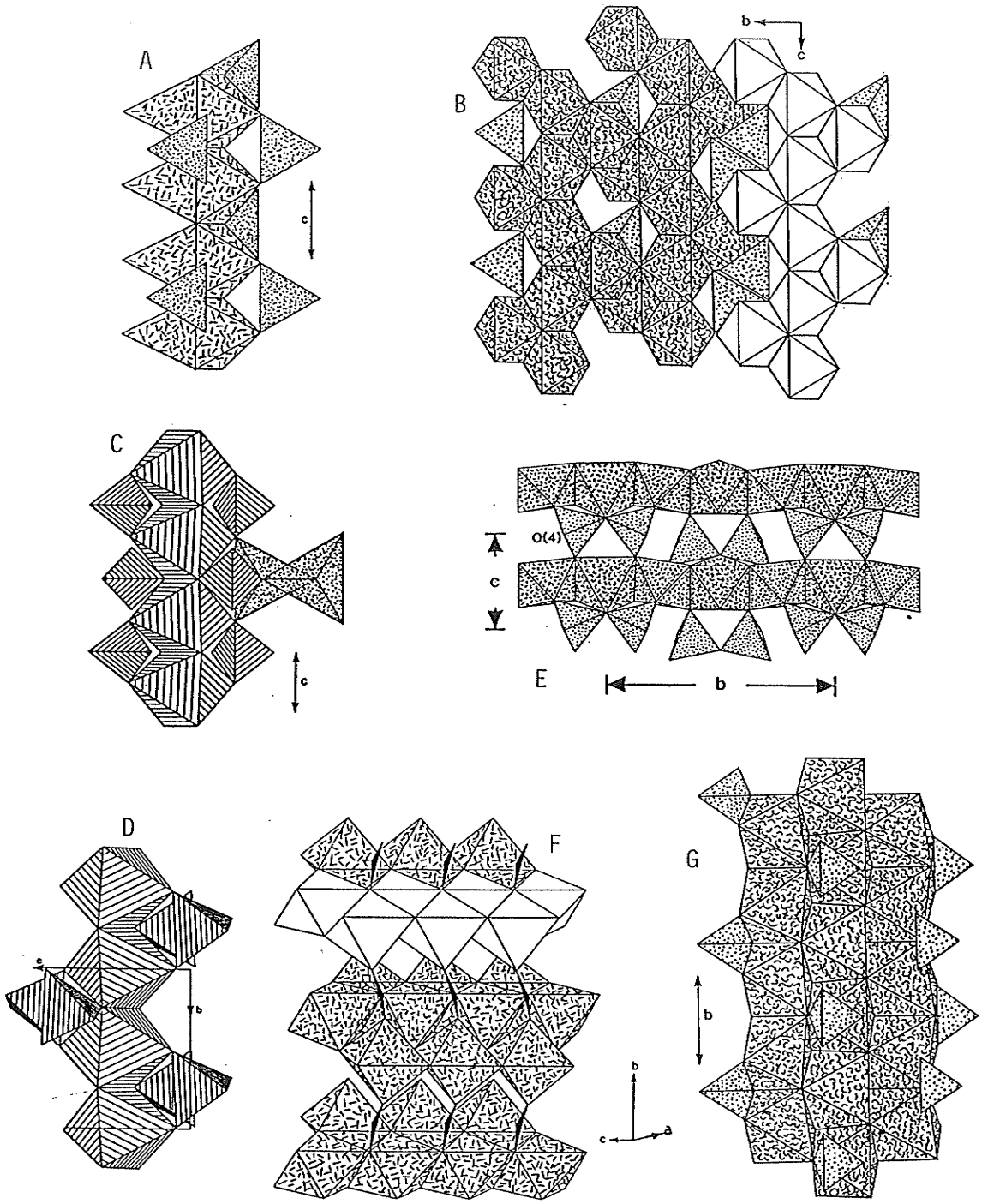

Figure 3.40: Chain Components of the Wallpaper Structures. (a) mixite chain type; (b) clinozoisite-type chains of idealized euchroite; c) olivenite-group chain with Cu_2O_8-dimer; (d) conichalcite type chain, similar in connectivity to vauquelenite; (e) papagoite, mixed Al-Cu octahedral chains with polymerized SiO_4 tetrahedra linking chains together, Al-dashed,Cu-curled, from Hawthorne & Groat (1986); (f) malachite double octahedral chains with carbonate triangles; g) antlerite triple-chains with SO_4 tetrahedra.

true for the whole mixite group. The A-cations are [9]-coordinate in a tri-capped trigonal prismatic arrangement. Because of the hexagonal arrangement of the octahedral chains, only one of the apical bonds is attached to (XO_4) tetrahedra, resulting in a unique tetrahedral-octahedral chain (Figure 3.40a). The repeat distance of the mixite wallpaper pattern parallel to the chain is 6Å.

Euchroite was first described by Finney (1966) as a hydrated derivative of the olivenite structure, with one octahedral Cu(1) site, and a square pyramidal Cu(2) site. The structure is better described with Cu(2) also in a J-T distorted octahedral coordination, because the sixth Cu-O distance is 2.80Å (quite acceptable; see Chapter 2). It is now evident that euchroite has clinozoisite-type octahedral chains, idealized in Figure 3.40b. The wallpaper representation made from the idealized chains (Figure 3.39b) has a 9Å repeat distance. Idealizing the structure shifts the position of neighboring octahedral chains because of tetrahedral linkage requirements (the topology remains the same). Therefore, the CCP packing arrangement of the idealized chains is different from the actual distorted structure shown in Figures 3.41a,b.

Olivenite and libethenite are part of the isostructural series: $^{6}M^{5}M(TO_4)(OH)$; which includes adamite, $Zn_2AsO_4(OH)$, and andalusite $Al_2(SiO_4)O$. As in the mixite group, the substitution of M^{2+} for M^{3+} is compensated by $(OH)^-$ for O^{-2}, except that the hydroxyl ion is part of the Cu-octahedron. Figure 3.42a shows the tetrahedral-octahedral network, and ^{5}M sites. The repeat distance of this wallpaper pattern is 6Å. The ^{5}M-O bonds are actually stronger that those in the octahedral

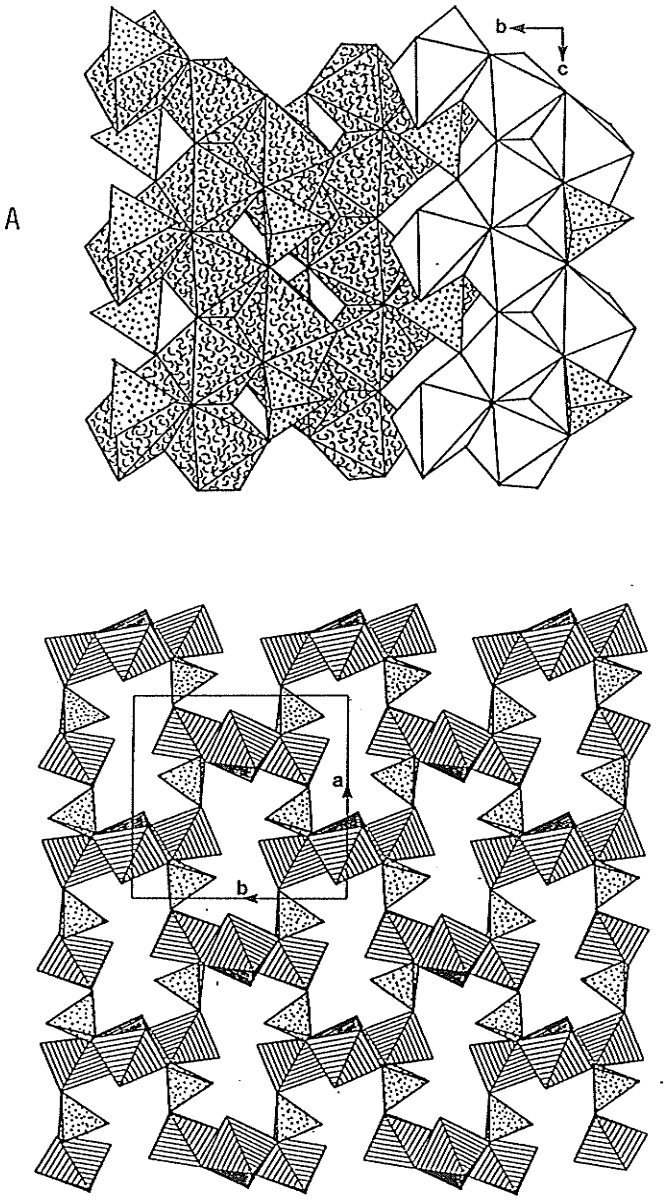

Figure 3.41: Structure of Euchroite. (a) distorted octahedral chains (one unshaded for clarity) cross-linked by tetrahedra; (b) a distorted packing arrangement viewed down the octahedral chains (shaded) with crosslinking tetrahedra.

chains, but for convenience in understanding the connectivity of the structure, it is classified based on the octahedral chains. The connectivity of the tetrahedra to the octahedral chains (Figure 3.40c) is different from those in conichalcite (Figure 3.40d). One can also see how the trigonal bipyramidal Cu_2O_8 dimers link to the rutile-like chains. Olivenite possesses a slight monoclinic distortion, whereas, its chemical analogues are orthorhombic. Consequently, the two apical oxygens of the Cu-octahedra in olivenite have different bond lengths, whereas, the apical octahedral oxygens in the other structures are symmetrically equivalent. The octahedra in all the minerals of this group have (4+2) distortions. Since only the copper members possess the J-T effect, the 4+2 distortion is an intrinsic property of this structural arrangement.

The tetrahedral-octahedral framework of conichalcite is quite similar to the olivenite group framework, and can be made into the same wallpaper pattern by rotation of the actual arrangement of octahedral chains. Figure 3.42b shows the framework with the chain rotation mechanism, and with the [8]-coordinate Ca. As shown in Figure 3.43, the CaO_8 polyhedron is equivalent to the Cu_2O_8 dimers in olivenite. The placement of these two type of polyhedra within their respective frameworks probably controls the topological differences of the two frameworks. Tetrahedral attachment to the octahedral chains is identical to the vauquelenite chains (Figure 3.12f). However, the lower proportion of ^{8}Ca to ^{6}Cu in conichalcite, relative to ^{8}Pb:^{6}Cu in vauquelenite, makes for the higher connectivity of the polymerized units.

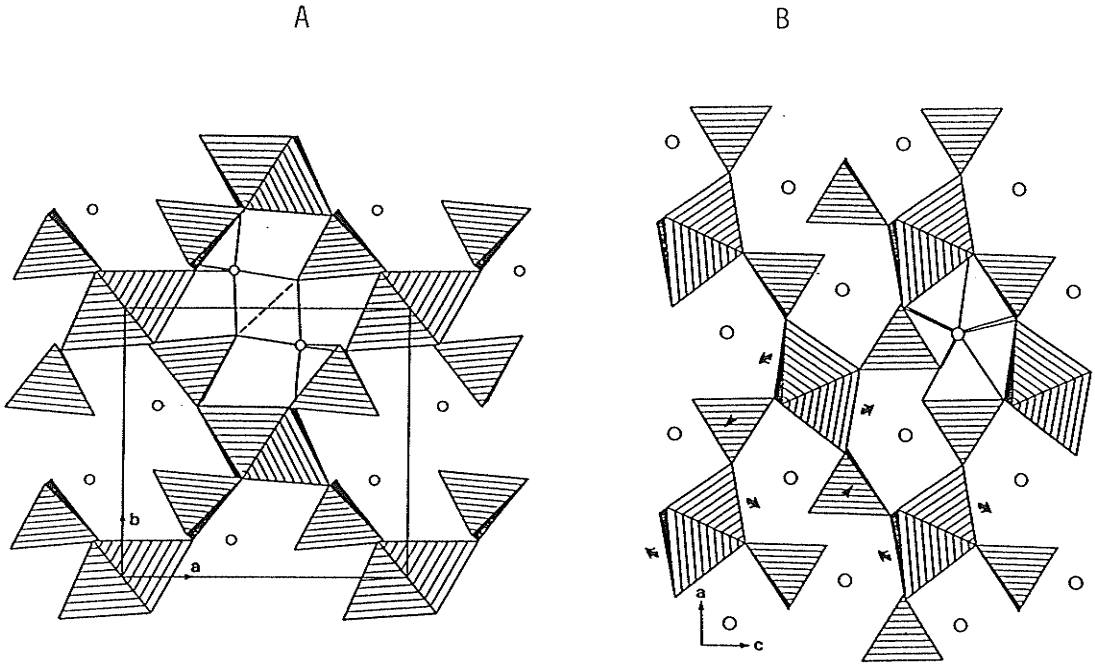

Figure 3.42: Structures of Olivenite and Conichalcite. (a) tetrahedral-octahedral framework of olivenite, with CuO_5 sharing edges to form dimers (shared edge dashed); (b) polyhedral framework of conichalcite, with [8]-coordinate Ca between the chains of polyhedra.

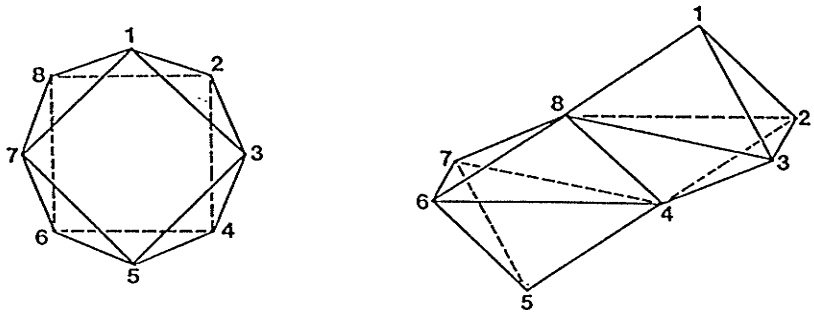

Figure 3.43: Equivalent Polyhedral Units. The eight coordinate square antiprism is equivalent to the Cu_2O_8 dimer (two edge sharing CuO_5 trigonal bipyramids), as both have 8 ligands.

Conichalcite is isostructural with austinite $CaZnAsO_4(OH)$ (Povarennykh, 1972), Ni-austinite (Cesbron et al., 1987), and the duftite and descloizite groups are structurally very similar, differing only in the coordination at the large cation sites. Thus, the general structural formula: $(^{7+8}A<->^{5}M)^{6}M(TO_4)(OH)$ has a large variety of chemistries with structural frameworks that are very similar, and seem to be controlled by the identity of the A or ^{5}M cations. The face-centred packing (FCP) arrangement of octahedral chains is present in all of these structures.

Papagoite contains chains of alternating Al^{3+} and Cu^{2+}-octahedra. Linking these chains together are rings of four SiO_4 tetrahedra, and CaO_6 polyhedra (Figure 3.40d). The idealized wallpaper representation of papagoite (Figure 3.39e) has a repeat distance of 12Å. The unique bond-valence features introduced by this structure are discussed in Chapter 5.

Malachite was first recognized as a wallpaper structure by Moore & Araki (1974), (Figure 3.39f). However, this structure has never been considered with both Cu-sites in octahedral coordination. With the coordination of both Cu(1) and Cu(2) as six with J-T distortions, the true wallpaper character of malachite is apparent. Double chains of octahedra are corner-linked to one another and to carbonate triangles into a network with a repeat distance of 3Å down the chains. The double chains are seen lengthwise in Figure 3.40f.

Antlerite is a wallpaper structure with a 6Å repeat distance (Figure 3.39g). It consists of strips of edge-sharing octahedral triple-chains, corner-linked together by SO_4 tetrahedra. The details of the chains are seen in Figure 3.40g. Viewed down (102), in Figure 3.44, this structure has a distorted cubic close-packed arrangement of oxygens (CCP).

Mammothite has a complex framework composed of euchroite-type chains of Cu-octahedra (Figure 3.45a), crosslinked by ordered arrangements of Al^{3+} and Sb^{5+} octahedra (Figure 3.45b). Within this framework of chains are isolated SO_4 tetrahedra and [9]-coordinate Pb^{2+}. Effenberger (1985a) described Cu(1) as square planar and Cu(2) an square pyramidal, but indicated the presence of apically situated anions in both positions. Bond-valence sums on these apical anions include valence contributions from copper, yet these bonds were not considered part of the Cu coordinations. If Cu contributes to the bond-valence of anions, then the anions should belong in the coordination of Cu. Both Cu(1) and Cu(2) should be considered in six coordination, with different degrees of J-T distortion. The topological relationships to euchroite (and clinozoisite) are then evident.

Chalcocyanite and trippkeite are stoichiometrically and structurally very simple minerals with a high degree of connectivity. Looking down the axes of their rutile-type chains (Figures 3.46a,b) these structures do not fit into the wallpaper family. Chalcocyanite cannot be idealized on to the 3^6 grid because the tetrahedral connection to the octahedra prohibits such an arrangement. Trippkeite does not have monomers, and it also fails to fit onto the 3^6 grid. Schaffarskite, $FeAs_2O_4$, is isostructural with trippkeite (Fischer & Pertlik, 1975). Figure 3.46c,d

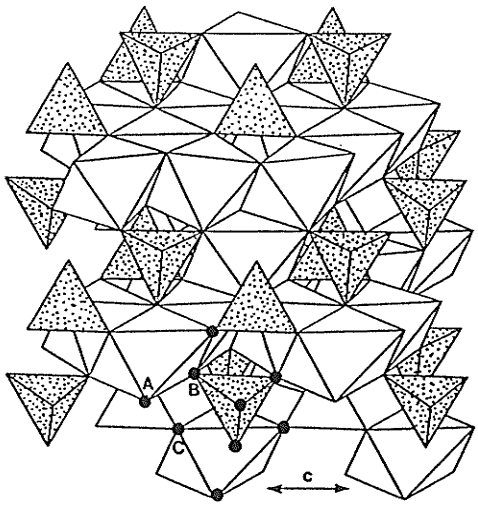

Viewed down (102), the oxygen array is a distorted variation of cubic-close packing; the different oxygen layers are indicated by circles.

Figure 3.44: Cubic-Close Packing of Antlerite.

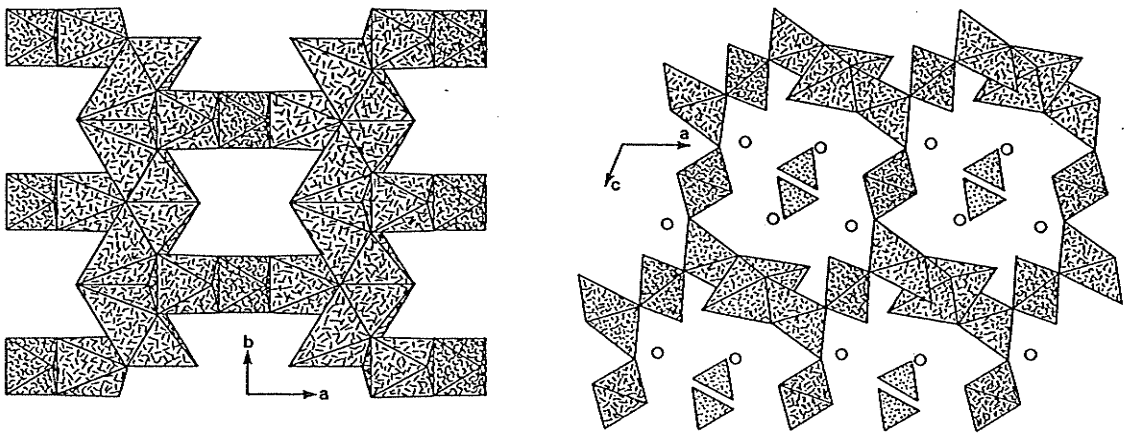

Figure 3.45: The Structure of Mammothite. (a) Euchroite-type chains of Cu-octahedra (straight dashes) crosslinked by Al octahedra (curled dashes); b) corner-linked network of Cu chains and ordered Al & Sb octahedra (Sb-straight dashes); Pb (circles) and SO_4 tetrahedra (dotted) are within the framework cavities.

shows the difference between the linkage of the complex oxyanions to the octahedral chains in chalcocyanite and trippkeite. Trippkeite has a higher degree of connectivity because each octahedral apical oxygen is bonded to two (AsO_3) pyramids, but only one SO_4 tetrahedra is linked to each apical oxygen in the octahedra of chalcocyanite.

Lindgrenite (Figures 3.47a,b) consists of strips of edge-sharing octahedra, crosslinked by MoO_4 tetrahedra. Alternate strips are canted 25° along (100), resulting in a commensurately-modulated structure (Hawthorne & Eby, 1985). This structure has a distorted HCP arrangement of anions, but idealization of the structure results in a shift to CCP (Figure 3.48a).

Lammerite is another modulated close-packed derivative (Hawthorne 1986a). Figure 3.48c,d shows αPbO_2-type chains of Cu(2), crosslinked by very distorted Cu(1) octahedra, and AsO_4 tetrahedra. As in lindgrenite, this structure has a distorted HCP array of anions, but idealization of a single layer results in a shift to CCP (Figure 3.48b). This structure is more densely packed than lindgrenite.

Azurite is another structure based on αPbO_2-type chains. Zigan & Schuster (1972) originally described the structure with Cu(1) in square planar configuration, and Cu(2) in square pyramidal coordination. With Cu(2) in a very distorted octahedral coordination, the bond-valence sums of azurite balance (Table 3.7). The resulting structure (Figures 3.49a,b) is very interesting. αPbO_2-type chains of Cu(2) are packed somewhat like M1-chains in pyroxenes. J-T distorted Cu(2) octahedra

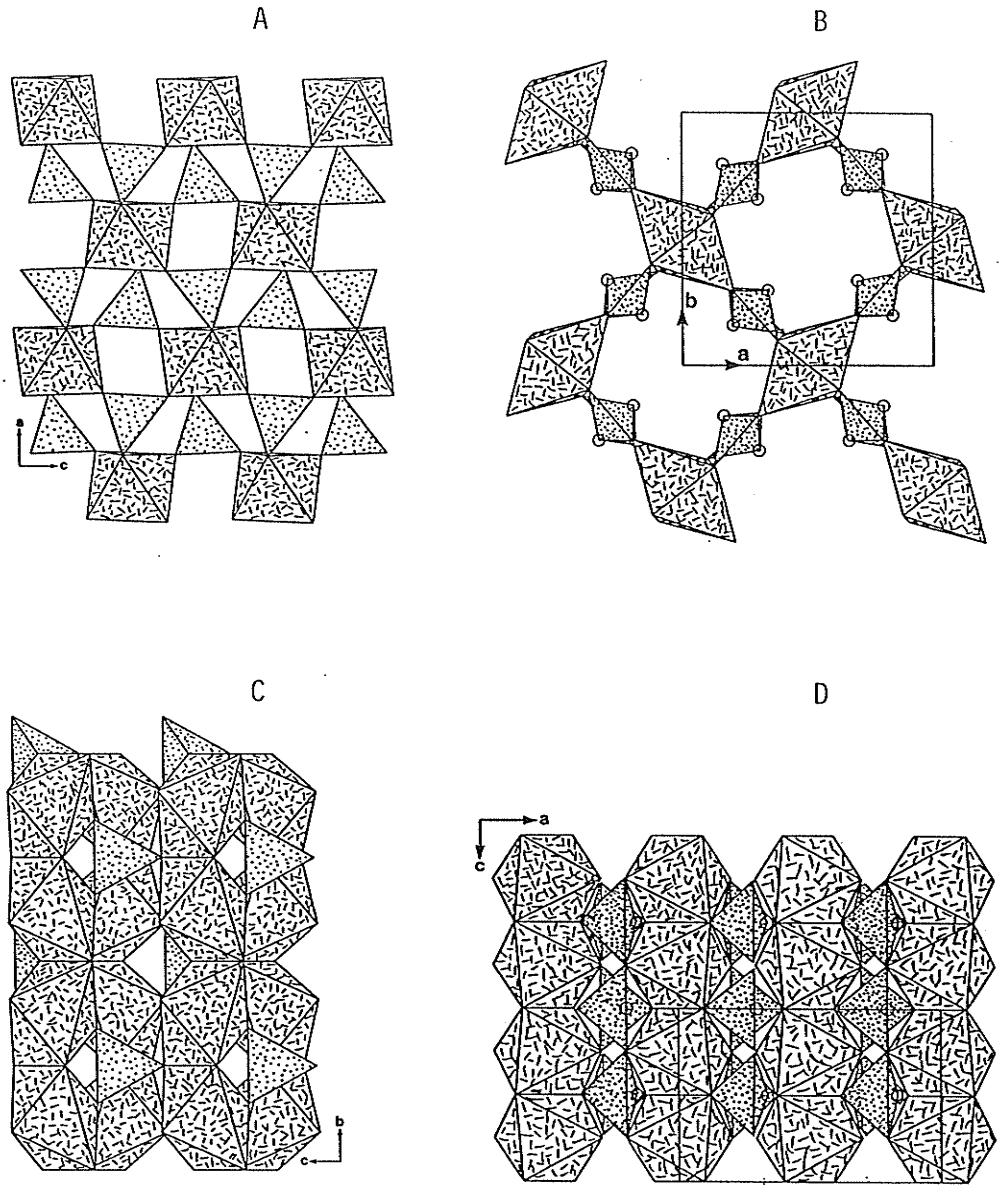

Figure 3.46: Structures of Chalcocyanite and Trippkeite. (a) looking down the rutile-type chains of Cu-octahedra in chalcocyanite with high connectivity to SO_4; (b) looking down octahedral chains of trippkeite, with a high degree of connectivity to AsO_3 pyramids; c) viewing the tetrahedral linkage to octahedral chains of $CuSO_4$; (d) $2(AsO_3)$ pyramids are attached to each apical octahedral oxygen in trippkeite.

share an edge with CO_3 triangles. CO_3 and square planar Cu(1) crosslink the octahedral chains. As was the case for chalconatronite, considering Cu in octahedral coordination reveals the edge-sharing component with CO_3.

3.5.2 Category B: Frameworks of sheets

Cu^{2+} oxysalt structures made from polyhedral frameworks with structural subunits of polymerized sheets are listed in Table 3.8.

Cu-Octahedral Sheets, Partially Occupied:

Cornubite and volborthite have octahedral sheets with 3/4 occupancy by copper, and the other 1/4 of the possible cation sites are empty. Holding together the sheets in cornubite are solitary AsO_4 tetrahedra, all corners of which link to adjacent sheets. Three corners link to one sheet, as in chalcophyllite (refer Fig.3.21a), and the remaining corner to an adjacent sheet (Figures 3.50a,b). Volborthite has V_2O_7 corner-sharing dimers linking together the octahedral sheets (Figures 3.50c,d). Both tetrahedra in each dimer share three corners with the sheets, in the same way as in cornubite. The stacking sequence in volborthite and cornubite is different. All vacant sites must be vertically superimposed in volborthite, whereas, they are staggered in cornubite (Figure 3.50b).

The formula $Cu_5(PO_4)_2(OH)_4 \cdot H_2O$ has three polymorphs: pseudomalachite (PM), reichenbachite (PPM), and QPM, described by Shoemaker et

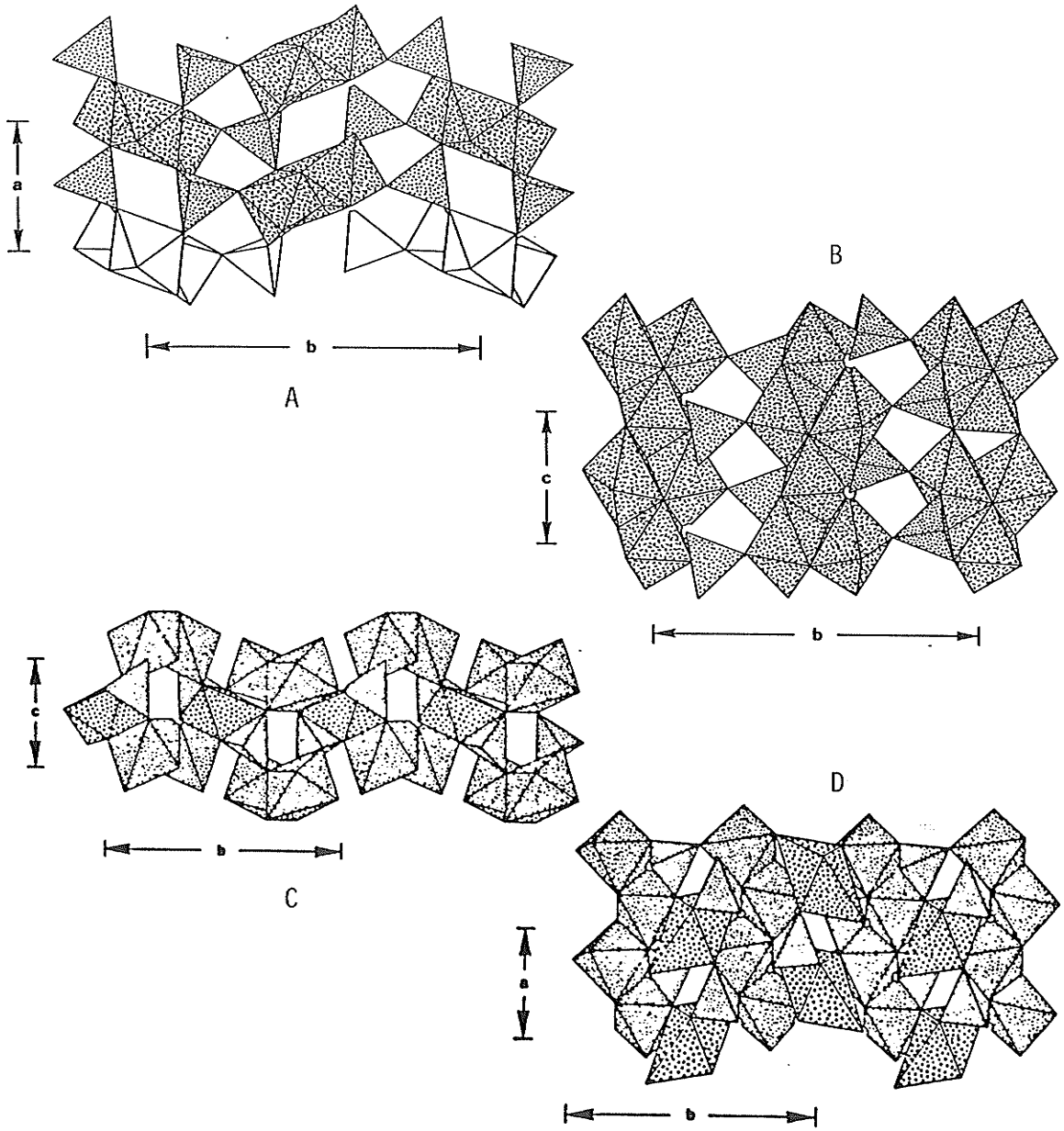

Figure 3.47: Structures of Lindgrenite and Lammerite. (a) looking down the modulated octahedral strips of lindgrenite; (b) looking onto the octahedral strips, with linking MoO_4 tetrahedra, a distorted HCP array; c) modulated polyhedral layers of Cu-octahedra and AsO_4 tetrahedra in lammerite; (d) looking onto the distorted HCP array of octahedral chains and crosslinking polyhedra; lindgrenite drawings from Hawthorne & Eby (1985) lammerite from Hawthorne (1986b)

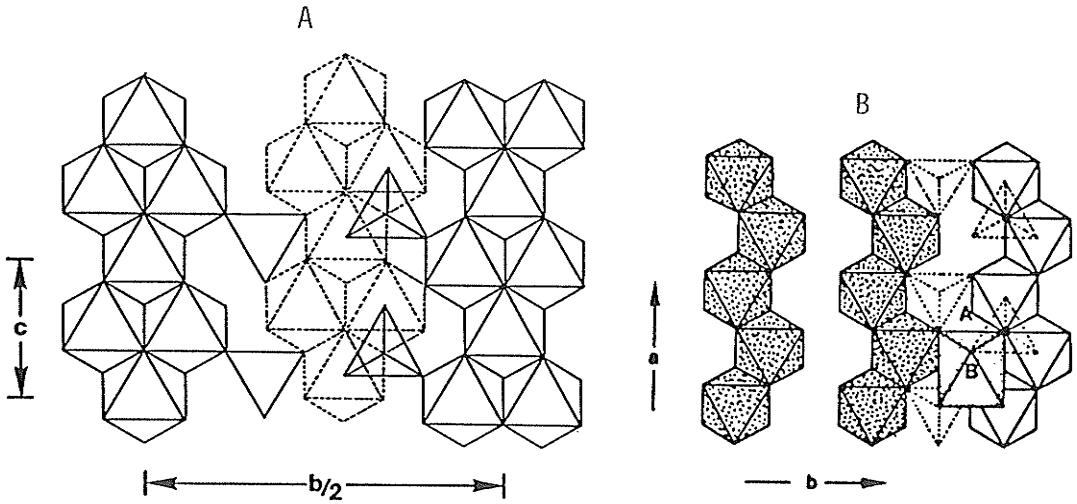

Figure 3.48: Idealized CCP in Lindgrenite and Lammerite. (a) idealized CCP layer of lindgrenite; (b) idealized CCP layer of lammerite; Hawthorne & Eby (1985) and Hawthorne (1986b) respectively

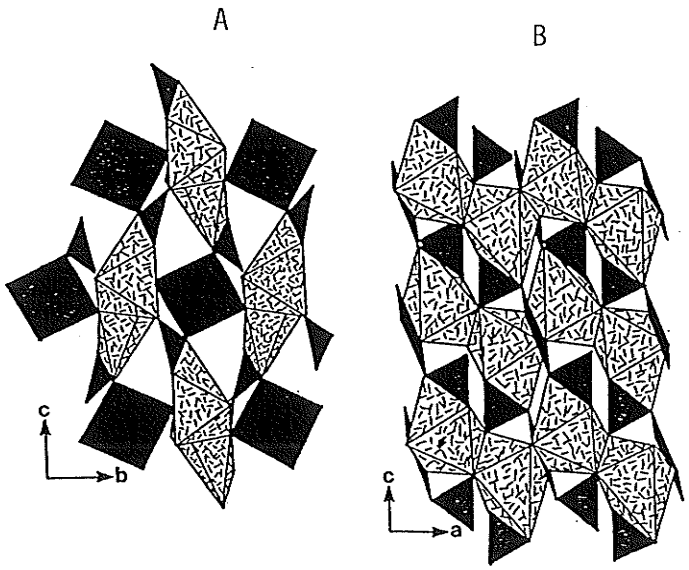

Figure 3.49: Structure of Azurite. (a) Looking down the distorted Cu(2) octahedral chains, crosslinked by CuO_4 square-planar and CO_3 triangular groups; (b) looking across the αPbO_2-chains, showing edge-sharing between octahedra and CO_3 triangles.

TABLE 3.7

Bond-Valences for Azurite

Numbers in brackets are for Cu(2) in six coordination.

	Cu(1)	Cu(2)	C	H	O^{-2}	
O1	.498 (x2)	(.058)	1.335		= 1.833	(1.891)
O2		.485,.150	1.321		= 1.955	
O3		.478	1.362	.14	= 1.980	
O4	.472 (x2)	.414,.447		.79	= 2.214	
	1.942	1.974 (2.032)	4.018	0.93		

Bond-lengths used are from Zigan & Schuster, 1972.
Values obtained using equations from BROWN, 1981.

al.(1977a), Anderson et al.(1977), and Shoemaker et al.(1981), respectively. Shoemaker & Kostiner (1981) described the unique octahedral patterns within the sheets of these structures, revealing the topological differences between the polymorphs. The octahedral-sheet skeletons in Figures 3.51a-c show the relationship between the sheets. Distortion of the ideal anion arrangements, with placement of another Cu-octahedron into the sheets, results in the arrangements of the three polymorphs (Figures 3.52a-c). PO_4 tetrahedra corner-link above and below the vacant areas left in the sheets. By observing that the sheet vacancies are geometric outlines of the tetrahedra, it is apparent that the Jahn-Teller distortions have arranged themselves to accomodate tetrahedral linkage between the sheets. The tetrahedral-octahedral layers are stacked differently in each polymorph, shown for QPM in Figure 3.53.

TABLE 3.8

Category B: Frameworks of Sheets

i. Cu-octahedral sheets (partially occupied) -

Cornubite	$Cu_5(AsO_4)_2(OH)_4$
Volborthite	$Cu_3(VO_4)_2 \cdot 3H_2O$
Pseudomalachite	$Cu_5(PO_4)_2(OH)_4 \cdot H_2O$
Reichenbachite	" "
QPM	" "
Fingerite	$Cu_{11}O_2(VO_4)_6$
McBirneyite	$Cu_3V_2O_8$
Cornetite	$Cu_3(PO_4)(OH)_3$

ii. fully occupied sheets of Cu-octahedra -

Derriksite	$Cu_4(UO_2)(SeO_3)_2(OH)_6$
Shattuckite	$Cu_5(SiO_3)_4(OH)_2$
Plancheite	$Cu_8Si_8O_{22}(OH)_4 \cdot H_2O$

iii. complex sheets of mixed polyhedra -

Arthurite	$CuFe_2^{3+}(AsO_4)_2(OH)_2 \cdot 4H_2O$
Balyakinite	$CuTeO_3$
Salesite	$Cu(IO_3)(OH)$
Veszelyite	$(Cu,Zn)_3(PO_4)(OH)_3 \cdot 2H_2O$
Dolerophanite	$Cu_2(SO_4)O$

Fingerite, a recently discovered mineral (Hughes & Hadidiacos, 1985), has a framework consisting of open Cu-octahedral sheets (Figure 3.54a). crosslinked by VO_4 tetrahedra and CuO_5 trigonal bipyramids (Figure 3.54b). The octahedral sheets have 5/7 cation occupancy, which is unique among the Cu^{2+} oxysalts. The arrangement of the vacancies within the sheets is quite similar to the octahedral skeleton of PPM (Figure 3.51b). However, instead of filling another octahedral site, the remaining Cu in fingerite goes into trigonal bipyramidal coordination between the sheets.

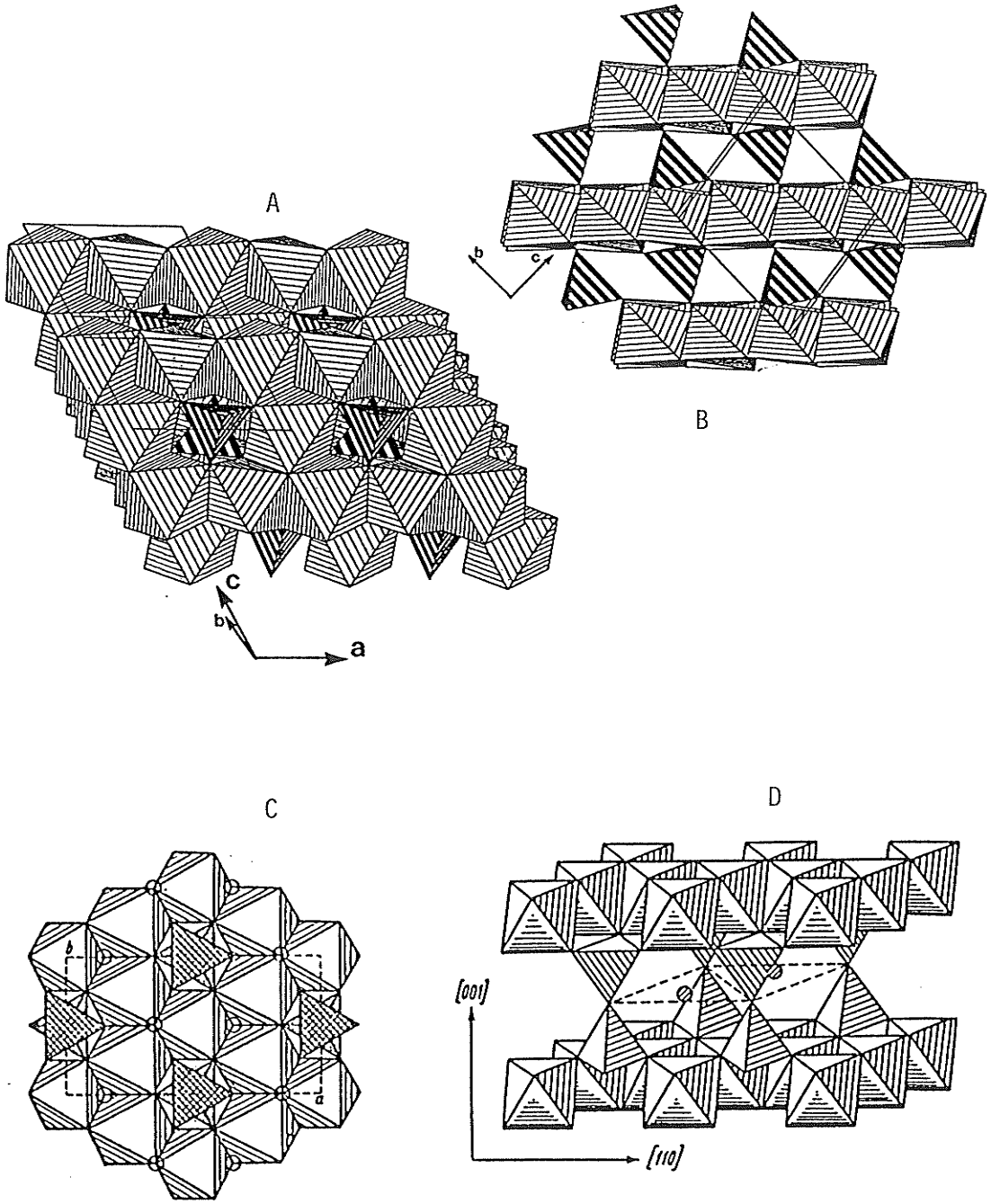

Figure 3.50: Structures of Cornubite and Volborthite. (a) packing of 3/4 occupied sheets in cornubite, with vacancies staggered due to tetrahedral connectivity; (b) tetrahedral-octahedral sequences in cornubite; c) octahedral sheet of volborthite with VO_4 tetrahedra linked only to vacancies; (d) stacking of volborthite sheets, with V_2O_7-dimers in vertical allignment with octahedral vacancies, from Kashayev & Bakakin, 1968.

$Cu_3V_2O_8$ was synthetically prepared by Shannon & Calvo (1972), and was later found to be a natural volcanic sublimate. It was named mcBirneyite (Christian & Hughes, 1986), and is the lowest symmetry structure of the series: $M^{2+}{}_3V_2O_8$, with M= Cu,Ni,Co,Zn and Mg. It has an interesting structure composed of zig-zag octahedral sheets with 3/4 cation occupancy (Figures 3.55a,b) that are corner-linked to VO_4 tetrahedra in a way similar to cornubite. Figure 3.55c shows a dense wallpaper-like arrangement of the close-packed sheets. Looking obliquely down the sheets (Figure 3.55d) one can see a CCP array. This is the only Cu^{2+} oxysalt structure with octahedral sheets that does not show corrugation. The zig-zag arrangement of the sheets in mcbirneyite accomodates the J-T distortion of the octahedra by virtue of its topology, which does not require a geometrical corrugation to attain axially elongated octahedra.

Fehlmann et al.(1964) described the structure of cornetite with Cu in both 5 & 6 coordinations, and explanation of the structure seemed overly complicated. However, refinement of cornetite (details in Chapter 2), and re-description of the structure, with Cu all [6]-coordinate, shows a more understandable polyhedral arrangement. The structure consists of edge-sharing octahedral chains of Cu(1) & Cu(2) along [001], and edge-sharing octahedral dimers of Cu(3) that share an edge with PO_4 tetrahedra (Figure 3.56a). These components are cross-linked, by shared edges along [010], into complex polyhedral layers (Figure 3.56b). The layers are further corner-linked along [100] to form a densely packed framework of commensurately modulated polyhedral layers (Figure 3.56c). The modulation direction is along [010] (shown by wavy arrows).

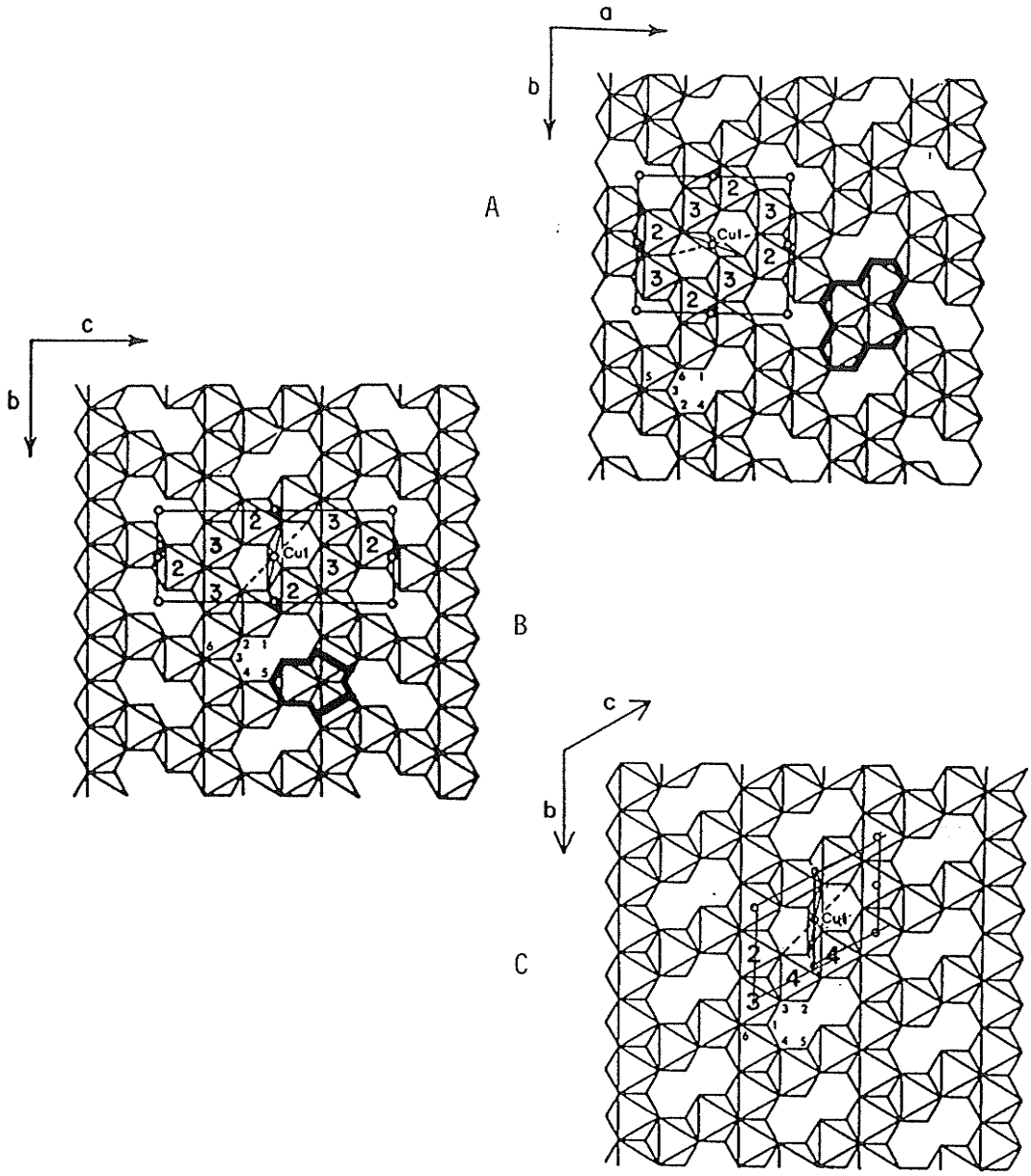

Figure 3.51: Octahedral Skeletons of PM Polymorphs. Idealized octahedral chains as polyhedral derivatives of octahedral sheets in (a) PM, (b) PPM, and c) QPM; these skeleton-sheets are missing Cu(1) sites which require severe geometrical distortions; from Shoemaker & Kostiner, 1981.

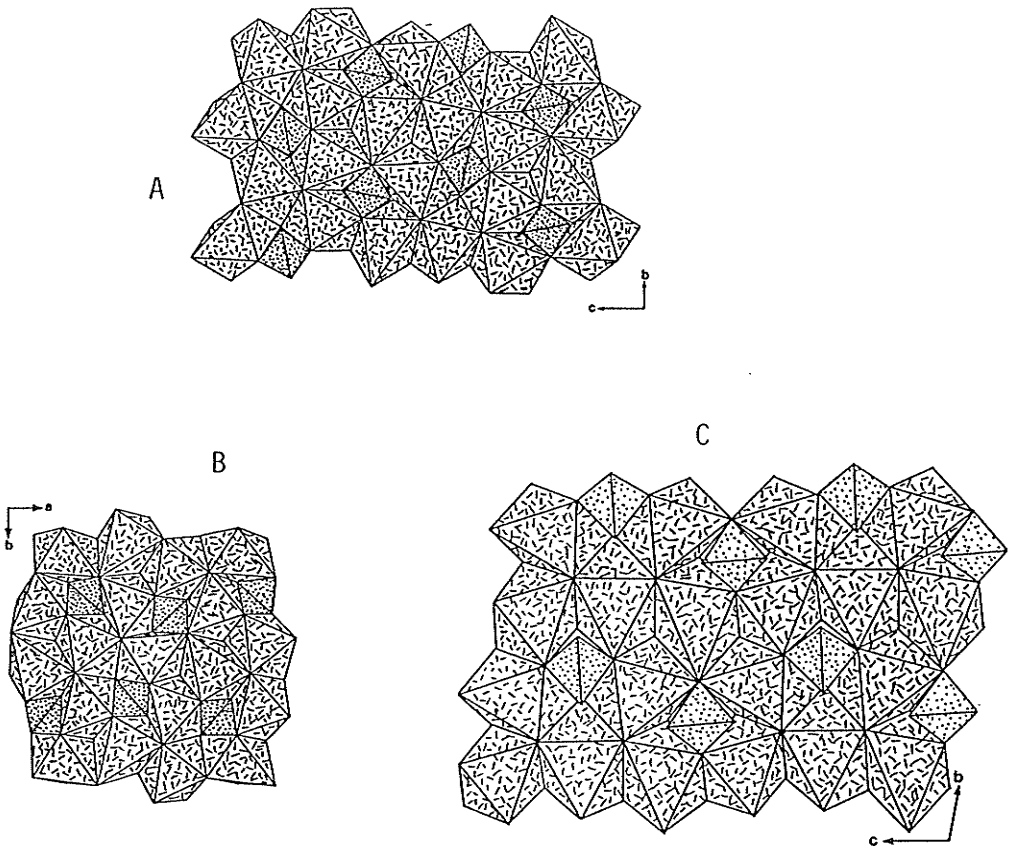

Figure 3.52: Structures of PM, PPM, QPM. Octahedral sheets of: (a) PM; (b) PPM, c) QPM, with sizable distortions. Notice their arrangements accomodate linkage to PO_4 tetrahedra, which outline the cation vacancies.

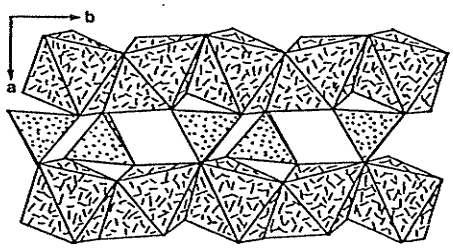

Figure 3.53: Tetrahedral/Octahedral Layer Stacking The unique tetrahedral-octahedral stacking in QPM.

Fully Occupied Cu-Octahedral Sheets:

Derriksite is an elaborate structure composed of Cu-octahedral sheets, alternating with layers of obliquely running U-Se polyhedral chains. SeO_3 pyramids corner-link together the polyhedral layers (Figure 3.57).

Shattuckite and plancheite are copper silicates with pyroxene- and amphibole-like structures. Shattuckite has pyroxene-like silicate chains which attach to both sides of a corrugated Cu-octahedral sheet (Figure 3.58a). The tetrahedral-octahedral-tetrahedral layers (t-o-t sandwich) are held strongly together by very distorted Cu-octahedra (which share equatorial oxygens) forming a layered network of polyhedra. Plancheite has essentially the same style of t-o-t sandwich (Figure 3.58b), except that the silicate chains are amphibole-like double chains (Figure 3.58c). Along with the solitary Cu-octahedra, H_2O groups further aid in linkage of the t-o-t sandwiches.

Complex Sheets of Mixed Polyhedra:

Arthurite is made of t-o-t layers linked together by solitary Cu-octahedra, in an arrangement somewhat similar to shattuckite (Figure 3.59a). However, the octahedral sheets are made of Fe_2O_{10}-dimers, corner-linked together, giving sheets half occupied by cations (Figure 3.59b). AsO_4 tetrahedra share three corners with the sheet, and one corner with Cu-octahedra (Cu-octahedra linking t-o-t layers). This network is rather open, and the H_2O groups bonded to Cu-octahedra aid in

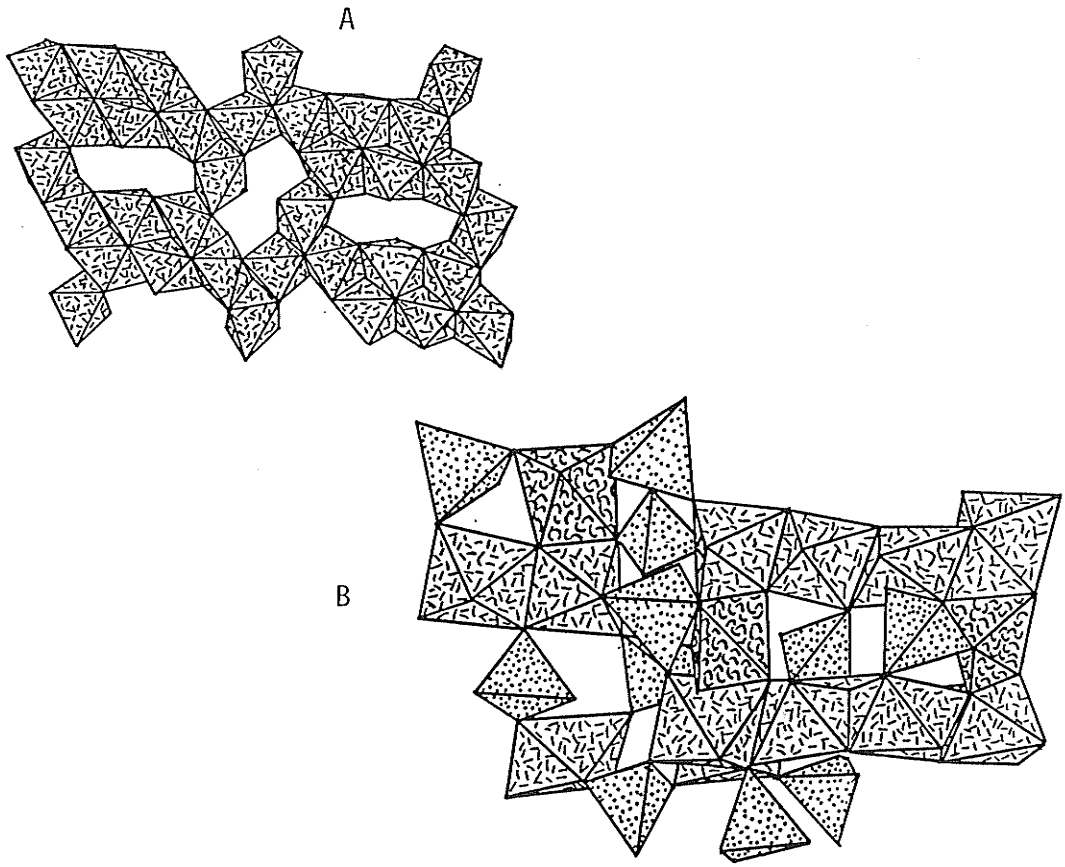

Figure 3.54: Structure of Fingerite. (a) very distorted Cu-octahedra make up the sheet of fingerite; (b) between the octahedral sheets are VO_4 tetrahedra (dotted) and trigonal bipyramids of Cu (curled dashes); a densely packed framework structure.

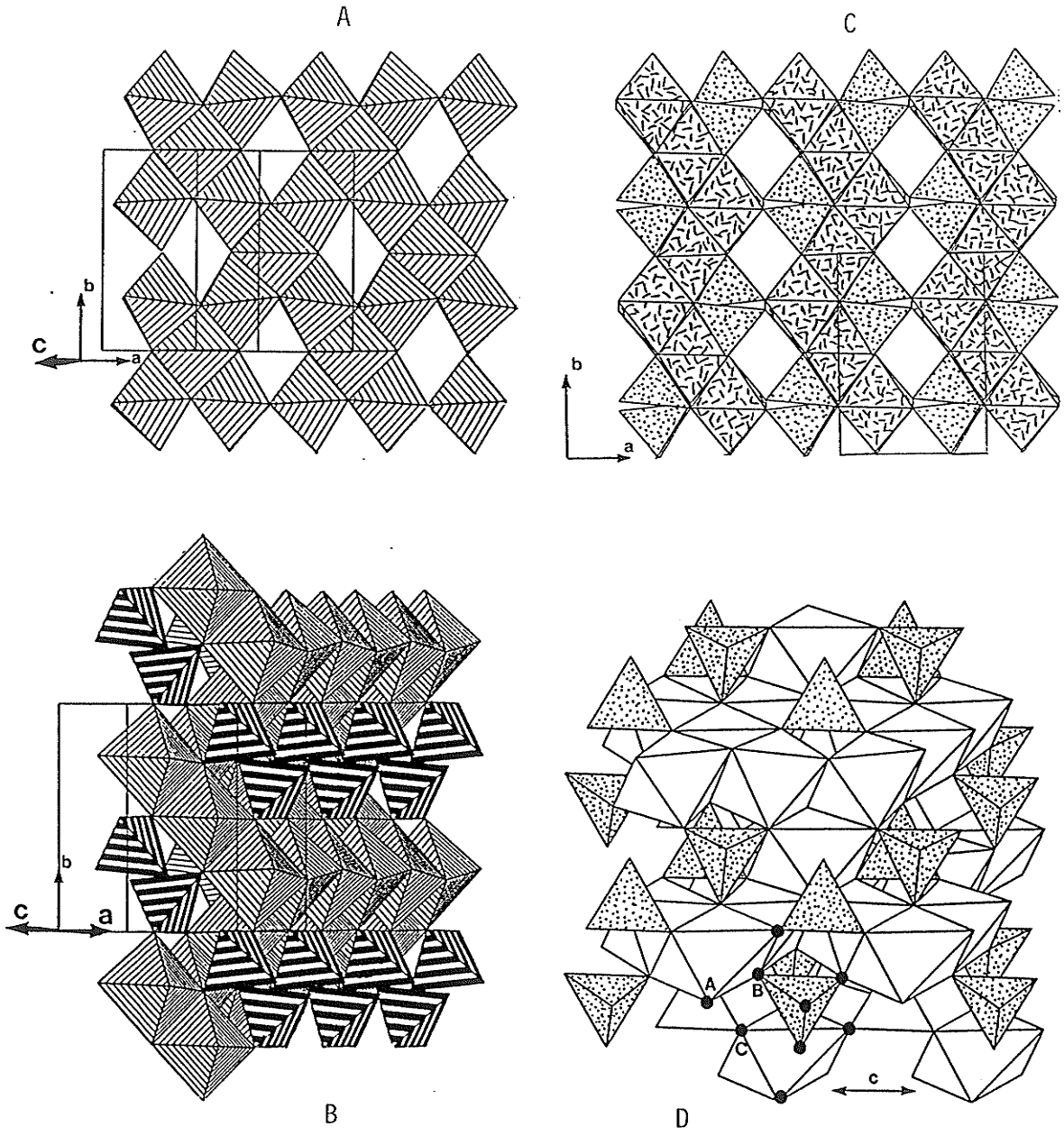

Figure 3.55: Structure of McBirneyite. (a) 3/4 cation occupancy of $Cu_3V_2O_8$ octahedral sheet; (b) oblique view of the zig-zag sheet with VO_4 tetrahedral linkage style like cornubite; c) densely packed arrangement of sheets and tetrahedra in a framework; (d) cubic close-packed array of anions, looking down [120].

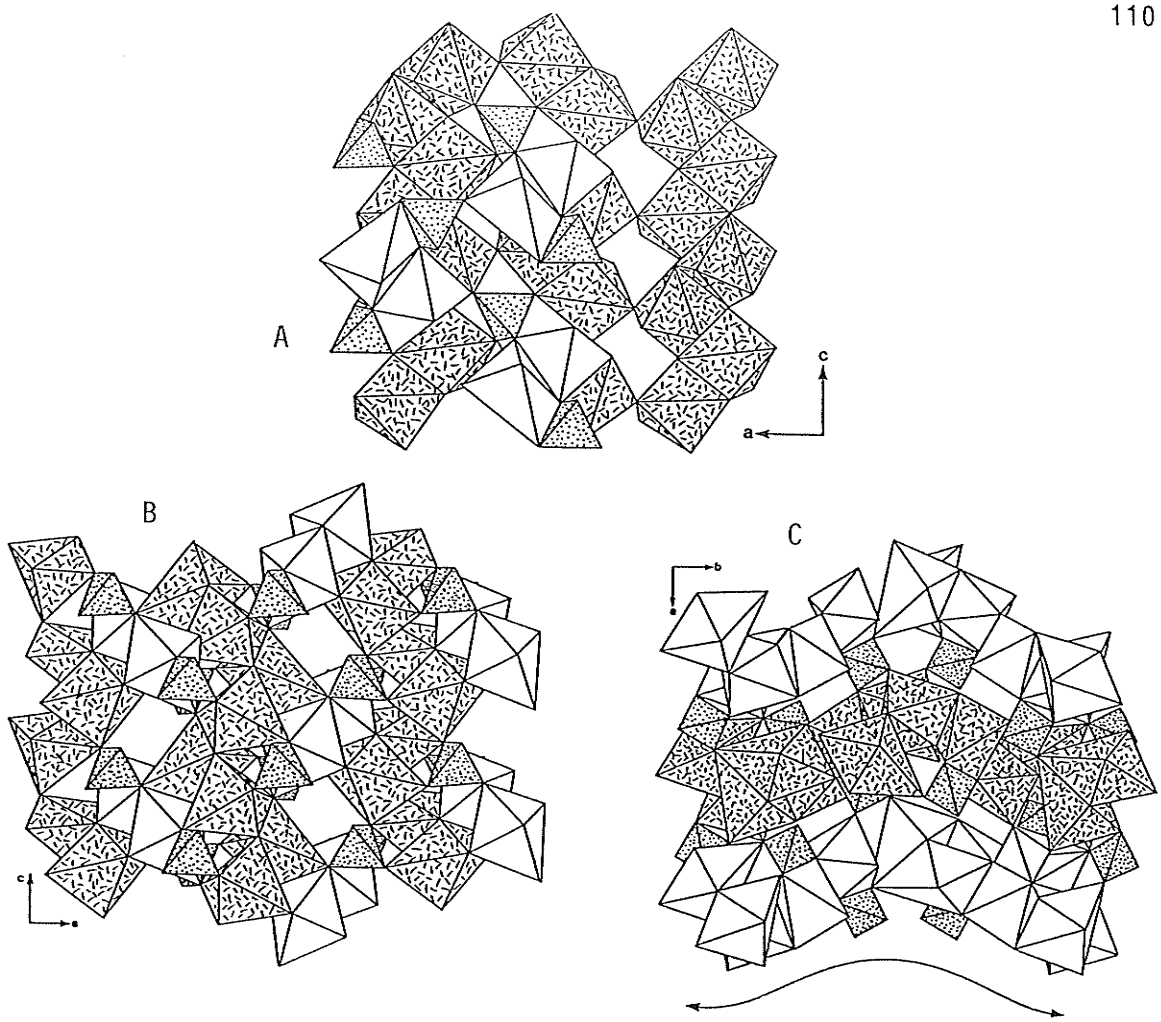

Figure 3.56: Structure of Cornetite. (a) chains of Cu(1) and Cu(2) octahedra (dashes) crosslinked by Cu(3) octahedral dimers (unshaded) & PO_4 tetrahedra (dotted); (b) edge-sharing between the dimers and chains along [010] to form complex layers; c) densely-packed modulated polyhedral layers. The modulation is commensurate with translational periodicity along [010] (wavey arrow); Only the middle polyhedral layer of octahedra is shaded for clarity.

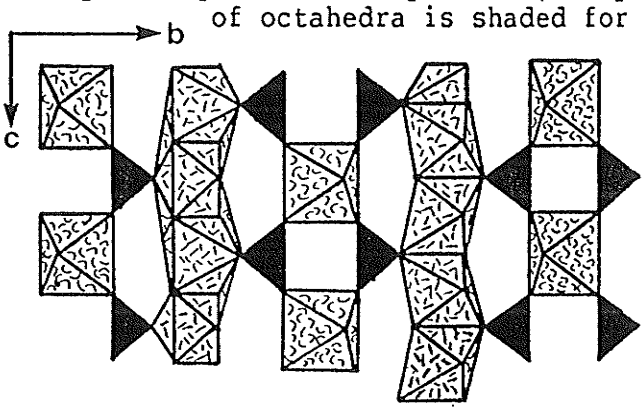

Figure 3.57: Structure of Derriksite. Sheets of Cu-octahedra (straight dashes), corner-linked to cornerlinking chains of SeO_3 (shaded) and UO_6 (curled dashes).

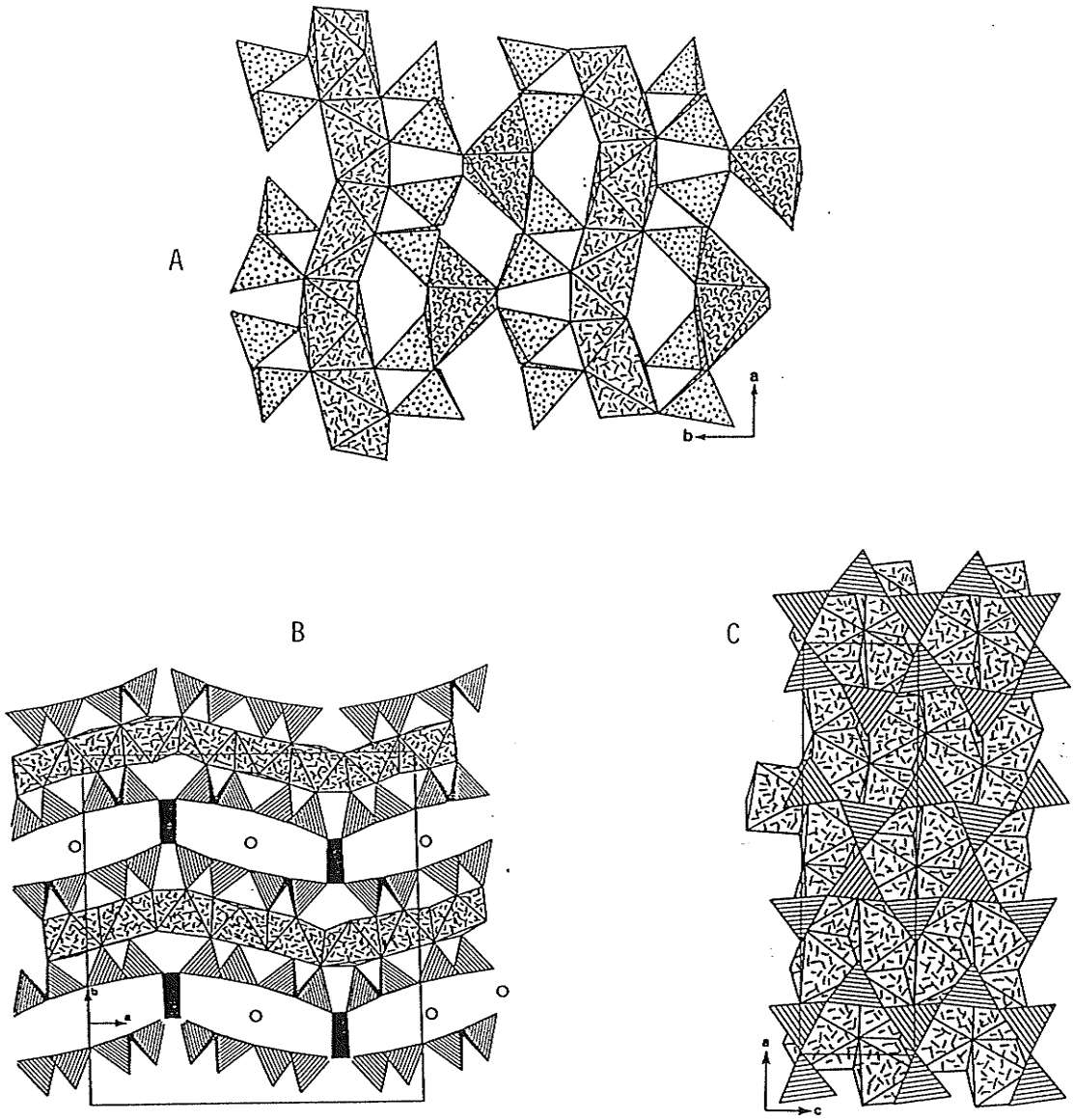

Figure 3.58: Structures of Shattuckite and Plancheite. (a) shattuckite with modulated t-o-t layers, crosslinked by solitary and very distorted Cu-octahedra (curled dashes); corner-linking silicate chains are pyroxene-like; (b) t-o-t layers in plancheite, crosslinked by both Cu-octahedra and H_2O; (c) amphibole-like silicate chains of plancheite.

linking the t-o-t layers together. Stronger equatorial Cu-O bonds are linked to the AsO_4 corners.

Synthetic $CuTeO_3$ is synonymous with balyakinite. Balyakinite is a complicated structure of distorted 3+1 Te-O coordinations and CuO_5 square pyramids which corner- and edge-share to form sheets parallel to (001), (Figure 3.60). Square pyramids share edges to form Cu_2O_8 dimers. Adjacent sheets are corner-linked together into a framework.

Salesite has an elegant structure for such a simple stoichiometry. Distorted IO_6 octahedra corner-share to form sheets of 1/2 cation occupancy (Figure 3.61a). These sheets are corner-linked to rutile-like Cu-chains. The packing of the sheets and chains has a HCP arrangement stacked on [100] (Figure 3.61b). Chain positions are staggered up the stacking sequence, and IO_6 octahedra occupy the positions above a layer of chains which are vacant in I-sheets below the chains (Figure 3.61a).

Veszelyite is made of two intricately polymerized types of sheets (Figures 3.62a,b). Edge sharing Cu-octahedra form eight-membered rings within their sheets. Zn and P tetrahedra alternate in corner-sharing 4- and 8-membered rings, forming tetrahedral sheets with half the polyhedra in each ring pointing up, the other half pointing down (linking to opposite octahedral sheets). This type of tetrahedral sheet is found in some framework silicates such as paracelsian and $BeAl_2Si_2O_6$, Ghose et al.(1974). The linkage of the tetrahedral and octahedral sheets is illustrated in Figure 3.62c,d.

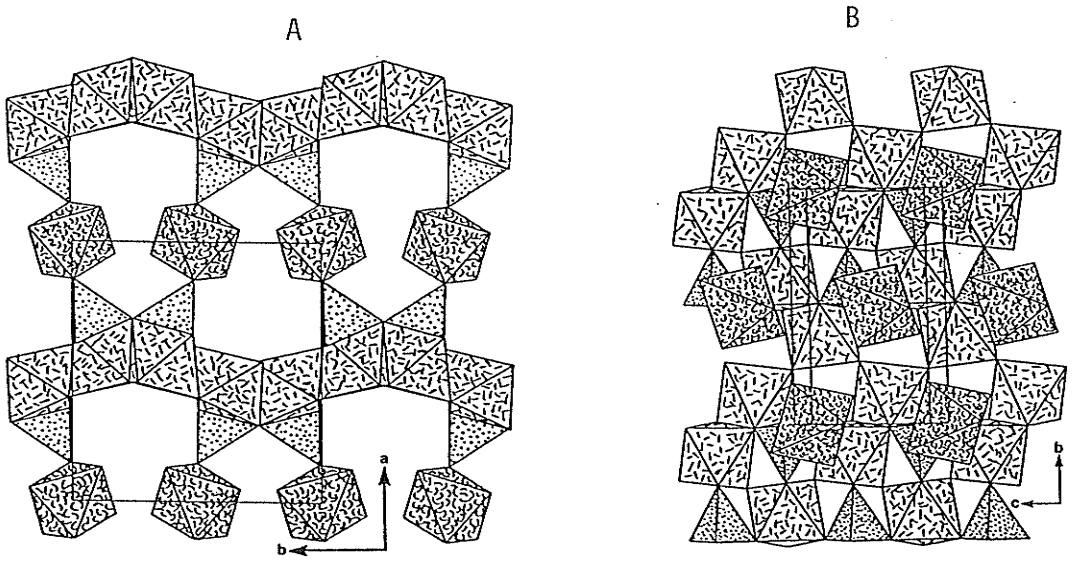

Figure 3.59: Structure of Arthurite. (a) t-o-t layers, crosslinked by CuO_6 octahedra (curled dashes); (b) corner-sharing sheet of Fe-octahedral dimers, and accompanying corner-sharing AsO_4 tetrahedra.

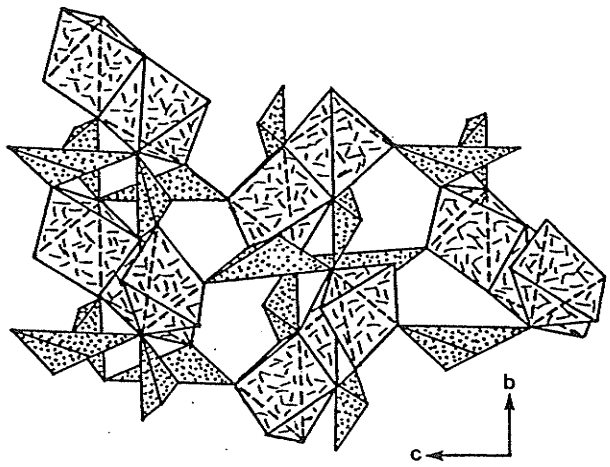

Figure 3.60: Structure of Balyakinite.
(3+1) Te-polyhedra and Cu_2O_8 dimers within a complex sheet.

A

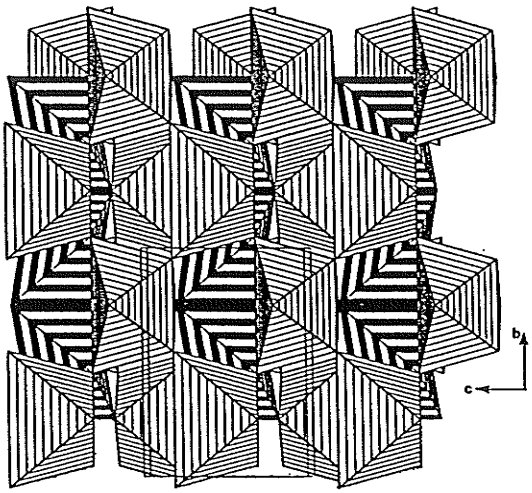

B

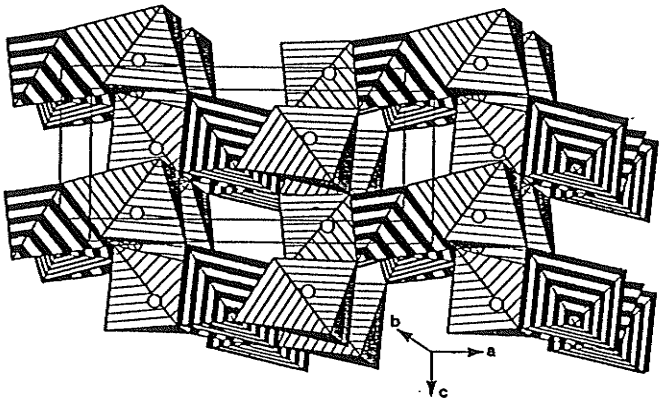

Figure 3.61: Structure of Salesite. (a) IO_6 corner-sharing octahedral sheet, and edge-sharing Cu-octahedral chains (banded); (b) packing sequence of the sheets and chains (HCP); Iodine octahedra have circles in figure (b).

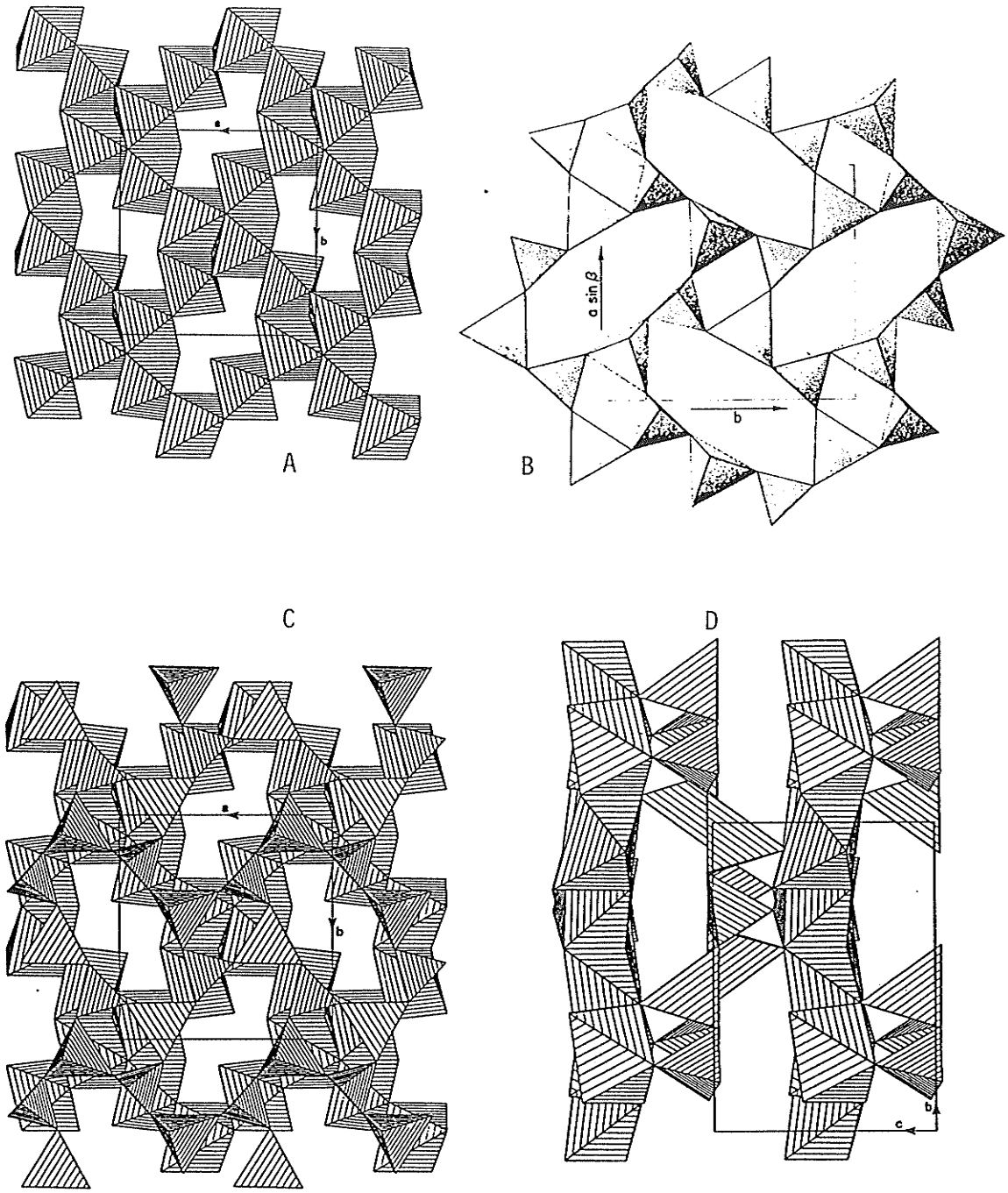

Figure 3.62: Structure of Veszelyite. (a) octahedral sheet; (b) tetrahedral sheet of alternating Zn and As cations; c) superposition of corner-linking sheets in figures a,b; (d) cross sectional view of layer linkage; (b) from Ghose et al.1974.

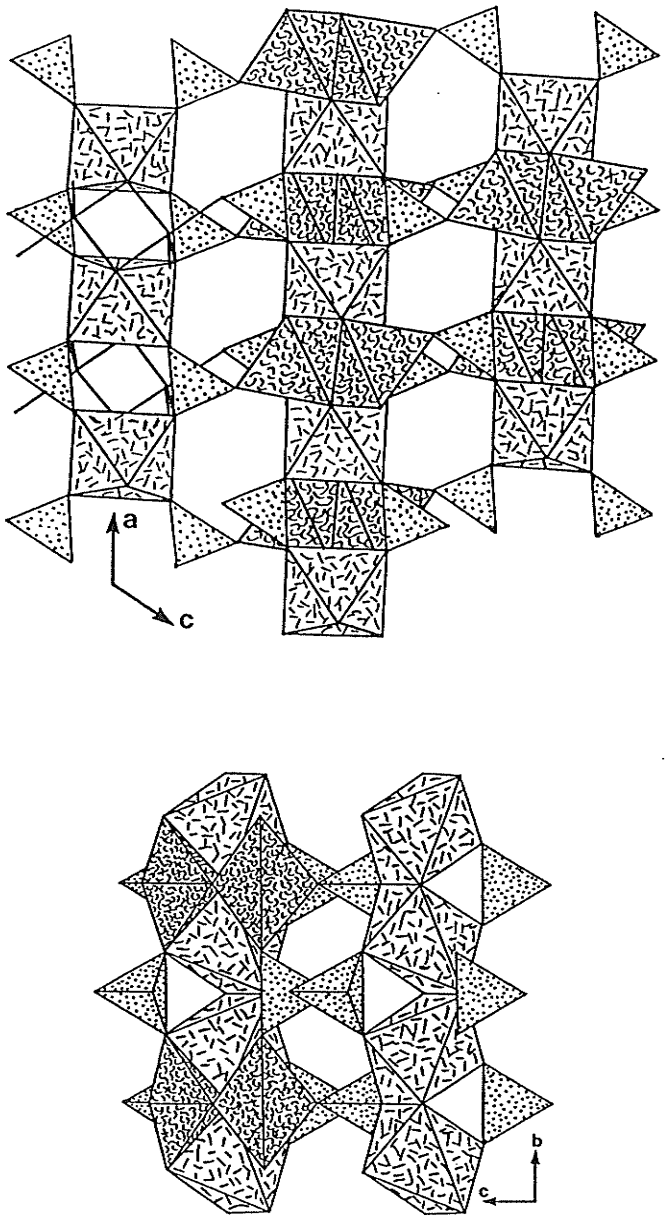

Figure 3.63: Structure of Dolerophanite. (a) mixed polyhedral sheets of rutile-type chains, trigonal bipyramidal dimers of Cu, and SO_4 tetrahedra; (b) conichalcite-type chains, with Cu_2O_8 dimers attached, forming dense sheets. are unshaded, and CuO_5 dimers are dashed.

Dolerophanite consists of rutile-type Cu-chains edge-sharing with Cu_2O_8 trigonal bipyramidal dimers to form mixed polyhedral sheets (Figure 3.63a). SO_4 tetrahedra crosslink adjacent sheets by corner-sharing with CuO_5 polyhedra. The SO_4 and CuO_6 chains of dolerophanite (Figure 3.63b) are identical to those of conichalcite (refer Figure 3.40d). Note how CuO_5 dimers fill the spaces between the tetrahedral-octahedral chains to form sheets. The trigonal bipyramidal dimers have taken different structural positions than in olivenite. Consequently, the connectivity between the tetrahedra and octahedra is different.

3.5.3 Category C: Complex Octahedral Frameworks

This category is composed of frameworks of octahedra that can be divided into subunits other than simple chains or sheets. The minerals in this category are in Table 3.9.

Zeolite-Like Frameworks:

Buttgenbachite and connelite are isomorphous structures made of a rigid octahedral framework with large cylindrical cavities (Figures 3.64a,b). Within the channels are complex oxyanions which distinguish the two end members: NO_3 for buttgenbachite, and SO_4 for connellite. There is some degree of substitution of nitrate for sulphate groups in these two minerals. Both structures have Cu sites at the cell origin with 0.5 cation occupancy, and due to symmetry constraints this Cu-octahedron does not show Jahn-Teller distortion. Connellite has a

TABLE 3.9

Category C: Complex Octahedral Frameworks

i. zeolite like -	
Buttgenbachite	$Cu_{19}Cl_4(NO_3)_2(OH)_{32}\cdot 2H_2O$
Connellite	$Cu_{19}Cl_4(SO_4)(OH)_{32}\cdot 3H_2O$
Lyonsite	$Cu_3Fe_4(VO_4)_6$
Dioptase	$CuSiO_2(OH)_2$
ii. spinel type -	
Atacamite	$Cu_2Cl(OH)_3$
Paratacamite	$Cu_2(OH)_3Cl$
iii. octahedral dimers & trimers -	
Bellingerite	$Cu_3(IO_3)_6\cdot 2H_2O$
Clinoclase	$Cu_3(AsO_4)(OH)_3$
Cu-Barbosalite	$CuFe_2PO_4{}_2(OH)_2\cdot 2H_2O$

novel [7]-coordinate Cu(3) site, with the longest apical H_2O group jutting into the channels and H-bonding to SO_4 tetrahedra; the wedge-shaped end pointing towards the cell origin. Buttgenbachite reportedly has a square-planar coordinated site instead of the 7-coordinate polyhedron in the isostructural connelite. However, it seems reasonable that Cu(3) is pup-tent shaped (without the apical bond towards the channel) rather than square-planar, because the framework isostructural with connellite.

Lyonsite is an interesting Cu^{2+} oxysalt mineral, with novel Cu-coordination features. The structure consists of rings made from HCP oxygens of FeO_6-VO_4 polyhedra (packed on 001), which form tubular units (Figure 3.65a). These tubular polyhedral columns are crosslinked by

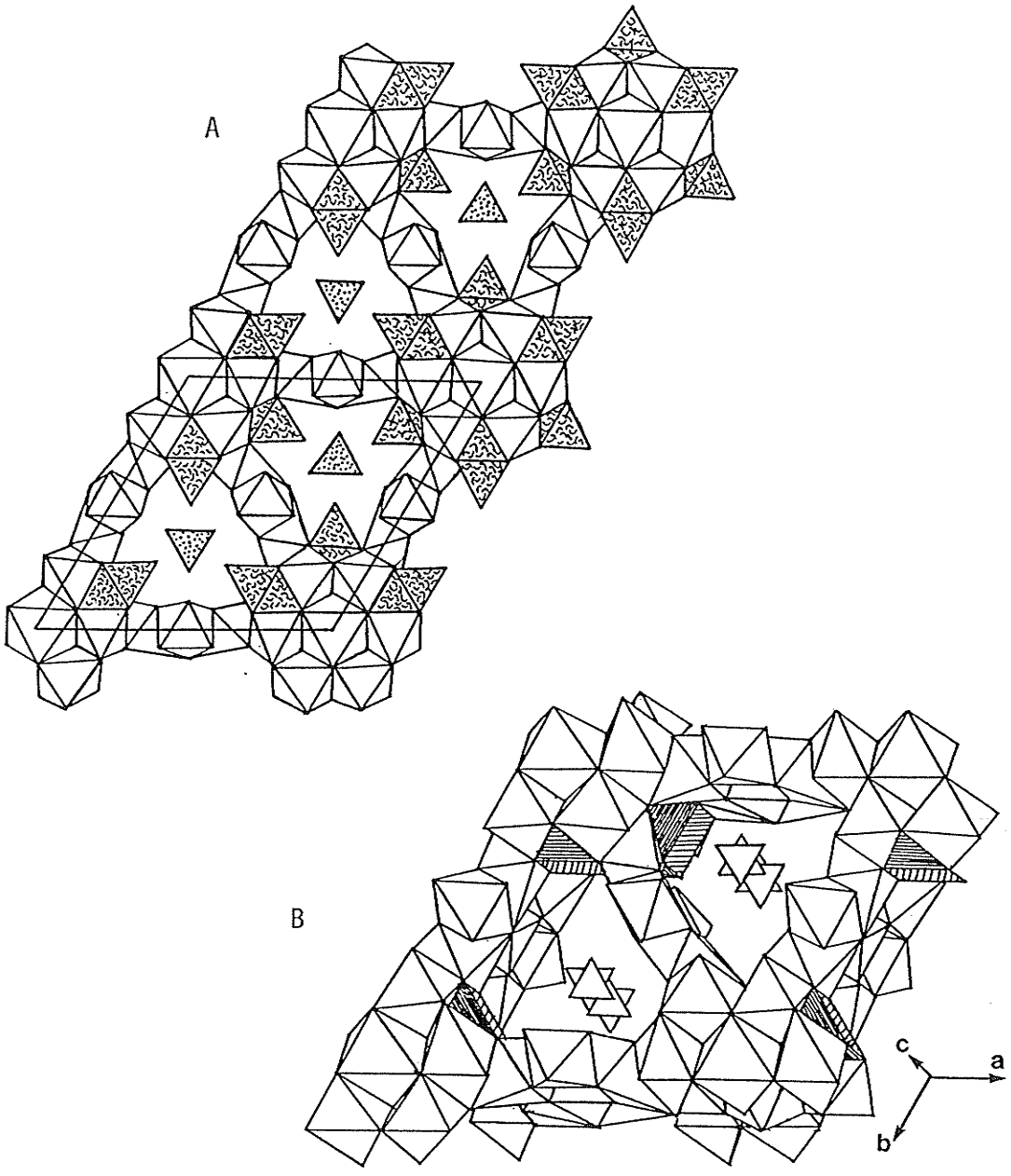

Figure 3.64: Structures of Buttgenbachite and Connellite. (a) framework of connellite, with 7-coordinate polyhedron (dashed) pointing towards the SO_4 tetrahedra; (b) buttgenbachite framework with NO_3 planar triangles in the channels, and a tent-shaped CuO_6 polyhedron instead of CuO_7.

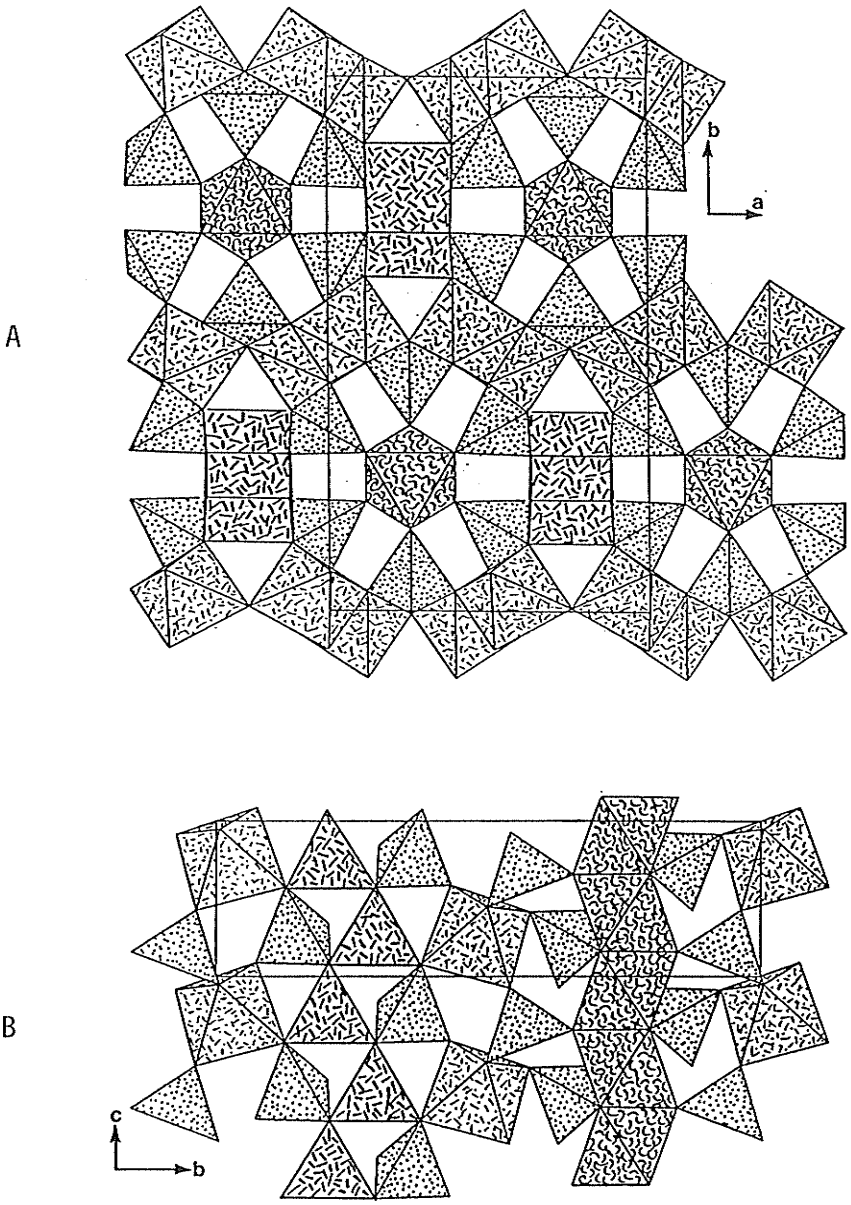

Figure 3.65: Structure of Lyonsite. (a) an elegant framework of FeO_6 octahedral-VO_4 tetrahedral rings (FeO_6 dotted & dashed). Regular shaped Cu-octahedra on two-fold axes occupy the centre of the columns (curled dashes); (b) chains of trigonal prismatic CuO_6 connect adjacent columns, and face sharing Cu-octahedral chains fill the columns (trig. prisms straight dashes).

edge-sharing chains of 4+2-cis trigonal prisms of CuO_6 (Figure 3.65b). The 4+2-cis polyhedron is very similar to that of buttgenbachite. Within the tubular columns are chains of face sharing Cu(1) octahedra (Figure 3.65b). The Cu(1) octahedron does not exhibit the J-T distortion. This position is reportedly only half occupied (Hughes et al., 1987), suggested by stoichiometric considerations and unique thermal vibrational data. Adjacent Cu(1) sites are only 2.455Å apart, and suggest that special conditions, such as positional disorder, are necessary for stability, and are more favorable without the static Jahn-Teller distortion.

Dioptase has an intricate framework of spiralling and winding octahedral chains, corner-linked to Si_6O_{18} tetrahedral rings which occupy the large framework cavities (Figure 3.66a). Within the rings are ordered arrays of H_2O groups (Figure 3.66b). The tetrahedral rings stack along the diagonal of the unit cell. Ribbe et al.(1977) considered Cu to be in [5]-coordination, but clearly the sixth Cu-O bonds are within a reasonable distance, producing fairly regular-shaped polyhedra. The interpretation of silicate rings within a framework of CuO polyhedra is not realized when considering Cu as [5]-coordinate.

Spinel-Type Frameworks:

Atacamite and paratacamite are polymorphs of botallackite. Their structures are radically different from botallackite, and consist of octahedral frameworks that are essentially a spinel-type skeleton

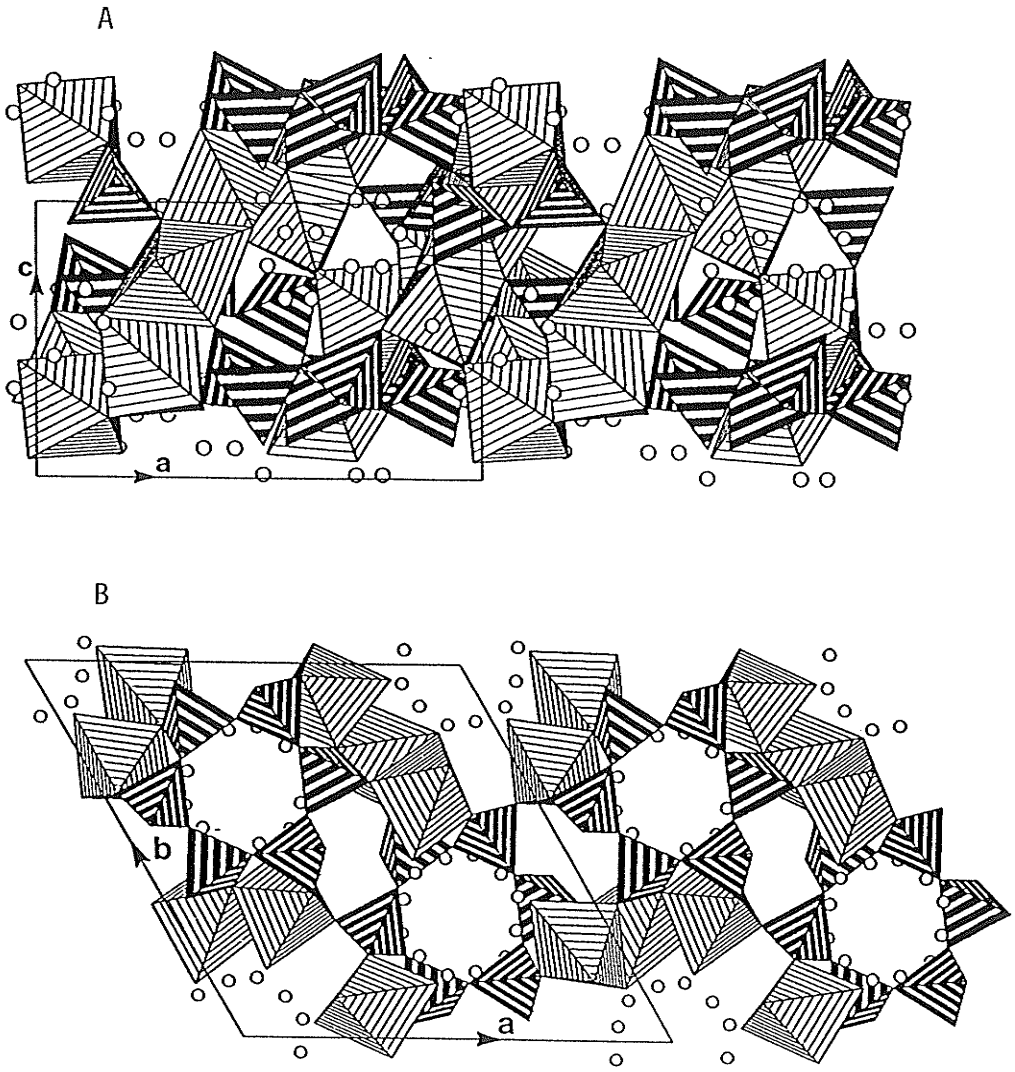

Figure 3.66: Structure of Dioptase. (a) winding octahedral framework with silicate rings in cavities; (b) looking down on the silicate rings, we see an orderly arrangement of H_2O groups (open circles are hydrogens).

structure without tetrahedra. Atacamite and paratacamite are only subtley different, due to slight symmetry differences. The anions are in CCP arrangement, seen from the perspective of cross-linked layers of hexagonal octahedral rings (Figure 3.67a). We can also view the structure from the perspective of interpenetrating octahedral chains (Figure 3.67b) which can be considered as rod packings of half occupancy in perpendicular directions. An oblique view of the framework (Figure 3.67c) shows structural corrugation of the layers parallel to (001), due to prominent J-T distortions. The higher symmetry of paratacamite (hexagonal) is due to the geometrical requirements of 1/4 of the octahedra, which link together the layers along (001). One-sixteenth of the copper is constrained to adopt a non-distorted configuration of six equal Cu-O bond lengths (at the cell origin). Three-sixteenths of the Cu-octahedra have reverse (2+4) symmetry, also a result of symmetry constraints. Orthorhombic atacamite has only the normal (4+2) J-T distortions, because the lower symmetry allows the electronic relaxation of the J-T distortion throughout the structure. Figure 3.67d shows the atacamite framework with a different distortion pattern from that of paratacamite in Figure 3.67c.

Octahedral Dimers and Trimers:

Bellingerite consists of edge-sharing Cu-octahedral dimers and solitary Cu-octahedra, each surrounded by IO_5, IO_6 and IO_7 polyhedra to form a framework (Figures 3.68a,b). The mixed coordinations of I^{5+} polyhedra lead to a low symmetry arrangement, because of the variability in the style of polymerization.

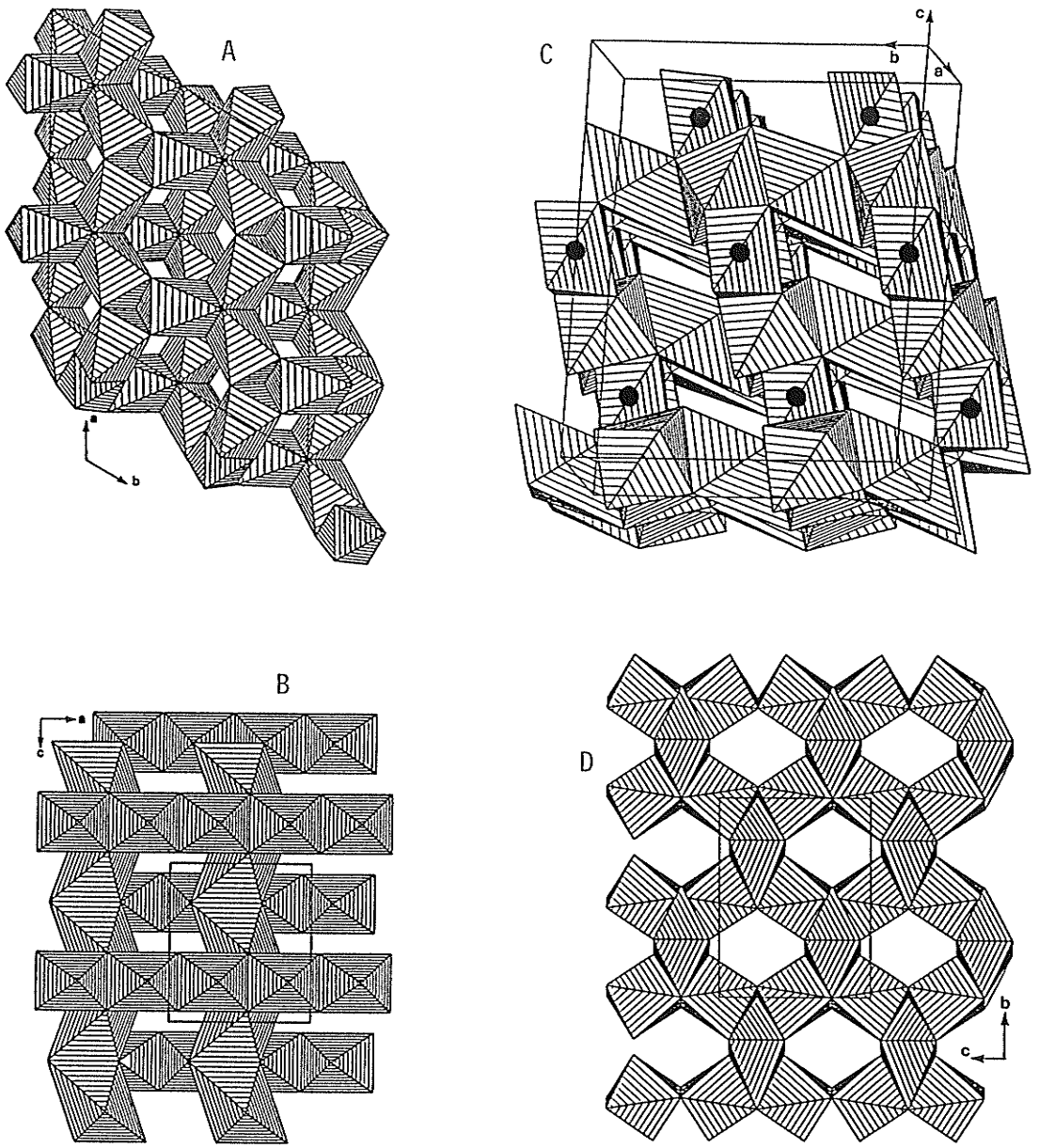

Figure 3.67: Structures of Atacamite and Paratacamite. (a) CCP array of anions looking down hexagonal octahedral layers that are crosslinked by octahedra on symmetry elements; (b) rodpacking of distorted chains with 1/2 cation occupancy in two directions; (c) oblique view of paratacamite with symmetrically constrained octahedral sites at symmetry elements (with circles); (d) atacamite framework with full (4+2) J-T distortion in all octahedra.

Clinoclase is a complicated structure made of edge-sharing CuO_5-CuO_6 dimers and edge-sharing Cu_2O_8 dimers corner-sharing together, and corner-linked by AsO_4 tetrahedra into a complex polyhedral framework (Figures 3.69a,b). Although the [5]-coordinate polyhedra have nearby sixth oxygens, the bond angles for octahedral coordination are extremely distorted, and bond-valence contributions are minimal. With this in mind, there is also no topological advantage to describing the Cu as octahedral. The structural linkage is complex, and quite different from the rest of the oxysalts, whose polymerizations are readily described and related to one another. Crystals of clinoclase cleave into sheets, and there is a layered aspect to the polyhedral arrangement on [010].

The structure of a recently described mineral, now called hentschellite, has been solved by Sieber (1985), and is part of the lazulite-scorzalite-barbosalite series (Mg-Al;Fe-Al;Fe-Fe respectively). It has a Cu-barbosalite composition, with monoclinic symmetry ($P2_1/n$) as opposed to the tetragonal symmetry of barbosalite. The loss of holosymmetric coordination around Cu^{2+} is probably the cause of the lowering from tetragonal symmetry in Fe-barbosalite. The structure consists of face-sharing trimers of Al-Cu-Al, densely packed into a network by corner-sharing to each other and to PO_4 tetrahedra. Figures 3.70a,b show the complicated polyhedral arrangement of hentschelite along two different axes.

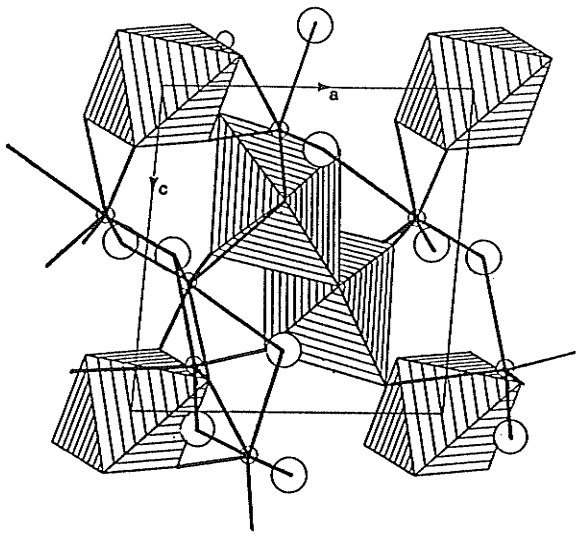

Isolated Cu-octahedra and edge-sharing dimers surrounded by I-polyhedra forming a framework.

Figure 3.68: Structure of Bellingerite.

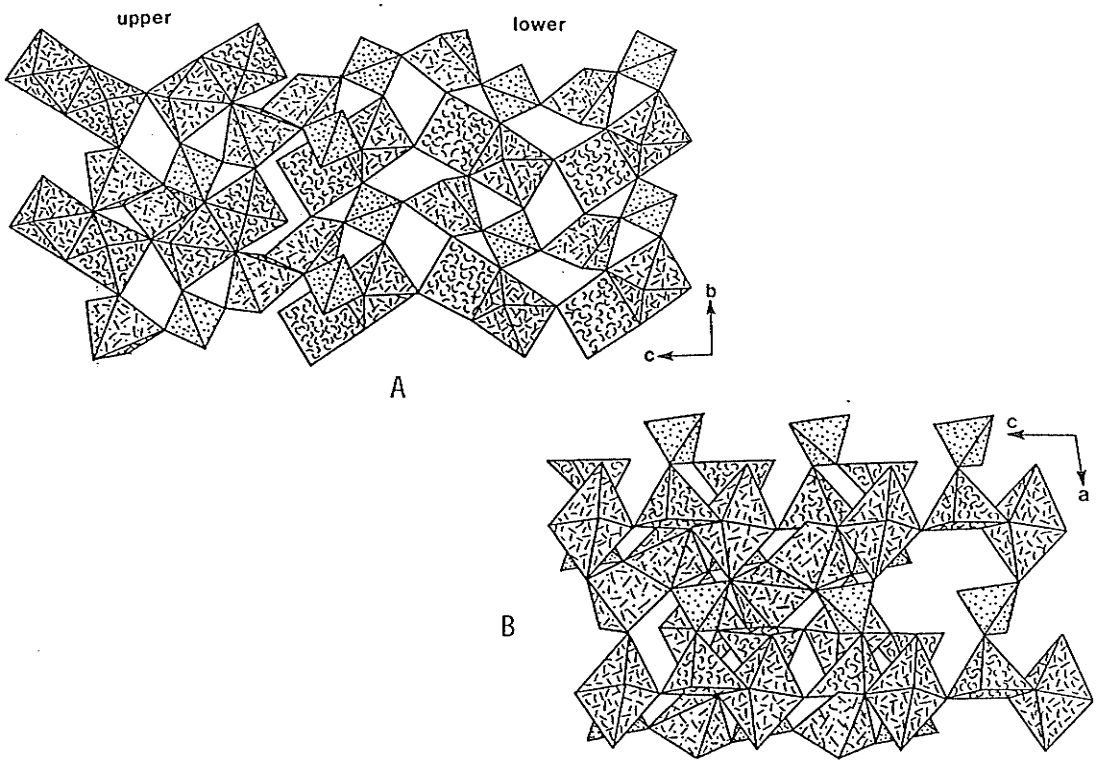

Figure 3.69: Structure of Clinoclase. (a) & (b) two perpendicular views of the dimeric framework; square pyramids have curled dashes, octahedra have straight dashes, tetrahedra dotted.

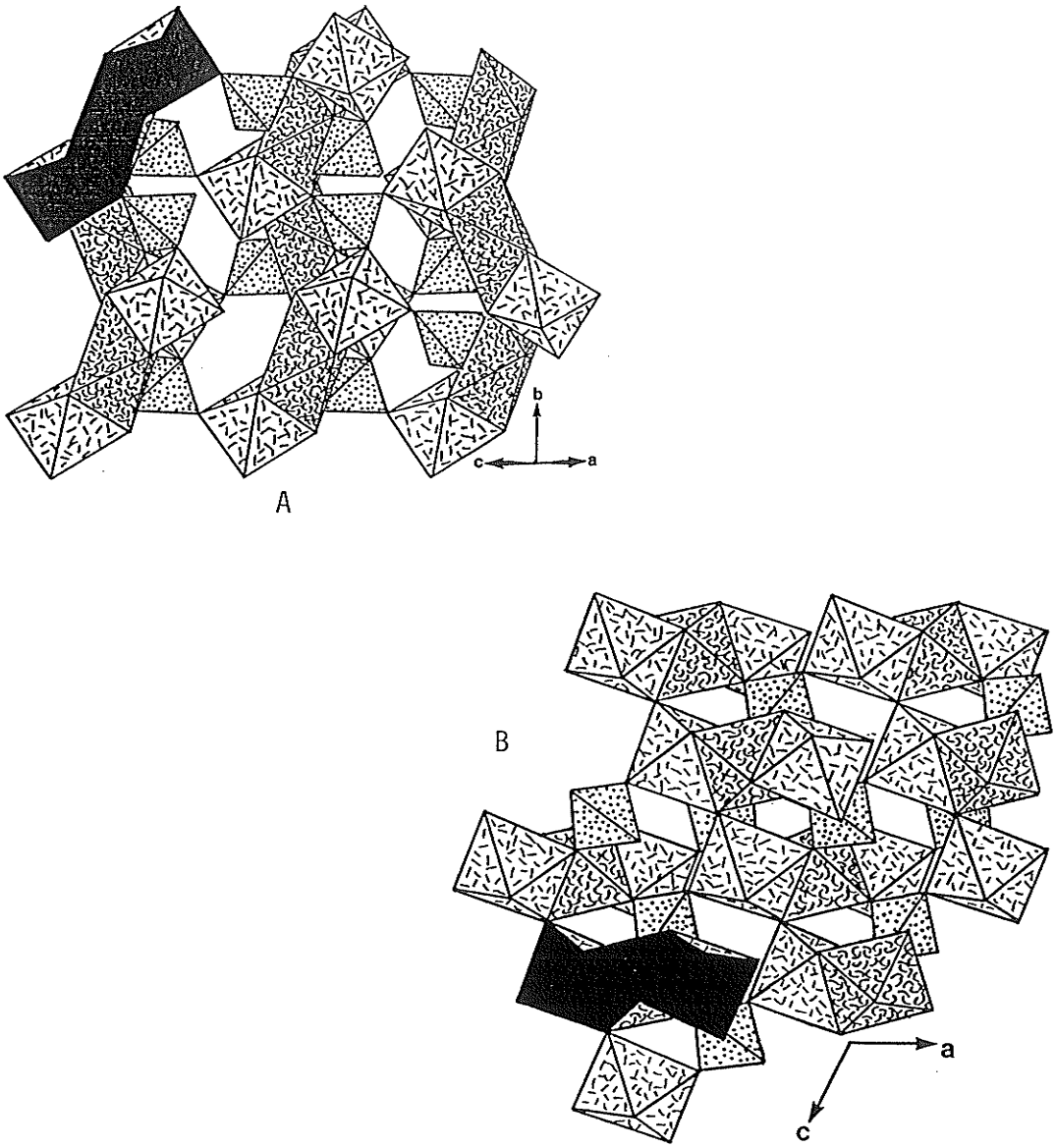

Figure 3.70: Structure of Hentschelite. (a) looking across the face-sharing trimers (Fe-Cu-Fe), linked by PO_4 tetrahedra and corner-sharing into a framework; (b) looking down on the trimers, notice the chain-like array. The connectivity is much more complex than corner-sharing chains; Fe-octahedra have straight dashes, Cu-octahedra have curled dashes. Several trimers are blackened for emphasis.

3.6 SUMMARY

When considering the total connectivity of the Cu^{2+} oxysalt structures, by incorparating the full coordination of Cu^{2+}, one finds that these structures are not enigmatic. Rather, there are many topological similarities between Cu^{2+} oxysalts and non-Cu oxysalts, which were not previously evident. It is apparent that all oxysalt structures afford the same possibilities for description with heteropolyhedral representations. The features that give Cu^{2+} oxysalts their unique structural character will now be explored; starting with an in-depth look at the Jahn-Teller distortion around Cu^{2+}.

Chapter IV

THE JAHN-TELLER EFFECT AND LOCAL Cu^{2+} ENVIRONMENT

4.1 A DETAILED EXPLANATION OF THE JAHN-TELLER EFFECT

Distortions of Cu^{2+}-ligand polyhedra are a small part of what is predicted by the Jahn-Teller theorem. Jahn & Teller (1937) proposed a general theorem for the distortion of molecular systems. The energy of a distorted molecule can be described by the power expansion series:

$$E(S_i) = E^{\circ} + F_i S_i + \frac{1}{2} F_{ii} S_i^2 + \frac{1}{6} F_{iii} S_i^3 + \cdots \qquad (4.1)$$

where S_i is a coordinate of the molecule, along which we may describe a distortion; E^0 is the energy of the undistorted geometry; the other parameters $F_{i,ii,iii}$ are the energy derivatives (Burdett, 1980). $F_i S_i$ describes the first-order Jahn-Teller term involving orbital degeneracy; $(1/2)F_{ii}S_i^2$ is the second-order Jahn-Teller term, involving more subtle forces associated with spin phenomena of the electrons (F_{ii} is the vibrational force constant); F_{iii} is the cubic anharmonicity. It is the first-order Jahn-Teller term which is significant in this discussion of Cu^{2+} (with a d^9 orbital degeneracy).

Jahn & Teller (1937) showed that any non-linear polyatomic molecule with an electronic orbital degeneracy is unstable, and must undergo distortion. The distortion is spontaneous, and relieves the molecule of its instability by a lowering of symmetry that results in orbital energy splitting of the degenerate state. The degenerate state

necessarily entails a symmetrical coordination environment about the central atom (in this case, a cation). This symmetrical ligand field is unstable because of its interaction with the unsymmetrical electronic configuration (degenerate) of the central atom. In a linear molecule, stability and degeneracy are simultaneously possible, and distortion is not required. However, for higher coordinations, stability and degeneracy are not compatible, and a spontaneous distortion occurs.

The Jahn-Teller theorem does not predict the geometrical nature of the distortion, nor its magnitude. The configuration with the lowest overall energy should be the favored geometry of equilibrium (Cotton & Wilkinson, 1972). In free molecules, the distortion is resonant, and called the dynamic Jahn-Teller effect. Resonance occurs because of the unrestricted nature of free molecules, with the bond lengths continually changing to establish an average state of lowest energy. Conversely, in crystalline solids, the most stable configuration is usually preserved in the static state. This is called the static Jahn-Teller effect, and it is this form of the Jahn-Teller theorem which concerns our study of oxysalt minerals. It is hereafter assumed that reference to the Jahn-Teller effect is to the static Jahn-Teller distortion.

Details of the Jahn-Teller (J-T) distortion in Cu^{2+} compounds are readily understood with the use of ligand field theory. In a holosymmetric octahedral ligand field, the d-orbital energies of the central cation are split into T_{2g} and e_g levels (Figure 4.1), due to their interaction with the ligand field. Being of lower energy, the T_{2g}

orbitals are more fully occupied, and the e_g orbitals receive the remaining d-electrons. There are two important points here:

1. One e_g orbital is occupied by two (spin-paired) electrons, and the other e_g orbital is occupied by one electron.
2. The two e_g orbitals are energetically degenerate.

This means that a splitting of the e_g orbitals must result in a lower energy. As the energy of the electrons in the spin-paired orbital decreases with an increase in cation-ligand distance towards that orbital, the energy of the electron in the singly-occupied orbital increases with a corresponding shortening of the cation-ligand distance. A net lowering of energy results, and is the driving force for the Jahn-Teller distortion (the amount E-stabilization in Figure 4.2). The change in bond lengths results in a lowering of symmetry. The symmetrical configuration is thus of a higher energy than an unsymmetrical configuration, and is hence unstable with respect to geometrical distortion (which occurs spontaneously). The instability of d^9 degeneracy is therefore removed by octahedral distortion, because of a net stabilization energy. This e_g orbital splitting is secondary to the general case of octahedral stabilizations (Figure 4.1). No net stabilizations occur in the T_{2g} orbitals because of balanced energy shifts by the fully spin-paired orbitals. Minor secondary adjustments of the T_{2g} orbital energies also occur, but are much lower in energy than e_g (not drawn to scale in Figure 4.1).

The nature of the distortion is not predicted by the J-T theorem, but if we consider which orbital is singly occupied, we can predict the

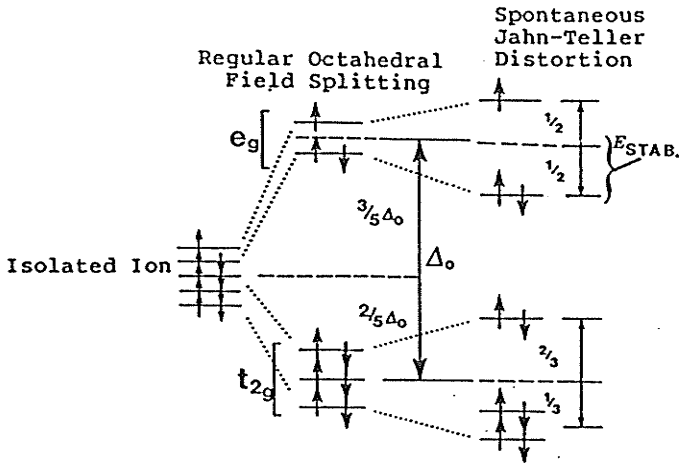

Figure 4.1: Octahedral Field Splittings. Orbital energy states for different environments of d^9 transition-metal complexes in: the isolated ion; the non-degenerate complex; and the degenerate Jahn-Teller distorted Cu^{2+} complex.

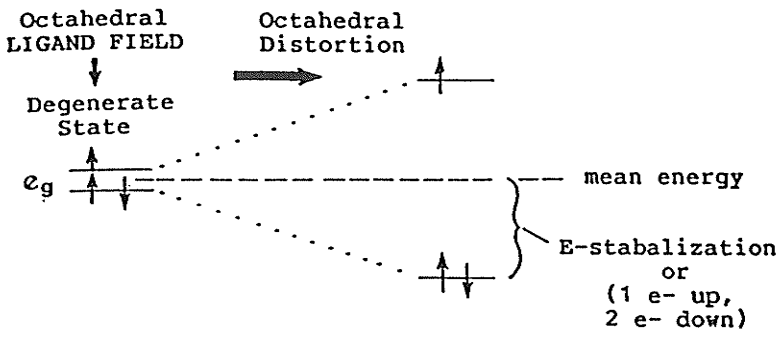

Figure 4.2: Net Stabilization Energy in the e_g Orbitals. The driving force for Jahn-Teller distortion.

type of distortion. A half-filled dx^2-y^2 orbital will cause less shielding of the ligands along the x- and y- axes, relative to the z-axis. The equatorial Cu-ligand bonds will therefore contract, and in response to equilibrium requirements, the co-linear bonds along z will proportionately lengthen (called a (4+2) distortion). Alternatively, if the dz^2 orbital is half occupied, the co-linear bonds along z are less shielded, relative to dx^2-y^2, and the two bonds along z shorten. The equatorial bonds simultaneously lengthen, and a compressed octahedron is the result (termed 2+4). Both of these J-T distortion models are ideal tetragonal distortions, represented by the secondary field splitting in Figure 4.1.

Opik & Pryce (1957) showed that (4+2) distortions have a marginally greater stability than (2+4) distortions, due to their accompanying second and third-order J-T terms (see equation 4.1). The rarity of the (2+4) octahedron supports their conclusion.

For tetrahedral ligand complexes (also of cubic symmetry), T_{2g} orbitals interact directly with the ligands, and e_g orbitals are between the ligands (Figure 4.3a). With Cu^{2+}, degeneracy of the cubic ligand field is lifted by a tetragonal distortion of the tetrahedral complex. The resulting field splitting is quite different from the octahedral distortion (Figure 4.3b). Helmholtz & Kruh (1952) report tetrahedral coordination in Cs_2CuCl_4. The tetrahedron is flattened, removing the 3-fold symmetry axis. This is called a T1 distortion by Dunitz & Orgel (1957). Miyahira & Ohinshi (1956) established that

$c/a<1$ in $CuCr_2O_4$ (synthetic spinel), and is consistent with T1 flattening of the CuO_4 tetrahedron (Dunitz & Orgel, 1957). T1 & T2 (T2=elongated tetrahedral) distortions are exclusive to certain d-orbital states (Figure 4.4). No more will be said about tetrahedral J-T distortions of Cu^{2+}, because no Cu oxysalt minerals (found so far) have Cu^{2+} in tetrahedral coordination.

Any transition-metal complexes with octahedral or tetrahedral coordinations and half-filled d-orbitals should show the J-T effect. High-spin Cr^{2+} and Mn^{3+}, and low spin Co^{2+} and Ni^{2+} show octahedral and tetrahedral distortions. Mn^{3+}, the most abundant of these cations in mineralogy, has been well-recognized in more recent studies for displaying the J-T distortion, e.g. Moore & Araki (1974), Dunn et al. (1987).

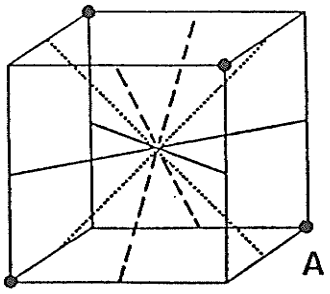

Showing the symmetrical relationship of the d_{xy}, d_{xz} and d_{yz} orbitals which form the triply degenerate t_2 orbital in a tetrahedral complex.

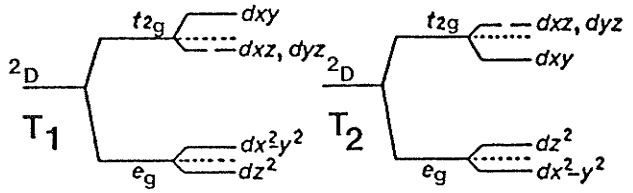

B Splitting of d orbital energy levels in a regular tetrahedral field and in tetragonally distorted fields with $c/a < 1$ (left) and $c/a > 1$ (right). These distortions may be described as flattening or elongation respectively of the tetrahedron along an S_4 axis.

Figure 4.3: Tetrahedral Ligand Field Splitting from Dunitz & Orgel (1957)

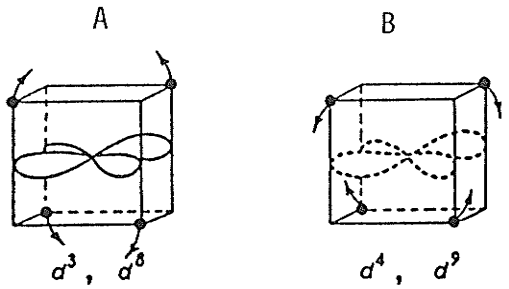

Effect of (a) a single electron in the t_2 orbital (T_2 state), (b) a single hole in the t_2 orbital (T_1 state) on the stereochemistry of a tetrahedral complex. Only tetragonal distortions are considered.

Figure 4.4: T_1 & T_2 Distortion Types from Dunitz & Orgel (1957)

4.2 THE COORDINATIONS OF Cu^{2+}

Cu^{2+} assumes a variety of coordination geometries in oxysalt mineral structures (Figure 4.5). A reaction path series is outlined in Figure 4.5, and is established throughout this chapter. Because minerals are the most stable chemical compounds, we must assume that the degeneracy of Cu^{2+} has been lifted in the oxysalt structures to a suitable degree of equilibrium. Recall that the nature of the J-T distortion in crystals is static, but the specific geometry of the J-T distortion is not prescribed. As the orbital degeneracy is lifted, Cu^{2+} coordination geometries need to conform to bond-valence theory and the topological/geometrical constraints of the crystalline environment. The driving force for polyhedral distortion must therefore operate within structural constraints.

Differentiating between coordinations is usually based on simple geometrical criteria and bond-valence theory. However, the application of both factors is not always straight forward. Recall, stringhamite has two different copper positions which border on octahedral and square planar. Bond-valence sums on Cu(2) and O(2) suggest that Cu(2) could be considered as an extremely distorted octahedron, with the apical bonds 3.06Å in length (2x0.035v.u. contributed). However, Cu(1) has two oxygens 3.38Å away from it, and these are too long to be considered significant (only 0.02v.u. per apical bond). Stranskiite and agardite test the limits of bond length significance (around 3.15Å). However, as in teinite, the assignment of octahedral coordination with "bonds" >3.20Å helps to relate the structure to another. The cutoff for

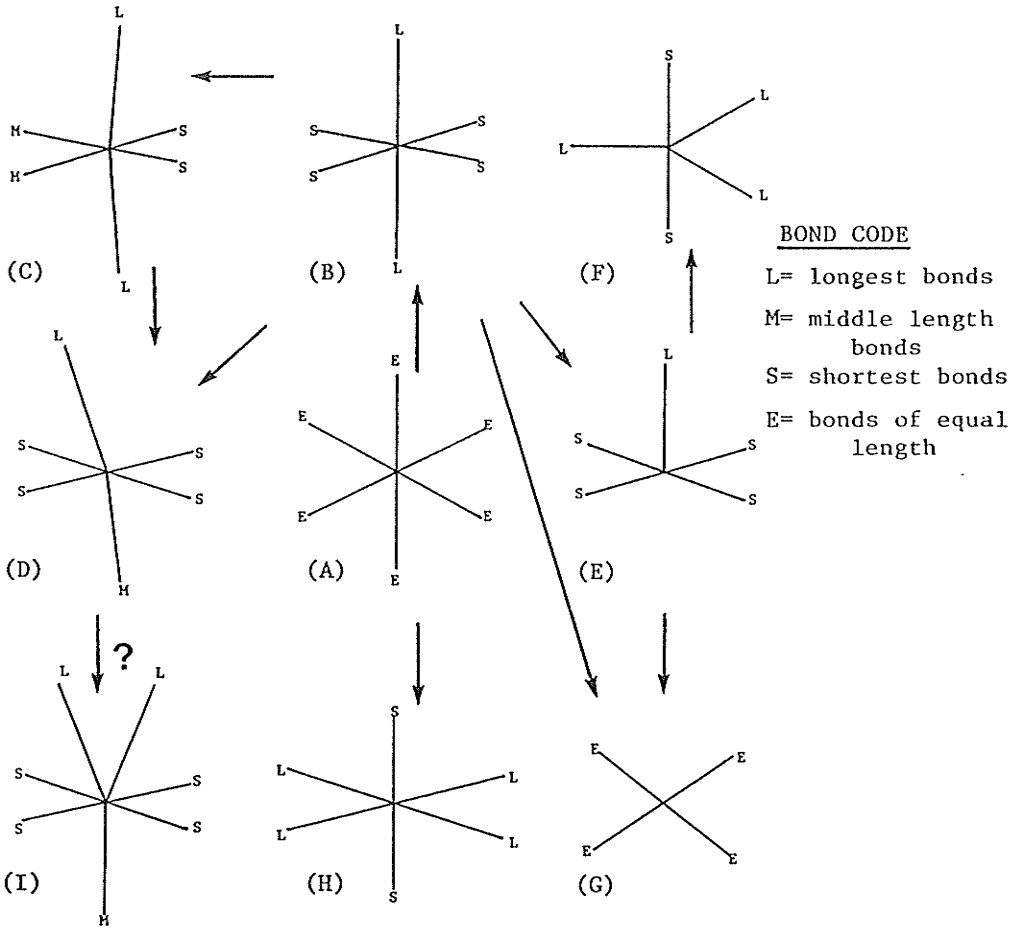

Figure 4.5: Coordination Types for Cu^{2+}. The varieties of Cu-polyhedra, as derived from the regular octahedron, are presented as a multi-path reaction series. (a) regular octahedron of six equal bond lengths and a 6-axis; (b) tetragonally distorted (4+2) octahedron, derived from a; (c) non-tetragonal (2+2)+2 distortion, non-centrosymmetric, derived from b; (d) non-tetragonal 4+1+1 distortion, non-centrosymmetric, from b; (e) square pyramidal 4+1, derived from non-tetragonal distortion of b; (f) trigonal bipyramidal 2+3, derived from either b or e; (g) square-planar, 4 equal bond lengths, extreme distortion of e (or b); (h) tetragonally distorted (2+4) (reverse) octahedron, from a; (i) non-tetragonally distorted 4+1+2 capped octahedron, from d.

including very long apical bonds is somewhat arbitrary. Bond-valence theory does not support or deny the validity of including these longest bonds, because they are so weak. Their significance lies purely in the better description of certain structures. If including a distant sixth oxygen helps to relate the Cu^{2+} structure to another, it is significant. If a sixth-nearest oxygen does not exist, then the cation is [5]- or [4]-coordinate.

Bond angles also play a role in determining the coordination of Cu^{2+}. Bond angles in stringhamite, between the apical and equatorial oxygens of Cu(2), allow the assignment of octahedral coordination (O2-Cu-O4=60.5°). Those in Cu(1) stretch past the limits of practicality (O3-Cu-O2=53.1°), making an octahedral coordination unrecognizable and inconvenient. Cu(1) is therefore square planar. Azurite also stretches the limit of bond angles allowed for octahedral coordination of Cu(2) (apical-equatorial=73.5°). Bond-valence theory suggests that the apical bond to Cu(2) is significant, completing the octahedral coordination. Cu(1) in azurite has an oxygen within 3.00Å of its square planar coordination. But a bond angle of 48.1° (O2-Cu-O1), and lack of contribution to the bond-valence sums, indicates that Cu(1) is square planar.

Discriminating between trigonal bipyramidal and square pyramidal coordinations is discussed in part 4.2.2. Most of the Cu polyhedra are not borderline cases. Bond angle and bond length data usually indicate distinct coordination types, regardless of the J-T distortions superimposed on the polyhedra.

4.2.1 Octahedral Coordinations

Octahedral coordination is by far the most common type of Cu^{2+} polyhedron in the oxysalt minerals. Examples of octahedral geometry in Figure 4.5 are only some of the forms found in Cu-structures. Table 4.1 lists geometrical and related structural data for all symmetrically distinct octahedra in the Cu oxysalts. Many variations of (4+2) distortion are observed. In fact, the ideal tetragonal distortion (the model described by Figure 4.1) is very rare.

In the Cu^{2+} oxysalt minerals, all bonds to Cu^{2+} are from O^{-2}, OH^-, H_2O, and Cl^-. There were no observed correlations between the type of oxygen ligand and octahedral geometry, so no distinctions were made between oxyanion types in Table 4.1. All bonds to Cl^- are labelled. The coding of the coordinations is based on bond lengths. 4+2 means that the short equatorial and longer apical bonds are in two distinct groups, each with bond length variations <0.06Å. The other coordinations are variations of this basic type of J-T distortion. 4+1+1 means the apical bonds differ more than 0.11Å in length, but are still appreciably longer than the equatorial bonds. Bond groups within parentheses (x+x) indicate bonds which differ by 0.06-0.11Å. eg. (2+2)+2 means the equatorial bonds are paired in length, and these pairs differ 0.06-0.11Å. Numbers in square brackets [x+x] designate equatorial bonds which differ significantly in length, but are still much shorter than apical bonds. The column labelled Δ indicates polyhedral distortion, and the column BVS indicates the bond-valence sum on Cu^{2+}.

TABLE 4.1

Geometrical Parameters for $Cu^{2+}O_6$ Octahedra

Mineral	Cu(#)	Coordination	<Cu-O> (Å)	Δ (x10³)	BVS	Other	
Isolated Polyhedral Structures							
aubertite		4+2	2.097	9.8	2.12	C	
cyanochroite		[2+2]+2	2.100	4.7	1.97	C	
Tutton's Salts		(2+2)+2	2.090	2.7	1.96	C	o
henmilite		4+2	2.318	52.2	2.00	C	
Chain Structures							
chalcanthite	(1)	4+2	2.107	8.6	2.05	C	
	(2)	4+2	2.109	11.8	2.14	C	
krohnkite		4+2	2.215	12.9	2.14	C-M	
chalconatronite		4+1+1	2.138	12.8	1.96	N	
chlorothionite		(2+2Cl)+2Cl	2.430		2.07	N-M	o
eriochalcite		(2+2Cl)+2Cl	2.433		1.95	N-M	o
chloroxiphite		4+2Cl	2.314		1.91	C	o
caledonite		4+(1+1)	2.128	8.6	1.92	N	
linarite		4+2	2.147	16.6	2.06	C	
schmeiderite		4+(1+1)	2.175	19.2	1.97	N	
vauquelinite	(1)	[2+2]+2	2.067	13.3	2.15	C *	o
	(2)	(2+2)+2	2.147	8.7	1.88	C *	o
fornacite		4+(1+1)	2.118	10.0	2.02	N	
Sheet Structures							
botallackite	(1)	4+1+1Cl	2.237		1.96	N-M	o
	(2)	(2+2)+2Cl	2.183		2.17	C-M	o
wroewolfeite	(1)	4+(1+1)	2.137	7.1	1.85	N	
	(2)	(2+2)+(1+1)	2.135	9.4	1.91	N	
	(3)	(2+2)+1+1	2.143	17.8	2.08	N	
	(4)	(1+3)+1+1	2.146	16.9	2.06	N	
langite	(1)	(3+1)+1+1	2.147	17.6	2.07	N	
	(2)	(3+1)+1+1	2.142	16.3	2.03	N	
	(3)	4+1+1	2.135	11.2	1.98	N	
	(4)	4+2	2.123	6.9	1.91	N	
posnajakite	(1)	(1+3)+1+1	2.112	10.5	2.09	N	
	(2)	4+1+1	2.190	26.0	1.95	N	
	(3)	4+2	2.117	6.6	1.92	N	
	(4)	(1+3)+1+1	2.152	14.7	2.03	N	
spangolite	(1)	4+1+1Cl	2.188		2.09	N	o
	(2)	4+2	2.100	7.4	2.05	C	
gerhardite	(1)	(1+3)+1+1	2.119	10.5	2.04	N	
	(2)	4+(1+1)	2.118	6.0	1.90	N-M	

Table 4.1 continued

Mineral	Cu(#)	Coordination	<Cu-O> (Å)	Δ (x10³)	BVS	Other
serpierite	(1)	(1+3)+2	2.112	1.8	1.80	N Zn o
	(2)	(3+1)+(1+1)	2.115	11.6	2.08	N
	(3)	(1+3)+2	2.178	13.3	2.04	N
	(4)	6	2.110	0	1.75	N Zn o
	(5)	4+2	2.147	12.8	1.95	N
devillite	(1)	(1+2+1)+(1+1)	2.117	4.1	1.85	N
	(2)	(1+3)+2	2.123	8.0	1.93	N
	(3)	(1+3)+(1+1)	2.142	14.8	2.03	N
	(4)	(3+1)+2	2.092	10.1	2.27	N
	(5)	[1+1+2]+2	2.143	6.7	1.82	N
	(6)	[2+2]+2	2.122	8.6	1.95	N
	(7)	(2+2)+1+1	2.137	8.5	1.87	N
	(8)	[2+2]+2	2.122	14.0	2.16	N
campigliaite	(1)	2+(1+3)	2.202	8.4	1.62	R * o
	(2)	(1+2+1)+2	2.077	10.5	2.32	N * o
	(3)	(1+1)+(2+2)	2.152	7.7	1.85	R * o
	(4)	[1+3]+(1+1)	2.147	10.0	1.90	N * o
ktenasite	(1)	4+(1+1)	2.118	3.4	1.81	N Zn o
	(2)	(2+2)+2	2.150	9.0	2.01	N-M
bayldonite	(1)	[2+2]+2	2.118	11.2	2.10	C
	(2)	[2+2]+2	2.079	5.9	2.17	C Zn o
	(3)	(2+2)+2	2.126	12.1	2.05	C
chalcophyllite	(1)	4+2	2.120	10.1	2.04	C
	(2)	4+2	2.143	12.4	1.96	N
Mixed Polyhedral Sheets						
guildite		(2+2)+(1+1)	2.078	3.8	2.08	N-M
ransomite		(2+2)+2	2.140	10.0	1.94	C
metatorbernite		4+1+1	2.117	20.3	2.33	4-M * o
sengierite		4+1+1	2.113	15.8	2.06	N
cuprosklodowskite		4+2	2.133	13.2	2.04	C
roubaultite		4+2	2.110	10.9	1.96	N
turquoise		[2+2]+2	2.183	2.9	1.48	C * o
stringhamite	(2)	4+2	2.313	50.7	1.89	C
likasite	(1)	4+2	2.113	7.5	1.97	N-M
	(2)	4+1+1	2.188	22.9	1.94	N-M
	(3)	4+2	2.240	34.7	2.00	C
Frameworks of Chains						
bonattite		4+2	2.108	11.3	2.07	N
chalcomenite		4+1+1	2.220	36.6	1.97	N
liroconite		(1+3)+1+1	2.181	23.9	2.05	N
bandylite		4+2Cl	2.253	29.4	2.04	T o
stranskiite		(2+2)+2	2.349	56.2	1.92	C

Table 4.1 continued

Mineral	Cu(#)	Coordination	<Cu-O> (Å)	Δ (x10³)	BVS	Other
stoiberite	(1)	(2+1+1)+1+1	2.200	26.0	1.99	N
	(2)	(2+2)+1+1	2.168	20.1	2.02	N
	(4)	[2+2]+(1+1)cis	2.151	10.7	1.91	N
agardite		(2+2)+1+1	2.211	39.0	2.03	N-M
euchroite	(1)	4+1+1	2.120	11.7	2.068	N
	(2)	4+1+1	2.179	21.0	1.97	N
olivenite	(1)	(3+1)+(1+1)	2.117	8.4	1.97	N
libethenite	(1)	4+2	2.112	9.2	2.03	C-M
conichalcite		(2+2)+2	2.113	5.9	1.93	N *
papagoite		4+1+1	2.203	32.5	2.04	N-M
malachite	(1)	[2+2]+1+1	2.167	16.7	2.00	N
	(2)	[2+(1+1)]+2	2.122	7.5	1.96	N
antlerite	(1)	4+1+1	2.125	10.7	1.99	N-M
	(2)	[2+2]+(1+1)	2.107	8.9	2.07	N
mammothite	(1)	4+2Cl	2.453		1.88	C
	(2)	4+1+1	2.140	17.0	2.07	N
chalcocyanite		[2+2]+2	2.083	9.3	2.23	C * o
trippkeite		4+2	2.121	13.7	2.13	4-M
lindgrenite	(1)	4+2	2.116	10.5	2.04	C
	(2)	4+1+1	2.104	9.5	2.09	N
lammerite	(1)	4+2	2.277	40.5	1.96	C
	(2)	4+1+1	2.165	19.8	2.02	N
azurite	(2)	4+1+1	2.162	9.9	2.03	N
Frameworks of Sheets						
fingerite	(1)	4+2	2.143	8.1	1.82	C
	(2)	(1+3)+1+1	2.128	8.8	1.94	N
	(3)	4+1+1	2.168	26.9	2.08	N
	(4)	(2+2)+1+1	2.178	29.5	2.10	N
	(5)	(3+1)+1+1	2.122	11.6	2.02	N
cornubite	(1)	[2+2]+2	2.133	12.2	2.02	C-M
	(2)	4+2	2.097	6.2	1.98	N
	(3)	4+2	2.122	9.0	2.03	N
pseudomalachite	(1)	[2+2]+2	2.170	30.6	2.05	C
	(2)	4+1+1	2.172	20.2	1.99	N
	(3)	4+1+1	2.128	9.8	1.97	N
reichenbachite	(1)	(2+2)+2	2.207	27.5	2.01	C
	(2)	4+1+1	2.175	26.0	2.03	N
	(3)	4+(1+1)	2.122	10.1	2.01	N
QPM	(1)	[2+2]+2	2.180	17.3	1.92	C
	(2)	(2+2)+2	2.080	5.3	2.12	C
	(3)	4+2	2.200	25.9	2.02	C
	(4)	4+1+1	2.180	24.3	2.02	N
mcbirneyite	(1)	(2+2)+2	2.162	20.2	2.08	N
	(2)	4+1+1	2.129	14.7	2.06	N

Table 4.1 continued

Mineral	Cu(#)	Coordination	<Cu-O> (Å)	Δ (x10³)	BVS	Other	
cornetite	(1)	4+1+1	2.233	36.3	1.96	N	
	(2)	4+1+1	2.208	25.6	1.96	N	
	(3)	(2+2)+1+1	2.163	21.7	2.03	N	
derriksite	(1)	4+(1+1)	2.114	9.1	2.02	N	
	(2)	4+1+1	2.102	6.8	2.02	N	
	(3)	(2+1+1)+2	2.110	10.9	2.12	N	
shattuckite	(1)	4+2	2.173	18.1	1.95	C	
	(2)	(2+2)+1+1	2.151	12.5	1.91	N	
	(3)	(2+2)+(1+1)	2.191	31.2	2.19	N	
arthurite		4+2	2.146	14.2	1.99	C	
salesite		4+2	2.157	15.0	1.97	C	
veszelyite	(1)	4+1+1	2.137	8.7	1.92	N	
	(2)	(2+2)+1+1	2.168	15.7	1.87	N	
dolerophanite	(1)	[2+2]+2	2.153	15.9	2.01	C	
		Frameworks of Octahedra					
connellite	(1a)	4+2Cl			1.97	C	o
	(1b)	(2+2)+2Cl			2.22	C	o
	(2a)	4+1+1Cl			2.17	N	o
	(2b)	[2+2]+1+1Cl			1.76	N	o
	(4)	(2+2)+2	2.227	26.7	1.89	C-M	
	(5)	6	2.250	0	1.19	**P	o
buttgenbachite	(1)	4+2	2.222	26.3	1.90	C-M	
	(2)	4+2Cl			2.06	C	o
	(4)	4+1+1Cl			1.95	N	o
	(5)	6	2.210	0	1.32	**P	o
lyonsite	(1)	6	2.044	0.5	2.12	C P	o
dioptase		4+1+1	2.163	18.5	1.99	N	
atacamite	(1)	(2+2)+2Cl	2.247		2.08	C	o
	(2)	4+1+1Cl	2.185		1.93	N-M	o
paratacamite	(1)	6	2.120	0	1.70	**	o
	(2)	2+4	2.107	9.3	1.91	R	o
	(3)	4+2Cl	2.245		2.10	C	o
	(4)	[(1+2)+1]+2Cl	2.245		2.01	N	o
bellingerite	(1)	4+2	2.123	13.3	2.08	C	
	(2)	4+2	2.147	16.0	2.06	N	
clinoclase	(1)	(2+1+1)+1+1	2.184	24.0	1.98	N	
hentschelite		4+2	2.110	9.0	2.13	C	

KEY for "Other" column: N=non-centrosymmetric; C=centrosymmetric; T= tetragonal distortion; M=mirror plane; 4=equivalent equatorial bonds; *=poor structural data; o=omission from statistical plots; **=symmetrically constrained position; Zn=substitution by Zn; P=partial occupancy

In the "Other" column, letter codes designate the symmetry of the octahedra, and other special features (see table key). Figure 4.6 shows how the symmetry codes relate to some of the different polyhedral shapes. eg. (3+1)+2 octahedra must be non-centrosymmetric (N). So must (2+2)+1+1, but it may have a mirror plane across the axis of the apical bonds (N-M). 4+2 need not be (C) if all bonds differ from each other within ±0.06Å.

The rarity of the ideal (4+2) distortion may suggest that the J-T effect is not a sufficient explanation for Cu^{2+} coordination geometries. Skeptics of the existence of the J-T effect in Cu^{2+} compounds (Miller et al., 1973) suggest that it is only truly present when all six donor sites are equivalent. Miller states,

> Non-equivalent ligands remove the degeneracy, and any distortions occurring cannot be attributed to the Jahn-Teller effect.

Orgel & Dunitz (1957) suggest the contrary,

> If the six ligands are not identical, a "regular" octahedral environment by definition is impossible. None the less, the physical picture is unchanged although the e_g orbitals are no longer strictly degenerate.

A plot of $Cu-O_6$ bond lengths (Figure 4.7) confirms the latter statement. Although O^{-2}, OH^- and H_2O bonds are randomly grouped in the plot, a well-defined bimodal distribution exists, and maxima are evident. The bond length maxima are approximately 1.97Å and 2.43Å. There are actually two apical maxima (2.39Å and 2.47Å) with a gap in between, and the average is 2.43Å. The equatorial population is approximately twice as large as the apical population, which is expected with the (4+2) distortion model.

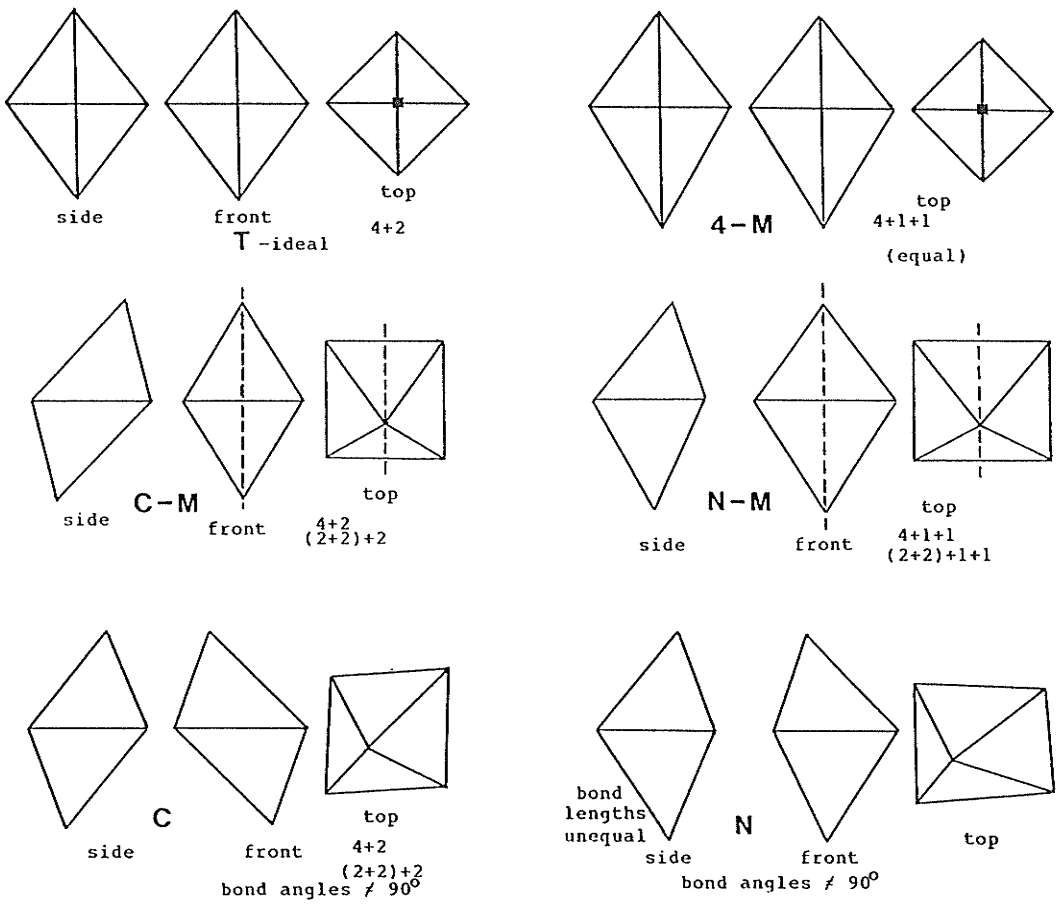

Figure 4.6: Possible Symmetries from CuO_6 Octahedra. The different perspectives of these types of octahedral symmetry help to relate various shapes of octahedra to the symmetry coding of the "Other" column in Table 4.1; note: the different shapes are arranged in a decending order of symmetry, from top left to bottom right.

A correlation between <Cu-O>equatorial vs <Cu-O>apical (Figure 4.8) illustrates the equilibrium mechanism for J-T electronic relaxation. As the apical bonds lengthen, the equatorial bonds shorten (although the variation in apical bond lengths, Figure 4.7, is much greater). This correlation also complies with bond-valence requirements on Cu^{2+} (bond lengths must adjust for proper bond-valence sums of 2). However, the mechanism of adjustment between apical and equatorial bonds cannot be attributed to bond-valence requirements. The octahedral distortion operates within the guidelines of bond-valence requirements in crystals, but the driving force for distortion is controlled by the J-T effect (from degeneracy to relaxation).

It should not be surprising that the actual geometries of Cu^{2+}-octahedra in oxysalt structures deviate from the model of ideal tetragonal distortion described in part 4.1. Structural symmetry and bond-valence constraints demand variability in the coordination environment of Cu^{2+}. A triclinic crystal structure will not normally have an octahedron with tetragonal symmetry as the major feature of its polyhedral linkage. Copper at the cell origin of a monoclinic structure (usually with symmetry C in Table 4.1) must have non-tetragonal symmetry. (2+2)+2 distortions indicate different bond-valence requirements along the 3 axes of an octahedron. Variations from tetragonal J-T distortion must involve more complex styles of orbital splitting to remove the degeneracy. The variations observed in octahedral geometry can be assembled into the reaction path series of Figure 4.5. This pathway is a continuous series because of the wide

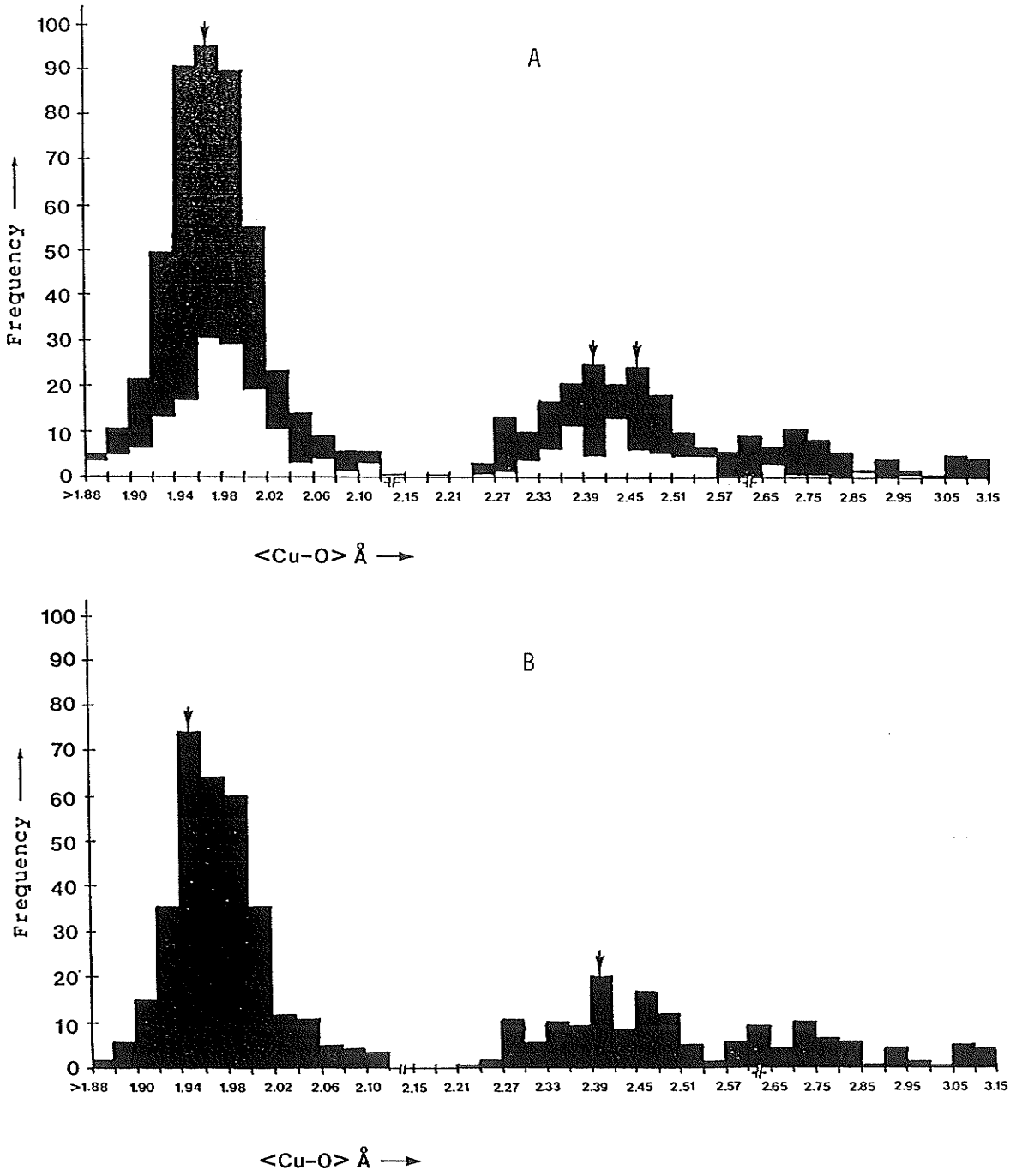

Figure 4.7: Octahedral (4+2) Bond Frequency Distributions. (a) distributions for all octahedra (solid) and for those only bonded to sulfate tetrahedra (open); (b) distributions of octahedra not bonded to SO_4 tetrahedra. The bond frequency maxima (arrows) are different for each distribution indicating that the SO_4 linkage group influences the position of the maxima. Note: the bond length scale has three stages.

distribution in apical bond lengths, and the wide variations observed in bond angles and octahedral geometry.

It is also not surprising that there are no correlations between bond-valence sums and octahedral geometry (or structure type). Each unique structure has a different bond-valence environment around Cu^{2+}, to which the J-T effect must conform for structural stability. Bond-valence requirements are not specific to styles of polyhedral linkage or particular coordination environments, but apply to all oxysalt structures.

The J-T distorted octahedron is apparently quite flexible in its ability to assume a wide range of bond lengths. Figure 4.7 shows the large bond length variations possible for Cu^{2+}, and Figure 4.8 shows its only restrictions (equilibrium must be maintained between apical and equatorial bonds). It is interesting to note that the position of the apical bond length maximum (Figure 4.7) is heavily influenced by sulfate structures. Apparently, the bond length requirements of Cu-octahedra linked to sulfate tetrahedra are much more restricted than for other groups. The rigid bond-valence requirements of sulfate tetrahedra are responsible for the range of apical bonds observed (this will become more apparent in Chapter 5). Therefore, there exists no true "most stable" range of apical bond lengths, but rather a continuum of possible distortions. Apical bonds can extend beyond 3.15Å to form pyramidal and square planar coordinations.

Figure 4.8: Average Equatorial vs. Average Apical Bond Lengths

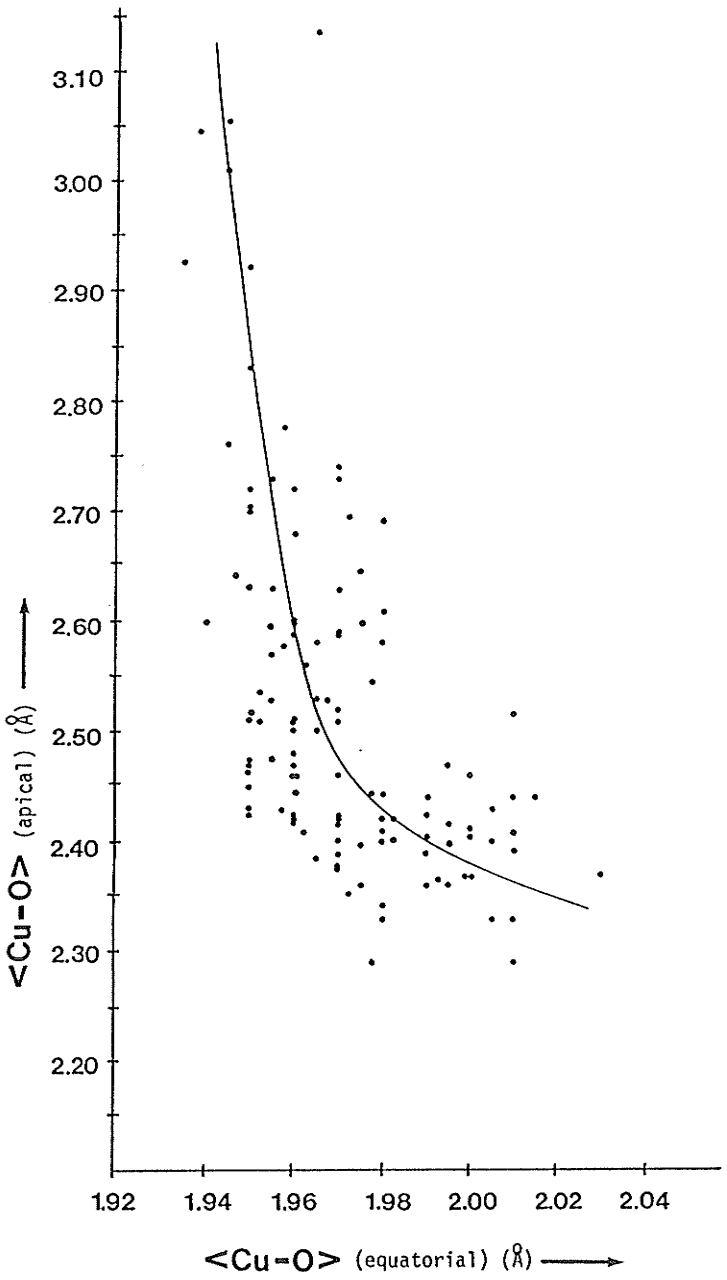

A wide range of angular distortions in Cu^{2+}-octahedra are possible because of the long apical bond lengths. This fact is best understood in light of Figure 4.9. Consider that apical anions are much farther from Cu^{2+} than equatorial anions. An apical anion is therefore able to move "overtop" of the equatorial anion and still maintain a short octahedral edge without additional anion-anion repulsion (Figure 4.9b). Such is not the case for regular octahedra (Figure 4.9a). In addition to the short equatorial-apical edges, Cu-octahedra also have short equatorial-equatorial edges. The short equatorial edge is formed by oxygen overlap as the equatorial bonds shorten due to the Jahn-Teller distortion, the force of which must be greater than anion repulsive forces. These distortion features, made possible by the Jahn-Teller effect, facilitate edge-sharing with small TO_4 and TO_3 groups. Elements without the Jahn-Teller distortion have anion repulsive forces which prohibit the occurrence of extremely shortened edges.

In structures with low connectivity (caledonite, kröhnkite), the geometrical requirements imposed on Cu-octahedra are minimal. The J-T distortions in these octahedra are roughly equal to the maxima of the bond lengths in Figure 4.7, and fall at the centre of the distribution in Figure 4.8. Conversely, structures with high connectivity (cornetite, pseudomalachite) have large and diverse octahedral distortions. These latter structures test the limits of Cu^{2+} flexibility, balancing J-T forces with structural requirements. This is supported by one of the few trends in Table 4.1. Structures with lower connectivity have more simple octahedral coordinations, whereas, those with more complex connectivies (network chains, dense octahedral sheets)

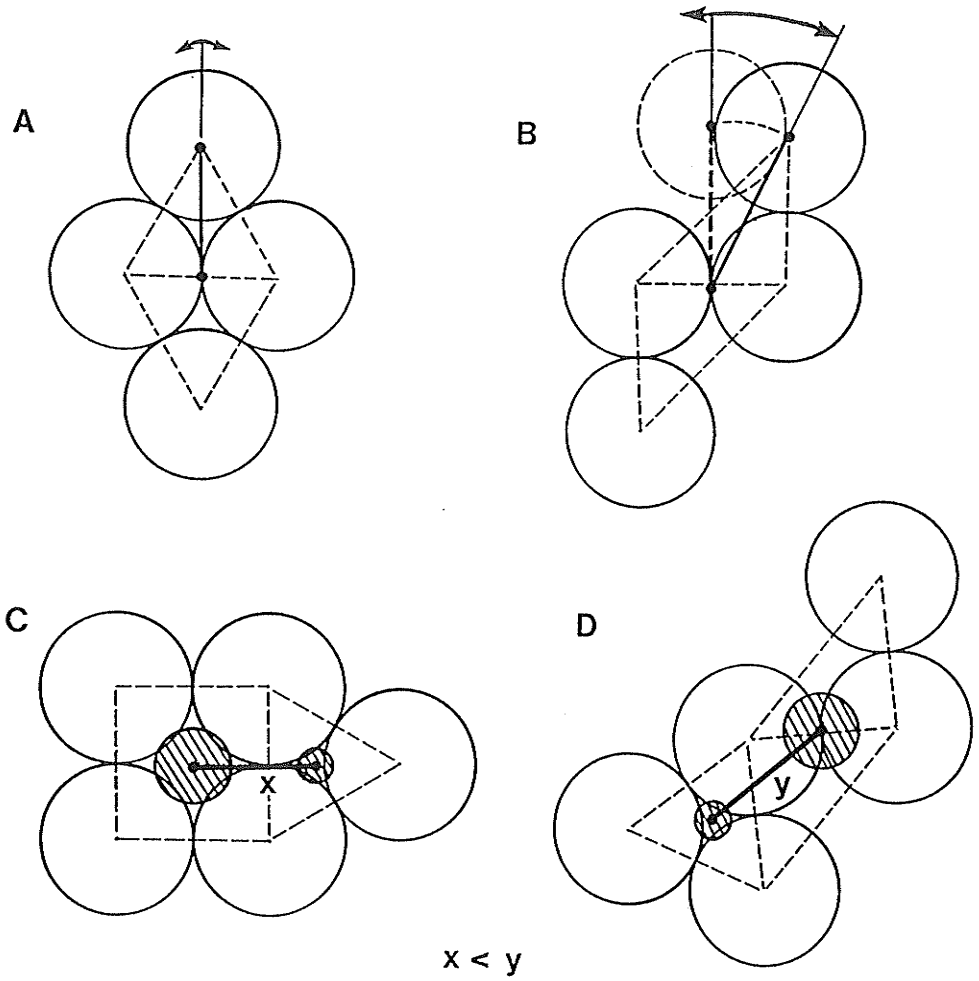

Figure 4.9: Angular Distortion Mechanism of the Cu^{2+}-octahedron. (a) regular octahedron, and lateral bond angle distortions are restricted (arrows); (b) angular distortion is much easier for apical bonds of J-T distorted octahedra; (c) consequently, the cation-cation distance between edge-sharing polyhedra is shorter across the equatorial edges (indicated by the bold line-x) than across the apical-equatorial edge in (d), with large angular distortion (bold line-y). Cation-cation repulsion should be greater in case (c) than in (d).

have very diversified octahedral bond lengths. Thus, fully occupied octahedral sheets require diverse bond length patterns, because of the geometrical requirements of fitting distorted octahedra into a layer. When the sheets are 3/4 occupied, the octahedral geometries are simpler, because the geometrical requirements are less demanding for specific bond lengths.

Shannon (1976) assigns a [6]-coordinate ionic radius of 0.73Å for Cu^{2+}. The bimodal distribution of Figure 4.7 suggests that Cu^{2+} is not spherical, but is better represented by a prolate ellipsoid. The maximum values of the bond lengths are 1.97Å and 2.43Å; subtracting an average value of 1.36Å for (O,OH, H_2O) in various coordinations, gives ellipsoidal dimensions of 0.61Å and 1.07Å, respectively. The equivalent spherical value (weighted for the different bond frequencies) is 0.75Å, larger than Shannon's (1976) value of 0.73Å. This difference results from the different criteria to assign Cu^{2+} coordinations, used here and by Shannon (1976).

The Δ parameter of Table 4.1 is the distortion index of an octahedron, and is calculated by the equation:

$$\Delta = \frac{1}{6}\sum_{1}^{6}\left(\frac{l_o - \bar{l}}{\bar{l}}\right)^2 \qquad (4.2)$$

from Hawthorne (1977), where $\bar{l}$ is the average bond length, l_o is the individual bond length, and the squared deviations are summed for all six bonds and then averaged. Correlations are not readily apparent between Δ and the other parameters, except for <Cu-O> (Figure 4.10).

Structures with very long apical bonds will have greater Δ and <Cu-O> values, as predicted by the distortion theorem of bond-valence theory (Brown, 1981). The more complex structures (with greater geometrical demands on the octahedra) generally have longer apical octahedral bonds, and have a greater number of high Δ values. This is observed in Figure 4.10, where the framework structures have a far greater number of octahedra with large Δ values than the non-framework structures.

Extrapolation to Δ=0 in Figure 4.10 gives a bond length of 2.084Å (i.e. for an undistorted octahedron). This is equal to the R_0 value used by Brown and Shannon (1973) for the bond-valence curve of [6]-coordinate Cu^{2+}, and indicates that a holosymmetric CuO_6 octahedron would have a bond-valence sum of exactly 2.00vu at the central Cu^{2+} cation. This contrasts with the R_0 value of 2.065Å used by Brown (1981); this latter value gives a bond-valence sum of 1.88vu for a holosymmetric CuO_6 octahedron with <Cu-O> = 2.084Å, and may be less appropriate for use in minerals than the earlier value.

Significant deviations from the ideal bond-valence sum of 2.00 (±0.20v.u.) usually have a reasonable explanation (referring to those in Table 4.1) Quite often, the structural data are of poor accuracy (marked with * in Figure 4.10) and the result is a large deviation in the bond-valence sums. Some Cu-octahedra have a significant amount of Zn substitution (marked Zn), and this significantly affects the bond lengths of the octahedra.

High symmetry Cu^{2+} positions in hexagonal structures prevent J-T distortions from showing. In buttgenbachite and connellite, the Cu(5)

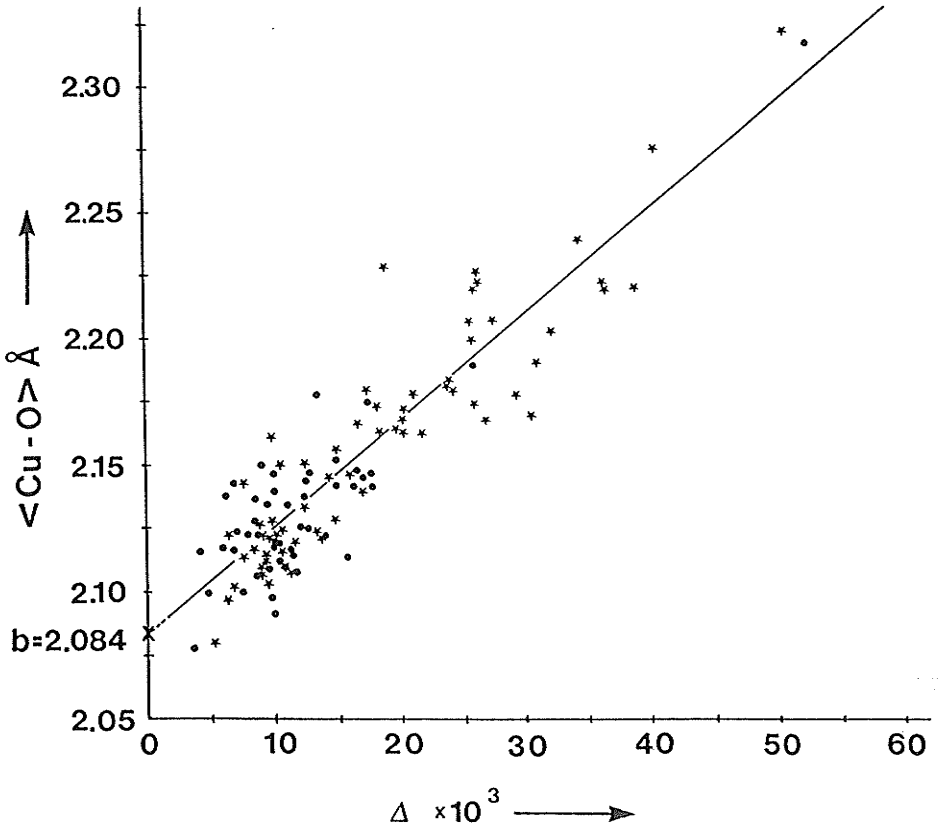

Figure 4.10: Average Octahedral Bond Length vs. Distortion Index. The line is fitted to the linear equation: y=mx+b; where b=2.084Å; and slope=m=0.004216. Framework structures have star symbols, and non-framework structures are as solid circles.

lies on a $\bar{6}$-axis, but has approximately 0.5 occupancy. Consequently, the J-T effect is prevented from occurring by crystallographic restrictions. The bond lengths are much larger than most <Cu-O>, due to partial occupancy. Is there a dynamic J-T distortion within the enlarged octahedral cavity of Cu(5), or is the J-T distortion dispersed in different directions at different Cu(5) positions throughout the structure, as a space-average of 2.25Å?

Lyonsite, although not symmetrically constrained, shows partial occupancy within a position of pseudo-hexagonal symmetry (Cu(1)). This pseudo-symmetry is imposed by hexagonally close-packed oxygens. Lack of J-T distortion at Cu(1) indicates that this position is not an ordinary site. Perhaps partial occupancy of Cu^{2+}, in sites of higher symmetry, allows the coordination of Cu^{2+} to be holosymmetric?

Paratacamite is a high-symmetry (hexagonal) polymorph of (the nearly isostructural) atacamite. Cu(1) has six equal bond lengths of 2.11Å and is on a $\bar{6}$-axis. However, this octahedron makes up only 1/16 of the total number of octahedra in the framework. This low proportion of the total structure is constrained to an electronically degenerate state. Three-sixteenths of the copper, Cu(2), has the rare (2+4) symmetry (compressed octahedral), and also lies on a high symmetry position. Although this geometry is supposedly less stable than 4+2 (c f. 4.1), the difference in stability presumably is small enough across the whole of the structure for (2+4) to exist.

Clearly, the undistorted Cu-octahedra are rare exceptions. However, these anomalies show that equal bond lengths can occur in high symmetry structures at positions of low equipoint rank. Presumably, the increased energy caused by the electronic degeneracy is offset by greater energetic advantages in the rest of the high-symmetry structure.

4.2.2 Square Pyramids & Trigonal Bipyramids

Table 4.2 lists all of the trigonal bipyramidal and square pyramidal coordinations observed in Cu^{2+} oxysalt minerals, together with some from selected synthetic compounds. Square pyramidal coordinations (Figure 4.5e) are one extreme form of octahedral distortion by the J-T effect. Starting with an octahedron, a single apical bond is removed from Cu^{2+} along the z-axis (when the dx^2-y^2 orbital is half-occupied) and the equatorial bonds shorten. This non-centrosymmetric distortion would require a more complex orbital splitting from that of Figure 4.1. Square pyramids (SPY) are the second most common Cu^{2+} coordination in oxysalt minerals.

Trigonal bipyramidal (TBD) Cu^{2+} (Figure 4.5f) must undergo an even more complex field splitting from that of SPY, because of the drastic departure from an octahedral arrangement. Although not first apparent, SPY and TBD are closely related in their geometries. The two coordinations are drawn as plan views of their molecular shapes (Figure 4.11), and in reference to a stereonet (bold circle). They are related by a simple distortion of two bonds (shown by arrows). The ideal SPY has 8 bond angles of 90°, and 2 trans-equatorial bonds are 180°. Ideal

TABLE 4.2

Parameters for Five Coordinate Cu-Polyhedra

Mineral	(#)	Shape	<Cu-O> (Å)	Δ (x10³)	BVS
clinoclase	(2)	SPY	2.061	12.8	2.02
	(3)	SPY	2.039	3.6	1.91
litidionite		SPY	2.092	12.0	1.81
callaghanite		SPY	2.052	10.8	2.02
kinoite	(1)	SPY	2.016	3.6	2.03
	(2)	SPY	2.045	10.0	2.00
teinite		SPY	2.031	5.4	1.99
mixite		SPY	2.024	4.1	2.01
ziesite		SPY	2.004	4.0	2.12
blossite		SPY-TBD	2.058	13.9	2.05
balyakinite		SPY-TBD	2.048	6.7	1.93
stoiberite	(3)	TBD	2.029	4.4	1.99
	(5)	TBD	2.010	3.6	2.08
dolerophanite	(2)	TBD	2.025	3.0	1.99
fingerite	(6)	TBD	2.011	2.3	1.90
olivenite	(2)	TBD	2.018	1.7	1.95
libethenite	(2)	TBD	2.003	0.9	2.03
synthetic compounds					
$Cu_3P_2O_8$	(1)	TBD	2.005	1.7	2.04
	(2)	TBD	2.017	1.3	1.98
$CuSeO_3$		TBD	2.029	2.2	1.91

TBD have 3 angles of 120° between their equatorial bonds, 6 angles of 90° between equatorial and apical bonds, and one 180° angle between the apical bonds. Actual geometries rarely approach these ideal values in Cu^{2+} polyhedra. However, the two can be differentiated by noting that equatorial bond angles in TBD are closer to 120°, while all those for SPY are on average 90°.

Because the TBD & SPY polyhedra are not ideal, there must be a common reference point for stereonet plotting of all the different geometries. The following method relates the two geometries most conveniently:

1. for SPY, the shortest equatorial bond is plotted at the S pole, and the next shortest bond is plotted near to the W pole, in the horizontal plane.
2. for TBD, the shortest apical bond is plotted at the S pole, and the shortest equatorial bond is plotted near to the W pole, in the horizontal plane.
3. for both SPY & TBD, the longest bond cis to the S pole is made the upward pointing bond.

Figure 4.12 shows stereonet plots of the SPY and TBD of Table 4.2. The bond poles of the two types of polyhedra form distinct zones. These zones are spatially related to the bonds of the end member geometries in Figure 4.11. Therefore, the distortion mechanism in Figure 4.11 can be applied to the plotted bond zones in Figure 4.12. However, we do not see a continuum of distortions between SPY and TBD, because of the separation in bond angle zones. Perhaps an analysis of bond length variations between TBD and SPY will complement the angular relationships, and reveal a more complete reaction series.

Projections of SPY and TBD show bond length and bond angle relations between these two polyhedra (Figure 4.13). Observing changes along the path (outlined by the arrows), the longest bonds show a continuous progression in length, from TBD -> SPY. The other four bonds become (on average) shorter as well, along with the changes in bond angles, from

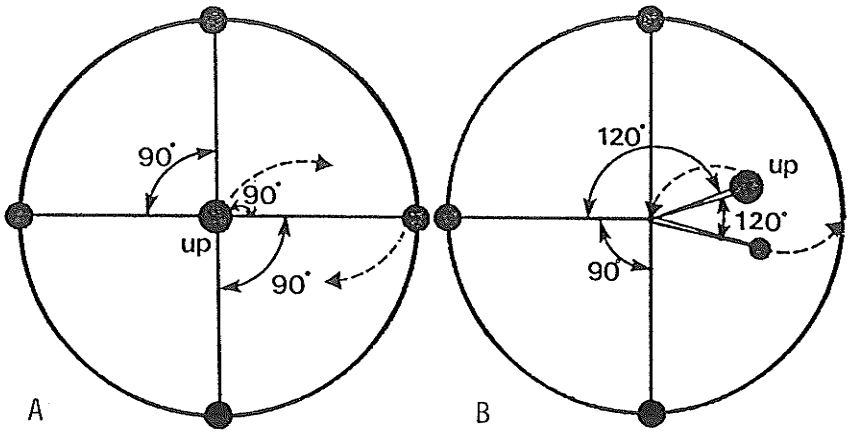

Figure 4.11: Views of the End-Member TBD and SPY Coordinations. (a) Square pyramid; (b) Trigonal bipyramid; viewed slightly obliquely. These two similar coordination geometries are related by a distortion mechanism (dashed arrows) when they are viewed in the above orientation. Their ligands can be plotted with reference to a stereonet, hence the molecules are circled with a stereonet.

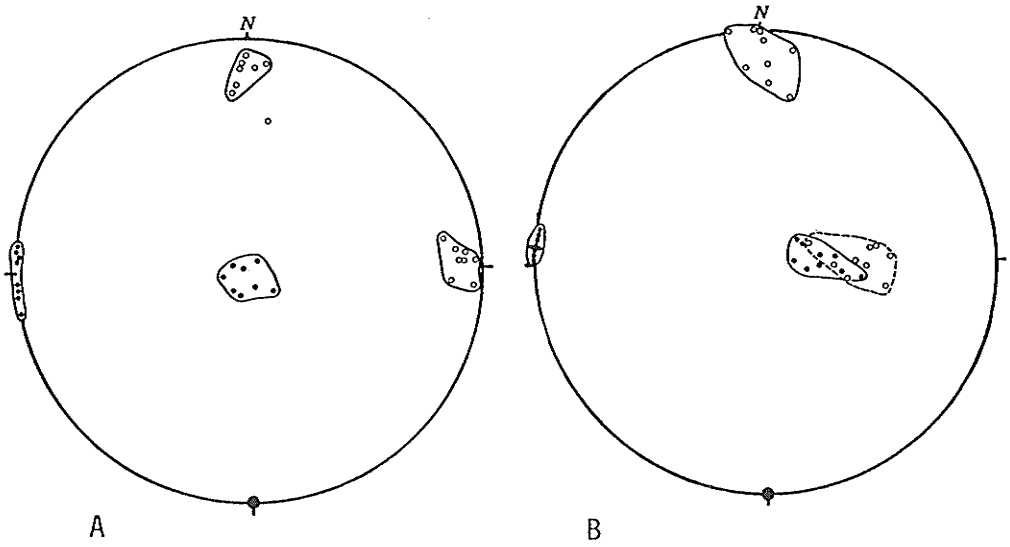

Figure 4.12: Stereonet Plots of TBD and SPY Geometries. Stereonet plots of (a) SPY and (b) TBD, oriented analogously to the end-member geometries. Bond angles are from polyhedra of Table 4.2 Note how the bond-pole zones are in the same positions as the ligands drawn in Figure 1.12. Also note the distinct separation between the E-pole bond zone of SPY and the lower E-bond zone of TBD.

120° -> 90°. However, the progression in bond length patterns is more continuous than for bond angles, which show a definite break (in Figure 4.12). Therefore, either there exists an energy gap between the progression in bond angle changes, or the data set is too small and inconclusive. The geometries shown represent a partial reaction path series between TBD and SPY.

SPY have longer apical bonds than the longest bonds in TBD (Figure 4.13). Therefore, the Δ parameter is characteristically higher for SPY, as shown in Table 4.2. The Cu^{2+} ion is usually above the basal plane in an SPY. Continued distortion of equatorial bonds in the basal plane, away from the apical anion, would result in the TBD geometry (via the reaction path).

Blossite, the polymorph of ziesite, has a more distorted SPY geometry than ziesite. The bond angles show similarity to a TBD, but the apical bond is distinctly SPY (hence the large Δ). Five-coordinate Cu^{2+} polyhedra in selected synthetic compounds also show these relationships in between similar structures (listed in Table 4.2). $CuSeO_3$ (Hawthorne et al., 1986), the near isomorph of balyakinite, illustrates a subtle change in geometry for polyhedra transitional between TBD and SPY, when Te is replaced by Se (Figure 4.13). $Cu_3P_2O_8$ is isostructural with stranskiite. The extra Cu relative to stranskiite goes into the TBD positions (which are occupied by Zn in the mineral), and are regular in shape.

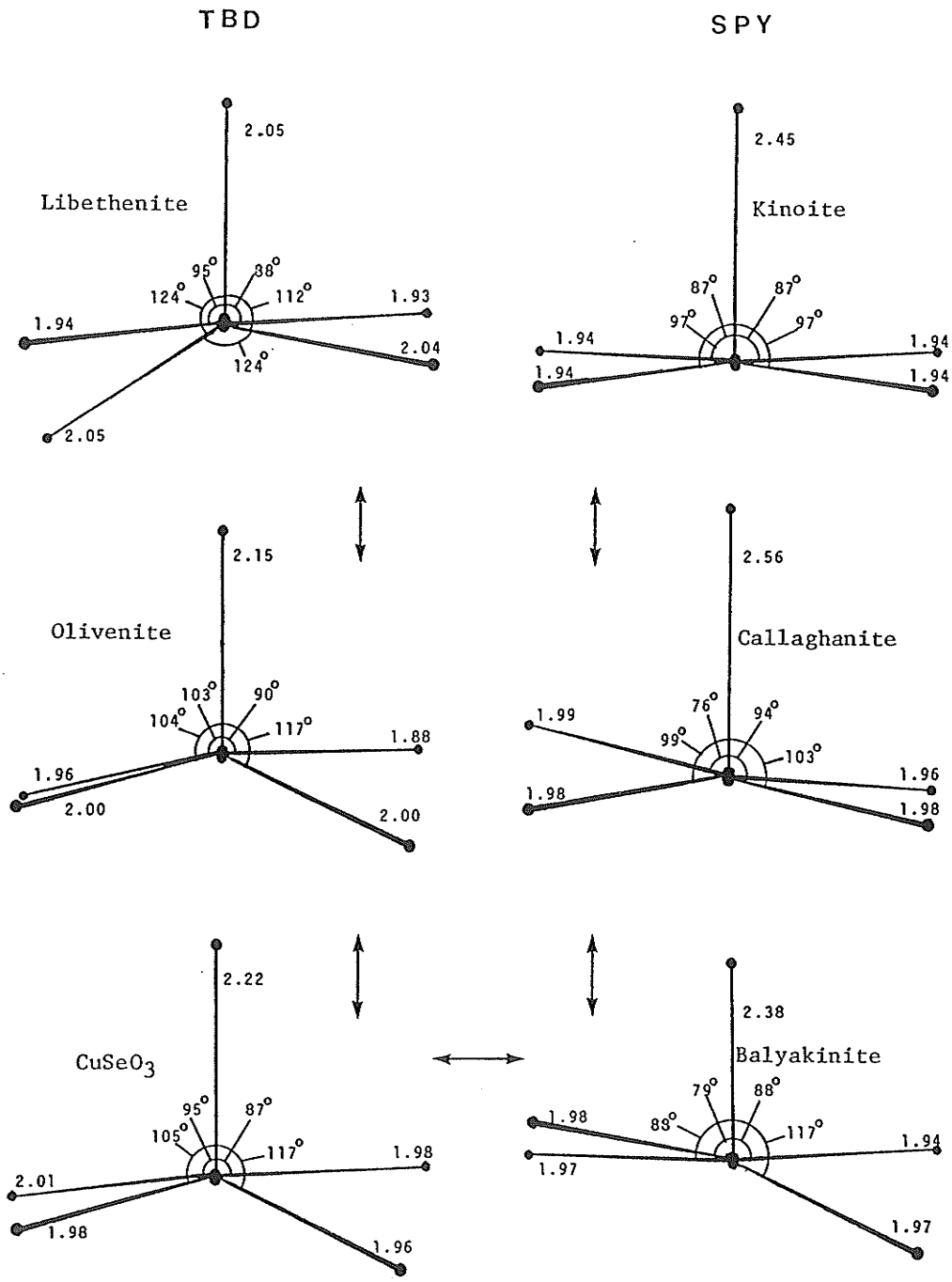

Figure 4.13: Reaction Pathway Between TBD & SPY

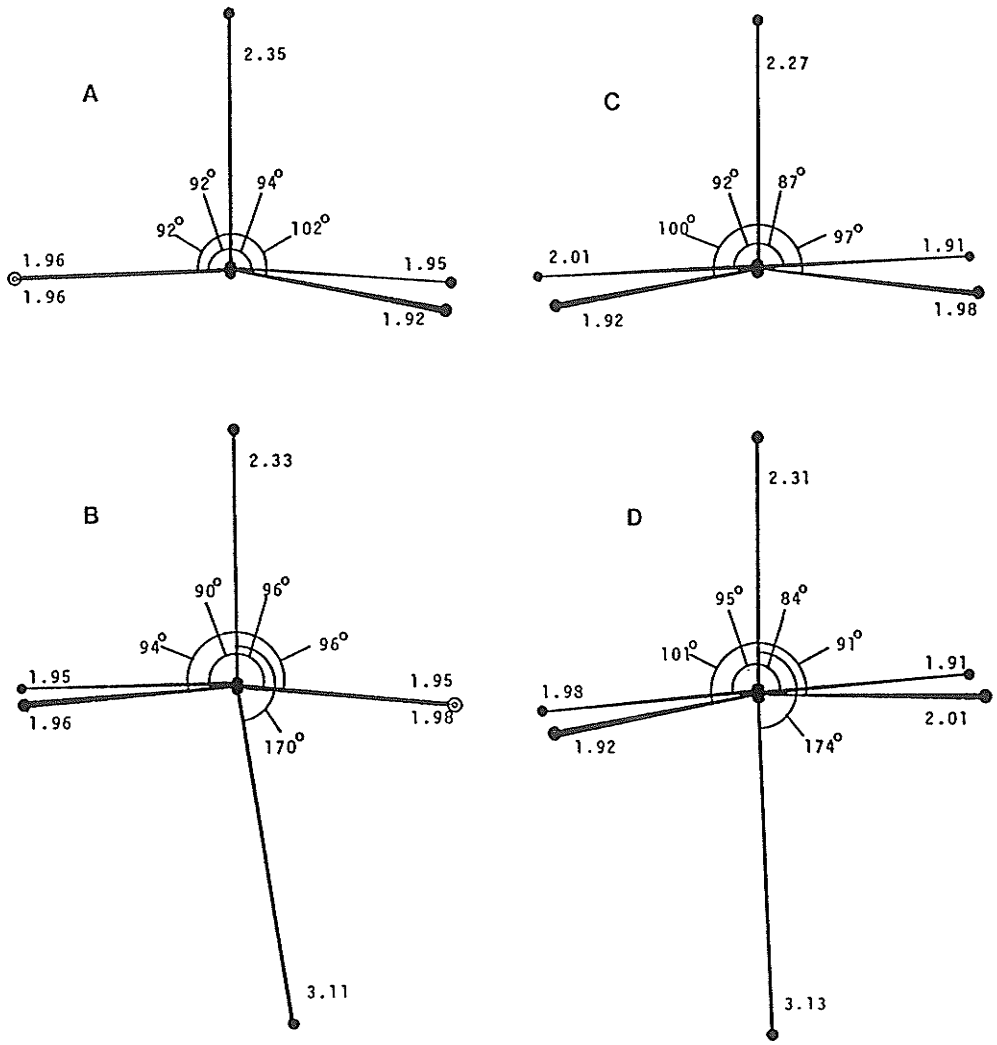

Figure 4.14: Reaction Path Between the Square Pyramid and Octahedron. (a) square pyramidal Cu in teinite; (b) octahedral coordination of Cu in chalcomenite; note the similar geometries between these two coordinations. (c) square pyramidal Cu in mixite; (d) octahedral Cu in agardite; these coordinations are geometrically very similar as well; bond lengths in Å.

We have established that the TBD and SPY represent a partial reaction path series. It can also be shown that the SPY is an extreme form of J-T octahedral distortion, as was suggested in the first paragraph of this section. Figure 4.14 illustrates how structurally similar minerals can have octahedral and SPY counterparts in related structural positions. Teinite has the SPY coordination, whereas chalcomenite has the borderline case of octahedral (4+1+1) coordination. The bond angles and bond lengths are very similar for the two Cu-polyhedra, regardless of the sixth bond in chalcomenite. Mixite and agardite show the same respective relationships, although under different structural circumstances. These related structures represent an important look at the fine line between [5]- and [6]-coordinations, and how neighboring chemical groups may affect what coordination is formed. As suggested before, the far end of the apical bond length distribution (Figure 4.7) represents the pathway of distortion from [6]-coordination to [5]- and [4]-coordinations.

It is also possible that the TBD is a direct product of octahedral distortion. This could happen by significant angular distortion of equatorial bonds away from the remaining apical bond, as the sixth apical bond is simultaneously removed. This hypothesis is not supported by the same type of structural evidence as that for SPY in Figure 4.14. Thus, it seems sufficient to propose the linear reaction series: Octahedron->Square Pyramid->Trigonal Bipyramid. The square pyramid forms the intermediate link of the distortion pathway. Therefore, the J-T effect is a potential continuum of electronic relaxation between

these three coordinations, and justifies the method of relating these coordinations in Figure 4.5.

4.2.3 Square Planar Cu^{2+}

Oxysalt minerals with square planar Cu^{2+} are listed in Table 4.3. The Cu^{2+}-oxides are included in Table 4.3 because they add to the data base of square planar CuO_4 (tenorite from Åsbrink & Norrby, 1970; paramelaconite from O'Keefe & Bovin, 1978), although they are not discussed in Chapter 3. It is interesting to note that the bond-valence sums in Table 4.3 are all consistently below 2.0v.u., except for cuprorivaite (which needs structural refinement). This suggests that the equatorial bonds may not be able to statically shorten enough to attain the ideal bond-valence sums. A dynamic J-T distortion could

TABLE 4.3

Square Planar CuO_4

Mineral	(#)	<Cu-O> (Å)	BVS
cuprorivaite		1.910	2.12
azurite	(1)	1.938	1.94
paramelaconite		1.941	1.93
stringhamite	(1)	1.945	1.91
tenorite		1.95	1.87

possibly compensate for this.

Another point of interest is the lack of variation in bond lengths within each square planar group. Bond lengths are either all equal, or they are in two pairs. Square planar sites are often in positions of higher symmetry than octahedral sites. Considering these features, the square planar coordination is most suited to higher symmetry positions in oxysalt structures. Four equal bond lengths in square planar Cu^{2+} may therefore represent an extreme case of J-T distortion, via the tetragonal model in Figure 4.1. Stringhamite has two Cu positions, of which one is octahedral, and the other is square planar. The borderline nature between these two coordinations has already been discussed. These coordinations suggest that the square plane can be a direct product of an octahedron, because the implied distortion mechanism involves the simultaneous removal of two apical bonds (Cu on centrosymmetric positions).

For the square pyramid to be an intermediate coordination between [6]- and [4]-coordinations of Cu^{2+}, the distortion must be non-centrosymmetric. Azurite may support the existence of SPY as an intermediate in some cases. As was said earlier, the square planar site has a fifth oxygen within 3.00Å. The environment of square planar Cu(1) is therefore not centrosymmetric, and may be a transitional coordination between the SPY and the square plane. The reaction path of Figure 4.5 can be justified by these arguments.

4.2.4 Unusual Cu^{2+} Coordinations

This category contains coordinations that are very unusual for transition metals in general, and which occur very infrequently in the Cu^{2+} oxysalt structures (Table 4.4).

The (4+2+1) polyhedron has one square pyramidal end and the other end is wedge shaped. The latter end is referred to as pup-tent shaped by Maclean & Anthony (1972). Connellite apparently provides a unique opportunity for this coordination geometry. Bond-valence analysis

TABLE 4.4

Unusual Cu^{2+} Coordinations

mineral	(#)	shape	BVS
connellite	(3)	4+2+1	2.02
buttgenbachite	(3)	4+2-cis "pup-tent"	>1.84
lyonsite	(2)	4+2-cis trig-prism	1.92

(Table 4.4) confirms the presence of all 7 bonds in Cu(3). Isostructural buttgenbachite is described as having square planar coordination in its Cu(3) position (Fanfani et al., 1973), without all three apical bonds. The difference of complex anion type within the channels of these two structures is responsible for the lack of the longest apical bond in Cu(3) of buttgenbachite. However, the octahedral framework of both structures is the same, and it is therefore logical to assume that the remainder of the Cu(3) position in both structures is

pup-tent shaped. The bond-valence sum on the Cu(3) position in buttgenbachite is low for square planar coordination, and suggests that the (4+2)-cis coordination is a valid assumption (which would increase the BVS). Lyonsite displays a very similar coordination geometry, and is termed trigonal prismatic. Bond-valence analysis supports this coordination assignment by Hughes et al. (1987).

Figure 4.5i shows seven coordinate Cu as a product of the (4+1+1) octahedron. This distortion path seems logical, although there is a lack of data to support the idea. Similarly, the (4+2)-cis coordination can be considered a product of (4+2+1) coordination, simply by loss of the longest apical bond.

4.3 SUMMARY

We have now reached the crux of the matter in relating the local environment of Cu^{2+} to its long-range crystalline environment. The variety of Cu-coordinations observed and their close relationships indicate the great flexibility of Cu^{2+}. The Jahn-Teller effect provides the driving force for this flexibility, in terms of both bond angles and bond lengths. This feature provides the Cu^{2+} polyhedron with the potential to polymerize with other polyhedra in unique ways. The following chapters will discuss this flexible ion in terms of how the long-range structural features are controlled or influenced by the Jahn-Teller effect.

Chapter V

BOND-VALENCE FEATURES OF Cu^{2+} OXYSALT STRUCTURES

It is now established that the Jahn-Teller effect provides a geometrically flexible environment for Cu^{2+}, allowing for a variety of different bond-valence distributions around Cu^{2+}. Therefore, the potential for different topological combinations of Cu-octahedra and other polyhedra is very great. This chapter explores the bond-valence features which give Cu^{2+} oxysalts their unique character, and focuses on the questions:

1. Why do some Cu^{2+} oxysalt structures have non-Cu analogues?
2. Why are some Cu^{2+} oxysalt structures unique?

5.1 BOND-VALENCE DISTRIBUTIONS

5.1.1 Octahedral Variations

Because of the Jahn-Teller (J-T) distortion, bond-valence (bv) distributions around Cu^{2+} are significantly different than for other M^{2+} cations in more regular coordinations. The variety of bv distributions around Cu^{2+}-octahedra and related coordinations are illustrated in Figure 5.1. In most non-Cu^{2+} oxysalt structures, the bv distributions for octahedra do not vary appreciably ($< \pm 0.1$v.u.) from the ideal Pauling (1960) bond strengths. Because the J-T effect provides a continuum of distortions, the bv distributions around Cu^{2+} have a wide range of values available for varying contributions to polyhedral

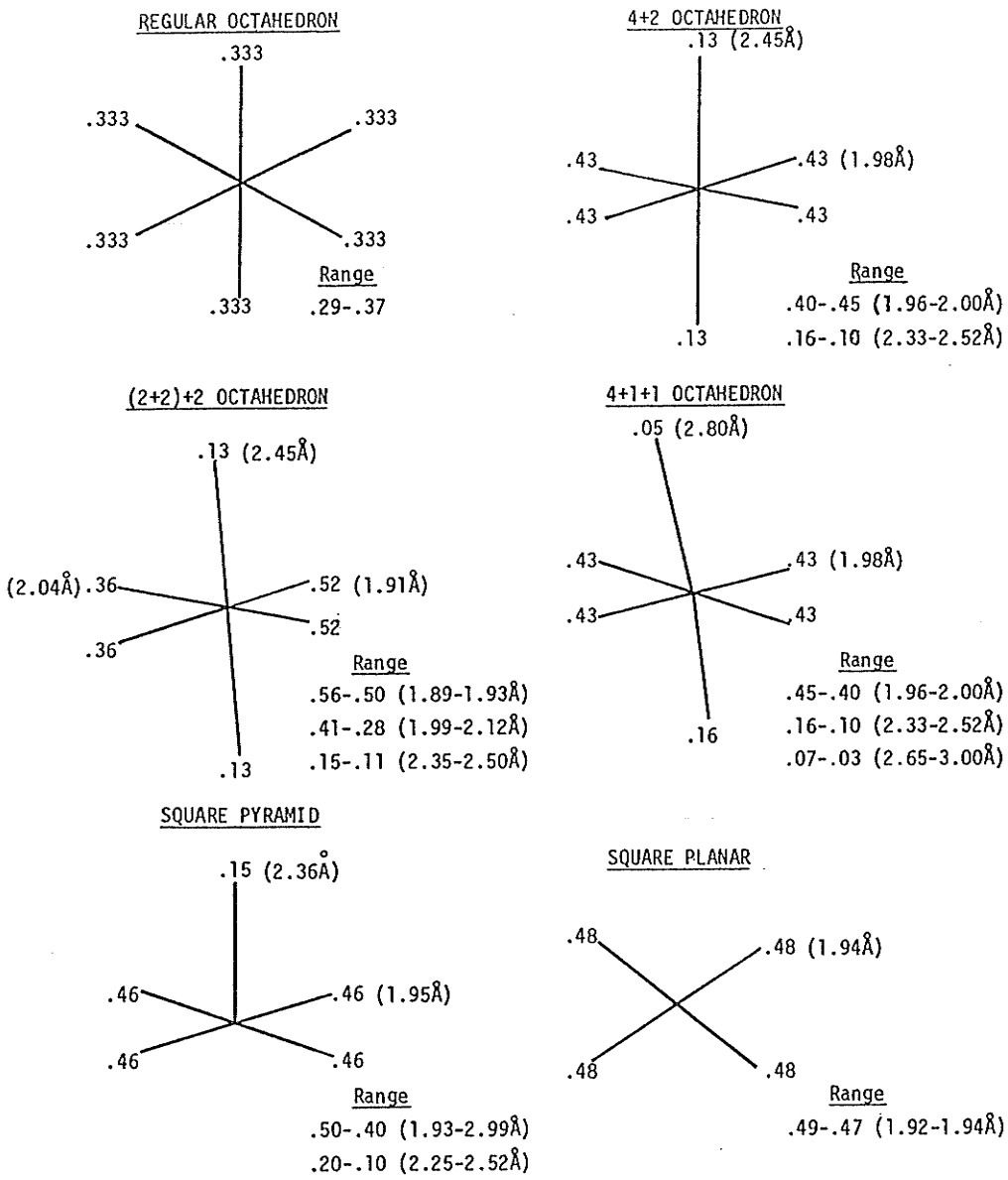

Figure 5.1: Bond-valence Distributions Around Octahedra. Skeleton models of the geometrical variations of an octahedron; average bond-valence contributions are given at the end of each bond, with a representative bond length (in brackets); also listed for each polyhedron are the range of bond lengths (in brackets) and bond-valences observed for a particular octahedral geometry.

linkages. It is this variation in bv distributions, relative to regular octahedra, which provide unique possibilites for polymerization.

5.1.2 Polymerization Features

Bond-valence sums (bvs) around linking oxygen anions are the deciding factor for the topologic combinations possible between cation polyhedra. bvs on oxygen must approach 2.00v.u. for structural stability in oxysalts. The oxygen coordination numbers in divalent metal oxysalts are usually [3] and [4]. This "rule of thumb" limits the combinations possible for linkage between regular octahedra and small complex oxyanions with high cation charges (scowhcacs).

There is a limit to the type of scowhcac that can polymerize to the octahedra. Figure 5.2 shows the polymerizations possible for adequate bvs, together with the bv distributions that are involved. Hydrogen-bonding doubles the number of polymerizations allowed with different scowhcacs, indicating the ever-important role of hydrogen-bonding in oxysalt mineralogy. Restrictions on polymerization with regular octahedra are essentially the charge of the cation in the scowhcac. CO_3 and SO_4 groups have higher bv contributions to the linking oxygens than most scowhcacs, and they require lower connectivities for structural stability. Octahedral sheets are usually restricted to polymerization with scowhcacs of 1.00v.u. contributions (i.e. silicate tetrahedra), unless cation vacancies are present within the sheets. If the M^{2+}-O bonds, which link to the scowhcac, can lengthen enough, then T^{5+} cation tetrahedra can also polymerize to the

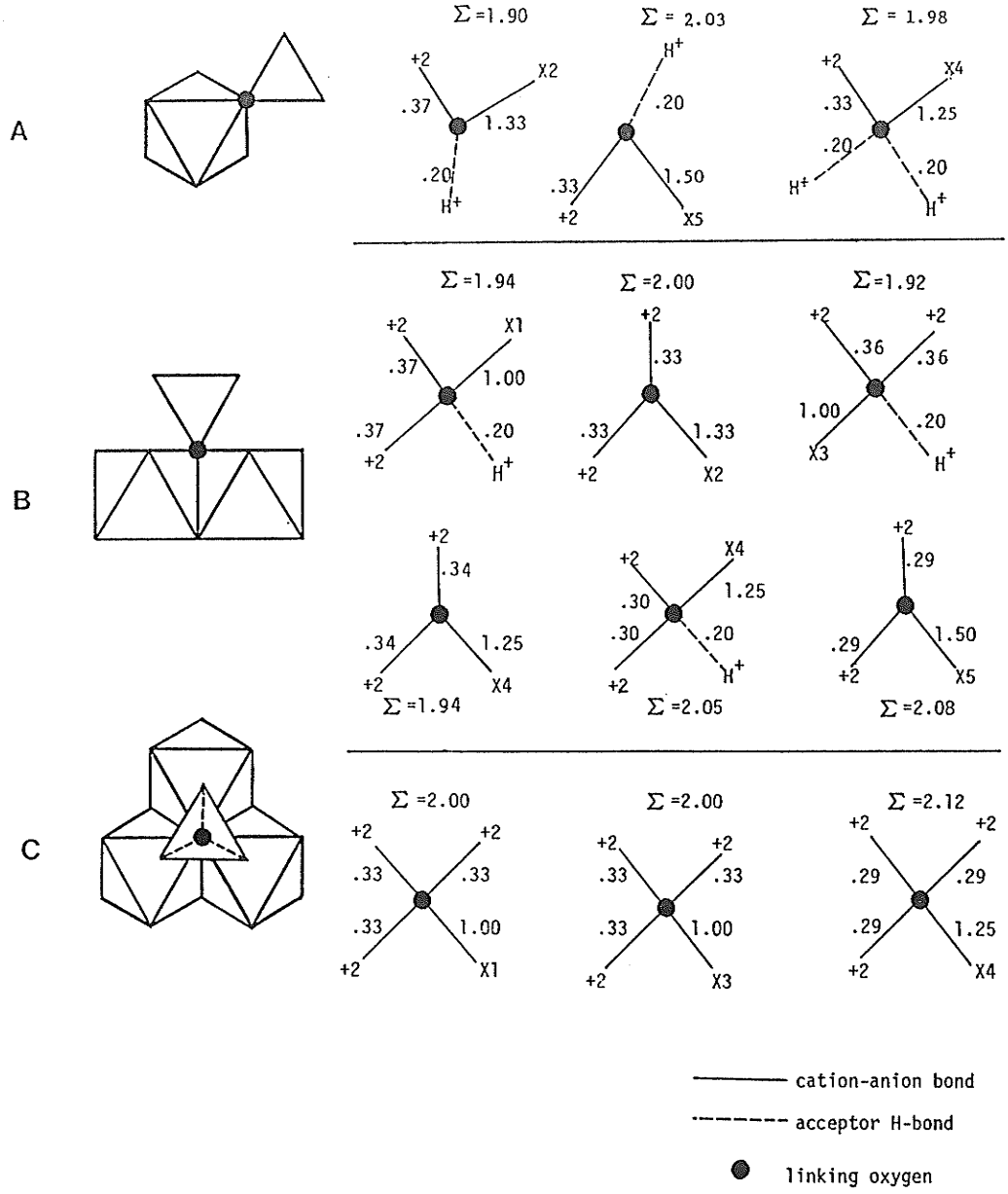

Figure 5.2: Bond-valence Distributions in Regular Octahedra. These are models of the variation in bond-valence distributions observed for regular octahedra; to the left are the basic types of polyhedral linkage, the triangular groups are either TO_4 or TO_3 polyhedra; to the right are models of bond-valence distributions around the linking oxygen anions (solid circles), which pertain to the type of linkage on the left; the range of bond-valences for regular octahedra is 0.29–0.37v.u. with minimal distortions; the symbol +2 indicates an octahedral cation of +2 charge; H^+ is a hydrogen bond (acceptor); and the X-values are types of complex oxyanion with high cation charges, as follows: X1= $T^{3+}O_3$; X2=$T^{4+}O_3$; X3= $T^{4+}O_4$; X4=$T^{5+}O_4$; X5=$T^{6+}O_4$; the bond-valence sums are listed for each unique bond-valence distribution, and indicate a stable topology.

sheets. With SO_4 or CO_3 groups, linkage to an oxygen in an octahedral sheet would result in overbonding of the linking oxygen. Thus, these complex anions are restricted to polymerizations with one or two regular octahedra on a linking oxygen.

With the wide variety of bv combinations possible between apical and equatorial bonds of edge-sharing Cu-octahedra, there is no connectivity with regular octahedra that Cu-octahedra cannot achieve. Figure 5.3 shows the combinations of bond-valences for different linkages, which are equivalent to those of regular octahedra in Figure 5.2. These analogous bv conditions are what make it possible for isostructuralism between Cu^{2+} and other M^{2+} compounds.

There are polymerizations unique to Cu^{2+} oxysalt structures, and they are a result of the weaker apical bond-valences. Polymerization between Cu^{2+}-octahedra and SO_4, NO_3 or CO_3 groups can have a greater degree of connectivity than with regular octahedra. Recall the significant number of Cu-octahedral sheets that have SO_4 tetrahedra attached to three octahedra. This is possible because three weak apical bonds of the octahedra are all linked to the sulphate tetrahedron (Figure 5.4). The total bond-valence contribution from these three octahedra is less than that from two regular edge-sharing octahedra. The linkage between three Cu-octahedra and one CO_3 or NO_3 planar triangle is also made possible by weak apical bond contributions. For example, the polymerization in malachite has a stable bv distribution around the linking oxygen (Figure 5.5). Two equatorial bonds and one weak apical bond make contributions

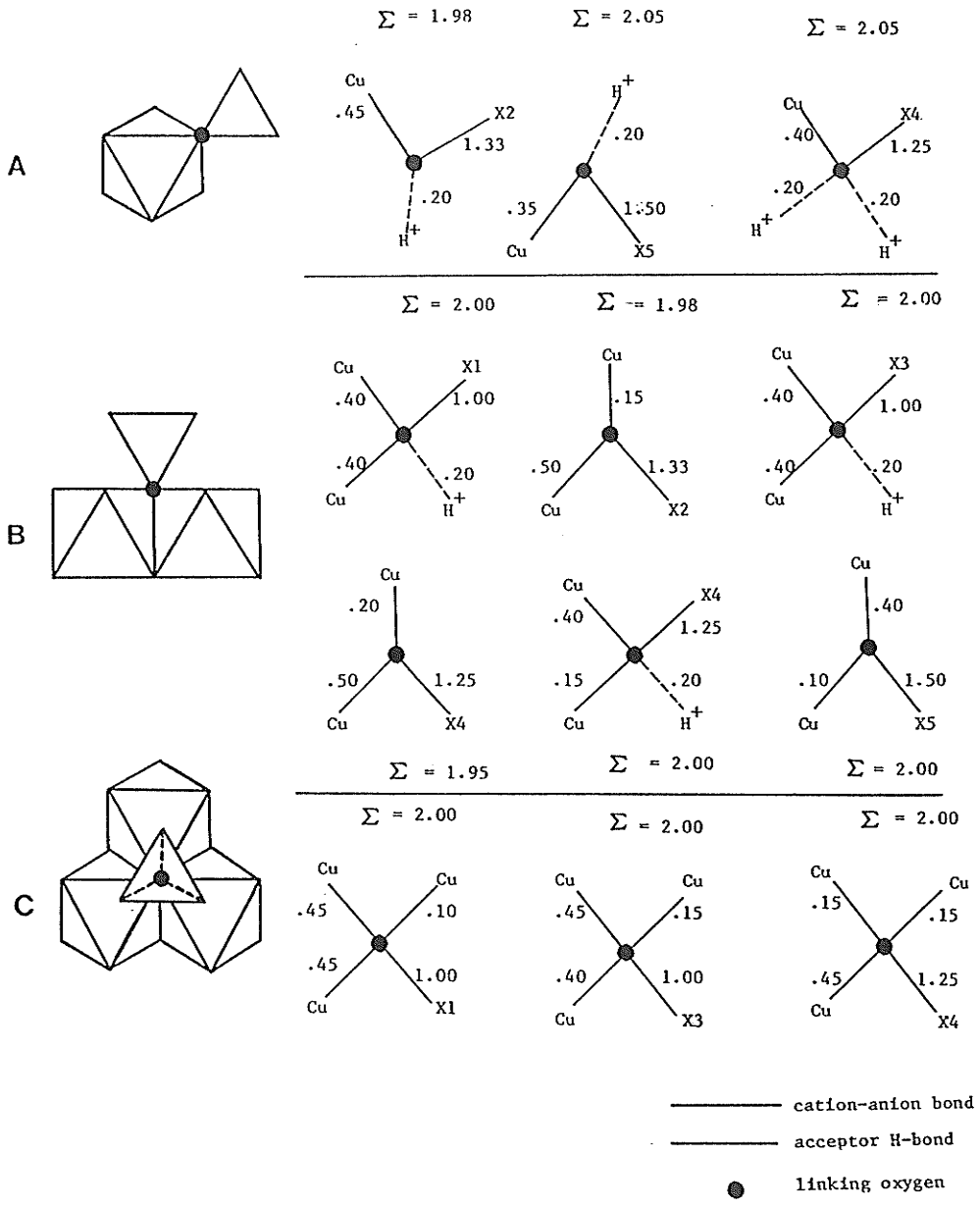

Figure 5.3: Bond-valences Around Cu^{2+}-octahedral Linkages. This is a collection of bond-valence distributions and linkages for Cu^{2+}-octahedra; these linkages are equivalent in style to those for regular octahedra (Figure 5.2), although the bv values differ as a result of the various combinations of equatorial and apical octahedral bonds to the linking oxygen; codings are the same as Figure 5.2.

to the linking oxygen, along with the carbonate triangle. Figure 5.6 shows a bond-valence arrangement in gerhardite that is very similar to the Cu-sulphate sheet in Figure 5.4. Structures with scowhcacs giving bond-valence contributions greater than 1.30 v.u. are unique to Cu^{2+} oxysalts because of the obvious restrictions on bond-valences of the linking anion. Polymerization between two regular-shaped edge-sharing octahedra and a $T^{6+}O_4$ tetrahedron (Figure 5.2b) requires some distortion of the octahedral bond lengths, to prevent overbonding. However, the same topology and bond-valence distribution is achieved in antlerite (Figure 5.7), with the addition of hydrogen-bonding. Overbonding is not a problem with arrangements of this type using Cu^{2+}.

Some structures with both Cu^{2+} and non-Cu analogues show isostructuralism because of flexibility in the bv requirements of the polyhedral arrangement. The function of Cu^{2+}-octahedra in some uranyl-layer structures (discussed in Chapter 3) is essentially that of an interlayer cation. The interlayer cavities are flexible enough to accomodate [8-10]-coordinate cations as well. The bond-valence contributions of these highly coordinated cations to the oxygens in the layers are approximately the same as the linking apical bonds of Cu^{2+}-octahedra (around 0.16v.u.).

The bond-valence arrangements of some structures with a low degree of of polymerization (discussed in Chapter 3) have the potential for substitution between Cu and other octahedral cations. This structural flexibility is possible because of the flexible nature of

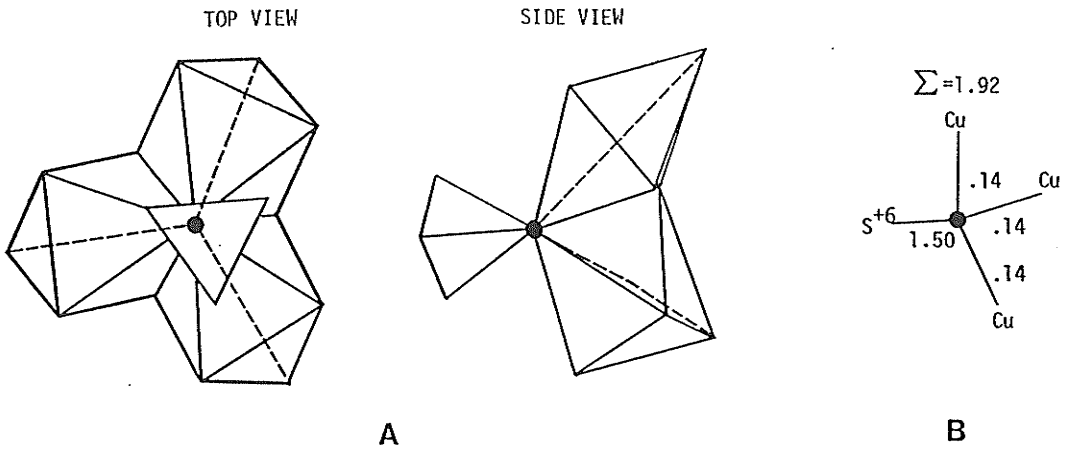

Figure 5.4: Bond-valence Distribution in a Copper-Sulphate Sheet. (a) polyhedral fragment of a Cu-octahedral sheet structure and cornerlinking SO_4 tetrahedron; notice that the three apical octahedral bonds (dashed) are attached to the linking oxygen (solid circle); (b) the bond-valence distribution of (a), with weak apical bond-valences.

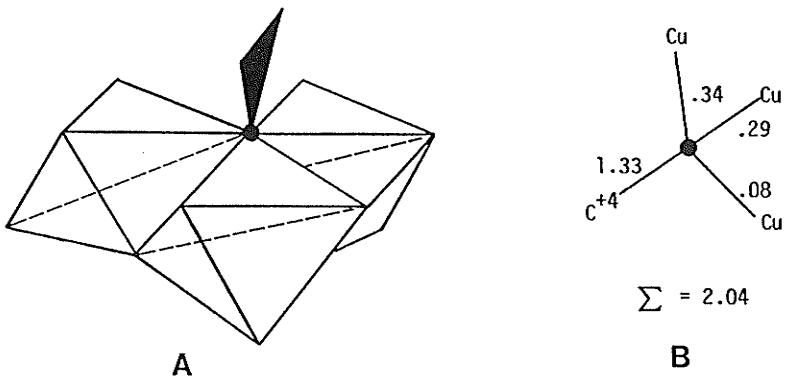

Figure 5.5: Bond-valences in Part of the Malachite Structure. (a) polyhedral fragment of the double-octahedral chains in malachite, with the apical bonds (dashed) and the linking oxygen (solid circle); (b) the bond-valence distribution of (a), with two equatorial and one apical octahedra bonds linked to a carbonate bond.

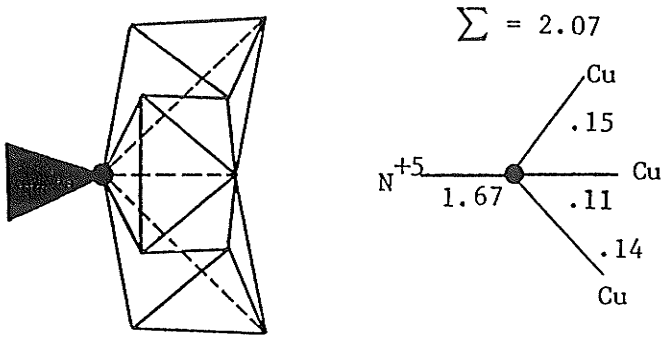

Figure 5.6: Bond-valence Distribution in Gerhardite. A polyhedral fragment of gerhardite, the sheet of Cu-octahedra cornerlinked (solid circle) to a nitrate triangle (left), with apical bonds dashed; to the right, the bond-valence distribution of the polyhedral fragment, similar to that of Figure 5.5.

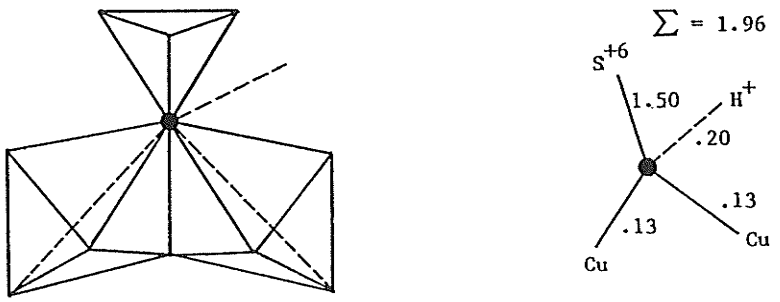

Figure 5.7: Bond-valences in Part of the Antlerite Structure. (a) edge-sharing octahedra corner-linked to a sulphate tetrahedron, with hydrogen-bonding as well (dashed), in antlerite; (b) the bond-valence distribution of (a).

hydrogen-bonding conditions surrounding the octahedra. The H-bonds buffer modifications in the bond-valences that result from changes in the bond lengths of the octahedra. Therefore, substitution is possible between J-T distorted octahedra and non-distorted octahedra. Figure 5.8 shows the accomodation of regular M^{2+}- and Cu^{2+}-octahedra into a structure, made possible by changes in H-bonding.

Considering the geometrical factors which influence polymerization, recall that many common rock-forming silicates (pyroxenes, amphiboles, and micas specifically) require significant geometrical distortions in their octahedra to accomodate the bond-valence requirements. The geometrical distortions of Cu^{2+}-octahedra are also quite varied (c f. chapters 3 & 4). However, a feature which is nearly unique to Cu^{2+}-octahedra is edge-sharing with scowhcacs. The geometrical flexibility of Cu^{2+}-octahedra allows the apical bonds to deviate significantly from 90° with equatorial bonds. The angular distortion mechanism involved (discussed in Chapter 4) provides a very short edge for sharing with scowhcacs, as do the already shortened equatorial edges (a result of the J-T effect). Cu^{2+} oxysalts with this edge-sharing feature (Figure 5.9) have unique bond-valence distributions around the linking oxygens of the shared polyhedral edges. The bvs of the linking anions are stable in these structures. Nesquehonite, $MgCO_3 \cdot 3H_2O$, is the only non-Cu mineral that shows this special edge-sharing feature (Hawthorne, 1986b).

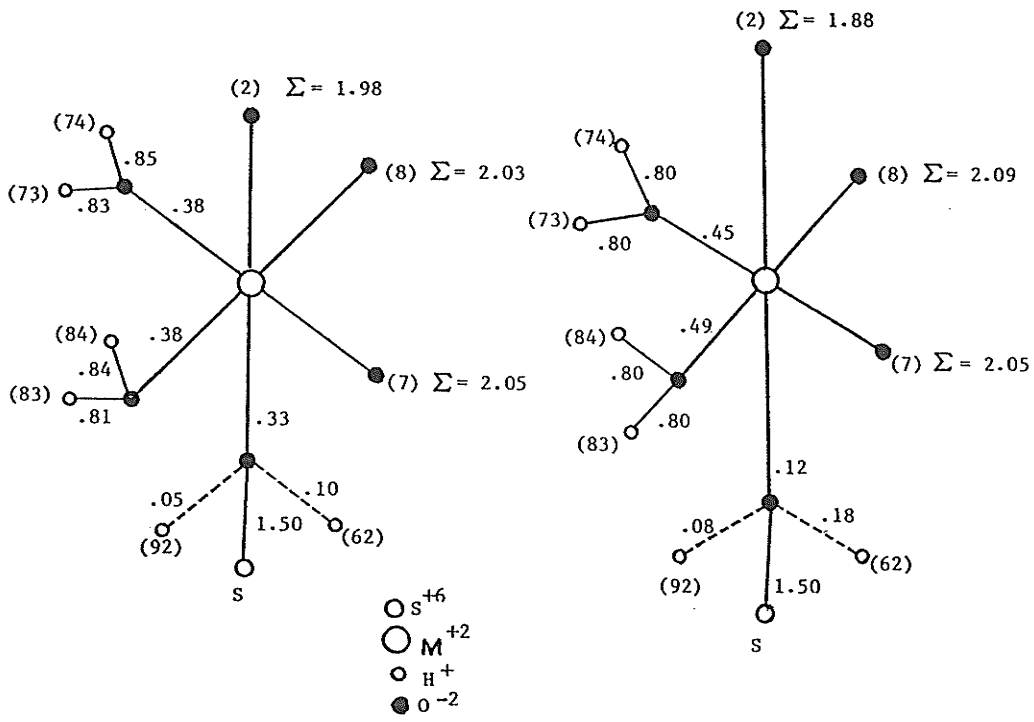

Figure 5.8: Bond-valences Around Flexible Octahedral Sites. To the left is the bond-valence distribution around an Mg octahedron, and to the right, around a Cu-octahedron; The changes in octahedral bond length produce different bv contributions to the linking oxygens (centrosymmetrically related about M^{2+}); H-bonding conditions are therefore also different, assuring that bvs of the anions are adequate. H-bonds are dashed; O^{2-} and H^{+} sites are numbered in brackets; the data are from the M(2) sites of the cyanochroite structure.

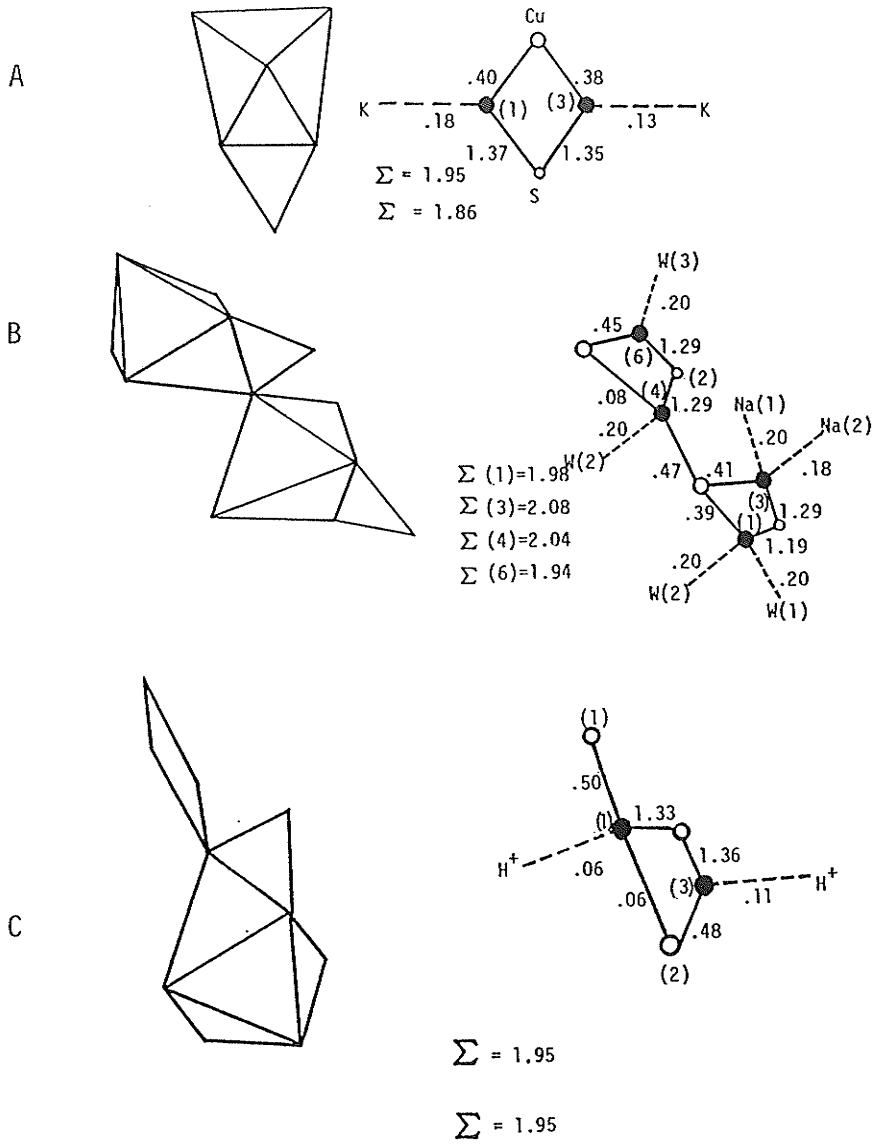

Figure 5.9: Bond-valences in Unique Edge-Sharing Polyhedra. Bond-valence distributions around unique edge-sharing polyhedral linkages; the polyhedra are to the left, and the bond-valence patterns are to the right; linking oxygens (large solid circles) are numbered (in brackets); scowhcacs->small open circles; Cu->large open circles; (a) the arrangement in chlorothionite, with K^+-O bonds dashed; (b) the arrangement of chalconatronite, with two carbonate sites, one sharing an edge with two equatorial Cu-bonds, while the other shares an edge with one apical and one equatorial Cu-bond; the hydrogen-bonding is idealized to 0.20vu; (c) the arrangement of azurite, with square planar Cu included, the carbonate triangle shares an edge with one apical and one equatorial bond; the bvs of all the linking oxygens in these examples are adequate.

5.2 SUMMARY

In observing the bond-valence characteristics of oxysalt structures, one finds that the Jahn-Teller distortion of Cu^{2+}-octahedra provides a wide variablity of bond-valence distributions for linkage to other polyhedra. This variability is unparalleled in the M^{2+}-octahedra of non-Cu oxysalt structures. The variability in bond-valence distributions provides Cu^{2+} with the ability to polymerize to a higher degree with complex oxyanions of higher cation charges (i.e. S^{6+}, N^{5+}, C^{4+}). The adaptability of Cu^{2+}-octahedra to the bond-valence conditions of non-Cu polyhedra allows for isostructuralism with non-Cu structures.

Chapter VI

DISTANCE LEAST-SQUARES MODELLING OF Cu^{2+} OXYSALT STRUCTURES

In this chapter, the Distance Least Squares method (DLS) is used to explore long-range structural effects of local polyhedral distortions in Cu^{2+} oxysalts, and non-Cu analogue structures. Such calculations help to answer the two key questions of this thesis:

1. Why do some Cu^{2+} oxysalts have structural analogues without Cu^{2+}?
2. Why are some Cu^{2+} oxysalts structurally unique?

6.1 THE DLS METHOD

Usually, a crystal structure has more unique interatomic distances than structural parameters. Thus one can express the structural parameters in terms of the interatomic distances. Given an initial structure (model), it is possible to calculate the most plausible final structure (target) by means of least-squares adjustments of interatomic distances prescribed for the target structure. Meier & Villager (1969) formalized these ideas and wrote a computer program called DLS. The coordinates of the model structure, refined towards the final target, represent an idealized structure (with respect to the ideal bond lengths assigned by the user).

DLS operates on the basis of the minimization function:

$$R(x) = \sum_{j=1}^{n} w_j^2 \left[d_{j(x)} - d_{j(pr)} \right]^2 \qquad (6.1)$$

where: $d_j(pr)$ is the prescribed interatomic distance (bond length); $d_j(x)$ is the interatomic distance calculated from the model; and w_j is the weight assigned to the prescribed bond lengths. The sum of R(x) is calculated from all the distances specified within the smallest polyhedral representation of the structure. Hence, using the model structure with distances d(x), the atomic coordinates are shifted successively by least-squares adjustments towards the target structure with bond lengths d(pr). The minimization function is called the error equation (Meier & Villager, 1969). The final R(x) value represents the degree of fit between the refined bond lengths of the model and those proposed for the target.

Baur (1981) emphasizes the importance of proper weighting in DLS refinement. The conventional method is to weight cation-anion distances proportional to their Pauling (1960) bond strengths; anion-anion distances are weighted much lower. This allows cation polyhedra to be flexible, and makes the weighted bonds proportional to the force constants within molecules. Baur (1981) suggests that a properly weighted DLS calculation resembles a classical mechanical model of interconnected springs, with the function:

$$V = \frac{1}{2} k (r - r_e)^2 \qquad (6.2)$$

where: r_e= the equilibrium length; r= the stressed length; k= the force constant; and V= the total potential energy. V reaches a minimum by the springs adjusting themselves to minimize the potential energy. Similarly, R(x) corresponds to the minimum potential energy of a system of atomic springs, with weights equal to the force constants of their equilibrium distances d(pr). Therefore, the DLS method is a model

building technique using elastically flexible coordination polyhedra (Baur, 1981). A significant difference between the simple spring model and DLS is that translational symmetry plays a profound role in constraining the refinement process of DLS.

DLS is a very flexible program, because is allows the user to manipulate the model structure towards the target in a variety of ways. Cation ordering, pressure/temperature effects, and partial structural refinement have all been studied using DLS. Discretion by the user is necessary because bond lengths, weights, and control of unit cell parameters are left to the programmer to decide. A low R value can be meaningless without proper use of the program to achieve the desired results; e.g., constraining cell dimensions profoundly affects the manner of atomic rearrangement, and thus the degree of fit R(x). Manipulation of symmetry between the model and target is tricky, and requires good judgement; e.g., if model symmetry is lowered, does one still have a valid mechanism of structural rearrangement?

6.2 APPLICATION TO CU^{2+} OXYSALT STRUCTURES

6.2.1 The General Problem

By idealizing the geometry of polyhedra while maintaining the topology of the more strongly bonded polymerized units, one can gain an understanding of the structural effects of polyhedral distortion. Therefore, the effects of Jahn-Teller distortions can be well characterized by using DLS. Bond-valence analysis is used in conjunction with DLS to understand the effects of (4+2)- distortions on the bonding of several structure types.

Structures of Cu^{2+} oxysalts which have non-Cu analogues are generally not a mystery. The great flexibility of cation polyhedra within structures that have a low degree of polymerization is obvious (bond-valence constraints are not strict). DLS is not necessary in this case because the J-T distorted Cu^{2+}-octahedra are readily substituted for by other elements with more regular coordinations. However, some structure types require further study. For example, the olivenite group of structures all have (4+2) distortions, but the minerals without copper lack the electronic driving force (J-T effect) for the (4+2) distortion. The kieserite structure shows the same relationship. Why do the non-copper analogues have M^{2+} polyhedra which mimic the J-T distortion? Polyhedral idealization using DLS will answer this question.

Many Cu^{2+} oxysalts are structurally unique. The reasons for their exclusiveness are often apparent solely by bond-valence analysis (non-distorted octahedra violate bond-valence rules within certain topologies). However, by studying some very distorted structures with DLS, and attempting to refine towards a target, interesting results lead to important conclusions about certain structures.

6.2.2 The Method of Analysis

To study the effects of large polyhedral distortions, it is necessary to make the polyhedra regular and examine the resulting structural changes. By studying the idealized structure, one can answer why distortions are necessary in the real structure, using bond valence (bv) theory and simple geometrical arguements. The general criterion is to idealize

those polyhedra which define the structural identity of the mineral in terms of polymerization. The non-polymerized units (usually more weakly bonding) are left to adjust freely in response to polyhedra which are idealized. This is done by weighting the idealized polyhedra in the least-squares process much more than the freely adjusting units.

Polyhedral idealization will cause a structure to expand and contract in certain directions, in response to the changes in polyhedral shape and volume. Therefore, cell parameters are allowed to freely adjust with structural modifications (within the constraints of symmetry). Constraining the unit cell could result in stifling the idealization process. Cell dimensions of the original model are input, and are then refined as least-squares variables.

Figure 6.1 outlines the program steps taken for structural idealization. Model input is data from the real structure which will be shifted towards the target structure. Atomic coordinates of symmetrically unique atoms are accompanied by their symmetrically related atoms within the smallest polyhedral representation of the structure. Each x,y,z coordinate of a symmetrically dependent atom is coded with its symmetry relation to the unique atom. This procedure fixes the symmetry of the structure within the program, and the coding remains constant throughout execution. Interatomic distances within the polyhedral arrangement are listed as pairs of atoms, and a target bond length is given to each atom pair.

The target input determines how the model will be modified. Bond lengths for ideal polyhedra were chosen from Brown & Shannon (1973), and

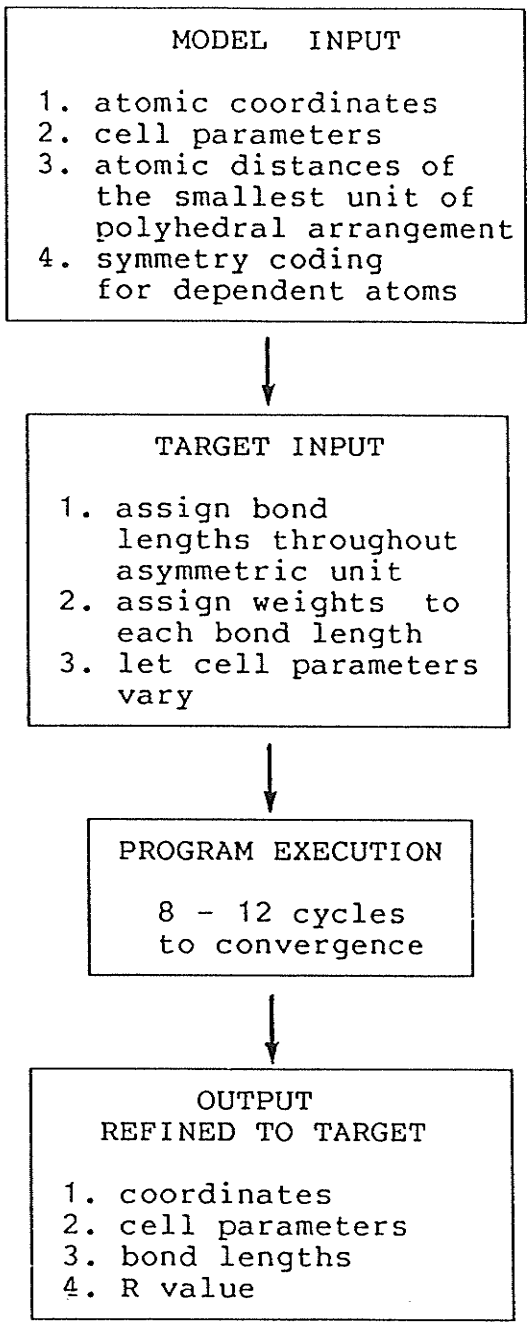

Figure 6.1: Flowchart of the DLS Program Parameters and Operation

represent ideal bond-valences. The Cu-O bond length of 2.084Å represents zero octahedral distortion and an ideal bond-valence (established in Chapter 4). This value is in agreement with Brown & Shannon (1973), and is used for DLS. Oxygen-oxygen distances are $2\sqrt{2}$ of cation-anion distances for octahedra, and 2cos35.24° of cation-anion distances in tetrahedra.

Weights assigned to idealized polyhedra were initially set equal to Pauling's (1960) bond strengths. However, if structures resist idealization with these starting weights, then the polyhedra which deviate most from their ideal are weighted higher. Usually, R(x) grows and indicates that there is some inherent structural resistance to idealization. Anion-anion distances are usually weighted between 0.1 and 0.3 of the strongest bond-valences. Non-idealized polyhedra are characteristically weighted below 0.1 of the strongest weighted distance. Cation-cation distances are initially weighted <0.05, and if the distance refines to an unacceptably low level, then the weight is increased to prevent cation collisions (if necessary). Each unique bond length for the target input is assigned a corresponding weight.

Refinements of 8-10 cycles are usually sufficient for convergence, unless the structural changes are not realistically possible. R values below 0.01 indicate that the refinement has proceeded without significant structural problems. R values above 0.01 indicate that idealization is incomplete in the strictist sense, and a compromise was reached between the atoms in competition for space.

Occasionally, the final coordinates reflect a symmetry which is higher than that of the starting structure. The symmetry cannot be lowered. Raising of symmetry can be expected, because polyhedral idealization can make certain atoms equivalent on a symmetry element where they were originally distinct.

Refined structures have bond-valence relations which require examination. As well, there are atomic distances which often violate the accepted limits.

Isostructural members usually have identical symmetry, and the correlation between their DLS input files is 100%. That is, one member can be idealized using the other member's bond lengths e.g. libethenite refined towards ideal andalusite. However, if a structure is nearly isostructural with another mineral (psuedo-orthorhombic olivenite and orthorhombic libethenite), the degree of compatibility between the two can be tested by simulation of the structures. Refinement can be towards the actual (non-ideal) structure of the related mineral using the best approximation of true bond lengths that the user has available. This procedure verifies the applicability of DLS to the structural series being studied.

If a structure resists idealization (R will not converge), then the structure is either incorrectly modeled, or it is of the type that cannot be idealized without modification of topology (upon which the identity of the structure is lost). After testing and ruling out the former possibility, graphical analysis of the structure should confirm that the structure cannot be idealized.

6.3 DLS MODELING OF RELATED STRUCTURE TYPES

6.3.1 The Olivenite Group

The olivenite group consists of olivenite $Cu_2(AsO_4)(OH)$, libethenite $Cu_2(PO_4)(OH)$, adamite $Zn_2(AsO_4)(OH)$, and andalusite $Al_2(SiO_4)O$ (structural data of adamite from Hawthorne, 1976; and of andalusite from Winter & Ghose, 1979). This isostructural group has a structure of edge-sharing octahedral chains cross-linked by tetrahedra into a framework (discussed in Chapter 3). It will be shown here that a (4+2) distortion is inherent in the octahedra of this structure type. The Cu-members have a more pronounced distortion, because of the J-T effect. Because the non-Cu members do not possess the J-T effect, a DLS study is used to analyse why their octahedra are not more regular in shape.

The first application of DLS to this structure series was to test the compatibility between olivenite ($P2_1/n$; $\beta=90°$) and the other fully isostructural members (Pnmm) during structural simulations. The a- and b-axes of libethenite are reversed to conform to the rest of the members. Olivenite was refined towards libethenite target values, and visa versa, using structural data from Toman (1977) and Corsden (1978) respectively. Appendix B1 lists the output for all refinements of the olivenite group, and these first two simulations are labelled "olivenite towards libethenite" and "libethenite towards olivenite".

The β angle was not allowed to vary in monoclinic olivenite, which keeps the structural changes in this mineral as similar as possible to changes in the other members. Cell dimensions from the simulated structures of olivenite and libethenite closely match the dimensions of the actual target structures (Table 6.1). The degree of fit between

idealized and actual structures is acceptable within the limits of the program. In other words, when a non-idealized structure is simulated, there is a limit to the degree of fit obtainable by the program structure, but the target input is only an approximation to these

TABLE 6.1

Cell Dimensions of the Olivenite Group

Actual Structures:	a(Å)	b(Å)	c(Å)	Volume
Olivenite	8.615	8.240	5.953	422.6
Libethenite	8.384	8.062	5.881	397.5
Adamite	8.304	8.530	6.047	428.3
Andalusite	7.798	7.903	5.557	342.5
DLS Simulations:				
Olivenite towards Libethenite	8.254	8.194	5.852	395.8
Libethenite towards Olivenite	8.614	8.263	5.916	421.1
DLS Idealizations:				
Olivenite	7.791	8.109	5.848	369.5
Libethenite	7.974	7.774	5.815	360.5
Adamite	8.135	8.200	5.872	391.7
Andalusite	7.694	7.626	5.382	316.0

values).

After being satisfied that the structures of this series behave the same way to DLS simulations, the structures were then idealized. The four and six coordinate polyhedra (framework components) are weighted to their Pauling (1960) bond strengths, and given ideal bond lengths of the particular cation anion bonds (As-O=1.68Å; P-O=1.537Å; etc.). The

[5]-coordinate dimeric polyhedra are given low weights, allowing them to freely adjust to framework idealizations. Refinement outputs are labelled "Mineral Idealized"; where mineral is the particular member (Appendix B1).

Cell dimensions of the idealized structures are significantly different from the those of the actual minerals (Table 6.1). Structural modifications from idealization are evident when observing the structure before and after DLS refinement (Figure 6.2). Although the topology of the framework is maintained, the arrangement of oxygens and ^{5}M cations is visibly altered. During idealization, the apical anions of Cu-octahedra in olivenite become symmetrically equivalent, thus making the ideal olivenite structure orthorhombic.

Rearrangement of ^{5}M cations and framework anions, due to idealization, has resulted in characteristic violations of accepted interatomic distances in all members of the olivenite structure type (Table 6.2). Three types of violations occur:

1. Bonds from apical octahedral oxygens to ^{5}M are too short (labelled as Trig-Bipmd in Table 6.2 under the symptoms column). The ^{5}M-O(1) bonds are also too short (labelled as Trig-Bipmd).
2. Unshared corners of the tetrahedra have moved too close to $(OH)^{-}$ groups on the shared edges of the octahedra (labelled tetra-OH under symptoms column).
3. The unshared tetrahedral oxygens have also moved too close to each other (O(1)-O(1); labelled as tetra-tetra), representing collision between neighboring tetrahedra.

A

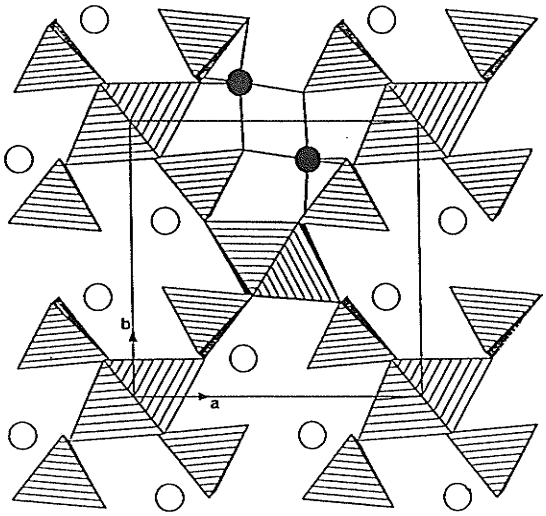

B

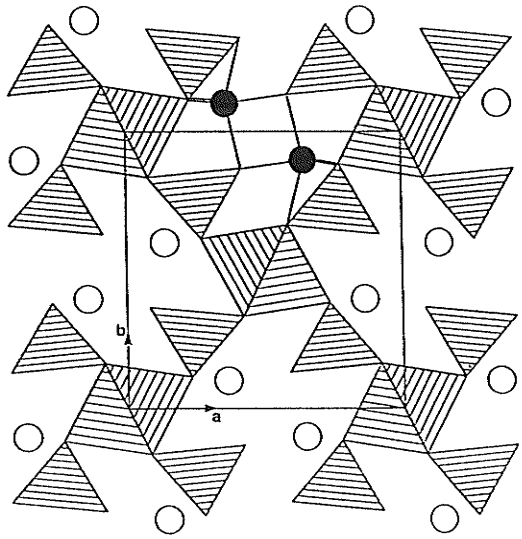

Figure 6.2: Actual and Idealized Olivenite Framework. (a) Distorted octahedra of the olivenite framework structure, and ^{5}Cu (as circles); (b) the idealized olivenite framework structure, with octahedral chains rotated relative to the actual structure.

TABLE 6.2

Atomic Distance Violations in the Idealized Olivenite Group

Mineral	Atom Pairs in Violation	Violation Symptoms
Olivenite	^{5}Cu - O(1) = 1.796(Å)	Trig-Bipmd
	^{5}Cu - O(4) = 1.841	Trig-Bipmd
	^{5}Cu - O(5) = 1.830	Trig-Bipmd
	O(1) - OH = 1.992	tetra - OH
Libethenite	^{5}Cu - O(1) = 1.814	Trig-Bipmd
	^{5}Cu - O(4) = 1.818 (x2)	Trig-Bipmd
	O(1) - OH = 2.267	tetra - OH
	O(1) - O(1)= 2.430	tetra - tetra
Adamite	^{5}Zn - O(1) = 1.875	Trig-Bipmd
	^{5}Zn - OH = 1.877 (x2)	Trig-Bipmd
	O(1) - OH = 2.207	tetra - OH
	O(1) - O(1)= 2.489	tetra - tetra
Andalusite	^{5}Al - O(1) = 1.672	Trig-Bipmd
	^{5}Al - O(4) = 1.737 (x2)	Trig-Bipmd
	O(1) - OH = 2.097	tetra - OH
	O(1) - O(1)= 2.186	tetra - tetra

Numbers for the atoms from all members are made equivalent to olivenite; e.g. O(1) of libethenite is O(3) from Corsden (1978)

Another structural problem, due to idealization, is evident for all members of the olivenite group. When bond-valence tables are constructed for the different members (Table 6.3), their bond-valence (bv) distributions are very similar, both before and after DLS refinements. Bond-valence sums (bvs) for ^{5}M cations are beyond the accepted levels of stability, and the oxygen bvs show overbonding in all sites except the shared octahedral edges.

TABLE 6.3

Bond-Valence Tables for the Idealized Olivenite Group

Before Idealization

OLIVENITE

Bond lengths from Toman, 1977

	Cu(1)	Cu(2)	As	H	Σ O⁻²
O(1)	0.405(x2)→		1.316		= 2.126
O(2)		0.491,0.409	1.158		= 2.058
OH	0.575	0.249,0.456		0.80	= 2.080
O(4)	0.260	0.167	1.102	0.20	= 1.729
O(5)	0.440	0.130	1.442		= 2.012
M⁺	2.085	1.902	5.018	1.00	

LIBETHENITE

Bond lengths from Corsden, 1978

	Cu(1)	Cu(2)	P	H	Σ O⁻²
O(1)	0.483,0.356		1.220		= 2.059
O(2)		0.450(x2)→	1.179		= 2.079
OH	0.503	0.429(x2)→		0.88	= 2.241
O(4)	0.344(x2)↓	0.137(x2)↓	1.321(x2)↓	0.12	= 1.922
M⁺	2.032	2.030	5.041	1.00	

ADAMITE

	Zn(1)	Zn(2)	As	H	Σ O⁻²
O(1)	0.650,0.474		1.240		= 2.364
O(2)		0.335(x2)→	1.240		= 1.910
OH	0.430	0.335(x2)→		1.0	= 2.100
O(4)	0.645(x2)↓	0.333(x2)↓	1.250(x2)↓		= 2.228
M⁺	2.844	2.007	4.980	1.00	

ANDALUSITE

Bond lengths from Winter & Ghose, 1979

	Al(1)	Al(2)	Si	Σ O⁻²
O(1)	0.598,0.511		1.034	= 2.143
O(2)		0.522(x2)→	0.959	= 2.003
O(3)	0.636	0.617(x2)→		= 1.870
O(4)	0.639(x2)↓	0.312(x2)↓	1.00(x2)↓	= 1.951
M⁺	2.902	3.023	3.993	

After Idealization

OLIVENITE

	Cu(1)	Cu(2)	As	H	Σ O⁻²
O(1)	0.701,0.491		1.250		= 2.442
O(2)		0.346(x2)→	1.250		= 1.942
OH	0.468	0.340(x2)→		0.80	= 1.948
O(4)	0.646(x2)↓	0.340(x2)↓	1.250(x2)↓	0.20	= 2.433
M⁺	2.952	2.052	5.000	1.00	

LIBETHENITE

	Cu(1)	Cu(2)	P	H	Σ O⁻²
O(1)	0.448,0.664		1.250		= 2.362
O(2)		0.337(x2)→	1.250		= 1.932
OH	0.657	0.337(x2)→		1.00	= 2.331
O(4)	0.523(x2)↓	0.333(x2)↓	1.250(x2)↓		= 2.106
M⁺	2.816	2.014	5.000	1.00	

ADAMITE

Bond lengths from Hawthorne, 1976

	Zn(1)	Zn(2)	As	H	Σ O⁻²
O(1)	0.430,0.371		1.198		= 1.999
O(2)		0.367(x2)→	1.308		= 2.042
OH	0.398	0.382(x2)→		1.0	= 2.162
O(4)	0.424(x2)↓	0.211(x2)↓	1.233(x2)↓		= 1.868
M⁺	2.047	1.920	4.972	1.00	

ANDALUSITE

	Al(1)	Al(2)	Si	Σ O⁻²
O(1)	0.928,0.625		1.004	= 2.557
O(2)		0.499(x2)→	1.004	= 2.002
O(3)	0.626	0.499(x2)→		= 1.624
O(4)	0.782(x2)↓	0.495(x2)↓	1.004(x2)↓	= 2.281
M⁺	3.734	2.986	4.016	

It is now evident why a (4+2) octahedral distortion is required in the olivenite group framework structure. Idealization results in crowding of the [5]-coordinate cation polyhedra in the framework cavities, causing overbonding of both ^{5}M cations and the associated oxygens. Therefore, the characteristic 4+2 geometry of Cu^{2+} is well-suited to this structure type. Other cations must mimic the (4+2) distortion (without the J-T effect) to achieve structural stability. Limits on the magnitude of distortions possible for other elements control their potential to crystallize in the olivenite structure. These limits are not well-defined. Fe^{2+} shows the second order J-T effect, and should be a likely candidate for the olivenite structure.

6.3.2 The Kieserite Structure Group

The kieserite group of minerals (Table 6.4) has the general formula $^{6}M^{2+}(SO_4)\cdot H_2O$, and is a structural subgroup of the titanite group of minerals (Hawthorne et al., 1987), with the formula $^{7}A^{6}M(TO_4)(O,OH,H_2O,F)$. The A-site is vacant in the kieserite subgroup. The kieserite series contains the copper member poitenvenite, whose structure is unrefined. The kieserite structure was discussed in Chapter 3. It is suspected that this structural series contains an inherent (4+2) octahedral distortion, because kieserite (the only structure so far refined) has such a distortion pattern. Kieserite has four equatorial bonds (ave.=2.030Å) and two apical bonds (2.172Å); the latter are H_2O groups that corner-link the octahedra into chains along [001]. Poitenvenite presumably has the same distortion, because of the

characteristic J-T effect of Cu^{2+}. The relatively simple framework of this structural series is a flexible one, allowing rearrangement for A-site occupancy. The reasons for an Mg-member to mimic the J-T

TABLE 6.4

Minerals Structurally Related to Kieserite

Mineral	Formula	a(Å)	b(Å)	c(Å)	β(°)	Sp.Gr.
Dwornikite	$[Ni(SO_4)(H_2O)]$	6.839	7.582	7.474	117.85	C2/c
Gunningite	$[Zn(SO_4)(H_2O)]$	6.954(8)	7.586(8)	7.566(8)	115.93(3)	C2/c
*Kieserite	$[Mg(SO_4)(H_2O)]$	6.912(2)	7.624(2)	7.642(2)	117.70(2)	C2/c
Poitevinite	$[Cu(SO_4)(H_2O)]$	7.176(10)	7.426(10)	7.635(10)	116.15(3)	C2/c
Szmikite	$[Mn(SO_4)(H_2O)]$	7.120(1)	7.666(1)	7.766(1)	115.85(1)	C2/c
Szomolnokite	$[Fe^{2+}(SO_4)(H_2O)]$	7.123	7.468	7.624	115.9	C2/c

(from Hawthorne et al., 1987)

distortion are a problem to be answered with DLS.

Kieserite structural data was used as model input. As the symmetry for all the members of this series is C2/c, we can assume that all the structures are equivalent to simulations using DLS. Target input for the idealized structure and the refinement output are in Appendix B2. Idealization produced no polyhedral collisions. The R value (0.000015) is essentially zero, indicating that structural changes to ideality were fully completed. Therefore, polyhedra in the kieserite structure can be idealized without any geometrical structural problems.

Bond-valence tables of the kieserite structure, before and after idealization (Table 6.5), show interesting results. In the actual

structure, the bvs on the O(3) apical bond deviates somewhat from the formal valence. In addition, O(1) is close to being underbonded. Idealizing the structure has exaggerated the imbalance of bvs on both O(1) and O(3), with O(3) becoming significantly overbonded, and O(1) becoming underbonded. The O(2)-O(3) distance of 2.780Å indicates that the H-bonding potential is not significantly affected by polyhedral

TABLE 6.5

Bond-Valence Tables for Kieserite

Before ->

	Mg	S	H	Σ O^{-2}
O(1)	0.391(x2)	1.543(x2)		= 1.934
O(2)	0.373(x2)	1.490(x2)	0.20	= 2.063
O(3)	0.286(x2)		0.80(x2)	= 2.172
M^+	2.100	6.066	1.00	

After ->

	Mg	S	H	Σ O^{-2}
O(1)	0.333(x2)	1.500(x2)		= 1.833
O(2)	0.333(x2)	1.500(x2)	0.17	= 2.003
O(3)	0.333(x2)		0.83(x2)	= 2.326
M^+	2.000	6.000	1.00	

Bond-valence curves used from Brown (1981)
(bond lengths of actual kieserite from Hawthorne et al., 1987)

rearrangements.

By idealization, the (4+2) distortion is removed, and the bv conditions of both the corner-linking H_2O groups and the anions not involved in H-bonding, become unstable. Conversely, increasing the

magnitude of the (4+2) distortion beyond that of kieserite octahedra should bring the bvs of the anions closer to their formal valences. Poitenvenite is thus a natural candidate for this structure type.

Because the cell dimensions of poitenvenite are known, it should be possible to predict the atomic coordinates of poitenvenite by refining the kieserite model with DLS. When the model refines to the cell dimensions of poitenvenite, the resulting atomic coordinates and bond lengths should be close to the target Cu-member (providing no atomic collisions occur).

The first refinement towards poitenvenite involved the use of a simple target approximation (labelled "simple model" in Appendix B2). Simple octahedral and tetrahedral distortions were modeled, using only nine unique target bond lengths. Bond-valence sums of this refinement are quite acceptable (Table 6.6). The O(2)-O(3) distance (2.829Å) is preserved for necessary H-bonding conditions. Cell dimensions (Table 6.6) are reasonably well-modeled for the a- and b-axes, but the c-axis and ß angle are poorly represented. Nevertheless, this quick and easy refinement has merit, showing that larger (4+2) distortions are geometrically valid in this structure type, and H-bonding conditions are preserved. Therefore, we can assume that poitenvenite has a "normal" (4+2) distortion.

A more elaborate attempt at predicting the structure of poitenvenite produced results that are not much better than the simple model (labelled "complex model" in Appendix B2). Sixteen unique target distances were used (the maximum allowable). These extra distances were

TABLE 6.6

Bond-Valence and Cell Data for DLS Towards Poitenvenite

Simple Model ->

	Cu	S	H	Σ O^{-2}
O(1)	0.443(x2)↓	1.550(x2)↓		= 1.993
O(2)	0.443(x2)↓	1.450(x2)↓	0.14	= 2.033
O(3)	0.116(x2)→		0.86(x2)→	= 1.952
M^+	2.004	6.000	1.00	

Complex Model ->

	Cu	S	H	Σ O^{-2}
O(1)	0.373(x2)↓	1.550(x2)↓		= 1.923
O(2)	0.495(x2)↓	1.450(x2)↓	0.11	= 2.055
O(3)	0.164(x2)→		0.89(x2)→	= 2.108
M^+	2.064	6.000	1.00	

Bond-valence curves used from Brown (1981)

Cell Dimensions

Simple model - a: 7.170 b: 7.428 c: 8.428 ß: 122.03°
Complex model - a: 6.782 b: 7.422 c: 7.639 ß: 117.90°

an attempt to control polyhedral tilting to achieve the correct cell dimensions. A Cu-Cu distance of half the length of the poitenvenite c-axis was weighted high, thereby fixing the c-axis (Cu at the cell origin, and c/2). Thus, Cu-O rearrangements must involve polyhedral tilting, because c is fixed. The resulting cell dimensions (Table 6.6) are close, except for the a-axis. Polyhedral tilting is not fully represented by the target distances, because the cell volume is not well reproduced.

Bond-valence analysis shows that the structure created is acceptable from a bonding standpoint. The O(2)-O(3) distances (2.894Å) are preserved for H-bonding, although other neighboring O(2) atoms are encroaching upon the H_2O groups (other O(2)-O(3)=2.521Å). This distance may be too close, indicating possible collision of neighboring octahedral chains. As the simple model duplicated the a and b axes, and the more complex model arrived close to the b,c and ß parameters, the true structure of poitenvenite should be representable by DLS. Somewhere between the two target approximations, there exists a compromise which represents the true poitenvenite structure.

6.3.3 The Chalcomenite - Teinite Structure

The topological features of the chalcomenite and teinite structure are discussed in Chapter 3, as are the relationships to the kieserite structure group. The cutoff between octahedral and square pyramidal coordinations in the chalcomenite structure is based on topological considerations. The extreme J-T distortions in the chalcomenite structure should be removable because of the similarity to the keiserite structure (whose structure permits idealization of the octahedra). The idealized chalcomenite structure should therefore resemble the ideal kieserite structure.

Some important differences exist between the chalcomenite structure and the kieserite structure, and they are related to the Se and Te coordinations and connectivity. Bond-valence analyses of chalcomenite and teinite indicate that Se and Te should be considered as (3+3) coordinate (Table 6.7). The three longer bonds (approximately 3.1Å)

greatly improve the bvs of Se and Te. The connectivity of the structure is better described with TO_3 pyramids, because of the irregular shape of the (3+3) coordination. Of course, the opposite is true for the very distorted (4+1+1) coordinations of Cu. The unshared corners of Cu-octahedra are H_2O groups, a result of the TO_3 group rather than TO_4 in kieserite. Therefore, the chalcomenite structure has a more complex arrangement of hydrogen-bonding. The bond-valence distribution is more diverse than in kieserite, and there are more unique oxygen atom positions.

Structural differences from kieserite become quite evident after idealization. Although the geometrical arrangements of this structure type seem to be the same as in kieserite, the bond-valence characteristics that result have different consequences (recall: kieserite H-bonding was preserved). The program output from idealizations are in Appendix B3. Analysis of O(4)-O(1)/O(3) distances (>3.10Å) indicates that the H-bonding potential of H(5) atoms is destroyed after idealization. The bond-valence conditions of the donor and acceptor oxygens (Table 6.7) are thus profoundly altered from those of the actual structures. O(5)-O(5) distances remain about the same for ideal chalcomenite, but this atom pair is farther away in ideal teinite, resulting in the loss of O(5)-H(5)···O(4) bonding. The difference in teinite is presumeably due to the effect of the larger Te^{4+} atom as compared with Se^{4+} in chalcomenite. As in the kieserite structure, idealization causes overbonding of the H_2O group oxygens that corner-link the octahedra together. Similarly, the oxygens of the TO_3 group become underbonded, but moreso than in kieserite. The lower

TABLE 6.7

Bond-Valence Tables for Chalcomenite & Teinite

Before

CHALCOMENITE

	Cu	Se	H4	H4'	H5	H5'	Σ O^{-2}
O(1)	0.443	1.243	0.25				= 1.966
O(2)	0.465	1.240,0.12			0.19		= 2.015
O(3)	0.449	1.211,0.13		0.27			= 2.060
O(4)	0.423		0.75	0.73		0.09	= 1.993
O(5)	0.163,0.028	0.11			0.81	0.91	= 2.021
M+	2.001	4.054	1.00	1.00	1.00	1.00	

After

CHALCOMENITE

	Cu	Se	H4	H4'	H5	H5	Σ O^{-2}
O(1)	0.333	1.240	X				= 1.573
O(2)	0.333	1.240,0.10			0.08		= 1.753
O(3)	0.333	1.240,0.11		X			= 1.683
O(4)	0.333		1.00	1.00		0.08	= 2.413
O(5)	0.333(x2) ↳	0.10			0.92	0.92	= 2.566
M+	2.000	4.030	1.00	1.00	1.00	1.00	

TEINITE

	Cu	Te	H4	H4'	H5	H5'	Σ O^{-2}
O(1)	0.51	1.16	0.25				= 1.92
O(2)	0.46	1.25,0.14			0.23		= 2.08
O(3)	0.45	1.22,0.13		0.26			= 2.08
O(4)	0.48		0.75	0.74		0.08	= 2.04
O(5)	0.18,0.01	0.13			0.77	0.92	= 2.00
M+	2.08	4.05	1.00	1.00	1.00	1.00	

TEINITE

	Cu	Te	H4	H4'	H5	H5'	Σ O^{-2}
O(1)	0.333	1.240	X				= 1.573
O(2)	0.333	1.240,0.11			0.13		= 1.813
O(3)	0.333	1.240,0.11		X			= 1.683
O(4)	0.333		1.00	1.00		X	= 2.333
O(5)	0.333(x2) ↳	0.11			0.87	1.00	= 2.646
M+	2.000	4.050	1.00	1.00	1.00	1.00	

Bond-valence curves of Brown (1981) were used; bond lengths of chalcomenite from Asai & Kiriayama (1973), and for teinite from Effenberger (1977).

charge of the T^{4+} group, relative to T^{6+} in kieserite, demands a greater contibution of H-bonding to oxygens of the TO_3 groups.

One can arrive at conclusions similar to those for the kieserite structure type. The patterns of bvs are quite similar. The chalcomenite and teinite structures require the (4+2) arrangement for proper bond-valence conditions at the anions. But in addition, the arrangement of the octahedra controls the more complex system of H-bonding in this structure type. Distortion requirements on the octahedra are more extreme than in kieserite, because of the H-bonding requirements. Therefore, the chalcomenite and teinite structure will allow only Cu^{2+} with the J-T distortion. Perhaps Mn^{3+} is a candidate for substitution (with proper charge-balance at the T-group).

6.3.4 The Kröhnkite Group

The kröhnkite group of minerals have a structure based on isolated chains of $^{6}M^{2+}(TO_4)_2\emptyset$ building blocks, discussed in Chapter 3. Octahedra of the different members have a (4+2) distortion, although only kröhnkite contains Cu^{2+} with the J-T effect. This distortion requirement is very interesting, because most structures with lower connectivity, having Cu^{2+} and non-Cu analogues, are flexible enough to permit both regular and distorted octahedral geometries. The structure of the kröhnkite group is studied by idealization with DLS, in order to find out why this loosely bonded arrangement does not accomodate regular shaped octahedra.

Idealization of the kröhnkite structure is not as straight forward as the structure types previously described, because DLS is more suitable for use with framework structures. Care must be exercised with refinement of non-framework structures, so that neighboring polymerized units do not collide, simply by lack of control on the rearrangement of weakly bonded structural units. Fortunately, interchain bonding units of the kröhnkite structure are large-cation polyhedra rather than H_2O groups (the latter would be too difficult to model).

The first idealization refinement was done without precautions for polyhedral collisions between neighboring chains (labelled "without restraint" in Appendix B4), using kröhnkite as the model structure. Several major problems arise in this refinement procedure:

1. The OW - O(4) distance between octahedra and tetrahedra in neighboring chains (1.753Å) indicates a collision has occurred.
2. The OW - O(1) distance (2.508Å) between octahedra and tetrahedra within the same chains is too close, and suggests another collision.
3. Considering the bond-valence characteristics of kröhnkite, before and after idealization (Table 6.8), the H-bonding conditions are profoundly altered. OW - H(2)···O(4) is destroyed by polyhedral collision, and OW - H(1)···O(1) is considerably shortened (producing an unusually strong donor bond to O(1)).
4. The Na^+ is more overbonded than in the actual structure, as are OW and O(2). O(4) has become underbonded by the loss of H-bonding.

TABLE 6.8

Kröhnkite Bond-Valence Tables, Before/After Idealization

Before DLS Refinement

	Na	Cu	S	H1	H2	Σ O^{-2}
O1	0.14		1.55	0.26		= 1.95
O2	0.17,0.14	0.14	1.50			= 1.95
O3	0.15	0.44	1.38			= 1.97
O4	0.16,0.15		1.49		0.20	= 2.00
OW	0.19	0.49		0.74	0.80	= 2.22
M^+	1.10	2.14	5.92	1.00	1.00	

Idealization Without Restraints

	Na	Cu	S	H1	H2	Σ O^{-2}
O1	0.151		1.500	0.38		= 2.031
O2	0.120,0.175	0.333	1.500			= 2.128
O3	0.226	0.335	1.500			= 2.061
O4	0.146,0.178		1.500		XX	= 1.824
OW	0.216	0.333		0.62	1.00	= 2.169
M^+	1.212	2.003	6.000	1.00	1.00	

Bond lengths before DLS from Hawthorne & Ferguson (1975); Bond-valence curves used from Brown (1981).

In viewing the structure before and after idealization (Figure 6.3), one can observe the relative change in Na positions with reference to the chains (hence the overbonding of Na). One also sees that the distance between tetrahedra and octahedra in neighboring chains has become appreciably closer (dashed line for OW - O(4) distance).

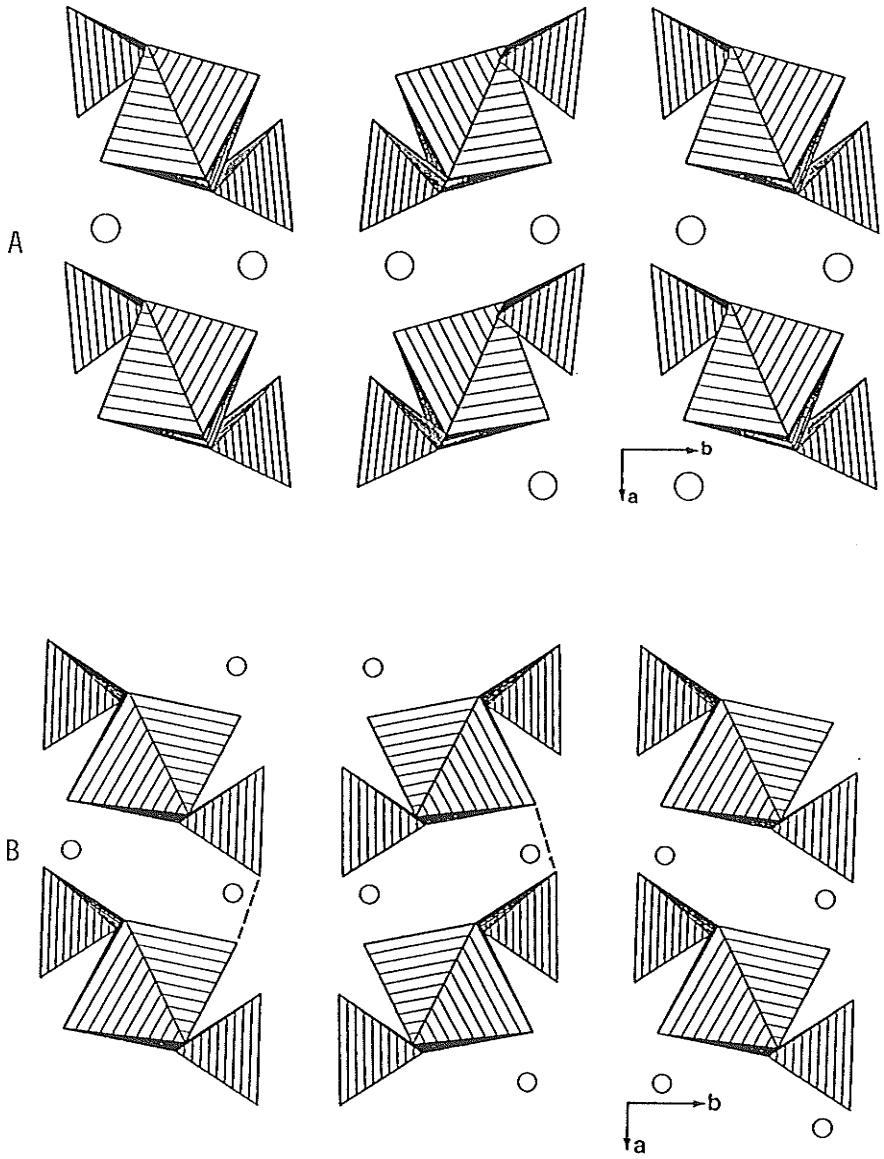

Figure 6.3: Kröhnkite, Before and After Idealization. (a) before idealization, the distorted chains; (b) after idealization, the neighboring chains are closer (dashed line), and the Na cavity is smaller than in the actual structure.

Roselite model data was refined towards the cell dimensions of idealized kröhnkite to verify that the two structures are in fact identical. In this procedure, the target bond lengths used for kröhnkite are put into the roselite program file. The simulation was successful (labelled "roselite to kröhnkite" in Appendix B4), and the cell dimensions are nearly identical.

Roselite was then idealized in the same unrestrained manner as kröhnkite, but using ideal bond lengths for Mg-O, Ca-O and As-O. Bond-valence tables for roselite before and after idealization (Table 6.9) indicate that the bonding environment of Ca^{2+} does not change significantly, unlike Na^{+} in kröhnkite. It should be noted that bvs in the non-ideal roselite structure are far from ideal. bvs of the anions are made worse by idealization. Although this structure is the same as kröhnkite, structural rearrangements are slightly different in roselite, because of the diffences in ideal target bond lengths used. Instead of collision with OW and O(4), these atoms move away (>3.2Å). However, the H-bonding to O(4) is still destroyed. Also, O(1) - O(3) = 2.497Å indicates tetrahedral collision within the chains, rather than the tetrahedral-octahedral collisions in kröhnkite.

Roselite and kröhnkite were then idealized with structural constraints. Extra target distances are used in these refinements, and are intended to prevent collisions in these non-framework structures (output labelled "With Constraints" in Appendix B4). The OW - O(4) and OW - O(1) distances which collided in kröhnkite (without restraint) were

TABLE 6.9

Roselite Bond-Valence Tables, Before/After Idealization

Before DLS Refinement

	Ca	Mg/Co	As	H1	H2	ΣO^{-2}
O1	0.315		1.282	0.13		= 1.727
O2	0.244,0.232	0.262	1.200			= 1.938
O3	0.274	0.374	1.178			= 1.826
O4	0.240,0.277		1.218		0.18	= 1.915
OW	0.292	0.368		0.87	0.82	= 2.349
M^+	1.873	2.008	4.878	1.00	1.00	

Idealization Without Restraints

	Ca	Mg/Co	As	H1	H2	ΣO^{-2}
O1	0.246		1.240	0.16		= 1.646
O2	0.255,0.272	0.333	1.240			= 2.100
O3	0.291	0.334	1.240			= 1.865
O4	0.218,0.283		1.240		XX	= 1.741
OW	0.269	0.333		0.84	1.00	= 2.442
M^+	1.834	2.000	5.000	1.00	1.00	

Bond lengths before DLS from Hawthorne & Ferguson (1977); Bond-valence curves used from Brown (1981).

weighted relatively high at distances equal to the actual structure. The OW - O(4) distance in roselite was also fixed to prevent separation. Bond-valence analyses of the constrained idealizations (Table 6.10) show significant improvement in the bonding conditions of the atoms. H-bonding to O(1) and O(4) is preserved. However, new atomic collisions are produced as a consequence of the structural constraints preventing

earlier collisions (OW - O(1b) = 2.286Å in kröhnkite; O(3) - O(3) = 2.377Å in roselite).

TABLE 6.10

Bond-Valence Tables for Constrained Idealizations

Kröhnkite

	Na	Cu	S	H1	H2	Σ O^{-2}
O1	0.153		1.500	0.27		= 1.923
O2	0.186,0.138	0.333	1.500			= 2.157
O3	0.168	0.334	1.500			= 2.002
O4	0.126,0.192		1.500		0.24	= 2.058
OW	0.244	0.334		0.73	0.76	= 2.068
M^+	1.207	2.002	6.000	1.00	1.00	

Roselite

	Ca	Mg/Co	As	H1	H2	Σ O^{-2}
O1	0.262		1.240	0.20		= 1.702
O2	0.250,0.303	0.333	1.240			= 2.126
O3	0.261	0.335	1.240			= 1.836
O4	0.161,0.288		1.240		0.21	= 1.899
OW	0.245	0.333		0.80	0.79	= 2.168
M^+	1.770	2.002	5.000	1.00	1.00	

Bond-valence curves used from Brown (1981)

Although the members of this structure type behave somewhat differently, a (4+2) distortion in the octahedra seems to produce the most convenient arrangement of polyhedra. The (4+2) distortion provides

a spatial balance between required O-H···O geometries and the avoidance of polyhedral collisions. It is interesting to note that the $M(TO_4)_2$ chains do not become ideally straight (in the geometrical sense) with idealization refinements, because the large interchain cations, although weakly bonding, still exert a spatial control on the geometry of the chains. Straight chains would radically alter the bonding environment of the larger cations.

6.4 DLS REFINEMENT OF UNIQUE STRUCTURE TYPES

Upon studying several structures which have unique topologies, it became apparent that a few of them cannot be idealized to have regular polyhedra. DLS idealization procedures will not work on these minerals. The program fails, and the least-squares process will not converge. This indicates that there are reasons for the unique nature of some Cu^{2+} oxysalt structures, other than just bond-valence constraints. Jahn-Teller distortions provide unique possibilities for Cu-octahedral topologies. Other elements are not able to substitute into the very distorted octahedral sites, and regular octahedra would destroy the topology of the unique structures. The following examples of DLS represent a search for unique structure types which require J-T distortions.

6.4.1 Lammerite

Lammerite was the first structure tested with DLS to determine its topological response to idealization. Refinements with various target input parameters were unsuccessful. Using bond lengths of greater or lesser values than ideal distances for Cu-O and As-O were also

unsuccessful (in attempts to fit different sized polyhedra into an ideal arrangement). After confirming that the input files were not flawed, further attempts at idealization were made. The program still would not converge.

It was suspected that the commensurate modulation of closed-packed polyhedral layers was responsible for the properties exhibited during DLS refinement. Graphical reconstruction of lammerite proved this suspicion to be true. When the octahedra are made regular and the layer modulation is flattened out, the tetrahedral sites are stretched well beyond acceptable limits (Figure 6.4). Therefore, the tetrahedral connectivity between octahedral layers is made possible only by the special arrangement of the distorted octahedra (which coupled together form the modulation). It is the modulation which allows the tetrahedra to fit into the places they occupy in lammerite. Other elements cannot substitute into the lammerite structure because they cannot achieve equivalent octahedral distortions.

6.4.2 Lindgrenite

Lindgrenite is another modulated layer structure, and is a logical candidate for DLS analysis. The unique topology of this structure suggests that it too may not allow idealization. However, upon using the standard method of idealization, lindgrenite acquires polyhedra of reasonably regular shapes. The R-value (0.020, Appendix B5) indicates that the structure undergoes some resistance to total idealization, but the polyhedra have only minute distortions. The presence of one atomic violation (O(3)-OH=2.144Å) is however significant. Upon inspection of

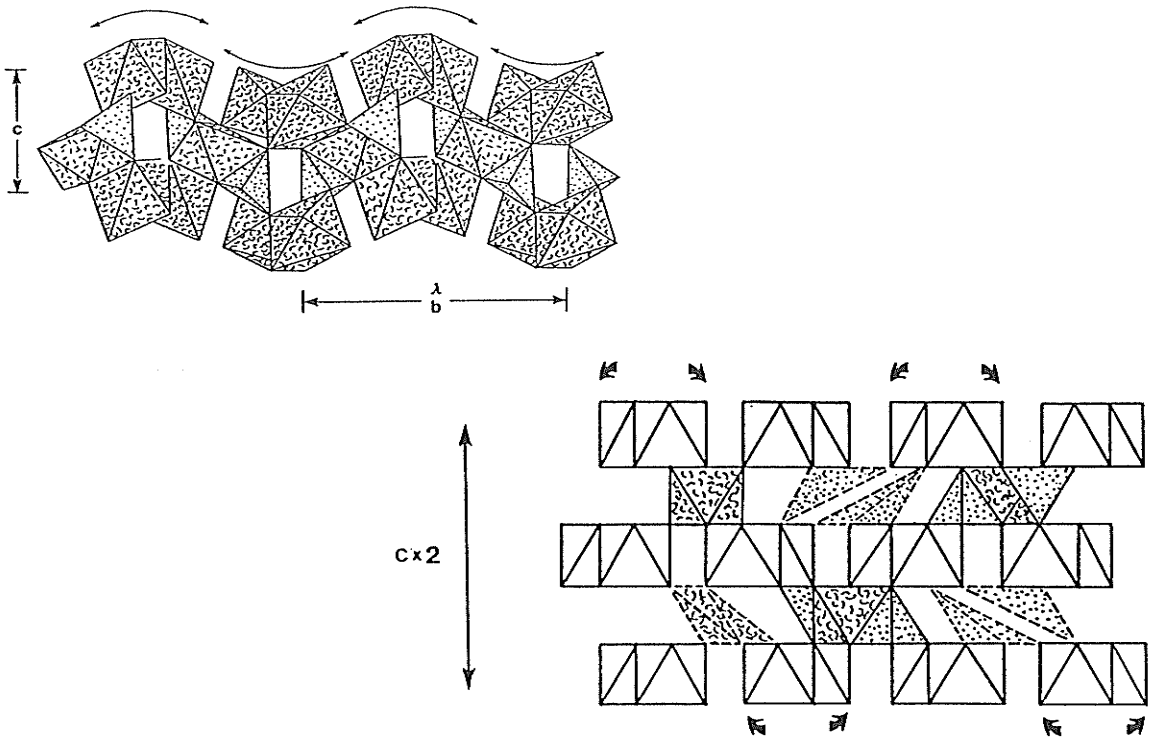

Figure 6.4: Lammerite Graphical Non-Idealization. An attempt at graphical idealization of the polyhedra fails. As the octahedral chains of Cu(2) are flattened out (shown by arrows) the tetrahedra and Cu(1) octahedra, between the layers of Cu(2)-chains, are stretched out past acceptable limits (dashed arrows).

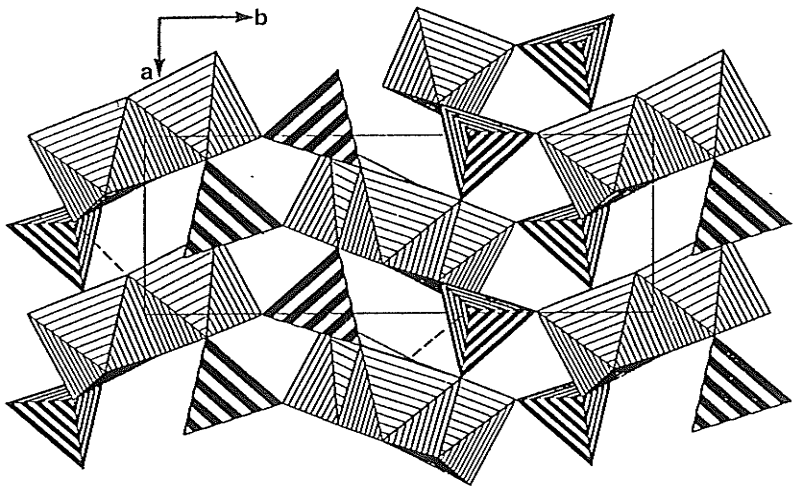

Figure 6.5: Lindgrenite Structure After Idealization Looking across the modulated polyhedral layers, adjacent layers are too close (atomic violation is dashed); the arrangement is otherwise not significantly different from the actual structure.

the structure before and after idealization (Figure 6.5), there is little difference in polyhedral arrangements and shapes. In the actual structure, the OH^- position (where the three octahedral apices meet) is puckered in away from the nearest tetrahedral apex. In the ideal structure, this distance is much shorter (O(3)-OH), and is dashed in Figure 6.5.

Interestingly, the modulation in lindgrenite is not removed by idealization. The nature of this modulation must therefore be purely topological, while that of lammerite is geometrical as well as topological.

Bond-valence analysis provides us with another clue as to why this Cu^{2+} is unique (Table 6.11). The stable bvs in the actual structure are altered to much less stable conditions in the idealized arrangement. Although the O(3)-OH distance (2.767Å) is preserved for H-bonding, the anion bvs are made unstable as a whole.

Lindgrenite requires the (4+2) octahedral distortion because of bond-valence requirements, and to prevent adjacent polyhedral layers from getting too close. Perhaps the latter constraint could be satisfied with some other distortion mechanism as well, but the bond-valence distributions of lindgrenite are best suited with (4+2) distortions. Other elements cannot achieve these distortion magnitudes; however, Zn seems to be able to approach Cu^{2+} in its distortions. Therefore, the bv conditions of a Zn-analogue may be sufficiently stable.

TABLE 6.11

Bond-Valence Tables of Lindgrenite

Before Idealization

	Cu(1)	Cu(2)	Mo	H	ΣO^{-2}
O(1)		0.459	1.585		= 2.044
O(2)	0.129(x2)↓	0.175	1.552		= 1.856
O(3)		0.501	1.402	0.15	= 2.053
O(4)	0.472(x2)↓	0.114	1.426		= 2.012
OH	0.419(x2)↓	0.425,0.407		0.85	= 2.101
M^+	2.040	2.081	5.965	1.00	

After Idealization

	Cu(1)	Cu(2)	Mo	H	ΣO^{-2}
O(1)		0.334	1.505		= 1.839
O(2)	0.330(x2)↓	0.331	1.499		= 2.160
O(3)		0.338	1.500	0.18	= 2.018
O(4)	0.344(x2)↓	0.331	1.513		= 2.188
OH	0.323(x2)↓	0.334,0.333		0.82	= 1.810
M^+	1.994	2.002	6.017	1.00	

Bond-valence curves used from Brown (1981); bond lengths of actual lindgrenite structure from Hawthorne & Eby (1985).

6.4.3 Chalcocyanite

Graphical analysis of chalcocyanite indicates that it cannot be idealized into a wallpaper structure. The question arose as to whether this structure can be idealized at all. Substitution by Zn to form zincocyanite (Kokkoros & Rentzeperis, 1958), indicates that this structure is not unique to Cu^{2+}, although zincocyanite is very unstable

in the presence of moisture. If the structure is not unique to Cu^{2+}, can it still have a topologically restricted arrangement, like lammerite?

Idealization with DLS is possible (Appendix B5). Therefore, we have an explanation for the substitution by Zn. Bond-valence sums of the ideal structure are better than values for the actual structure (Table 6.12). However, they are still not acceptable as stable values for oxysalts, because none of the anion bvs approach ideality. The structure needs refinement, because the bvs of the actual mineral are unacceptable.

TABLE 6.12

Bond-Valence Tables for Chalcocyanite

	Before Idealization			After Idealization		
	Cu	S	ΣO^{-2}	Cu	S	ΣO^{-2}
O(1)	0.147(x2) →	1.221	= 1.515	0.333(x2) →	1.500	= 2.166
O(2)	0.407(x2) →	1.057	= 1.871	0.333(x2) →	1.500	= 2.166
O(3)	0.559(x2) →	1.534(x2) ↓	= 2.093	0.333(x2) →	1.500(x2) ↓	= 1.833
M^+	2.226	5.346		2.000	6.000	

Bond lengths before DLS from Kokkoros & Rentzeperis (1958); bond-valence curves used from Brown (1981).

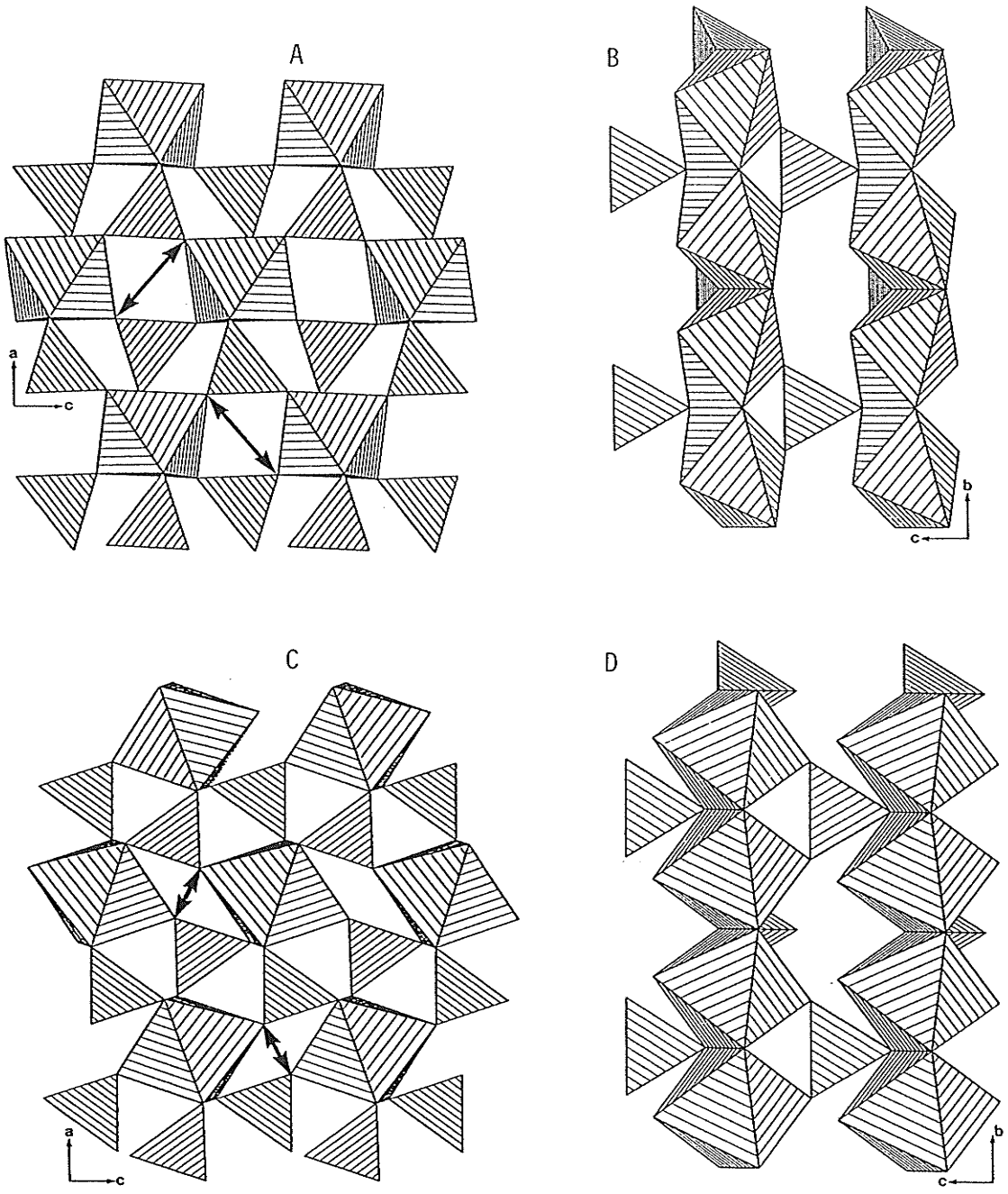

Figure 6.6: Chalcocyanite, Before and After Idealization. (a) before idealization of the tetrahedral-octahedral framework, looking down the rutile-like octahedral chains; (b) non-ideal octahedral chains and cross-linking tetrahedra; (c) idealized polyhedral framework, with rotation of the chains to produce collisions between neighboring chains (shown with arrows, collision is dashed); (d) idealized octahedral chains and tetrahedra.

Although bond-valence characteristics are inconclusive about the stability of regular octahedra in the structure, inspection of atomic distances reveals a problem with idealization. Observation of the structure before and after idealization (Figure 6.6) shows that the octahedral chains have undergone significant rotation due to oxygen rearrangements. Consequently, the distance between apical oxygens of neighboring octahedral chains is much too close (O(3)-O(3)=1.590Å). Rotation of the chains is caused from making the octahedra regular, and results in polyhedral collisions. The (4+2) distortion seems to be necessary to prevent atomic collisions. Bond-valence analysis suggests that the anions are not stable in an idealized octahedral arrangement, but poor structural data prevents comparison of bv characteristics between the ideal and actual structures.

6.5 SUMMARY

With application of the Distance Least Squares method, a number of important features in oxysalt mineralogy are revealed. There exist structures which require (4+2) octahedral distortions for the following reasons:

1. Bond-valence distributions are more favorable with the (4+2) distortion than with regular shaped octahedra.
2. Certain hydrogen-bonding arrangements are possible only with the (4+2) distortion in the structure. Making the octahedra regular destroys the O(donor)-O(acceptor) distances needed for proper bond-valence contributions by hydrogen to the anions.

3. Geometrical limitations require a particular arrangement of (4+2) octahedra. Idealizating these octahedra causes collision of neighboring polyhedra.
4. Certain topologies require a specific arrangement of (4+2) octahedra. Removal of the distortion alters the topology of the more tightly bonded units, thus obliterating the identity of the structure.

Chapter VII

THE ROLES OF Cu^{2+} IN THE LONG RANGE STRUCTURE OF OXYSALTS

The structural effects that the Cu^{2+} ion is responsible for (within a unique series of coordination geometries) have been discussed (Chapters 4-6). In this chapter, the features exhibited by Cu^{2+} and the Jahn-Teller distortion are considered in terms of their effects on the long range properties of the Cu^{2+} oxysalts. A final summary of this thesis is also provided.

7.1 A GEOMETRICAL CLASSIFICATION OF CU^{2+} OXYSALT MINERALS

Chapters 5 and 6 have addressed the two central questions of this thesis:

1. Why do some Cu^{2+} oxysalt structures have non-Cu analogues?
2. Why are some Cu^{2+} oxysalt structures unique to Cu?

However, in considering these questions, time allowed the detailed study of only a small part of the known Cu^{2+} oxysalt mineral structures. They are now classified here in terms of their geometrical properties with relation to Cu^{2+} and the Jahn-Teller distortion. There are TWO FUNDAMENTAL TYPES OF STRUCTURE:

I : Structures constructed from holosymmetric coordination polyhedra, the arrangement of which is also flexible enough to distort and accomodate local Jahn-Teller distortion of the octahedra.

II: Structures (polyhedral connectivities) that can only be constructed from very distorted coordination polyhedra.

The two structure types extend beyond the scope of Cu^{2+} oxysalt minerals. However, there are subcategories to structure type I which are defined on the basis of the role(s) of Cu^{2+} in the structure. The subcategories of structure type I are:

A: Structures flexible enough to accomodate Jahn-Teller distorted octahedra and/or regular octahedra. These structures lack rigid geometrical and/or bond-valence constraints on substitution at the octahedral positions.

B: Structures which must have Jahn-Teller-type distortions for structural stability.

Minerals with structure type II are those which resist idealization by DLS methods or simple graphical analysis.

The Cu oxysalt minerals are categorized according to the above classification scheme, and they are listed in Table 7.1. The rationale for deciding a structure type was developed from the results of chapters 5 and 6 (see summaries). There are three possible criteria for assigning a structure to type IA:

i) structural flexibility can be a result of the buffering nature of an elaborate and/or flexible hydrogen-bonding network (e.g. chalcanthite).

ii) Cu^{2+} in a structure can play a supportive and/or minor role, and is readily substituted for by other elements (e.g. interlayer cation role in uranyl-layer structures).

iii) certain topological arrangements allow for variability in bond-valence distributions of the octahedra (provided the anion bvs are satisfied), thus permitting regular or distorted octahedral polymerizations (e.g. the equivalence of certain linking models in Figures 5.1 and 5.2).

For structures of type IB, there are the following criteria:

i) bond-valence requirements impose constraints on the distortion of polymerized octahedra linked to certain complex anion polyhedra (e.g. octahedral-Cu···tetrahedral-S sheet structures are restricted to (4+2) distortions at linking anions).

ii) some hydrogen-bonding geometries require a particular arrangement of distorted octahedra, which cannot be made regular without destroying the H-bonding arrangement (e.g. chalcomenite).

iii) idealization of octahedra in a structure may cause instability in the bonding conditions of cations not involved in the polyhedral connectivity (e.g. ^{5}M cation dimers in olivenite)

iv) idealization of octahedra may cause unrealistic atomic geometry (e.g. atomic collisions, as in chalcocyanite).

The criterion decided upon for each mineral structure type is listed in Table 7.1. The minerals studied in depth, or which are clear cut examples of structure type, are marked with an asterisk. The other mineral structures are assigned their place by less thorough inspection. Further study is necessary to more conclusively determine the structure type for minerals only briefly inspected.

TABLE 7.1

Geometrical Classification of Cu^{2+} Oxysalts

These minerals are classified according to their type of structure, within the subcategories of the two structure types. The subcategories and criterion for categorization are described in the text. The criterion used are listed in abbreviated form for each mineral structure, and are coded as follows: Category IA - (i) HBF=hydrogen-bonding is flexible; (ii) SMR=copper plays a supportive or minor structural role; (iii) LAB=the linkage arrangement allows both regular and (4+2) octahedra; Category IB - (i) BV=bond-valence constraints; (ii) HBUF=hydrogen-bonding is unflexible; (iii) DCB=disturbance of cation bonding with idealization; (iv) AC=atomic collisions. The minerals marked with an asterisk were studied in greater detail than the rest, and represent more conclusive results.

STRUCTURE TYPE I : Structures Which Can Be Idealized

Category A - Geometrically flexible without constraints

	Minerals	Formula	Criteria
		(isolated polyhedra and clusters)	
	Aubertite	$CuAl(SO_4)_2Cl \cdot 14H_2O$	HBF
	Boothite	$CuSO_4 \cdot 7H_2O$	HBF
	Cyanochroite	$K_2Cu(SO_4) \cdot 6H_2O$	HBF
	Henmilite	$Ca_2Cu(OH)_4[B(OH)_4]_2$	HBF
		(infinite polyhedral chains)	
*	Chalcanthite	$CuSO_4 \cdot 5H_2O$	HBF
	Cuprocopiapite	$CuFe_4^{+3}(SO_4)_6(OH)_2 \cdot 20H_2O$	HBF,SMR
	Eriochalcite	$CuCl_2 \cdot 2H_2O$	HBF
		(infinite mixed-type polyhedral sheets)	
	Guildite	$CuFe^{+3}(SO_4)_2(OH) \cdot 4H_2O$	SMR
	Ransomite	$CuFe_2^{+3}(SO_4)_4 \cdot 6H_2O$	SMR
	Metatorbernite	$Cu(UO_2)_2(PO_4)_2 \cdot 8H_2O$	SMR
	Sengierite	$Cu_2(UO_2)_2V_2O_8 \cdot 6H_2O$	SMR
	Cuprosklodowskite	$Cu(UO_2)_2Si_2O_6(OH)_2 \cdot 6H_2O$	SMR
	Turquoise	$CuAl_6(PO_4)_4(OH)_8 \cdot 5H_2O$	HBF,SMR

Table 7.1 continued

Minerals	Formula	Criteria
	(polyhedral frameworks)	
Litidionite	$KNaCuSi_4O_{10}$	LAB
Ziesite	$\beta Cu_2V_2O_7$	LAB
Arthurite	$CuFe_2^{+3}AsO_4{}_2(OH)_2 \cdot 4H_2O$	HBF,SMR
McBirneyite	$Cu_3V_2O_8$	LAB
Atacamite	$Cu_2Cl(OH)_3$	LAB
Paratacamite	$Cu_2(OH)_3Cl$	LAB
Category B - Require (4+2) distortions for stability		
	(infinite polyhedral chains)	
* Kröhnkite	$Na_2Cu(SO_4)_2 \cdot 2H_2O$	BV,DCB
* Chalconatronite	$Na_2Cu(CO_3)_2 \cdot 3H_2O$	BV
* Chlorothionite	$K_2Cu(SO_4)Cl_2$	BV,HBUF
Caledonite	$Pb_5Cu_2(CO_3)(SO_4)_3(OH)_6$	BV,DCB
Linarite	$PbCu(SO_4)(OH)_2$	BV,DCB
Schmiederite	$PbCu(SeO_4)(OH)_2$	BV,DCB
Fornacite	$Pb_2Cu(CrO_4)AsO_4(OH)$	BV
Vauquelinite	$Pb_2Cu(CrO_4)(PO_4)(OH)$	BV
	(infinite polyhedral sheets)	
* Botallackite	$Cu_2Cl(OH)_3$	BV
* Wroewolfeite	$Cu_4(SO_4)(OH)_6 \cdot 2H_2O$	BV
* Langite	$Cu_4(SO_4)(OH)_6 \cdot 2H_2O$	BV
* Posnjakite	$Cu_4(SO_4)(OH)_6 \cdot H_2O$	BV
* Spangolite	$Cu_6Al(SO_4)(OH)_{12}Cl \cdot 3H_2O$	BV
* Gerhardite	$Cu_2(OH)_3NO_3$	BV
* Campigliaite	$Cu_4Mn(SO_4)_2(OH)_6 \cdot 4H_2O$	BV
* Ktenasite	$(Cu,Zn)_5(SO_4)_2(OH)_6 \cdot 6H_2O$	BV
* Devillite	$CaCu_4(SO_4)_2(OH)_6 \cdot 3H_2O$	BV
* Serpierite	$Ca(Cu,Zn)_4(SO_4)_2(OH)_6 \cdot 3H_2O$	BV
Bayldonite	$PbCu_3(AsO_4)_2(OH)_2 \cdot H_2O$	BV,DCB
Chalcophyllite	$Cu_{18}Al_2(AsO_4)_3(SO_4)_3(OH)_{27} \cdot 33H_2O$	BV,DCB
Cuprorivaite	$CaCuSi_4O_{10}$	AC
Likasite	$Cu_3(OH)_5NO_3 \cdot 2H_2O$	BV,HBUF
	(frameworks of chains)	
* Chalcomenite	$CuSeO_3 \cdot 2H_2O$	BV,HBUF
* Teineite	$CuTeO_3 \cdot 2H_2O$	BV,HBUF
* Poitevinite	$(Cu,Fe^{+2},Zn)SO_4 \cdot H_2O$	BV
Bandylite	$CuB(OH)_4Cl$	BV
Kinoite	$Ca_2Cu_2Si_3O_8(OH)_4$	BV

Table 7.1 continued

	Minerals	Formula	Criteria
	Stoiberite	$Cu_5V_2^{+5}O_{10}$	BV
	Euchroite	$Cu_2(AsO_4)(OH)\cdot 3H_2O$	BV,HBUF
*	Olivenite	$Cu_2AsO_4(OH)$	BV,DCB,AC
*	Libethenite	$Cu_2(PO_4)(OH)$	BV,DCB,AC
	Papagoite	$CaCuAlSi_2O_6(OH)_3$	BV
*	Malachite	$Cu_2(CO_3)(OH)_2$	BV
*	Antlerite	$Cu_3(SO_4)(OH)_4$	BV
	Mammothite	$Pb_6Cu_4AlSbO_2(OH)_{16}Cl_4(SO_4)_2$	BV
*	Chalcocyanite	$CuSO_4$	BV,AC
*	Trippkeite	$CuAs_2^{+3}O_4$	BV
*	Lindgrenite	$Cu_3(MoO_4)_2(OH)_2$	BV,AC
		(frameworks of sheets)	
*	Cornubite	$Cu_5(AsO_4)_2(OH)_4$	BV
*	Fingerite	$Cu_{11}O_2(VO_4)_6$	BV
	Dolerophanite	$Cu_2(SO_4)O$	BV,DCB
	Salesite	$Cu(IO_3)(OH)$	BV
	Derriksite	$Cu_4(UO_2)(SeO_3)_2(OH)_6$	BV
	Shattuckite	$Cu_5(SiO_3)_4(OH)_2$	BV
	Plancheite	$Cu_8Si_8O_{22}(OH)_4\cdot H_2O$	BV
	Clinoclase	$Cu_3(AsO_4)(OH)_3$	BV
	STRUCTURE TYPE II : Structures That Cannot Be Idealized		
*	Stringhamite	$CaCuSiO_4\cdot 2H_2O$	
	Stranskiite	$Zn_2Cu(AsO_4)_2$	
*	Lammerite	$Cu_3(AsO_4)_2$	
*	Azurite	$Cu_3(CO_3)_2(OH)_2$	
*	Pseudomalachite	$Cu_5(PO_4)_2(OH)_4\cdot H_2O$	
*	Reichenbachite	" "	
*	QPM	" "	
*	Cornetite	$Cu_3(PO_4)(OH)_3$	
	Dioptase	$CuSiO_2(OH)_2$	

TABLE 7.2

Structures Still Enigmatic

Class 1: Structures apparently unique to Cu^{2+}.

Chloroxiphite	$Pb_3CuCl_2(OH)_2O_2$
Roubaultite	$Cu_2(UO_2)_3(CO_3)(OH)_{10}\cdot 5H_2O$
Bonattite	$CuSO_4\cdot 3H_2O$
Liroconite	$Cu_2Al(AsO_4)(OH)_4\cdot 4H_2O$
Blossite	$\alpha Cu_2V_2O_7$
Callaghanite	$Cu_2Mg_2(CO_3)(OH)_6\cdot 2H_2O$
Mixite Group	$ACu_6(XO_4)_3(OH)_6\cdot 3H_2O$
Volborthite	$Cu_3(VO_4)_2\cdot 3H_2O$
Veszelyite	$(Cu,Zn)_3(PO_4)(OH)_3\cdot 2H_2O$
Buttgenbachite	$Cu_{19}Cl_4(NO_3)_2(OH)_{32}\cdot 2H_2O$
Connellite	$Cu_{19}Cl_4(SO_4)(OH)_{32}\cdot 3H_2O$
Lyonsite	$Cu_3Fe_4(VO_4)_6$
Bellingerite	$Cu_3(IO_3)_6\cdot 2H_2O$

Class 2: Structures with non-Cu analogues.

Osarizawaite	$PbCuAl_2(SO_4)_2(OH)_6$
Conichalcite	$CaCu(AsO_4)(OH)$
Balyakinite	$CuTeO_3$
Hentschelite	$CuFe_2PO_42(OH)_2\cdot 2H_2O$

Many Cu^{2+} oxysalt minerals (Table 7.2) have structures that have not been explained in terms of: 1) why the structures are unique; or 2) why they are isostructural with non-Cu analogues, (labelled class 1 and class 2 respectively). In otherwords, these structures do not yet fit into the geometrical classification scheme put forth in Table 7.1. Further study of these minerals may reveal another role of the distorted Cu^{2+}-octahedron in structures. The methods used in chapters 5 and 6 for determining the role of Cu^{2+} in a particular structure may not be sufficient to answer the questions posed by these structures (Table 7.2).

It must be stressed that the intentions of this classification are not for the purpose of developing an all encompassing classification scheme for oxysalt structures. Such a scheme already exists and has been applied to the Cu^{2+} oxysalts. The assignment of fundamental structure types shows how Cu^{2+} and the Jahn-Teller effect control the character of a structure in various ways. The distinction between styles of heteropolyhedral connectivity in Table 7.1 (categories in brackets) serves to outline the variety of roles which copper plays in structures with similar styles of connectivity. As well, oxysalts with markedly different polyhedral connectivity can possess the same fundamental type of structure, with respect to the role of Cu^{2+}.

7.2 LONG RANGE ADAPTATION OF CU^{2+} DISTORTIONS IN STRUCTURES

The relationship between fundamental structure type and the role which Cu^{2+} is playing in the oxysalt structures has been established. It is now necessary to describe the mechanism whereby the long range periodic structure adapts itself to the local Jahn-Teller distortion of Cu^{2+} polyhedra.

7.2.1 Periodic Electronic Relaxations as Waveforms

There are several geometrical features associated with specific styles of polymerization between J-T distorted octahedra. Each of these three wave-like features has its own unique identity, although collectively they are all commensurate waveforms. These waveforms become evident by inspection of the long range aspects of Cu^{2+} oxysalt structures. The three features are:

1. Zig-zag octahedral chains with rutile-like connectivity.
2. Corrugated edge-sharing octahedral sheets.
3. Commensurately-modulated layers of mixed-type polyhedra (that is, not just octahedra).

These three wave-like structural units (Figure 7.1) are simple modifications that have accomodated the local Jahn-Teller distortion into a long-range periodic structure. As copper octahedra are polymerized throughout structures, their (4+2) distortions are coupled across the shared edges (Figure 7.2). When the coupled distortions are repeated by translational symmetry operators, they form a commensurate wave pattern (Figure 7.3). The wave amplitude is perpendicular to the direction of polymerization. The wave patterns represent an accomodation of the spontaneous electronic relaxation of Cu^{2+}-octahedra within a periodically symmetric structure. The wave-like features are now termed "periodic electronic relaxation" (PER), and are a means of maintaining: (i) overall structural connectivity; (ii) local electronic equilibrium around Cu^{2+}; (iii) and satisfaction of anion bond-valence requirements.

7.2.2 Zig-Zag Octahedral Chains

We find the zig-zag form of PER in many of the oxysalts with rutile-like octahedral chains. Zig-zag PER is the most simple form of distortion coupling, involving amplitudinal modulation along a single direction. Only the octahedra are involved in the mechanism of distortion coupling within zig-zag PER. Other cation groups in these structures are auxilliary to the zig-zag feature.

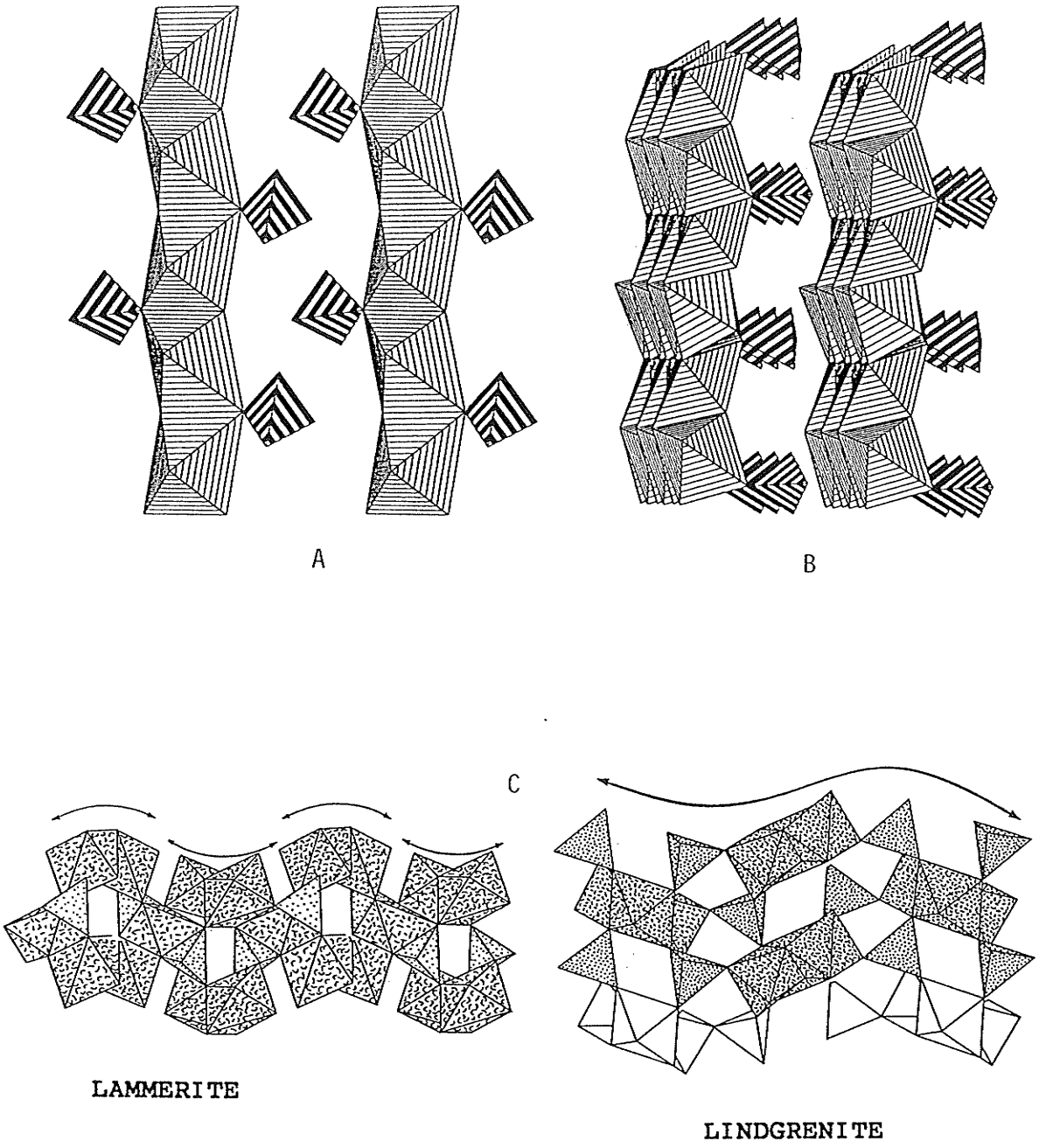

Figure 7.1: Polymerized Waveforms of Jahn-Teller Octahedra. The three forms of periodic electronic relaxation: (a) a zig-zag pattern is seen in the rutile-like edge-sharing octahedral chains of caledonite); (b) corrugation is pronounced in the edge-sharing sheets of distortion-coupled Cu-octahedra, an oblique view shows the two-dimensional propagation of the distortion wave; (c) successive layers of polyhedra are modulated with a wavelength commensurate with structural periodicity, on [001] in lammerite and on [100] in lindgrenite.

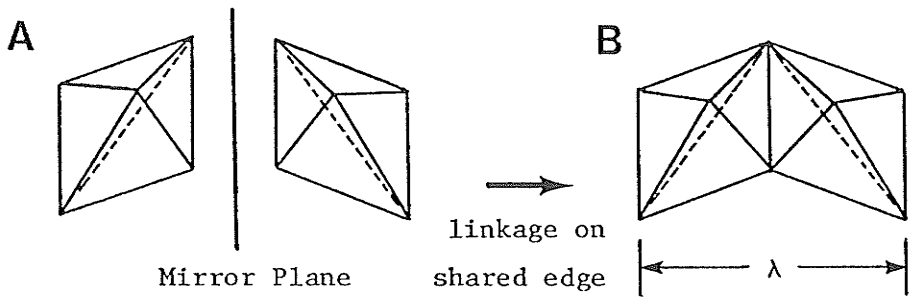

Figure 7.2: Coupling of Octahedral Distortions. a) two distorted (4+2) octahedra are symmetrically related by a mirror plane; b) by polymerization, the octahedra in (a) have their distortions coupled.

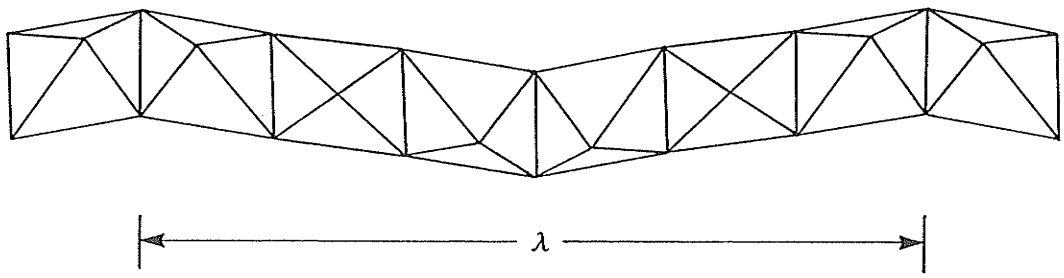

Figure 7.3: Periodic Electronic Relaxation by Polymerization. When coupled octahedral distortion is considered across the long range of a structure a periodic waveform is produced, and is commensurate within structural symmetry.

The presence of chain modulations is dependent on the specific combination of edge-sharing between adjacent octahedra. An apical bond must be linked along the shared-edges for zig-zag PER. Ordered octahedral chains with Cu^{2+} and other elements (e.g. Al^{3+} and Cu^{2+} in papagoite) do not show the zig-zag PER, because the 4+2 distortions are not coupled. Octahedral chains without apical bonds along the shared edges do not show PER either, because again the distortions are not coupled (e.g. trippkeite with apical bonds perpendicular to the chain direction; c f. chapter 3). The presence of apical bonds along shared edges is determined by bond-valence requirements of the structure. Dolerophanite is an example of zig-zag PER. The apical bonds are linked to shared edges, necessary for bond-valence satisfaction at the anion which links to a sulphate tetrahedron. The amplitude of PER is dependent on the magnitude of Jahn-Teller distortion. Minerals with large apical distortions (e.g. mammothite) show a greater amplitude of zig-zag PER than structures whose octahedral chains have lesser apical distortions (e.g. caledonite).

7.2.3 Corrugated Octahedral Sheets

All of the Cu^{2+} oxysalts whose structures have edge-sharing Cu-octahedral sheets (with brucite-like layers) possess corrugation in those sheets. Brucite-like sheets (consisting of regular-shaped octahedra) are made from double-layers of hexagonally close-packed oxygens, and they are flat (without corrugation). Introduction of a (4+2) distortion into the octahedra of an ideal brucite-like sheet

causes corrugation, because perturbation of the ideal HCP geometry requires flexure of the anion layers to maintain periodicity. The corrugation pattern must possess symmetry, because of the periodic nature of octahedral polymerizations (with distortion coupling) in oxysalts. Therefore, sheet corrugation in Cu^{2+} oxysalts is another form of PER.

Periodic electronic relaxation is more complex in octahedral sheets than in zig-zag chains. The propogation directions of distortion coupling in the octahedra occur in two directions across the plane of the two-dimensional sheet, rather than linearly along chains. This produces an undulating oceanwave-like pattern when the octahedral sheets are viewed at an oblique angle (Figure 7.1b). As in zig-zag chains, only the octahedra are involved in the mechanism of corrugation; the other polyhedra in such structures are auxilliary. It is interesting to note that this is the case even in framework structures with corrugated sheets (e.g. cornubite). The other polyhedral only link the sheets together. As we will see, such is not the case for framework structures with mixed type polyhedral modulation.

The specific pattern and symmetry of the corrugation are controlled by the style of linkage between the axial bonds of the (4+2) octahedra. When three axial bonds are linked together, they form areas of positive relief (high points) on the side of the sheet with the linking oxygen (refer Figure 5.4a). The pattern of triply-linked axial bonds that is imposed on an octahedral sheet (by symmetry rules) determines the areas of positive relief in the corrugation pattern. Octahedra whose axial bonds are not linked to two other axial bonds result in areas of lower

relief on the sheet (low points). Therefore, the arrangement of (4+2) octahedra within a sheet determines the areas of the high and low points, and thus the corrugation pattern of PER.

Corrugation patterns of octahedral sheets within the structures of the $[M_4X_n\,\phi_{8-n}]$-series (Hawthorne & Groat, 1985; discussed in Chapter 3) can be described by their axial bond patterns (ABP). Figure 7.4 shows the ABP of a large portion of this series, superimposed on an octahedral sheet. The solid circles represent high points (triple-junctions) where either SO_4, NO_3, Cl or H_2O groups can link (compatible with bond-valence arguements in Chapter 5). Thus, we see that the $[M_4X_n\,\phi_{8-n}]$-series has substitution of n spatially controlled by the ABP. The ABP of Figure 7.4 can be represented differently by showing the axial bonds without the octahedra, and including the linking complex anions specific to the different structures. This method (Figure 7.5) shows the type of ABP more clearly. Note that adjacent triple-junctions are on opposite sides of a sheet. The ABP of posnajakite and langite (Figure 7.6a) and serpierite-devillite (Figure 7.6b) have a higher degree of connectivity between the triple-junctions than those in Figure 7.5. However, the number of non-triple-junctions is the same (some seen as solitary dashes within rings of triple-junctions).

In zig-zag chains, the direction of propagation for the waveform of PER was along the chain. In octahedral sheets, the propagation vectors can be seen by drawing lines from adjacent triple-junctions that are on the same side of the sheet. The propagation vectors (Figures 7.5 and 7.6) are either 90° or 120° apart, and the combination of vectors for a particular structure depends on the ABP.

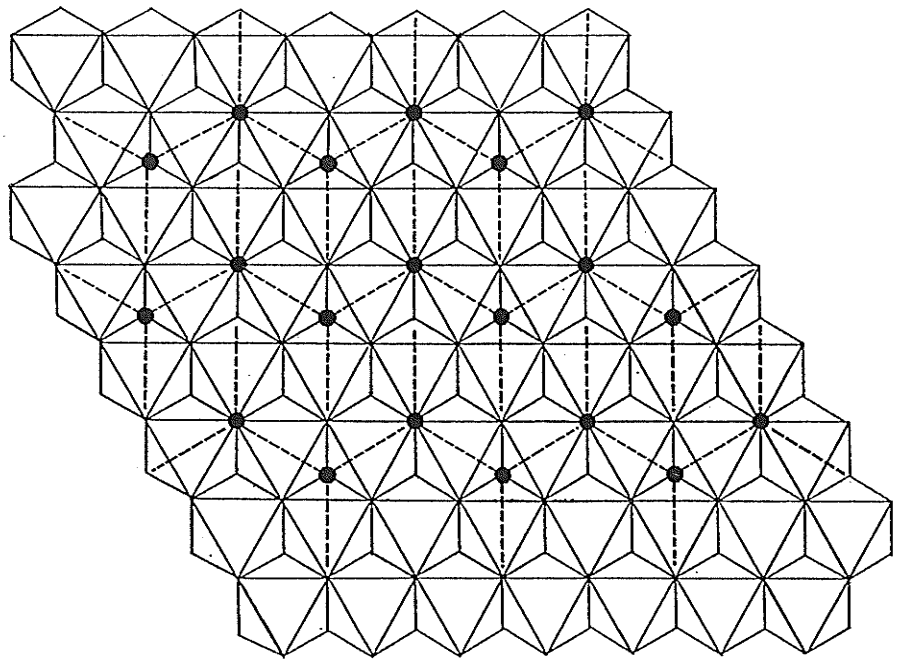

Figure 7.4: Axial Bond Pattern of a Corrugated Octahedral Sheet An axial bond pattern is superimposed onto an octahedral sheet. The axial bonds are dashed, and the triple-junctions of axial connectivity have solid circles. The triple-junctions represent areas where H_2O groups and complex anions can link, consistent with arguements of bond-valence theory in Chapt.5. This particular pattern is found in structures of the related minerals: bottallackite, wroewolfeite, gerhardite, campigliaite and ktenasite.

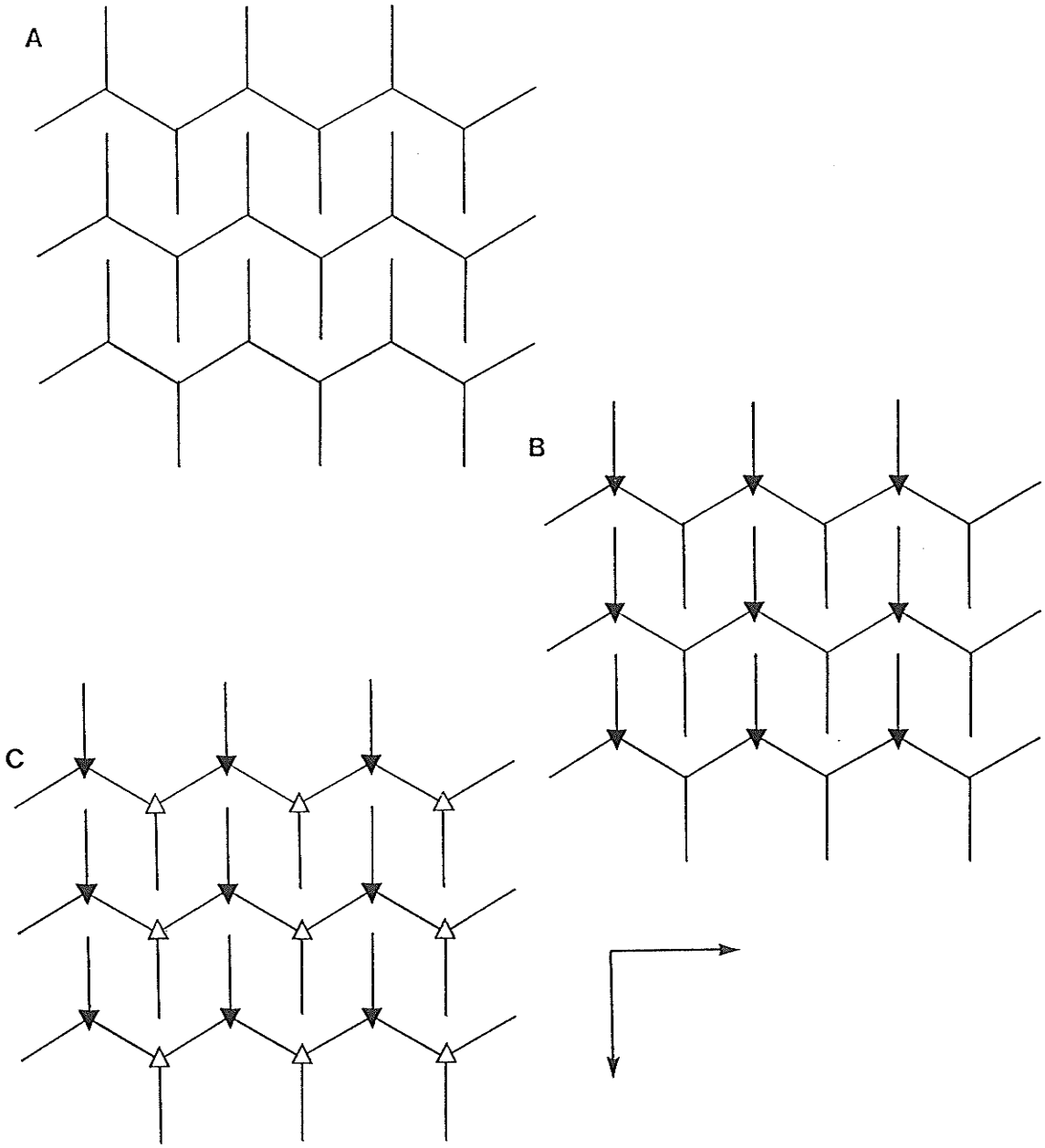

Figure 7.5: Axial Bond Patterns of Corrugated Octahedral Sheets. (shown without the octahedra) Linking complex anions are shown as triangles: solid triangles are on the top side of the sheet, open triangles are on the bottom side. Triple-junctions without triangles represent areas where H_2O or OH groups are bonded. The following ABP are: (a) bottallackite; (b) wroewolfeite; (c) gerhardite, campigliaite and ktenasite. Joining adjacent triple-junctions on the same side of the sheet reveals the propagation vectors of PER. The PER vectors (shown as arrows) are the same for (a), (b) and (c).

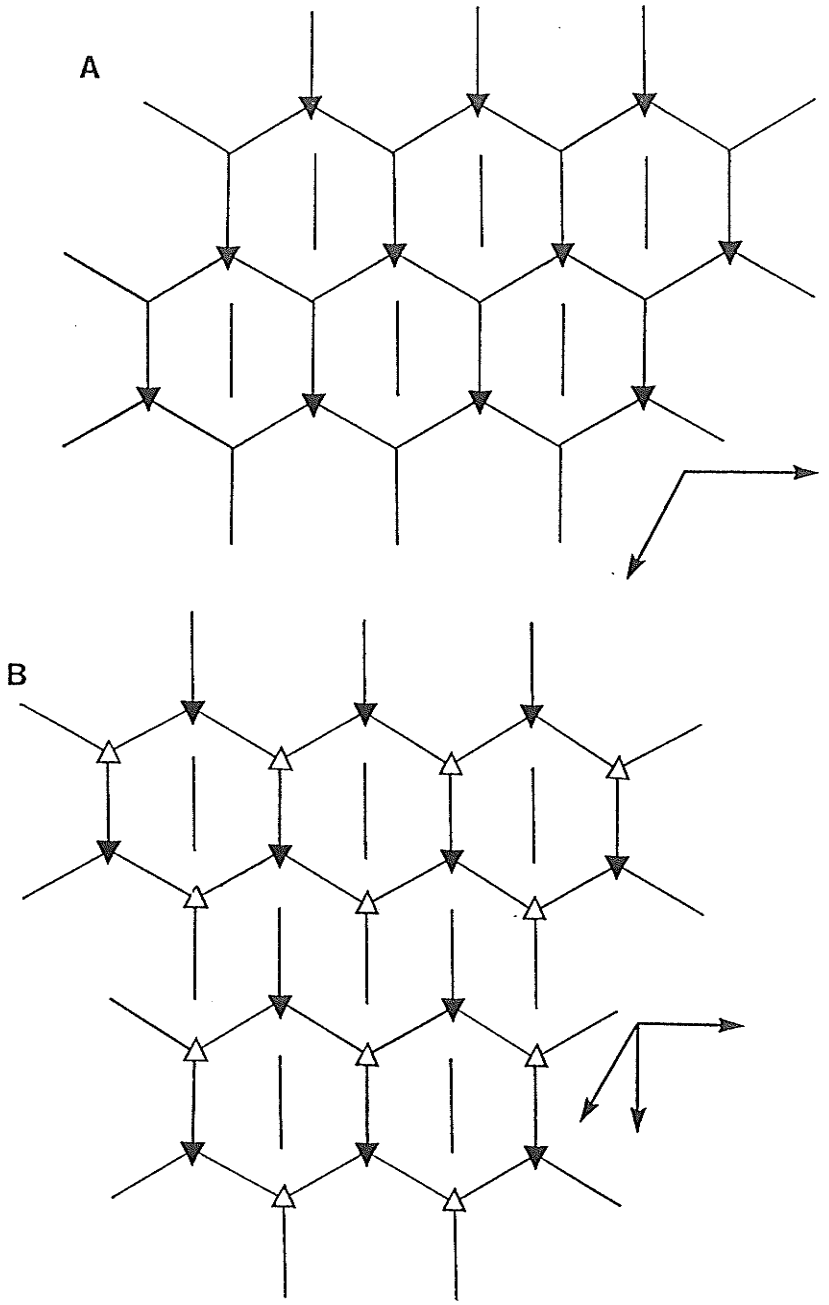

Figure 7.6: More Axial Bond Patterns. These are the axial bond patterns of: (a) posnajakite & langite; (b) serpeirite & devillite. See Figure 7.5 for explanation of pattern rules; solitary lines within the triple-junction rings represent octahedra that cannot bond to complex anion groups. The vectors of PER propagations are shown as arrows.

In structures that have octahedral sheets with more than just Cu^{2+}, or with cation vacancies, the axial bond patterns are different. There are less triple-junctions, but the coupling of octahedral distortions still results in a corrugation pattern. Because the linkage density of axial bonds is different, there are more possibilities for linkage to complex anions (e.g. two octahedra linked to one TO_4 in 3/4 occupied sheets, cornubite). The distribution of AlO_6 octahedra in the sheets of spangolite and chalcophyllite controls the symmetry of corrugation. Disordered substitution of Cu^{2+} into a non-Cu-octahedral sheet would result in aperiodic modulations, because of random distortion coupling. Cu-rich micas (if they exist) would be an interesting case for study of this feature.

7.2.4 Commensurate Modulation of Mixed-Type Polyhedral Layers

Commensurate modulation is a form of periodic electronic relaxation that involves both the distortion coupling of (4+2) octahedra and the linkage of other polyhedra (Figure 7.1c). This type of PER is fundamentally different from the other two types. In zig-zag chains and corrugated octahedral sheets, periodic waveforms are produced solely with the coupling of (4+2) octahedral distortions, whereas, the rest of the structural components are not involved in the PER. In commensurate modulation, all of the polyhedra in the structure are involved in the modulation function. The combination of distortion coupling by the octahedra and polymerization with other polyhedra results in a periodic waveform commensurate with structural symmetry.

In the latter two waveforms discussed, the propagation vectors of PER are parallel to the polymerization direction of the octahedra. In other words, the one- and two-dimensional styles of polymerization form wave propagations along one and two directions, respectively. With commensurate modulation, the vector of modulation is not necessarily parallel to the polymerization direction of the (4+2) octahedra. Rather, the structures concerned are three dimensional polymerizations with layered polyhedral arrangements, and the modulation is ridge-like in one direction, with the vector of PER perpendicular to the ridges. For example, lammerite (Figure 7.1c) is a densely-packed layered structure with a periodic waveform across the plane of the layers (on [001]). The crests of the ridge-like waveform are along the hinge axes of the distortion coupled octahedral chains (along [100]), which are perpendicular to the propagation vector of the modulation (along [010]).

Very few structures possess commensurate modulation of polyhedral layers, because this feature requires the unique arrangement of polyhedra with specialized octahedral distortion patterns. The structures involved do not have analogue structures, because their polymerizations are only possible with copper. This is unlike the wide variety of Cu^{2+} oxysalts with similar zig-zag chain components or octahedral sheets with similar corrugation patterns. Commensurate modulation has a unique character within each of the unique structures that possess it.

7.3 FINAL SUMMARY

This section summarizes the main points of this thesis. We must first recall the questions which have prompted this study:

1. Why are some Cu^{2+} oxysalts isostructural with non-Cu^{2+} minerals or synthetic compounds, whereas, many others are structurally unique?
2. What are some features of the local Cu^{2+} Jahn-Teller distortion, and how do they relate to the long-range properties of structures?
3. What are the different fundamental roles of distorted Cu^{2+}-polyhedra in oxysalt structures?
4. What are the characteristic features observed in the long-range aspects of these Cu^{2+} structures?

Similarities or differences between Cu^{2+} oxysalts and other oxysalts first became apparent when the entire family of Cu^{2+} oxysalts was described according to Hawthorne's (1983) classification of heteropolyhedral connectivities. When the full coordination number around Cu^{2+} is considered, the true style of connectivity between Cu^{2+}-polyhedra and other polyhedra in a structure reveals the relationship (or lack of) with non-Cu^{2+} structures.

By considering features of the local environment around Cu^{2+}, together with the long-range characteristics of Cu^{2+} oxysalts, the structural roles of Cu^{2+} can be explained. Cu^{2+} polyhedra exhibit a wide range of coordination geometries. The Jahn-Teller effect is the driving force for the large variation in bond lengths and angles of

Cu^{2+}-polyhedra (as a distortion series starting from a regular-shaped octahedron). The Jahn-Teller distortion makes possible a wide range of bond-valence distributions around Cu^{2+}-octahedra. This variability provides Cu^{2+}-octahedra with the means to polymerize to a higher degree with complex oxyanions of high cation charges, and is responsible for certain topologies unique to Cu^{2+} oxysalts.

Cu^{2+}-octahedra can also have topologies with bond-valence distributions that are similar to non-Cu^{2+} oxysalts. Several factors which result in isostructural (Cu^{2+} and non-Cu) minerals are:

1. The buffering nature of a flexible hydrogen-bonding network on the bond-valence requirements of octahedra.
2. Cu^{2+} in a structure can play a supportive and/or minor role, and is readily substituted for by other elements (e.g. interlayer cation role in layer structures).
3. Certain topological arrangements allow for variability in bond-valence distributions of the octahedra (provided the anion bvs are satisfied), thus permitting regular or distorted octahedral polymerizations.

The variety of linkage roles of Cu^{2+} is unparalleled by other M^{2+}-octahedra, and is an important factor in understanding how the local Cu^{2+} coordination controls the long-range identity of oxysalts.

Structural idealization of polyhedral distortions, using DLS, is useful in understanding why some oxysalts require local (4+2) octahedral distortions (as a means of attaining long-range stability); reasons for the (4+2) distortion are:

1. Bond-valence distributions are more favorable with (4+2) distortions than with regular shaped octahedra.
2. Certain hydrogen-bonding arrangements are possible only with (4+2) distortions in the structure, and making the octahedra regular destroys the O(donor)-O(acceptor) distances needed for proper bond-valence contributions.
3. Geometrical limitations require a particular arrangement of (4+2) octahedra. Idealizating the octahedra causes collision of neighboring polyhedra.
4. Certain topologies require a specific arrangement of (4+2) octahedra. Removal of the distortion alters the topology of the more tightly bonded units, thus obliterating the identity of a structure.

Cu^{2+}-octahedra are naturally tailored to these (4+2) structure types. The first three features are possible in both Cu^{2+} and non-Cu^{2+} structures, but the last feature is limited to Cu^{2+} oxysalts. The ability of other M^{2+}-octahedra to attain the required (4+2) distortion (for structural stability) will decide whether or not a non-Cu^{2+} composition can be isostrucutral with a Cu^{2+}-bearing oxysalt.

The Cu^{2+} oxysalts are classified in terms of their geometrical properties, with respect to the roles that Cu^{2+}-polyhedra play in a structure. There are two fundamental structure types:

1. Cu^{2+} oxysalt structures which can be idealized, but often require octahedral distortions. Some of these structures have non-Cu^{2+} analogues, but many do not, because of the unique character of Cu^{2+} and the Jahn-Teller distortion.

2. Cu^{2+} oxysalt structures which cannot be idealized, because of topological constraints. These structures are unique to Cu^{2+}.

Periodic electronic relaxation is the long-range mechanism whereby many oxysalt structures adapt to polymerizations of Cu^{2+}-octahedra with local Jahn-Teller distortions. The types of periodic waveform produced depend on the particular style of polymerization, and they are:

1. One-dimensional distortions, giving zig-zag octahedral chains.
2. Two-dimensional distortions, resulting in corrugated octahedral sheets.
3. Three-dimensional polymerizations combined with distortion coupling, resulting in ridge-like waveforms called commensurate modulation.

I have therefore explained how the Jahn-Teller effect around Cu^{2+} controls structural identity, and how structures adjust their long-range polyhedral arrangements to adapt to the local Jahn-Teller distortions.

REFERENCES

Anderson, J.B., Shoemaker, G.L., Kostiner, E. and Ruszala, F.A. (1977): The Crystal Structure of Synthetic $Cu_5(PO_4)_2(OH)_4$, a Polymorph of Pseudomalachite; Amer. Min., v.62, p.115-121.

Aruga, A. & Nakai, I. (1985): Structure of Ca-Rich Agardite; Acta Cryst., C41, p.161-163.

Asai, T. & Kiriyama, R. (1973): Optical and Magnetic Studies of $CuSeO_3 \cdot 2H_2O$ Based on the Refined Crystal Structure; Bull. Chem. Soc. Japan, v.46, p.2395-2401.

Åsbrink, S. & Norrby, L.J. (1970): A Refinement of the Crystal Structure of Copper(II) Oxide with a Discussion of Some Exceptional E.s.d.'s; Acta Cryst., B26, p.8-15.

Baur, W.H. (1964): On the Crystal Chemistry of Salt Hydrates. III. The Determination of the Crystal Structure of $FeSO_4 \cdot 7H_2O$ (Melanterite); Acta Cryst., v.17, p.1167-1174.

Baur, W.H. (1981): Structure and Bonding in Crystals, Vol.II. Academic Press, 1981; Chapt. 15, Interatomic Distance Predictions for Computer Simulation of Crystal Structures; p.31-52.

Baur, W.H. & Rolin, J.L. (1972): Salt Hydrates. IX. The Comparison of the Crystal Structure of Magnesium Sulfate Pentahydrate with Copper Sulfate Pentahydrate and Magnesium Chromate Pentahydrate; Acta Cryst., B28, p.1448-1455.

Baur, W.H. (1973): Criteria for Hydrogen Bonding. II. A Hydrogen Bond in the Edge of a Coordination Polyhedron Around a Cation; Acta Cryst., B29, p.139-140.

Birnie, R.W. & Hughes, J.M. (1979): Stoiberite, $Cu_5V_2O_{10}$, a New Copper Vanadate from Izalco Volcano, El Salvador, Central America; Amer. Min., v.64, p.941-944.

Bovio, B. & Locchi, S. (1982): Crystal Structure of the Orthorhombic Basic Copper Nitrate, $Cu_2(OH)_3NO_3$; Journ. of Cryst. and Spect. Rsrch., v.12, No.6, p.507-517.

Brown, G.M. & Chidambaram, R. (1969): The Structure of Copper Ammonium Sulfate Hexahydrate from Neutron-Diffraction Data; Acta Cryst., B25, p.676-687.

Brown, I.D. (1976): On the Geometry of O-H···O Hydrogen Bonds; Acta Cryst., A32, p.24-31.

Brown, I.D. (1981): Structure and Bonding in Crystals, Vol.II. Academic Press, 1981; Chapt. 14, The Bond-Valence Method: An Empirical Approach to Chemical Structure and Bonding; p.1-30.

Brown, I.D. & Shannon, R.D. (1973): Empirical Bond-Strength-Bond-Length Curves for Oxides; Acta Cryst., A29, p.266-282.

Brown, I.D. & Wu, K.K. (1976): Empirical Parameters for Calculating Cation-Oxygen Bond Valences; Acta Cryst., B32, 1957-1959.

Brunton, G. (1973): Refinement of the Callaghanite Structure; Amer. Min., v.58, p.551.

Burdett, J.K.: Theoretical Models of Inorganic Stereochemistry. New York: John Wiley & Sons, 1980; Chapt. 5, Molecular Orbital Models of Main Group Stereochemistry: The Jahn-Teller Theorems; p.64-88.

Calvo, C. & Faggiani, R. (1975): α Cupric Divanadate; Acta Cryst., B31, p.603-605.

Cocco, G., Fanfani, L. and Zanazzi, P.F. (1966): The Crystal Structure of Fornacite; Acta Cryst., A21, p.A47, part 5.24.

Collin, R.L. (1951): The Crystal Structure of Bandylite, $Cu_2B_2O_4Cl_2 \cdot 4H_2O$; Acta Cryst., v.4, p.204-209.

Corsden, A. (1978): A Crystal-Structure Refinement of Libethenite; Canad. Min., v.16, p.153-157.

Cotton, F.A. & Wilkinson, G. (1972): Advanced Inorganic Chemistry, 3rd ed. London: John Wiley & Sons, 1966; Chapt. 26, Stereochemistry of Cupric Compounds, p.660-718.

Carapezza, M. & Sanseverino, L.R. (1968): Crystallography and Genesis of Double Sulfates and Their Hydrates. II. Structure, Powder Pattern and Thermoanalysis of Cyanochroite, $K_2Cu(SO_4)_2 \cdot 4H_2O$; Miner. Petrogr. Acta, v.14, p.23-37.

Cromer, D.T. & Liberman, D. (1970): Relativistic Calculation of Anomalous Scattoring Factors for X-rays; J. Chem. Physcs., v.53, p.1891-1898.

Cromer, D.T. & Mann, J.B. (1968): X-ray Scattoring Factors Computed from Numerical Hartree-Fock Wave Functions; Acta Cryst., A24, p.321-324.

Dresdner, H.C. (1965): Determination and Refinement of the Crystal Structure of Turquoise, $CuAl_6(PO_4)_4(OH)_8 \cdot 4H_2O$; Zeit. für Krist., v.121, p.87-113.

Dunitz, J.D. & Orgel, L.E. (1957a): Electronic Properties of Transition-Metal Oxides-I, Distortions From Cubic Symmetry; J. Phys. Chem. Solids, v.3, p.20-29.

Dunn, P.J., Peacor, D.R., Ramik, R.A., Su, S. and Rouse, R.C. (1987): Franklinfurnaceite, a Ca-Fe^{3+}-Mn^{3+}-Mn^{2+} Zincosilicate Isotypic with Chlorite, From Franklin, New Jersey; Amer. Min., v.72, p.812-816.

Effenberger, H. (1977): Verfeinerung der Kristallstruktur von Synthetischem Teineit, $CuTeO_3 \cdot 2H_2O$; TMPM, v.24, p.287-298.

Effenberger, H. (1985a): The Crystal Structure of Mammothite, $Pb_6Cu_4AlSbO_2(OH)_{16}Cl_4(SO_4)_2$; TMPM, v.34, p.279-288.

Effenberger, H. (1985b): $Cu_2O(SO_4)$, Dolerophanite: Refinement of the Crystal Structure, with a Comparison of [OCu(II)$_4$] Tetrahedra in Inorganic Compounds; Montash. für Chemie, v.166, p.927-931.

Effenberger, H. (1986): Likasite: Revision of the Chemical Formula and Redetermination of the Crystal Structure; N. Jb. Miner. Mh., v.3, p.101-110.

Effenberger, H. (1987): Crystal Structure and Chemical Formula of Schmiederite, $Pb_2Cu_2(OH)_4(SeO_3)(SeO_4)$, with a Comparison to Linarite, PbCu(OH)2(SO4); Min. Pet., v.36, p.3-12.

Evans, H.T. & Mrose, M.E. (1977): The Crystal Chemistry of the Hydrous Copper Silicates, Shattuckite and Plancheite; Amer. Min., v.62, p.491-502.

Fanfani, L., Nunzi, A., Zanazzi, P.F. and Zanzari, A.R. (1973): The Crystal Structure of Buttgenbachite; Mineral. Mag., v.39, p.264-270.

Fanfani, L. & Zanazzi, P.F. (1968): The Crystal Structure of Vauquelenite and the Relationships to Fornacite; Zeit. für Krist., v.126, p.433-443.

Fehlmann, M. & Ghose, S. (1964): Direct Determination of the Crystal Structure of Cornetite, $Cu_3PO_4(OH)_3$, by the Monte Carlo Method; Journ. Chem. Phys., v.41, p.1910-1916.

Finger, L.W. (1985): Fingerite, $Cu_{11}O_2(VO_4)_6$, a New Vanadium Sublimates from Izalco Volcano El Salvador: Crystal Structure; Amer. Min., v.70, p.197-199.

Finney, J.J. (1966): Refinement of the Crystal Structure of Euchroite, $Cu_2(AsO_4)(OH) \cdot 3H_2O$; Acta Cryst., v.21, p.437-440.

Finney, J.J., Graeber, E.J., Rosenzweig, A. and Hamilton, R.D. (1977): The Structure of Chloroxiphite, $Pb_3CuO_2(OH)_2Cl_2$; Mineral. Mag., v.41, p.357-361.

Fischer, R. (1984): STRUPLO. A Plotprogram for Crystal Structure Illustrations.

Fischer, R. & Pertlik, F. (1975): Verfeinerung der Kristallstruktur des Schafarzikits, $FeSb_2O_4$; TMPM, v.22, p.236-241.

Fleet, M.E. (1975): The Crystal Structure of Paratacamite, $Cu_2(OH)_3Cl$; Acta Cryst., B31, p.183-187.

Gentsch, M. & Weber, K. (1984): Structure of Langite, $Cu_4[(OH)_6|SO_4]\cdot 2H_2O$; Acta Cryst., C40, p.1309-1311.

Ghose, S., Fehlmann, M. and Sundaralingam, M. (1965): The Crystal Structure of Clinoclase, $Cu_3AsO_4(OH)_3$; Acta Cryst., v.18, p.777-786.

Ghose, S., Leo, S.R. and Wan, C. (1974): Structural Chemistry of Copper and Zinc Minerals. Part I. Veszelyite, $(Cu,Zn)_2ZnPO_4(OH)_3\cdot 2H_2O$: A Novel Type of Sheet Structure and Crystal Chemistry of Copper-Zinc Substitution; Amer. Min., v.59, p.573-581.

Ghose, S. & Wan, C. (1974): Structural Chemistry of Copper and Zinc Minerals. II. Stereochemistry of Copper (II) and Iodine (V) in Bellingerite, $Cu(IO_3)_2\cdot 2H_2O$; Acta Cryst., B30, p.965-973.

Ghose, S. & Wan, C. (1978): Salesite, $CuIO_3(OH)$, and $Cu(IO_3)_2\cdot 2H_2O$: A Comparison of the Crystal Structures and Their Magnetic Behavior; Amer. Min., v.63, p.172-179.

Ghose, S. & Wan, C. (1979): Structural Chemistry of Copper and Zinc Minerals. VI. Bayldonite, $(Cu,Zn)_3Pb(AsO_4)_2(OH)_2$: A Complex Layer Structure; Acta Cryst., B35, p.819-823.

Giachovazzo, C., Menchetti, S. and Scordari, F. (1973): The Crystal Structure of Caledonite, $Cu_2Pb_5(SO_4)_3CO_3(OH)_6$; Acta Cryst., B29, p.1986-1990.

Giachovazzo, C., Scandale, E. and Scordari, F. (1976): The Crystal Structure of Chlorthionite, $CuK_2Cl_2SO_4$; Zeit. für Krist., v.144, p.226-237.

Ginderow, P.D. & Cesbron, F. (1979): The Crystal Structure of Aubertite, $AlCuCl(SO_4)_2\cdot 14H_2O$; Acta Cryst., B35, p.2499-2502.

Ginderow, P.D. & Cesbron, F. (1983): Structure de la Derriksite, $Cu_4(UO_2)(SeO_3)_2(OH)_6$; Acta Cryst., C39, p.1605-1607.

Ginderow, P.D. & Cesbron, F. (1985): Structure de la Roubaultite, $Cu_2(UO_2)_3(CO_3)_2O_2(OH)_2\cdot 4H_2O$; Acta Cryst., C41, p.654-657.

Goodenough, J.B. (1964): Jahn-Teller Distortions Induced by Tetrahedral-Site Fe+2 Ions; J. Phys. Chem. Solids, v.25, p.151-160.

Gopal, R. & Calvo, C. (1972): Crystal Structure of α-Zn2V2O7; Can. J. Chem., v.51, p.1004-1009.

Groat, L.A. & Hawthorne, F.C. (1987): Refinement of the Crystal Structure of Papagoite; TMPM, v.37, p.89-96. wefg

Giuseppetti, G. & Tadini, C. (1980): The Crystal Structure of Osarizawaite; N. Jb. Miner. Mh., v.9, p.401-407.

Harker, D. (1936): The Crystal Structure of Cupric Chloride Dihydrate, $CuCl_2 \cdot 2H_2O$; Zeit für Krist., v.93, p.136-145.

Hawthorne, F.C. (1976): A Refinement of the Crystal Structure of Adamite; Canad. Min., v.14, p.143-148.

Hawthorne, F.C. (1983): Graphical Enumeration of Polyhedral Clusters; Acta Cryst., A39, p.724-736.

Hawthorne, F.C. (1985a): Towards a Structural Classification of Minerals: The $^{6}M^{4}T_2\emptyset_n$; Minerals. Amer., v.70, p.455-473.

Hawthorne, F.C. (1985b): Refinement of the Crystal Structure of Bloedite: Structural Similarities in the $[^{6}M(^{4}T\emptyset_4)_2\emptyset_n]$ Finite-Cluster Minerals; Canad. Min., v.23, p.669-674.

Hawthorne, F.C. (1985c): Refinement of the Crystal Structure of Botallackite; Mineral. Mag., v.49, p.87-89.

Hawthorne, F.C. (1985d): The Crystal Structure of Stringhamite; TMPM, v.34, p.15-24.

Hawthorne, F.C. (1986a): Lammerite, $Cu_3(AsO_4)_2$, a Modulated Close-Packed Structure; Amer. Min., v.71, p.206-209.

Hawthorne, F.C. (1986b): Structural Heirarchy in $^{6}M_X{}^{3}T_Y\emptyset_Z$ Minerals; Canad. Min., v.24, p.625-642.

Hawthorne, F.C. & Eby, R.K. (1985): Refinement of the Crystal Structure of Lindgrenite; N. Jb. Miner. Mh., v.5, p.234-240.

Hawthorne, F.C. & Eby, R.K. (in print): The Crystal Structure of Spangolite.

Hawthorne, F.C., Ercit, T.S. and Groat, L.A. (1986): Structures of Zinc Selenite and Copper Selenite; Acta Cryst., C42, p.1285-1287.

Hawthorne, F.C. & Faggiani, R. (1979): Refinement of the Structure of Descloizite; Acta Cryst., B35, p.717-720.

Hawthorne, F.C. & Ferguson, R.B. (1975): Refinement of the Crystal Structure of Kröhnkite; Acta Cryst., B31, p.1753-1755.

Hawthorne, F.C. & Ferguson, R.B. (1977): The Crystal Structure of Roselite; Canad. Min., v.15, p.36-42.

Hawthorne, F.C. & Groat, L.A. (1985): The Crystal Structure of Wroewolfeite, a Mineral With $[Cu_4(OH)_6(SO_4)(H_2O)]$ Sheets; Amer. Min., v.70, p.1050-1055.

Hawthorne, F.C., Groat, L.A., and Eby, R.K. (in print): The Refinement of the Crystal Structure of Antlerite.

Hawthorne, F.C., Groat, L.A. and Raudsepp, M. (1987): Kieserite, $Mg(SO_4)(H_2O)$, a Titanite-Group Mineral; N. Jb. Miner. Ab., v.157, p.121-132.

Helmholtz, L. & Kruh, R.F. (1952): The Crystal Structure of Cesium Chlorocuprate, Cs_2CuCl_4, and the Spectrum of the Chlorocuprate Ion; J. Amer. Chem. Soc., v.74, p.1176-1181.

Hughes, J.M., Starkey, S.J., Malinconico, M.L. and Malinconico, L.L. (1987): Lyonsite, $Cu_3Fe_4(VO_4)_6$, a New Fumarole Sublimate from Izalco Volcano El Salvador: Descriptive Mineralogy and Crystal Structure; Amer. Min., v.72, p.1000-1005.

Jahn, H.A. & Teller, E. (1937): Stability of Polyatomic Molecules in Degenerate Electronic States, I - Orbital Degeneracy; Proc. Royal Soc., Sec.A, v.161, p.220-236.

Kashayev, A.A. & Bakakin, V.V. (1968): Crystal Structure of Volborthite $Cu_3(OH)_2V_2O_7 \cdot 2H_2O$; Doklady Akad. Nauk USSR, v.181, p.967-969.

Keller, P. & Hess, H. (1978): Die Kristallstruktur von Arthurit, $CuFe_2[(H_2O)_4|(OH)_2|(AsO_4)_2]$; N. Jb. Miner. Abh., v.133, p.291-302.

Keller, P., Hess, H. and Dunn, P.J. (1979): Die Ladungsbianz für eine Verfeinerte Kristallstruktur von Stranskiit, $Zn_2Cu(AsO_4)_2$; TMPM, v.26, p.167-174.

Kokkoros, P.A. & Rentzeperis, P.J. (1958): The Crystal Structure of the Anhydrous Sulphates of Copper and Zinc; Acta Cryst., v.11, p.361-364.

Kolesova, R.V. & Fesenko, E.G. (1968): Determination of the Crystal Structure of Liroconite, $Cu_2Al[AsO_4](OH)_4 \cdot 4H_2O$; Soviet Phys. - Cryst., v.13, No.3, p.324-328.

Laughton, R.B. (1971): The Crystal Structure of Kinoite; Amer. Min., v.56, p.193-200.

Liehr, A.D. & Ballhausen, C.J. (1958): Inherent Configurational Instability of Octahedral Inorganic Complexes in Eg Electronic States; Annals of Physics, v.3, p.304-319.

Lindqvist, O. (1972): The Crystal Structure of $CuTeO_3$; Acta Chem. Scand., v.26, p.1423-1430.

McLean, W.J. & Anthony, J.W. (1972): The Disordered, "Zeolite-Like" Structure of Connelite; Amer. Min., v.57, p.426-438.

Meier, W.M. & Villiger, H. (1969): A Fortran Computer Program for the Least-Squares Refinement of Interatomic Distances, Program Manual©; 26 pages.

Mellini, M. & Merlino, S. (1978): Ktenasite, Another Mineral with $[(Cu,Zn)_2(OH)_3O]^-$ Octahedral Sheets; Zeit. für Krist., v.147, p.129-140.

Mellini, M. & Merlino, S. (1979): Posnajakite: $[Cu_4(OH)_6(H_2O)O]$ Octahedral Sheets in its Structure; Zeit. für Krist., v.149, p.249-257.

Mercurio-Lavaud, D. & Frit, M.B. (1973): Structure Cristalline de la Variete Haute Temperature du Pyrovanadate de Cuivre: $\beta Cu_2V_2O_7$; C.R. Acad. Sc. Paris, v.277, p.1101-1104.

Mereiter, V.K. & Preisinger, A. (1986): Kristallstrukurdaten der Wismutminerale Atelestit, Mixit, und Pucherit; Anz. der Östchn. Akad. der Wiss., math.-natws. Klasse, v.123, p.79-81.

Miller, P.T., Lenhert, P.G. and Joesten, M.D. (1973): The Crystal and Molecular Structure of Tris(tetraisopropylmethylenediphosphonate)-copper(II) Perchlorate with Comments on the Jahn-Teller Effect; Inorg. Chem., v.12, No.1, p.218-223.

Miyahara, S. & Ohnshi, H. (1956): Cation Arrangement and Magnetic Properties of Copper Ferrite-Chromite Series; J. Phys. Soc. Japan, v.11, p.1296-1297.

Moore, P.B. & Araki, T. (1974): Pinakiolite, $Mg_2Mn^{3+}O_2[BO_3]$; Warwickite, $Mg(Mg,Ti)O[BO_3]$; Wightmanite, $Mg_5O(OH)_5[BO_3]\cdot nH_2O$: Crystal Chemistry of Complex 3-Å Wallpaper Structures; Amer. Min., v.59, p.958-1004.

Mosset, A., Bonnet, J.J. and Galy, J. (1978): Structure Cristalline de la Chalconatronite Synthetique: $Na_2Cu(CO_3)_2\cdot 3H_2O$; Zeit. für Krist., v.148, p.165-177.

Nakai, I. (1986): Henmilite, $Ca_2Cu(OH)_4[B(OH)_4]_2$, a New Mineral From Fuka, Okayama Prefecture, Japan. II. Crystal Structure; Amer. Min., v.71, p.1236-1239.

O'Keefe, M. & Bovin, J.O. (1978): The Crystal Structure of Paramelaconite, Cu_4O_3; Amer. Min., v.63, p.180-185.

Öpik, U. & Pryce, M.H.L. (1957): Studies of the Jahn-Teller Effect I. A Survey of the Static Problem; Proc. Royal Soc., A238, p.425-447.

Orgel, L.E. & Dunitz, J.D. (1957); Stereochemistry of Cupric Compounds; Nature, v.179, p.462-465.

Pabst, A. (1959): Structures of Some Tetragonal Sheet Silicates; Acta Cryst., v.12, p.733-739.

Palache, C., Berman, H. and Frondel, C.: The System of Mineralogy, Vol.II, 7th ed. New York: John Wiley & Sons, 1951; p.504-505.

Parise, J.B. & Hyde, B.G. (1986): The Structure of Atacamite and its Relationship to Spinel; Acta Cryst., C42, p.1277-1280.

Pauling, L.C.: The Nature of the Chemical Bond, III.ed. Ithaca, New York: Cornell Univ. Press, 1960; Chapt. 13, Structure of Complex Ionic Crystals, sec.6, p.543-562.

Pertlik, F. (1975): Verfeinerung der Kristallstruktur von Synthetischem Trippkeit, $CuAs_2O_4$; TMPM, v.22, p.211-217.

Piret, P., Declercq, J.P. and Wauter-Stoop, D. (1980): Structure Cristalline de la Sengierite; Bull. Mineral., v. 103, p.176-178.

Povarennykh, A.S.: Crystal Chemical Classification of Minerals. New York: Plenum Press, 1972; 2 volumes.

Quarashi, M.M. & Barnes, W.H. (1963): The Structures of the Minerals of the Descloizite and Adelite Goups: IV-Descloisite and Conichalcite (Part2) The Structure of Conichalcite; Canad. Min., v.7, p.561-577.

Ribbe, P.H., Gibbs, G.V. and Hamil, M.M. (1977): A Refinement of the Structure of Dioptase, $Cu_6[Si_6O_{18}]\cdot 6H_2O$; Amer. Min., v.62, p.807-811.

Rosenzweig, A. (1975): Refinement of the Crystal Structure of Cuprosklowskite, $Cu[(UO_2)_2(SiO_3OH_2]\cdot 6H_2O$; Amer. Min., v.60, p.448-453.

Ross, M., Evans, H.T. and Appleman, D.E. (1964): Studies of the Torbernite Minerals (II): The Crystal Structure of Meta-Torbernite; Amer. Min., v.49, p.1603-1621.

Sabelli, C. (1980): The Crystal Structure of Chalcophyllite; Zeit. für Krist., v.151, p.129-140.

Sabelli, C. (1982): Campigliaite, $Cu_4Mn(SO_4)_2(OH)_6\cdot 4H_2O$, a New Mineral from Campiglia Marittima, Tuscany, Italy, II. Crystal Structure; Amer. Min., v.67, p.388-393.

Sabelli, C. & Zanazzi, P.F. (1972): The Crystal Structure of Devillite; Acta Cryst., B28, p.1182-1189.

Sabelli, C. & Zanazzi, P.F. (1968): The Crystal Structure of Serpierite; Acta Cryst., B24, p.1214-1221.

Shannon, R.D. (1976): Revised Effective Ionic Radii and Systematic Studies of Interatomic Distances in Halides and Chalcogenides; Acta Cryst., A32, p.751-767.

Shannon, R.D. & Calvo, C. (1972): Crystal Structure of a New Form of $Cu_3V_2O_8$; Can. Journ. Chem., v.50, p.3944-3949.

Shannon, R.D. & Calvo, C. (1973): Crystal Structure of $Cu_5V_2O_{10}$; Acta Cryst., B29, p.1338-1345.

Sieber, N.H.W., Tillmans, E. and Medenbach, O. (1987): Hentschelite, $CuFe_2(PO_4)_2(OH)_2$, a New Member of the Lazulite Group, and Reichenbachite, $Cu_5(PO_4)_2(OH)_4$, a Polymorph of Pseudomalachite, Two New Copper Phosphate Minerals from Reichenbach, Germany; Amer. Min., v.72, p.404-408.

Shoemaker, G.L., Anderson, J.B. and Kostiner, E. (1977a): Refinement of the Crystal Structure of Pseudomalachite; Amer. Min., v.62, p.1042-1048.

Shoemaker, G.L., Anderson, J.B. and Kostiner, E. (1977b): Copper(II) Phosphate; Acta Cryst., B33, p.2969-2972.

Shoemaker, G.L., Anderson, J.B. and Kostiner, E. (1981): The Crystal Structure of a Third Polymorph of $Cu_5(PO_4)_2(OH)_4$; Amer. Min., v.66, p.169-175.

Shoemaker, G.L. & Kostiner, E. (1981): Polymorphism in $Cu_5(PO_4)_2(OH)_4$; Amer. Min., v.66, p.176-181.

Süsse, P. (1972): Crystal Structure and Hydrogen Bonding of Copiapite; Zeit. für Krist., v.135, p.34-55.

Tillmans, E., Hofmeister, W. and Petitjean, K. (1987): Cornubite, $Cu_5(AsO_4)_2(OH)_4$, First Occurance of Single Crystals, Mineral Description and Crystal Structure; Bull. Geol. Soc. Finland 57, Part 1-2, p.119-127.

Toman, K. (1977): The Symmetry and Crystal Structure of Olivenite; Acta Cryst., B33, p.2628-2631.

Varghese, J.N. & Maslen, E.N. (1985): Electron Density in Non-Ideal Metal Complexes. I.Copper Sulphate Pentahydrate; B41, p.184-190.

Wan, C., Ghose, S. and Rossman, G.R. (1978): Guildite, a Layer Structure with a Ferric Hydroxy-Sulphate Chain and its Optical Absorption Spectra; Amer. Min., v.63, p.478-483.

Winter, J.K. & Ghose, S. (1979): Thermal Expansion and High Temperature Crystal Chemistry of the Al_2SiO_5 Polymorphs; Amer. Min., v.64, p.573-586.

Wood, M.M. (1970): The Crystal Structure of Ransomite; Amer. Min., v.55, p729-734.

Zahrobsky, R.F. & Baur, W.H. (1968): On the Crystal Chemistry of Salt Hydrates. V. The Determination of the Crystal Structure of $CuSO_4 \cdot 3H_2O$ (Bonattite); Acta Cryst., B24, p.508-513.

Zigan, von F. & Schuster, H.D. (1972): Verfeinerung der Struktur von Azurit, $Cu_3(OH)_2(CO_3)_2$, durch Neutronenbeugung; Zeit. für Krist., v.135, p.416-436.

Zigan, von F., Joswig, W. and Schuster, H.D. (1977): Verfeinerung der Struktur von Malachit, $Cu_2(OH)_2CO_3$, durch Neutonenbeugung; Zeit. für Krist., v.145, p.412-426.

Appendix A

STRUCTURE FACTORS OF X-RAY REFINEMENTS

A.1 CORNETITE

OBSERVED AND CALCULATED STRUCTURE FACTORS FOR CORNETITE

H	K	L	10FO	10FC	H	K	L	10FO	10FC	H	K	L	10FO	10FC	H	K	L	10FO	10FC	H	K	L	10FO	10FC
1	8	8	624	598	4	10	8	543	524	3	2	9	477	465	0	4	9	248	236	5	5	9	166	156
2	8	8	784	763	1	11	8	223	166	4	2	9	638	627	1	4	9	247	233	0	6	9	307	323
5	8	8	169	14	3	11	8	281	232	6	2	9	413	403	2	4	9	253	62	1	6	9	290	311
3	9	8	180	187	1	1	9	388	388	1	3	9	203	228	3	4	9	595	597	2	6	9	495	475
5	9	8	564	572	2	1	9	284	305	2	3	9	164	104	1	5	9	170	89	3	6	9	274	324
0	10	8	476	437	4	1	9	200	165	3	3	9	335	311	2	5	9	431	440	4	6	9	462	439
1	10	8	427	420	1	2	9	428	431	4	3	9	244	224	3	5	9	258	255	1	7	9	230	168
2	10	8	209	117	2	2	9	471	488	5	3	9	560	549	4	5	9	170	94	3	7	9	288	248
3	10	8	605	565																				

OBSERVED AND CALCULATED STRUCTURE FACTORS FOR CORNETITE

H	K	L	10FO	10FC	H	K	L	10FO	10FC	H	K	L	10FO	10FC	H	K	L	10FO	10FC	H	K	L	10FO	10FC
2	0	0	1325	1339	4	5	0	1404	1420	6	10	0	207	210	0	18	0	743	248	2	3	1	2176	2106
4	0	0	474	513	6	5	0	635	647	8	10	0	654	629	2	18	0	399	421	3	3	1	284	295
6	0	0	798	795	8	5	0	2021	2062	10	10	0	1425	1440	4	18	0	718	714	4	3	1	233	308
8	0	0	525	542	10	5	0	601	629	2	11	0	1328	1389	6	18	0	755	737	5	3	1	213	191
10	0	0	2271	2251	12	5	0	1128	1124	4	11	0	722	736	2	19	0	688	681	6	3	1	131	45
12	0	0	275	244	14	5	0	612	600	6	11	0	189	38	4	19	0	356	380	7	3	1	319	302
14	0	0	571	634	0	6	0	1711	1752	8	11	0	892	890	1	1	1	757	736	8	3	1	505	492
2	1	0	1453	1451	2	6	0	2064	2043	10	11	0	492	524	2	1	1	135	160	9	3	1	863	905
4	1	0	748	768	4	6	0	468	459	12	11	0	211	174	3	1	1	843	858	10	3	1	965	937
6	1	0	2728	2713	8	6	0	296	305	0	12	0	1145	1147	4	1	1	247	202	11	3	1	646	661
10	1	0	352	374	10	6	0	954	937	2	12	0	2012	2058	5	1	1	2125	2071	12	3	1	891	919
12	1	0	1531	1528	12	6	0	590	597	4	12	0	478	471	6	1	1	1272	1248	14	3	1	372	345
0	2	0	399	355	14	6	0	329	288	6	12	0	299	320	7	1	1	749	782	15	3	1	346	332
2	2	0	2226	2209	2	7	0	612	618	8	12	0	1565	1553	8	1	1	1045	1066	0	4	1	1606	1609
4	2	0	1830	1793	4	7	0	1469	1495	10	12	0	477	448	9	1	1	183	136	1	4	1	1399	1307
6	2	0	2588	2564	6	7	0	2311	2293	12	12	0	277	371	10	1	1	694	695	2	4	1	245	274
8	2	0	1712	1760	8	7	0	1228	1212	4	13	0	1478	1499	11	1	1	514	502	3	4	1	624	670
12	2	0	425	480	10	7	0	250	273	6	13	0	520	536	14	1	1	198	143	4	4	1	314	340
14	2	0	229	235	12	7	0	261	258	10	13	0	636	602	15	1	1	292	304	5	4	1	492	458
2	3	0	1024	958	0	8	0	1587	1611	0	14	0	1308	1347	0	2	1	275	170	6	4	1	1045	1024
4	3	0	3203	3185	2	8	0	554	542	2	14	0	663	710	1	2	1	920	922	7	4	1	1005	1031
6	3	0	910	914	4	8	0	2214	2239	4	14	0	679	694	2	2	1	1340	1365	8	4	1	167	111
8	3	0	433	474	6	8	0	1757	1808	6	14	0	243	262	3	2	1	713	701	9	4	1	267	267
10	3	0	447	406	8	8	0	229	134	8	14	0	553	574	4	2	1	2302	2308	10	4	1	868	892
12	3	0	400	408	10	8	0	705	729	10	14	0	700	729	5	2	1	360	342	11	4	1	332	345
14	3	0	1385	1419	12	8	0	496	513	2	15	0	991	1035	6	2	1	1776	1745	12	4	1	171	167
0	4	0	890	832	14	8	0	185	73	4	15	0	228	186	7	2	1	1081	1093	13	4	1	604	583
2	4	0	3364	3352	2	9	0	1609	1634	6	15	0	738	731	8	2	1	149	196	14	4	1	460	451
4	4	0	1839	1785	4	9	0	708	709	8	15	0	443	443	9	2	1	459	431	1	5	1	1235	1156
6	4	0	847	850	6	9	0	955	954	0	16	0	1447	1441	10	2	1	181	173	3	5	1	235	199
8	4	0	2356	2375	10	9	0	541	532	4	16	0	231	240	12	2	1	154	179	4	5	1	858	840
10	4	0	779	748	12	9	0	887	877	6	16	0	941	957	14	2	1	199	188	5	5	1	239	218
14	4	0	200	132	0	10	0	2191	2247	4	17	0	778	774	15	2	1	238	266	6	5	1	154	116
2	5	0	1858	1962	4	10	0	190	159	6	17	0	944	921	1	3	1	1505	1530	8	5	1	231	231

OBSERVED AND CALCULATED STRUCTURE FACTORS FOR CORNETITE

H	K	L	10FO	10FC	H	K	L	10FO	10FC	H	K	L	10FO	10FC	H	K	L	10FO	10FC	H	K	L	10FO	10FC
9	5	1	414	396	8	8	1	322	309	12	11	1	192	141	6	16	1	303	272	7	1	2	1158	1149
10	5	1	1117	1090	10	8	1	428	428	0	12	1	634	627	7	16	1	385	349	8	1	2	652	650
11	5	1	167	144	11	8	1	153	74	1	12	1	500	505	8	16	1	505	526	10	1	2	353	359
12	5	1	579	591	12	8	1	220	220	3	12	1	336	305	3	17	1	176	185	12	1	2	225	227
0	6	1	1885	1851	13	8	1	276	279	4	12	1	163	183	6	17	1	238	181	13	1	2	611	591
1	6	1	412	403	1	9	1	1306	1315	5	12	1	171	25	7	17	1	240	240	14	1	2	753	768
2	6	1	2015	2004	2	9	1	1706	1682	6	12	1	165	148	0	18	1	920	944	0	2	2	950	897
3	6	1	919	940	3	9	1	190	192	8	12	1	300	308	2	18	1	322	337	1	2	2	2707	2721
4	6	1	755	743	4	9	1	616	625	9	12	1	361	394	3	18	1	478	471	3	2	2	363	380
5	6	1	328	343	5	9	1	943	956	12	12	1	327	261	5	18	1	175	174	5	2	2	441	448
7	6	1	486	490	6	9	1	510	522	2	13	1	322	390	6	18	1	182	221	6	2	2	185	193
8	6	1	318	295	8	9	1	270	234	5	13	1	689	701	1	19	1	429	433	7	2	2	194	218
9	6	1	288	284	9	9	1	532	520	8	13	1	655	665	2	19	1	381	364	8	2	2	427	417
10	6	1	531	541	10	9	1	865	890	9	13	1	298	275	3	19	1	235	205	9	2	2	1121	1118
11	6	1	683	713	11	9	1	288	217	10	13	1	519	441	4	19	1	183	184	10	2	2	239	114
12	6	1	627	631	12	9	1	765	755	2	14	1	564	569	0	0	2	1380	1371	11	2	2	971	965
13	6	1	636	620	1	10	1	224	234	3	14	1	563	591	1	0	2	201	158	12	2	2	263	254
1	7	1	1110	1111	2	10	1	691	712	4	14	1	1104	1128	2	0	2	1342	1399	13	2	2	263	286
2	7	1	1047	1024	3	10	1	204	202	5	14	1	280	266	3	0	2	2206	2284	1	3	2	2071	2096
3	7	1	200	203	4	10	1	1576	1599	6	14	1	681	673	4	0	2	473	402	2	3	2	689	653
4	7	1	1181	1185	5	10	1	555	559	7	14	1	815	832	5	0	2	839	801	3	3	2	557	553
7	7	1	437	433	6	10	1	787	807	9	14	1	326	315	6	0	2	858	854	4	3	2	528	503
8	7	1	334	306	7	10	1	268	229	1	15	1	522	554	7	0	2	1680	1686	5	3	2	577	599
9	7	1	640	637	9	10	1	372	370	3	15	1	183	195	8	0	2	1366	1343	6	3	2	1688	1689
10	7	1	685	726	1	11	1	343	324	4	15	1	159	238	9	0	2	1227	1248	7	3	2	890	883
11	7	1	486	458	2	11	1	566	555	5	15	1	258	262	10	0	2	157	137	8	3	2	507	506
12	7	1	685	694	3	11	1	982	980	6	15	1	240	244	11	0	2	997	994	9	3	2	572	547
14	7	1	400	406	5	11	1	818	797	8	15	1	475	454	13	0	2	1362	1346	11	3	2	1276	1301
0	8	1	396	393	6	11	1	832	839	9	15	1	176	129	1	1	2	537	523	12	3	2	387	375
2	8	1	258	210	7	11	1	721	741	0	16	1	603	631	2	1	2	1312	1264	13	3	2	724	745
3	8	1	1089	1102	8	11	1	823	824	1	16	1	594	593	3	1	2	1309	1369	14	3	2	378	364
4	8	1	401	378	9	11	1	410	413	2	16	1	347	346	4	1	2	601	587	0	4	2	1922	1974
6	8	1	472	466	10	11	1	442	451	3	16	1	547	550	5	1	2	1115	1117	1	4	2	2073	2031
7	8	1	283	303	11	11	1	324	308	4	16	1	561	563	6	1	2	617	575	2	4	2	478	493

OBSERVED AND CALCULATED STRUCTURE FACTORS FOR CORNETITE

H	K	L	10FO	10FC	H	K	L	10FO	10FC	H	K	L	10FO	10FC	H	K	L	10FO	10FC	H	K	L	10FO	10FC
3	4	2	657	629	12	6	2	185	187	0	10	2	929	960	8	13	2	277	286	7	17	2	564	547
4	4	2	230	219	1	7	2	1482	1451	1	10	2	597	587	9	13	2	535	508	1	18	2	686	684
5	4	2	339	317	2	7	2	140	82	3	10	2	1526	1551	10	13	2	180	141	2	18	2	284	272
6	4	2	894	900	3	7	2	2795	2759	4	10	2	459	445	11	13	2	514	479	3	18	2	274	305
7	4	2	1631	1629	4	7	2	1064	1061	5	10	2	165	73	0	14	2	217	193	4	18	2	217	158
8	4	2	599	604	5	7	2	458	448	7	10	2	1324	1268	1	14	2	256	281	5	18	2	297	258
10	4	2	724	727	6	7	2	412	400	8	10	2	214	184	2	14	2	207	141	1	1	3	564	547
11	4	2	1111	1103	7	7	2	1096	1099	9	10	2	393	389	3	14	2	665	649	2	1	3	1255	1287
12	4	2	420	394	8	7	2	376	368	10	10	2	304	304	4	14	2	212	194	3	1	3	1010	1013
13	4	2	200	195	9	7	2	568	608	12	10	2	213	213	6	14	2	207	207	4	1	3	1099	1131
14	4	2	314	286	11	7	2	898	891	1	11	2	816	820	7	14	2	862	853	5	1	3	1413	1412
1	5	2	634	610	13	7	2	654	675	3	11	2	341	321	8	14	2	260	182	6	1	3	831	856
2	5	2	931	904	0	8	2	733	715	4	11	2	211	135	9	14	2	356	322	7	1	3	856	880
3	5	2	498	474	1	8	2	1606	1614	5	11	2	1410	1407	1	15	2	603	610	8	1	3	734	757
5	5	2	3500	3471	2	8	2	1392	1404	6	11	2	789	815	2	15	2	385	416	10	1	3	239	190
6	5	2	576	574	3	8	2	365	357	7	11	2	372	343	3	15	2	569	549	11	1	3	299	301
8	5	2	238	217	4	8	2	390	389	8	11	2	315	350	4	15	2	282	288	12	1	3	990	982
9	5	2	660	653	5	8	2	540	504	9	11	2	323	298	5	15	2	703	690	14	1	3	300	276
10	5	2	256	295	7	8	2	307	308	11	11	2	413	362	6	15	2	303	331	0	2	3	1653	1627
12	5	2	753	737	8	8	2	844	815	0	12	2	1206	1240	7	15	2	176	189	2	2	3	796	771
13	5	2	337	365	9	8	2	1944	1949	1	12	2	1285	1317	8	15	2	396	389	4	2	3	625	610
14	5	2	275	337	10	8	2	243	190	2	12	2	393	390	9	15	2	360	394	5	2	3	916	942
0	6	2	139	177	11	8	2	229	191	3	12	2	817	799	0	16	2	516	558	6	2	3	184	112
1	6	2	779	778	1	9	2	482	456	4	12	2	523	532	1	16	2	391	344	7	2	3	1655	1698
2	6	2	754	715	2	9	2	281	270	6	12	2	458	470	2	16	2	546	528	8	2	3	685	685
3	6	2	1201	1208	3	9	2	1581	1575	7	12	2	258	273	3	16	2	686	669	9	2	3	766	748
4	6	2	518	503	4	9	2	453	453	9	12	2	532	486	4	16	2	223	166	10	2	3	518	497
5	6	2	437	442	5	9	2	1207	1212	11	12	2	1156	1147	5	16	2	322	347	11	2	3	211	189
6	6	2	161	181	7	9	2	371	372	1	13	2	1156	1168	6	16	2	212	205	12	2	3	497	464
7	6	2	1402	1399	8	9	2	791	802	2	13	2	259	210	8	16	2	463	448	13	2	3	493	491
8	6	2	455	466	9	9	2	631	650	3	13	2	522	502	2	17	2	215	130	1	3	3	2231	2180
9	6	2	816	821	10	9	2	549	560	5	13	2	455	445	3	17	2	738	709	2	3	3	840	850
10	6	2	419	415	11	9	2	225	195	6	13	2	632	613	4	17	2	489	471	3	3	3	830	815
11	6	2	549	562	13	9	2	506	501	7	13	2	309	261	5	17	2	304	301	4	3	3	410	367

OBSERVED AND CALCULATED STRUCTURE FACTORS FOR CORNETITE

H	K	L	10FO	10FC	H	K	L	10FO	10FC	H	K	L	10FO	10FC	H	K	L	10FO	10FC	H	K	L	10FO	10FC
5	3	3	177	146	8	6	3	436	412	2	10	3	811	822	2	14	3	439	462	11	0	4	1216	1228
8	3	3	738	693	9	6	3	384	400	3	10	3	253	237	3	14	3	273	355	12	0	4	332	315
9	3	3	529	554	10	6	3	409	382	4	10	3	549	565	5	14	3	217	152	14	0	4	486	507
10	3	3	398	401	11	6	3	750	779	5	10	3	743	747	7	14	3	897	835	1	1	4	1731	1701
11	3	3	427	416	13	6	3	823	806	6	10	3	251	244	9	14	3	529	543	2	1	4	1332	1330
13	3	3	265	205	1	7	3	1441	1450	7	10	3	587	568	1	15	3	454	468	3	1	4	379	392
0	4	3	2036	2036	3	7	3	599	599	9	10	3	427	447	3	15	3	453	486	4	1	4	987	1011
1	4	3	1043	1013	4	7	3	633	641	11	10	3	316	293	5	15	3	408	418	5	1	4	2194	2223
3	4	3	692	704	5	7	3	288	296	12	10	3	375	331	6	15	3	588	581	6	1	4	371	372
4	4	3	946	954	6	7	3	336	311	1	11	3	278	250	1	16	3	453	441	8	1	4	537	553
5	4	3	347	356	7	7	3	570	548	2	11	3	813	837	2	16	3	213	203	10	1	4	162	191
6	4	3	936	938	8	7	3	382	383	3	11	3	862	866	3	16	3	519	462	11	1	4	445	430
7	4	3	214	199	9	7	3	540	492	4	11	3	679	651	4	16	3	412	426	12	1	4	801	808
8	4	3	155	107	10	7	3	366	390	5	11	3	842	824	6	16	3	505	528	13	1	4	204	53
10	4	3	529	551	0	8	3	901	913	6	11	3	464	397	7	16	3	276	317	14	1	4	493	475
11	4	3	190	215	2	8	3	375	344	7	11	3	632	646	1	17	3	363	389	0	2	4	438	424
13	4	3	323	264	4	8	3	605	619	8	11	3	466	430	2	17	3	194	223	1	2	4	1392	1358
14	4	3	365	327	5	8	3	278	268	0	12	3	601	629	4	17	3	420	354	2	2	4	1374	1377
1	5	3	1435	1440	6	8	3	170	127	1	12	3	270	259	6	17	3	303	250	4	2	4	641	641
2	5	3	391	395	8	8	3	352	331	2	12	3	470	482	0	18	3	404	383	5	2	4	317	280
3	5	3	471	473	9	8	3	171	65	4	12	3	524	553	2	18	3	296	266	6	2	4	1467	1517
7	5	3	668	679	10	8	3	843	842	6	12	3	158	83	3	18	3	278	244	7	2	4	209	243
8	5	3	271	245	13	8	3	256	173	8	12	3	499	541	4	18	3	334	307	8	2	4	852	847
9	5	3	534	534	1	9	3	1137	1150	9	12	3	396	383	0	0	4	2756	2726	9	2	4	972	972
10	5	3	265	196	2	9	3	332	320	10	12	3	269	238	1	0	4	853	851	11	2	4	428	391
12	5	3	399	364	3	9	3	226	239	1	13	3	213	262	2	0	4	794	759	12	2	4	425	408
0	6	3	728	744	5	9	3	333	333	2	13	3	1066	1090	3	0	4	131	28	1	3	4	141	142
1	6	3	231	203	7	9	3	464	463	4	13	3	281	308	4	0	4	264	301	2	3	4	723	717
2	6	3	193	100	8	9	3	918	919	5	13	3	500	515	5	0	4	194	216	3	3	4	2302	2286
3	6	3	458	488	9	9	3	775	768	7	13	3	366	372	6	0	4	159	171	4	3	4	1537	1546
4	6	3	2123	2146	10	9	3	398	351	8	13	3	442	423	7	0	4	1562	1597	5	3	4	673	683
5	6	3	1032	1032	11	9	3	225	191	9	13	3	237	209	8	0	4	722	736	6	3	4	1751	1772
6	6	3	1346	1310	12	9	3	361	358	10	13	3	403	404	9	0	4	486	477	7	3	4	562	576
7	6	3	454	463	1	10	3	229	243	0	14	3	1020	1008	10	0	4	1327	1368	8	3	4	312	301

OBSERVED AND CALCULATED STRUCTURE FACTORS FOR CORNETITE

H	K	L	10FO	10FC	H	K	L	10FO	10FC	H	K	L	10FO	10FC	H	K	L	10FO	10FC	H	K	L	10FO	10FC
10	3	4	472	475	9	6	4	453	428	11	9	4	443	443	0	14	4	863	849	8	2	5	276	259
11	3	4	239	242	10	6	4	613	595	12	9	4	457	437	1	14	4	465	450	9	2	5	307	303
13	3	4	750	753	11	6	4	425	415	0	10	4	1406	1416	2	14	4	352	367	10	2	5	285	266
0	4	4	1840	1830	12	6	4	181	105	1	10	4	289	335	3	14	4	228	252	11	2	5	558	551
1	4	4	172	163	1	7	4	611	623	3	10	4	794	768	5	14	4	296	280	13	2	5	935	920
2	4	4	610	595	3	7	4	348	292	4	10	4	579	580	7	14	4	247	243	1	3	5	362	391
3	4	4	1859	1880	4	7	4	1017	1027	6	10	4	374	364	8	14	4	425	387	2	3	5	167	192
4	4	4	707	676	5	7	4	1262	1285	7	10	4	829	820	2	15	4	1051	1044	3	3	5	626	647
5	4	4	551	548	6	7	4	801	806	9	10	4	203	206	3	15	4	195	79	4	3	5	304	344
7	4	4	235	219	7	7	4	205	210	10	10	4	1120	1105	5	15	4	1006	985	5	3	5	846	856
8	4	4	461	485	8	7	4	430	448	1	11	4	160	95	7	15	4	176	7	7	3	5	491	489
9	4	4	1213	1216	9	7	4	397	396	2	11	4	519	529	0	16	4	424	418	8	3	5	158	189
10	4	4	799	778	10	7	4	256	102	3	11	4	929	931	1	16	4	542	536	11	3	5	282	230
11	4	4	550	518	11	7	4	559	540	4	11	4	596	603	2	16	4	323	286	12	3	5	367	338
12	4	4	332	320	0	8	4	178	167	6	11	4	339	336	6	16	4	282	253	0	4	5	379	422
13	4	4	495	512	1	8	4	1246	1228	7	11	4	417	392	1	17	4	798	770	1	4	5	613	603
1	5	4	1272	1281	2	8	4	653	653	8	11	4	165	160	4	17	4	628	609	3	4	5	847	854
2	5	4	1843	1866	3	8	4	543	526	10	11	4	239	219	0	18	4	363	334	4	4	5	349	332
3	5	4	1777	1813	4	8	4	860	860	1	12	4	470	448	1	1	5	1717	1739	5	4	5	207	214
4	5	4	215	189	6	8	4	813	813	2	12	4	738	753	5	1	5	741	745	7	4	5	824	833
5	5	4	159	52	7	8	4	475	456	4	12	4	602	594	6	1	5	171	162	8	4	5	178	84
7	5	4	882	884	8	8	4	654	682	5	12	4	320	348	7	1	5	349	424	9	4	5	453	457
8	5	4	853	818	9	8	4	286	268	6	12	4	655	647	8	1	5	447	478	10	4	5	408	393
9	5	4	381	383	10	8	4	191	88	8	12	4	494	484	9	1	5	1001	1000	1	5	5	992	987
11	5	4	196	122	11	8	4	1139	1109	9	12	4	1041	1031	11	1	5	499	493	2	5	5	299	293
12	5	4	878	864	12	8	4	325	288	1	13	4	310	270	13	1	5	538	533	3	5	5	415	425
13	5	4	336	338	1	9	4	1076	1077	2	13	4	177	175	0	2	5	234	193	4	5	5	350	359
0	6	4	887	887	2	9	4	777	756	3	13	4	994	1010	1	2	5	480	456	6	5	5	238	184
1	6	4	659	664	3	9	4	655	692	4	13	4	831	828	2	2	5	207	223	7	5	5	604	638
2	6	4	603	594	4	9	4	525	514	5	13	4	286	272	3	2	5	528	481	8	5	5	200	165
4	6	4	350	332	5	9	4	1289	1238	6	13	4	667	647	4	2	5	812	809	9	5	5	229	256
5	6	4	509	508	6	9	4	242	275	7	13	4	921	884	5	2	5	944	973	12	5	5	165	107
7	6	4	302	297	8	9	4	452	473	8	13	4	346	288	6	2	5	548	527	0	6	5	1150	1158
8	6	4	724	696	9	9	4	159	157	9	13	4	227	224	7	2	5	484	500	1	6	5	984	972

OBSERVED AND CALCULATED STRUCTURE FACTORS FOR CORNETITE

H	K	L	10FO	10FC	H	K	L	10FO	10FC	H	K	L	10FO	10FC	H	K	L	10FO	10FC	H	K	L	10FO	10FC
2	6	5	573	600	3	10	5	165	192	2	16	5	225	120	10	2	6	347	348	0	6	6	1318	1332
3	6	5	970	984	5	10	5	592	600	4	16	5	184	115	11	2	6	402	399	1	6	6	597	579
5	6	5	804	786	6	10	5	276	254	1	17	5	637	643	12	2	6	225	233	2	6	6	807	808
7	6	5	1593	1607	7	10	5	712	706	0	0	6	812	817	1	3	6	514	516	6	6	6	253	254
8	6	5	525	502	8	10	5	326	337	1	0	6	313	280	2	3	6	450	447	7	6	6	377	381
9	6	5	964	979	1	11	5	1169	1180	2	0	6	1210	1209	3	3	6	1289	1281	8	6	6	525	492
10	6	5	239	220	2	11	5	306	280	3	0	6	486	512	4	3	6	956	990	9	6	6	288	264
1	7	5	294	251	4	11	5	239	168	4	0	6	549	528	5	3	6	837	842	10	6	6	472	444
3	7	5	660	631	5	11	5	168	60	5	0	6	188	200	6	3	6	1036	1074	1	7	6	882	858
4	7	5	186	220	6	11	5	269	207	6	0	6	464	478	7	3	6	450	437	4	7	6	1246	1231
5	7	5	697	702	9	11	5	712	699	7	0	6	889	913	8	3	6	439	444	5	7	6	515	514
7	7	5	624	616	10	11	5	211	193	8	0	6	416	421	9	3	6	477	457	6	7	6	467	506
8	7	5	195	199	0	12	5	271	275	9	0	6	740	745	10	3	6	330	355	7	7	6	356	363
10	7	5	199	102	1	12	5	497	483	10	0	6	703	742	11	3	6	284	284	10	7	6	446	427
11	7	5	313	302	3	12	5	345	374	11	0	6	707	678	12	3	6	253	276	1	8	6	1081	1052
12	7	5	268	297	4	12	5	225	222	12	0	6	322	296	0	4	6	1417	1397	2	8	6	1195	1194
0	8	5	289	329	1	13	5	899	905	2	1	6	622	627	3	4	6	1019	1039	3	8	6	740	713
1	8	5	267	278	2	13	5	175	86	3	1	6	411	409	4	4	6	465	410	6	8	6	379	376
3	8	5	1059	1088	3	13	5	224	127	4	1	6	885	903	6	4	6	699	679	8	8	6	916	904
6	8	5	423	441	5	13	5	558	551	5	1	6	1238	1262	7	4	6	500	486	1	9	6	430	398
7	8	5	620	615	6	13	5	410	414	8	1	6	579	613	8	4	6	347	321	2	9	6	680	676
8	8	5	196	148	7	13	5	411	353	10	1	6	528	572	9	4	6	773	784	4	9	6	681	685
9	8	5	165	83	8	13	5	251	239	11	1	6	314	288	10	4	6	759	756	5	9	6	984	973
11	8	5	356	341	0	14	5	222	199	12	1	6	215	98	11	4	6	582	598	6	9	6	165	227
1	9	5	264	259	2	14	5	318	274	0	2	6	201	212	1	5	6	673	651	8	9	6	772	781
2	9	5	258	133	3	14	5	687	691	1	2	6	794	806	2	5	6	1105	1131	10	9	6	481	478
3	9	5	304	305	4	14	5	343	356	2	2	6	555	555	3	5	6	693	715	0	10	6	1239	1226
4	9	5	466	466	5	14	5	267	272	3	2	6	327	353	4	5	6	156	136	1	10	6	249	177
5	9	5	872	888	6	14	5	206	189	4	2	6	601	617	5	5	6	578	569	2	10	6	284	327
6	9	5	181	208	1	15	5	215	212	5	2	6	218	81	6	5	6	762	769	3	10	6	974	992
7	9	5	517	517	2	15	5	267	267	6	2	6	445	447	7	5	6	396	377	4	10	6	405	410
11	9	5	408	384	3	15	5	621	617	7	2	6	234	229	8	5	6	255	293	6	10	6	202	211
0	10	5	386	422	5	15	5	293	273	8	2	6	839	856	9	5	6	668	655	7	10	6	929	903
2	10	5	428	464	1	16	5	196	231	9	2	6	599	592	11	5	6	344	322	8	10	6	326	344

OBSERVED AND CALCULATED STRUCTURE FACTORS FOR CORNETITE

H	K	L	10FO	10FC	H	K	L	10FO	10FC	H	K	L	10FO	10FC	H	K	L	10FO	10FC	H	K	L	10FO	10FC
2	11	6	197	213	2	2	7	1017	1030	1	7	7	311	339	0	12	7	364	341	3	3	8	622	644
3	11	6	806	812	4	2	7	703	708	2	7	7	182	216	1	12	7	230	269	4	3	8	225	188
4	11	6	440	412	5	2	7	303	311	3	7	7	196	217	2	12	7	464	390	5	3	8	420	467
5	11	6	166	23	7	2	7	310	307	5	7	7	296	299	3	12	7	200	210	6	3	8	578	598
6	11	6	743	735	8	2	7	309	299	6	7	7	700	736	5	12	7	238	217	7	3	8	516	499
8	11	6	174	10	10	2	7	486	452	7	7	7	304	256	1	13	7	340	336	8	3	8	703	697
0	12	6	859	850	1	3	7	415	428	8	7	7	455	410	2	13	7	596	581	0	4	8	1212	1235
1	12	6	337	328	2	3	7	236	267	9	7	7	202	197	0	14	7	850	823	1	4	8	789	799
2	12	6	196	179	3	3	7	203	234	0	8	7	769	760	0	0	8	484	485	2	4	8	667	694
4	12	6	644	625	6	3	7	555	550	1	8	7	267	275	2	0	8	837	861	3	4	8	329	330
5	12	6	241	278	7	3	7	483	472	2	8	7	231	222	3	0	8	1173	1203	4	4	8	428	412
6	12	6	691	683	8	3	7	853	866	4	8	7	321	341	4	0	8	941	959	5	4	8	179	165
7	12	6	306	338	9	3	7	314	342	5	8	7	163	123	5	0	8	201	89	6	4	8	469	452
2	13	6	204	270	10	3	7	361	363	7	8	7	181	176	6	0	8	570	571	7	4	8	406	397
3	13	6	667	652	0	4	7	554	519	8	8	7	238	154	7	0	8	1143	1144	8	4	8	438	448
4	13	6	242	297	1	4	7	170	173	9	8	7	169	63	8	0	8	436	397	1	5	8	187	187
5	13	6	374	352	4	4	7	451	449	1	9	7	347	366	9	0	8	603	589	2	5	8	529	543
6	13	6	628	594	6	4	7	452	466	2	9	7	562	565	1	1	8	425	419	3	5	8	357	352
0	14	6	408	411	7	4	7	238	236	3	9	7	166	52	2	1	8	248	229	4	5	8	482	483
2	14	6	315	289	10	4	7	506	522	4	9	7	172	98	3	1	8	877	908	5	5	8	973	972
3	14	6	185	162	1	5	7	527	521	6	9	7	288	311	4	1	8	364	341	6	5	8	331	297
5	14	6	221	196	2	5	7	172	85	7	9	7	266	253	5	1	8	780	789	7	5	8	458	441
1	15	6	283	257	5	5	7	171	93	8	9	7	734	697	6	1	8	377	371	0	6	8	376	370
2	15	6	478	443	6	5	7	186	182	0	10	7	369	389	8	1	8	482	489	1	6	8	372	404
3	15	6	311	310	8	5	7	340	320	2	10	7	631	613	0	2	8	229	251	2	6	8	179	173
1	1	7	595	590	9	5	7	365	371	4	10	7	445	384	1	2	8	1028	1026	3	6	8	273	277
2	1	7	1312	1300	10	5	7	432	445	5	10	7	194	239	2	2	8	268	254	7	6	8	652	636
4	1	7	890	864	0	6	7	269	287	6	10	7	485	478	4	2	8	294	293	1	7	8	694	679
6	1	7	247	275	2	6	7	479	477	7	10	7	400	356	5	2	8	200	98	2	7	8	233	230
7	1	7	252	285	3	6	7	224	249	1	11	7	293	310	6	2	8	264	241	3	7	8	676	635
9	1	7	448	449	4	6	7	1196	1202	2	11	7	583	551	8	2	8	261	291	4	7	8	475	441
10	1	7	364	333	5	6	7	187	168	3	11	7	259	262	9	2	8	766	785	6	7	8	188	131
0	2	7	1201	1207	6	6	7	959	980	4	11	7	660	631	1	3	8	334	320	7	7	8	396	367
1	2	7	519	503	7	6	7	574	553	6	11	7	171	151	2	3	8	214	253	0	8	8	1132	1133

A.2 CLINOCLASE

OBSERVED AND CALCULATED STRUCTURE FACTORS FOR CLINOCLASE

H	K	L	10FO	10FC	H	K	L	10FO	10FC	H	K	L	10FO	10FC	H	K	L	10FO	10FC	H	K	L	10FO	10FC
1	1	15	260	263	-5	3	15	312	321	-1	4	15	452	428	-5	1	16	175	173	1	2	16	212	190
2	1	15	229	213	-4	3	15	107	21	0	4	15	217	232	-4	1	16	240	254	-3	3	16	182	188
-5	2	15	205	207	-3	3	15	224	208	-5	0	16	206	191	-3	1	16	180	172	-2	3	16	98	78
-4	2	15	292	286	-2	3	15	375	381	-3	0	16	170	144	-2	1	16	91	34	-1	3	16	192	195
-3	2	15	627	619	-1	3	15	373	362	-2	0	16	200	158	-1	1	16	328	296	-3	1	17	103	101
-1	2	15	558	541	0	3	15	169	155	-1	0	16	414	385	0	1	16	131	127	-1	1	17	259	244
0	2	15	547	516	1	3	15	559	522	0	0	16	210	205	1	1	16	178	168	0	1	17	182	136
2	2	15	408	391	2	3	15	387	373	1	0	16	712	685	2	1	16	131	113	-1	2	17	625	576
3	2	15	301	310	-3	4	15	348	352	2	0	16	504	486	-1	2	16	121	116					

OBSERVED AND CALCULATED STRUCTURE FACTORS FOR CLINOCLASE

H	K	L	10FO	10FC	H	K	L	10FO	10FC	H	K	L	10FO	10FC	H	K	L	10FO	10FC	H	K	L	10FO	10FC
1	0	0	510	574	8	3	0	204	199	1	9	0	100	86	9	2	1	185	122	7	4	1	99	89
2	0	0	2717	2759	9	3	0	108	93	-9	1	1	350	336	-9	3	1	384	363	8	4	1	283	299
3	0	0	1083	1092	0	4	0	2450	2701	-8	1	1	383	358	-8	3	1	343	320	-8	5	1	216	225
4	0	0	235	248	1	4	0	109	95	-7	1	1	739	735	-7	3	1	781	791	-7	5	1	152	122
5	0	0	1335	1356	2	4	0	1549	1498	-6	1	1	742	766	-6	3	1	910	964	-5	5	1	243	244
6	0	0	648	668	3	4	0	189	195	-5	1	1	520	527	-5	3	1	553	593	-4	5	1	152	133
7	0	0	323	290	4	4	0	198	220	-4	1	1	107	133	-4	3	1	340	340	-3	5	1	232	218
8	0	0	715	710	5	4	0	701	734	-3	1	1	953	977	-3	3	1	1042	1046	-2	5	1	342	325
9	0	0	189	183	6	4	0	365	376	-2	1	1	568	575	-2	3	1	260	254	-1	5	1	94	108
10	0	0	659	593	7	4	0	204	201	-1	1	1	740	684	-1	3	1	994	909	0	5	1	97	101
1	1	0	57	33	8	4	0	433	437	0	1	1	85	58	0	3	1	178	164	1	5	1	231	245
2	1	0	2130	2239	9	4	0	108	95	1	1	1	1554	1401	1	3	1	1091	990	2	5	1	85	17
3	1	0	1227	1269	1	5	0	402	399	2	1	1	710	655	2	3	1	886	853	3	5	1	196	206
4	1	0	1186	1255	2	5	0	1105	1069	3	1	1	1187	1214	3	3	1	1480	1517	6	5	1	158	126
5	1	0	375	357	3	5	0	439	430	4	1	1	778	834	4	3	1	1295	1346	-7	6	1	98	129
6	1	0	750	758	4	5	0	808	832	6	1	1	232	235	5	3	1	180	198	-6	6	1	245	235
7	1	0	111	107	5	5	0	445	462	7	1	1	321	309	6	3	1	520	552	-4	6	1	520	509
8	1	0	438	414	6	5	0	377	380	9	1	1	154	149	7	3	1	357	366	-3	6	1	281	270
0	2	0	880	922	8	5	0	363	364	-9	2	1	720	704	8	3	1	137	72	-2	6	1	390	355
1	2	0	391	366	0	6	0	811	872	-8	2	1	397	404	9	3	1	147	111	-1	6	1	623	604
2	2	0	264	252	1	6	0	274	275	-6	2	1	471	483	-9	4	1	150	162	0	6	1	130	155
3	2	0	125	131	2	6	0	485	467	-5	2	1	479	512	-8	4	1	261	261	1	6	1	696	706
4	2	0	115	110	3	6	0	410	420	-4	2	1	1199	1269	-6	4	1	186	164	2	6	1	453	439
5	2	0	102	111	4	6	0	110	112	-3	2	1	493	510	-5	4	1	224	241	3	6	1	177	153
6	2	0	90	60	5	6	0	80	51	-2	2	1	98	161	-4	4	1	196	182	5	6	1	370	395
8	2	0	81	21	1	7	0	538	544	-1	2	1	2167	1984	-2	4	1	238	215	6	6	1	208	220
9	2	0	86	19	2	7	0	157	147	0	2	1	731	769	-1	4	1	360	348	7	6	1	127	114
1	3	0	681	622	3	7	0	150	126	1	2	1	1649	1523	0	4	1	562	624	-6	7	1	446	450
2	3	0	1315	1305	4	7	0	257	242	2	2	1	1673	1584	1	4	1	462	458	-5	7	1	341	335
3	3	0	589	613	5	7	0	162	153	3	2	1	540	530	2	4	1	943	883	-4	7	1	336	313
4	3	0	894	968	6	7	0	113	112	4	2	1	375	388	3	4	1	138	112	-3	7	1	375	345
5	3	0	84	8	0	8	0	533	584	5	2	1	768	819	4	4	1	411	431	-1	7	1	366	340
6	3	0	362	366	2	8	0	403	376	6	2	1	514	534	5	4	1	229	240	1	7	1	356	375
7	3	0	393	401	3	8	0	111	118	8	2	1	309	291	6	4	1	365	384	2	7	1	260	244

OBSERVED AND CALCULATED STRUCTURE FACTORS FOR CLINOCLASE

H	K	L	10FO	10FC	H	K	L	10FO	10FC	H	K	L	10FO	10FC	H	K	L	10FO	10FC	H	K	L	10FO	10FC
3	7	1	672	672	-3	1	2	182	183	-1	3	2	409	379	1	5	2	225	229	0	8	2	182	167
4	7	1	702	709	-2	1	2	882	825	0	3	2	596	601	2	5	2	164	133	2	8	2	193	192
6	7	1	336	333	-1	1	2	418	385	1	3	2	728	681	3	5	2	269	262	3	8	2	175	182
-2	8	1	124	88	1	1	2	661	588	2	3	2	139	116	4	5	2	337	336	4	8	2	331	318
-1	8	1	163	172	2	1	2	235	192	3	3	2	375	369	5	5	2	584	606	0	9	2	87	91
0	8	1	275	303	3	1	2	321	292	4	3	2	504	524	6	5	2	886	934	-9	1	3	119	95
1	8	1	262	273	4	1	2	622	622	6	3	2	579	614	8	5	2	529	509	-7	1	3	101	99
2	8	1	716	732	5	1	2	704	753	7	3	2	99	140	-7	6	2	295	311	-6	1	3	119	100
3	8	1	168	199	6	1	2	1157	1222	8	3	2	440	413	-6	6	2	265	258	-5	1	3	969	990
4	8	1	291	294	7	1	2	101	117	-9	4	2	243	253	-5	6	2	208	209	-4	1	3	251	250
0	9	1	249	280	8	1	2	534	521	-8	4	2	102	67	-3	6	2	791	742	-3	1	3	1523	1470
-10	0	2	390	361	-9	2	2	173	156	-7	4	2	155	170	-2	6	2	544	537	-2	1	3	611	582
-9	0	2	422	397	-8	2	2	91	17	-6	4	2	661	682	-1	6	2	452	451	-1	1	3	426	437
-8	0	2	272	227	-7	2	2	104	134	-5	4	2	530	542	0	6	2	153	166	0	1	3	224	271
-7	0	2	283	262	-6	2	2	115	135	-4	4	2	360	350	1	6	2	436	445	1	1	3	500	501
-6	0	2	1228	1235	-5	2	2	263	280	-3	4	2	644	643	3	6	2	359	350	2	1	3	941	889
-5	0	2	929	971	-4	2	2	155	68	-2	4	2	645	614	4	6	2	279	285	3	1	3	718	684
-4	0	2	401	418	-3	2	2	699	688	-1	4	2	270	279	5	6	2	254	259	4	1	3	505	519
-3	0	2	795	791	-1	2	2	655	602	0	4	2	440	476	7	6	2	423	433	5	1	3	632	670
-2	0	2	742	768	1	2	2	133	97	1	4	2	212	206	-6	7	2	95	131	6	1	3	90	86
-1	0	2	54	20	2	2	2	554	488	2	4	2	885	855	-5	7	2	344	334	7	1	3	541	550
0	0	2	957	1079	3	2	2	298	296	3	4	2	573	559	-4	7	2	138	151	8	1	3	172	115
1	0	2	461	436	4	2	2	302	318	4	4	2	981	984	-3	7	2	295	268	9	1	3	135	126
2	0	2	1091	1035	5	2	2	299	322	5	4	2	170	204	-2	7	2	152	108	-9	2	3	256	255
3	0	2	1247	1253	6	2	2	92	43	6	4	2	317	327	0	7	2	262	287	-8	2	3	181	162
4	0	2	1537	1591	7	2	2	232	242	7	4	2	107	129	1	7	2	226	230	-7	2	3	645	664
6	0	2	207	201	8	2	2	139	125	8	4	2	496	472	2	7	2	155	151	-5	2	3	621	627
7	0	2	215	220	-9	3	2	89	79	-8	5	2	309	297	3	7	2	490	470	-4	2	3	577	578
8	0	2	679	652	-8	3	2	300	294	-7	5	2	640	648	4	7	2	117	20	-3	2	3	1106	1088
-10	1	2	131	113	-7	3	2	189	200	-6	5	2	99	102	5	7	2	366	346	-2	2	3	233	251
-8	1	2	582	581	-5	3	2	113	111	-5	5	2	887	907	6	7	2	99	64	-1	2	3	2321	2291
-7	1	2	795	810	-4	3	2	614	627	-4	5	2	713	707	-3	8	2	121	136	0	2	3	1412	1495
-5	1	2	680	717	-3	3	2	430	430	-2	5	2	451	426	-2	8	2	135	96	1	2	3	1396	1362
-4	1	2	827	849	-2	3	2	475	452	-1	5	2	283	282	-1	8	2	88	111	2	2	3	509	477

OBSERVED AND CALCULATED STRUCTURE FACTORS FOR CLINOCLASE

H	K	L	10FO	10FC	H	K	L	10FO	10FC	H	K	L	10FO	10FC	H	K	L	10FO	10FC	H	K	L	10FO	10FC
3	2	3	816	783	7	4	3	219	235	1	7	3	490	522	-8	1	4	373	372	-4	3	4	679	675
4	2	3	434	448	-8	5	3	101	100	2	7	3	681	694	-7	1	4	684	698	-2	3	4	837	820
5	2	3	349	361	-6	5	3	107	109	3	7	3	408	403	-6	1	4	385	392	-1	3	4	242	231
6	2	3	267	278	-5	5	3	308	307	4	7	3	252	252	-5	1	4	265	246	0	3	4	106	128
7	2	3	345	349	-4	5	3	246	239	5	7	3	522	524	-4	1	4	1169	1147	1	3	4	766	771
8	2	3	132	138	-3	5	3	382	357	-4	8	3	388	354	-3	1	4	704	665	2	3	4	580	552
9	2	3	673	647	-2	5	3	201	185	-3	8	3	539	505	-2	1	4	325	357	3	3	4	818	785
-8	3	3	112	38	-1	5	3	481	490	-2	8	3	223	213	-1	1	4	538	530	4	3	4	271	266
-6	3	3	156	130	0	5	3	395	417	-1	8	3	666	679	0	1	4	907	923	5	3	4	209	221
-5	3	3	1132	1155	1	5	3	108	118	0	8	3	210	227	1	1	4	471	516	7	3	4	135	124
-4	3	3	164	138	2	5	3	574	564	1	8	3	222	234	2	1	4	1147	1062	-9	4	4	367	374
-3	3	3	2214	2131	3	5	3	183	202	2	8	3	173	184	3	1	4	1496	1438	-8	4	4	313	314
-2	3	3	1062	1010	4	5	3	375	384	4	8	3	113	16	4	1	4	117	137	-7	4	4	128	104
-1	3	3	414	409	5	5	3	219	237	-10	0	4	420	371	5	1	4	455	483	-6	4	4	444	465
0	3	3	287	294	7	5	3	206	232	-9	0	4	661	637	6	1	4	105	122	-5	4	4	612	611
1	3	3	900	892	-7	6	3	387	389	-8	0	4	273	280	9	1	4	126	125	-4	4	4	97	52
2	3	3	1323	1268	-6	6	3	91	77	-7	0	4	96	26	-9	2	4	254	244	-3	4	4	860	848
3	3	3	800	777	-5	6	3	441	436	-6	0	4	637	656	-8	2	4	123	86	-2	4	4	1346	1312
4	3	3	427	422	-3	6	3	397	382	-5	0	4	575	585	-6	2	4	98	105	-1	4	4	1316	1348
5	3	3	901	939	-2	6	3	493	486	-4	0	4	236	226	-4	2	4	132	115	0	4	4	1471	1561
6	3	3	90	47	-1	6	3	1062	1081	-3	0	4	1214	1157	-3	2	4	111	99	1	4	4	1190	1214
7	3	3	728	746	0	6	3	723	764	-2	0	4	1881	1790	-2	2	4	510	489	2	4	4	105	115
8	3	3	237	226	1	6	3	888	939	-1	0	4	2414	2368	-1	2	4	611	607	3	4	4	302	290
-9	4	3	115	137	2	6	3	183	171	0	0	4	2061	2171	0	2	4	84	118	4	4	4	217	229
-7	4	3	124	108	3	6	3	524	513	1	0	4	1991	1941	1	2	4	454	437	5	4	4	642	648
-5	4	3	183	196	4	6	3	500	503	2	0	4	370	353	2	2	4	213	200	6	4	4	125	139
-4	4	3	526	529	5	6	3	320	324	3	0	4	75	46	4	2	4	244	248	7	4	4	251	256
-3	4	3	535	511	6	6	3	269	272	4	0	4	691	686	5	2	4	159	161	8	4	4	157	141
-2	4	3	410	397	7	6	3	229	215	5	0	4	1130	1169	8	2	4	92	97	-8	5	4	307	296
-1	4	3	1054	1034	-5	7	3	788	762	7	0	4	320	303	9	2	4	112	104	-7	5	4	541	554
0	4	3	530	550	-3	7	3	1102	1047	8	0	4	286	279	-9	3	4	273	276	-6	5	4	390	384
1	4	3	106	86	-2	7	3	311	308	9	0	4	148	152	-7	3	4	337	345	-5	5	4	293	270
2	4	3	98	82	-1	7	3	249	232	-10	1	4	204	179	-6	3	4	452	469	-4	5	4	890	860
6	4	3	155	159	0	7	3	151	141	-9	1	4	358	338	-5	3	4	380	398	-3	5	4	419	405

OBSERVED AND CALCULATED STRUCTURE FACTORS FOR CLINOCLASE

H	K	L	10FO	10FC	H	K	L	10FO	10FC	H	K	L	10FO	10FC	H	K	L	10FO	10FC	H	K	L	10FO	10FC
-2	5	4	571	566	1	8	4	206	221	8	2	5	191	178	-6	5	5	147	153	0	8	5	452	461
-1	5	4	560	559	3	8	4	122	141	-9	3	5	264	239	-5	5	5	271	273	1	8	5	417	421
0	5	4	807	830	-10	1	5	196	161	-8	3	5	784	798	-4	5	5	192	189	2	8	5	329	343
1	5	4	733	745	-8	1	5	683	685	-7	3	5	272	264	-3	5	5	338	328	3	8	5	396	387
2	5	4	593	585	-6	1	5	826	842	-6	3	5	819	812	-2	5	5	295	297	-10	0	6	170	164
3	5	4	1107	1102	-5	1	5	122	137	-5	3	5	520	518	0	5	5	222	235	-8	0	6	600	610
4	5	4	148	124	-4	1	5	168	202	-4	3	5	258	237	1	5	5	183	184	-7	0	6	311	308
5	5	4	404	417	-3	1	5	402	395	-2	3	5	174	186	3	5	5	254	240	-6	0	6	878	863
6	5	4	129	53	-2	1	5	343	325	0	3	5	99	55	7	5	5	104	116	-5	0	6	922	895
7	5	4	159	161	-1	1	5	498	462	1	3	5	673	685	-6	6	5	462	454	-4	0	6	773	744
-7	6	4	124	125	0	1	5	304	297	2	3	5	1047	1014	-5	6	5	123	107	-3	0	6	887	846
-4	6	4	98	93	1	1	5	714	717	3	3	5	347	335	-4	6	5	415	398	-2	0	6	1488	1447
-2	6	4	473	470	2	1	5	1003	934	4	3	5	572	552	-2	6	5	163	174	-1	0	6	2236	2268
-1	6	4	724	735	3	1	5	212	181	5	3	5	920	923	-1	6	5	198	197	0	0	6	843	845
0	6	4	340	346	4	1	5	485	472	6	3	5	288	287	0	6	5	287	291	1	0	6	677	694
1	6	4	935	962	5	1	5	622	611	7	3	5	464	456	1	6	5	258	264	2	0	6	1744	1727
2	6	4	301	290	6	1	5	370	382	8	3	5	240	236	3	6	5	510	517	3	0	6	263	244
3	6	4	119	134	7	1	5	329	341	-9	4	5	234	228	4	6	5	160	134	4	0	6	1244	1213
4	6	4	115	104	8	1	5	281	282	-8	4	5	143	122	5	6	5	189	216	5	0	6	174	171
5	6	4	144	147	-8	2	5	241	250	-7	4	5	390	412	6	6	5	126	116	6	0	6	136	164
-6	7	4	163	157	-7	2	5	224	247	-6	4	5	120	128	-6	7	5	466	439	7	0	6	405	403
-4	7	4	372	347	-6	2	5	779	781	-5	4	5	88	80	-5	7	5	340	323	8	0	6	598	583
-3	7	4	256	242	-4	2	5	1100	1083	-4	4	5	116	75	-3	7	5	119	69	-9	1	6	175	170
-2	7	4	342	327	-3	2	5	323	305	-3	4	5	248	239	-2	7	5	238	223	-7	1	6	294	273
-1	7	4	524	540	-2	2	5	300	290	-2	4	5	166	170	-1	7	5	119	110	-6	1	6	890	875
0	7	4	190	187	-1	2	5	287	285	-1	4	5	393	416	1	7	5	166	164	-5	1	6	404	415
1	7	4	307	317	0	2	5	562	608	0	4	5	417	428	2	7	5	448	458	-4	1	6	1528	1494
2	7	4	154	174	1	2	5	578	584	1	4	5	842	885	3	7	5	257	273	-3	1	6	1383	1355
4	7	4	298	288	2	2	5	612	603	2	4	5	473	482	4	7	5	349	356	-2	1	6	442	423
5	7	4	131	180	3	2	5	1680	1610	3	4	5	744	742	5	7	5	571	562	-1	1	6	385	393
-3	8	4	340	297	4	2	5	621	603	5	4	5	89	82	-4	8	5	114	137	0	1	6	585	582
-2	8	4	455	440	5	2	5	396	395	7	4	5	287	297	-3	8	5	263	235	1	1	6	1043	1069
-1	8	4	371	386	6	2	5	372	376	-8	5	5	211	199	-2	8	5	123	126	3	1	6	727	699
0	8	4	448	453	7	2	5	409	416	-7	5	5	195	192	-1	8	5	196	181	4	1	6	998	980

OBSERVED AND CALCULATED STRUCTURE FACTORS FOR CLINOCLASE

H	K	L	10FO	10FC	H	K	L	10FO	10FC	H	K	L	10FO	10FC	H	K	L	10FO	10FC	H	K	L	10FO	10FC
5	1	6	576	559	-6	4	6	445	426	3	6	6	177	165	-7	2	7	785	765	-1	4	7	123	145
6	1	6	962	968	-5	4	6	446	453	5	6	6	324	328	-6	2	7	242	240	0	4	7	647	649
7	1	6	499	518	-4	4	6	407	400	6	6	6	187	212	-5	2	7	392	394	1	4	7	340	369
8	1	6	149	158	-3	4	6	432	427	-6	7	6	201	183	-4	2	7	554	550	2	4	7	260	277
-8	2	6	183	172	-2	4	6	830	833	-5	7	6	151	122	-3	2	7	837	834	3	4	7	203	211
-6	2	6	88	72	-1	4	6	1073	1114	-2	7	6	185	179	-2	2	7	2502	2524	5	4	7	88	72
-5	2	6	146	153	0	4	6	623	613	0	7	6	259	253	-1	2	7	599	630	6	4	7	124	63
-4	2	6	466	463	1	4	6	432	437	1	7	6	204	180	0	2	7	2329	2374	7	4	7	143	54
-3	2	6	150	92	2	4	6	851	875	2	7	6	135	141	1	2	7	162	167	-8	5	7	178	163
-2	2	6	464	456	4	4	6	767	740	3	7	6	247	246	2	2	7	338	330	-6	5	7	308	292
0	2	6	210	222	5	4	6	126	113	-3	8	6	217	207	3	2	7	643	645	-5	5	7	196	180
2	2	6	204	176	6	4	6	153	170	-2	8	6	154	131	4	2	7	374	376	-4	5	7	328	321
3	2	6	223	215	7	4	6	314	302	-1	8	6	335	332	5	2	7	348	345	-3	5	7	446	444
5	2	6	168	145	-8	5	6	129	137	0	8	6	246	224	6	2	7	348	376	-2	5	7	119	128
8	2	6	133	117	-7	5	6	329	327	1	8	6	143	172	7	2	7	265	244	-1	5	7	291	324
-8	3	6	138	142	-6	5	6	862	844	2	8	6	293	305	8	2	7	522	517	0	5	7	422	417
-7	3	6	91	100	-5	5	6	302	312	-9	1	7	199	195	-8	3	7	331	318	1	5	7	232	273
-6	3	6	254	235	-4	5	6	873	840	-8	1	7	389	383	-7	3	7	117	156	2	5	7	369	381
-5	3	6	391	390	-3	5	6	664	647	-6	1	7	644	647	-6	3	7	598	613	4	5	7	232	242
-4	3	6	498	479	-2	5	6	236	238	-5	1	7	925	898	-5	3	7	884	863	5	5	7	196	198
-3	3	6	663	660	1	5	6	509	526	-4	1	7	1360	1349	-4	3	7	1421	1390	-7	6	7	288	279
-2	3	6	425	433	2	5	6	150	145	-3	1	7	873	884	-3	3	7	588	581	-6	6	7	110	107
-1	3	6	98	65	3	5	6	278	258	-2	1	7	673	682	-2	3	7	865	888	-5	6	7	243	241
0	3	6	281	283	4	5	6	734	734	-1	1	7	210	209	-1	3	7	124	135	-4	6	7	186	184
1	3	6	776	804	5	5	6	365	362	0	1	7	1200	1224	0	3	7	843	867	-3	6	7	190	191
2	3	6	345	331	6	5	6	671	650	1	1	7	286	298	2	3	7	1425	1451	-2	6	7	905	910
3	3	6	414	398	7	5	6	404	404	2	1	7	1401	1397	3	3	7	327	313	-1	6	7	219	192
4	3	6	508	503	-7	6	6	124	96	4	1	7	596	597	4	3	7	711	683	0	6	7	942	934
5	3	6	393	369	-5	6	6	328	310	5	1	7	373	377	5	3	7	207	180	2	6	7	165	207
6	3	6	565	552	-4	6	6	574	556	6	1	7	338	334	6	3	7	484	476	3	6	7	276	261
7	3	6	208	204	-2	6	6	624	618	7	1	7	141	137	-6	4	7	137	111	4	6	7	180	178
8	3	6	193	178	-1	6	6	126	143	8	1	7	90	77	-5	4	7	314	327	5	6	7	208	199
-8	4	6	494	489	0	6	6	274	259	-9	2	7	215	189	-3	4	7	468	481	-5	7	7	396	378
-7	4	6	304	302	2	6	6	124	144	-8	2	7	213	218	-2	4	7	386	396	-4	7	7	643	615

OBSERVED AND CALCULATED STRUCTURE FACTORS FOR CLINOCLASE

H	K	L	10FO	10FC	H	K	L	10FO	10FC	H	K	L	10FO	10FC	H	K	L	10FO	10FC	H	K	L	10FO	10FC
-3	7	7	245	235	-2	1	8	267	265	1	3	8	331	337	-2	6	8	178	179	-1	2	9	155	157
-2	7	7	484	483	-1	1	8	132	136	3	3	8	113	95	-1	6	8	678	674	0	2	9	685	702
-1	7	7	243	256	0	1	8	619	623	4	3	8	214	192	0	6	8	489	481	1	2	9	971	993
0	7	7	409	392	1	1	8	1119	1176	5	3	8	228	218	1	6	8	390	393	2	2	9	882	925
2	7	7	610	620	2	1	8	667	660	6	3	8	95	124	2	6	8	435	457	3	2	9	799	815
3	7	7	105	114	3	1	8	319	335	7	3	8	166	131	3	6	8	175	216	4	2	9	572	573
4	7	7	331	346	4	1	8	724	708	-8	4	8	90	58	5	6	8	173	178	6	2	9	290	281
-3	8	7	468	451	5	1	8	165	161	-7	4	8	148	137	-5	7	8	96	119	7	2	9	206	228
-2	8	7	388	375	6	1	8	339	340	-6	4	8	467	474	-4	7	8	215	210	-8	3	9	394	389
0	8	7	477	452	7	1	8	139	124	-5	4	8	210	192	-3	7	8	91	40	-7	3	9	724	743
1	8	7	302	302	8	1	8	157	140	-4	4	8	225	231	-2	7	8	307	313	-6	3	9	233	224
-9	0	8	310	286	-9	2	8	111	94	-3	4	8	660	680	0	7	8	135	111	-5	3	9	473	476
-8	0	8	100	41	-8	2	8	88	83	-1	4	8	1080	1091	2	7	8	216	207	-4	3	9	540	542
-7	0	8	202	197	-6	2	8	81	29	0	4	8	407	408	-1	8	8	286	271	-3	3	9	144	156
-6	0	8	594	586	-5	2	8	136	129	1	4	8	294	314	-9	1	9	133	138	-1	3	9	184	182
-5	0	8	404	401	-4	2	8	329	334	2	4	8	529	549	-8	1	9	247	251	0	3	9	250	246
-4	0	8	368	365	-3	2	8	184	185	3	4	8	550	556	-7	1	9	433	446	2	3	9	191	186
-3	0	8	1027	1010	-1	2	8	647	676	5	4	8	364	370	-6	1	9	282	262	3	3	9	588	608
-2	0	8	219	213	0	2	8	208	221	6	4	8	175	140	-5	1	9	227	210	4	3	9	571	565
-1	0	8	1905	1973	1	2	8	398	420	-7	5	8	511	501	-4	1	9	439	436	5	3	9	461	454
0	0	8	857	861	2	2	8	220	203	-6	5	8	243	259	-2	1	9	190	192	6	3	9	783	758
1	0	8	446	481	3	2	8	168	171	-5	5	8	308	317	-1	1	9	282	300	-8	4	9	105	106
2	0	8	863	876	4	2	8	183	183	-4	5	8	127	86	0	1	9	224	213	-7	4	9	132	134
3	0	8	818	822	5	2	8	102	118	-3	5	8	464	480	1	1	9	130	123	-6	4	9	356	359
5	0	8	387	381	6	2	8	106	136	-2	5	8	247	252	3	1	9	289	290	-5	4	9	364	378
6	0	8	104	161	-9	3	8	319	319	0	5	8	312	314	4	1	9	495	498	-3	4	9	262	277
8	0	8	194	163	-8	3	8	182	165	1	5	8	763	802	5	1	9	336	331	-2	4	9	205	190
-9	1	8	624	620	-7	3	8	247	236	2	5	8	411	434	6	1	9	591	586	-1	4	9	219	234
-8	1	8	236	242	-5	3	8	125	136	3	5	8	462	491	7	1	9	108	75	1	4	9	501	512
-7	1	8	556	549	-4	3	8	287	288	4	5	8	722	718	-9	2	9	345	336	2	4	9	159	188
-6	1	8	87	69	-3	3	8	232	239	5	5	8	177	184	-8	2	9	502	508	3	4	9	195	199
-5	1	8	369	373	-2	3	8	254	234	6	5	8	204	195	-6	2	9	794	793	4	4	9	200	208
-4	1	8	257	245	-1	3	8	323	328	-4	6	8	198	205	-5	2	9	411	423	5	4	9	299	298
-3	1	8	421	419	0	3	8	198	185	-3	6	8	231	241	-2	2	9	580	594	6	4	9	170	146

OBSERVED AND CALCULATED STRUCTURE FACTORS FOR CLINOCLASE

H	K	L	10FO	10FC	H	K	L	10FO	10FC	H	K	L	10FO	10FC	H	K	L	10FO	10FC	H	K	L	10FO	10FC
-7	5	9	138	126	3	0	10	389	403	0	3	10	438	428	3	6	10	164	188	-6	3	11	569	580
-6	5	9	138	90	4	0	10	223	212	1	3	10	317	324	-3	7	10	113	78	-5	3	11	127	143
-5	5	9	207	200	6	0	10	119	124	2	3	10	338	326	-2	7	10	308	313	-4	3	11	796	829
-4	5	9	226	226	7	0	10	565	528	3	3	10	406	420	-1	7	10	123	72	-3	3	11	470	500
-2	5	9	316	325	-8	1	10	147	160	4	3	10	113	66	0	7	10	269	256	-1	3	11	97	123
-1	5	9	297	291	-7	1	10	414	401	5	3	10	305	305	1	7	10	101	94	0	3	11	851	854
1	5	9	452	469	-6	1	10	280	280	6	3	10	172	132	-8	1	11	289	276	1	3	11	699	694
2	5	9	182	175	-5	1	10	1166	1179	-7	4	10	480	475	-7	1	11	301	303	2	3	11	314	299
3	5	9	225	230	-4	1	10	161	147	-6	4	10	87	93	-6	1	11	565	556	3	3	11	455	473
4	5	9	310	307	-3	1	10	857	897	-4	4	10	122	128	-4	1	11	760	776	4	3	11	114	15
-6	6	9	343	318	-2	1	10	148	147	-3	4	10	1090	1141	-3	1	11	97	91	5	3	11	166	168
-5	6	9	167	137	-1	1	10	254	183	-2	4	10	300	311	-2	1	11	128	114	-5	4	11	208	226
-3	6	9	94	13	0	1	10	388	399	-1	4	10	1153	1162	-1	1	11	131	118	-4	4	11	133	165
-2	6	9	373	374	1	1	10	723	741	0	4	10	190	162	0	1	11	754	758	-3	4	11	88	24
-1	6	9	120	115	2	1	10	417	442	1	4	10	586	595	1	1	11	645	652	-2	4	11	343	349
0	6	9	346	340	3	1	10	559	584	2	4	10	333	356	2	1	11	462	472	-1	4	11	605	597
1	6	9	390	393	4	1	10	226	225	3	4	10	281	292	3	1	11	376	398	0	4	11	170	138
2	6	9	477	495	5	1	10	748	746	4	4	10	267	276	-8	2	11	273	276	1	4	11	391	392
3	6	9	466	472	7	1	10	277	277	-7	5	10	368	360	-7	2	11	325	307	2	4	11	141	158
4	6	9	342	357	-8	2	10	93	124	-6	5	10	341	338	-6	2	11	126	135	3	4	11	122	110
-4	7	9	321	317	-7	2	10	201	218	-5	5	10	1110	1102	-5	2	11	316	321	-6	5	11	331	328
-1	7	9	142	133	-6	2	10	158	155	-3	5	10	758	797	-4	2	11	657	658	-4	5	11	281	288
2	7	9	94	85	-4	2	10	217	216	-2	5	10	132	125	-3	2	11	353	378	-3	5	11	344	368
-9	0	10	342	343	-3	2	10	278	296	-1	5	10	316	319	-2	2	11	1461	1506	-1	5	11	341	341
-8	0	10	304	302	-1	2	10	259	261	0	5	10	521	519	-1	2	11	976	967	0	5	11	237	233
-7	0	10	709	702	0	2	10	119	141	1	5	10	519	529	0	2	11	628	629	1	5	11	132	167
-6	0	10	204	214	3	2	10	109	99	2	5	10	274	265	1	2	11	461	465	2	5	11	328	323
-4	0	10	325	329	4	2	10	116	114	3	5	10	589	614	2	2	11	328	340	-5	6	11	174	176
-3	0	10	1227	1271	6	2	10	119	128	4	5	10	145	154	3	2	11	370	387	-4	6	11	446	440
-2	0	10	175	157	7	2	10	149	155	5	5	10	662	652	4	2	11	259	269	-3	6	11	265	261
-1	0	10	1549	1533	-7	3	10	248	241	-4	6	10	426	439	5	2	11	253	262	-2	6	11	695	684
0	0	10	496	499	-5	3	10	528	536	-3	6	10	552	580	6	2	11	176	197	-1	6	11	357	337
1	0	10	598	609	-3	3	10	491	514	-1	6	10	390	373	-8	3	11	256	264	0	6	11	358	345
2	0	10	246	247	-2	3	10	147	127	0	6	10	186	159	-7	3	11	258	252	1	6	11	128	138

OBSERVED AND CALCULATED STRUCTURE FACTORS FOR ELIKOCLASE

H	K	L	10FO	10FC	H	K	L	10FO	10FC	H	K	L	10FO	10FC	H	K	L	10FO	10FC	H	K	L	10FO	10FC
2	6	11	122	111	1	2	12	184	183	0	6	12	506	489	3	3	13	101	54	0	1	14	820	799
3	6	11	195	201	2	2	12	121	122	1	6	12	341	321	4	3	13	679	689	2	1	14	554	540
-2	7	11	91	46	3	2	12	90	126	-6	1	13	678	693	-5	4	13	150	153	3	1	14	284	271
0	7	11	421	389	4	2	12	121	90	-5	1	13	327	343	-4	4	13	249	277	4	1	14	305	306
-7	0	12	210	207	-7	3	12	92	109	-4	1	13	526	550	-2	4	13	310	303	-3	2	14	208	228
-6	0	12	644	624	-6	3	12	98	73	-3	1	13	126	112	-1	4	13	124	85	-2	2	14	285	285
-5	0	12	219	222	-4	3	12	203	207	-2	1	13	181	195	0	4	13	153	179	0	2	14	176	157
-4	0	12	271	261	-2	3	12	106	36	-1	1	13	501	488	2	4	13	231	228	1	2	14	93	24
-3	0	12	186	200	-1	3	12	245	239	0	1	13	138	133	3	4	13	193	165	2	2	14	109	97
-2	0	12	407	418	1	3	12	308	307	1	1	13	345	331	-5	5	13	201	225	3	2	14	115	13
-1	0	12	87	45	2	3	12	177	183	2	1	13	347	352	-4	5	13	240	217	-6	3	14	289	302
0	0	12	696	688	3	3	12	253	216	3	1	13	124	139	-2	5	13	257	231	-5	3	14	361	368
1	0	12	898	889	5	3	12	257	261	4	1	13	664	683	-1	5	13	292	284	-4	3	14	232	258
2	0	12	131	135	-6	4	12	348	354	5	1	13	231	224	1	5	13	315	308	-3	3	14	143	172
3	0	12	881	910	-4	4	12	209	240	-7	2	13	313	322	-2	6	13	314	284	-2	3	14	191	148
4	0	12	371	373	-3	4	12	92	80	-6	2	13	262	248	-1	6	13	256	224	0	3	14	413	403
-8	1	12	555	546	-2	4	12	225	208	-4	2	13	558	586	-7	0	14	436	418	2	3	14	270	261
-7	1	12	157	153	-1	4	12	103	79	-3	2	13	801	833	-5	0	14	419	425	3	3	14	164	146
-6	1	12	182	170	0	4	12	507	502	-2	2	13	799	793	-4	0	14	629	673	-5	4	14	203	223
-5	1	12	183	162	1	4	12	610	600	-1	2	13	591	569	-3	0	14	898	912	-4	4	14	493	502
-3	1	12	114	126	3	4	12	522	519	0	2	13	989	962	-2	0	14	1321	1304	-3	4	14	490	496
-2	1	12	354	360	4	4	12	206	183	1	2	13	202	177	-1	0	14	278	263	-2	4	14	854	835
-1	1	12	586	561	-5	5	12	152	165	2	2	13	1062	1061	0	0	14	487	468	-1	4	14	296	270
0	1	12	88	38	-4	5	12	190	158	3	2	13	126	90	1	0	14	246	231	0	4	14	467	435
1	1	12	249	245	-3	5	12	122	127	4	2	13	175	172	2	0	14	103	17	1	4	14	98	101
2	1	12	415	428	-2	5	12	321	319	5	2	13	148	140	3	0	14	157	146	-3	5	14	163	115
3	1	12	522	532	-1	5	12	346	340	-7	3	13	170	193	4	0	14	91	87	-1	5	14	186	163
4	1	12	167	160	1	5	12	105	95	-6	3	13	799	789	-7	1	14	433	427	0	5	14	614	583
5	1	12	654	636	2	5	12	475	480	-5	3	13	201	213	-6	1	14	451	448	1	5	14	94	30
6	1	12	134	129	3	5	12	525	512	-4	3	13	485	503	-5	1	14	732	750	-6	1	15	129	147
-5	2	12	131	165	-4	6	12	159	136	-3	3	13	197	179	-4	1	14	666	710	-5	1	15	190	199
-2	2	12	289	299	-3	6	12	106	85	-1	3	13	288	267	-3	1	14	151	160	-2	1	15	344	339
-1	2	12	221	215	-2	6	12	376	363	1	3	13	147	146	-2	1	14	103	126	-1	1	15	257	256
0	2	12	265	258	-1	6	12	133	93	2	3	13	306	325	-1	1	14	128	108	0	1	15	142	146

A.3 EUCHROITE

OBSERVED AND CALCULATED STRUCTURE FACTORS FOR EUCHROITE

H	K	L	10FO	10FC	H	K	L	10FO	10FC	H	K	L	10FO	10FC	H	K	L	10FO	10FC	H	K	L	10FO	10FC
4	5	7	229	261	0	7	7	446	438	0	0	8	106	101	5	1	8	114	116	4	3	8	298	293
5	5	7	102	117	1	7	7	184	196	1	0	8	316	303	0	2	8	145	135	0	4	8	125	130
6	5	7	135	134	2	7	7	120	111	3	0	8	158	146	1	2	8	234	239	1	4	8	252	229
0	6	7	127	122	3	7	7	97	98	0	1	8	367	361	3	2	8	544	530	2	4	8	173	163
1	6	7	89	65	4	7	7	167	163	1	1	8	317	314	0	3	8	149	141	3	4	8	109	90
2	6	7	268	256	1	8	7	125	116	2	1	8	271	259	1	3	8	343	315	0	5	8	347	325
3	6	7	223	220	2	8	7	164	159	3	1	8	287	280	2	3	8	262	240	1	5	8	222	183
4	6	7	135	120	3	8	7	199	188	4	1	8	201	198	3	3	8	301	296	2	5	8	185	165
5	6	7	183	160																				

OBSERVED AND CALCULATED STRUCTURE FACTORS FOR EUCHROITE

H	K	L	10FO	10FC	H	K	L	10FO	10FC	H	K	L	10FO	10FC	H	K	L	10FO	10FC	H	K	L	10FO	10FC
2	0	0	1685	1787	14	2	0	112	96	10	5	0	297	307	8	8	0	449	442	5	12	0	359	350
4	0	0	39	20	1	3	0	696	678	11	5	0	76	67	9	8	0	264	269	6	12	0	139	136
6	0	0	976	992	2	3	0	463	474	12	5	0	168	140	10	8	0	350	353	1	13	0	443	441
8	0	0	232	230	3	3	0	410	429	13	5	0	276	270	1	9	0	518	512	2	13	0	84	75
10	0	0	401	392	4	3	0	1067	1031	0	6	0	710	730	2	9	0	104	111	3	13	0	198	189
12	0	0	135	149	5	3	0	1139	1136	1	6	0	449	435	3	9	0	137	134	4	13	0	248	239
14	0	0	366	356	6	3	0	1206	1240	2	6	0	139	138	4	9	0	789	790	6	13	0	376	369
1	1	0	1356	1311	7	3	0	453	448	3	6	0	163	141	5	9	0	383	400	0	14	0	269	264
2	1	0	569	579	9	3	0	469	489	4	6	0	1017	1052	6	9	0	684	711	1	14	0	225	224
3	1	0	797	801	10	3	0	175	159	5	6	0	390	385	7	9	0	593	606	3	14	0	106	112
4	1	0	419	477	11	3	0	450	454	6	6	0	266	253	8	9	0	152	158	4	14	0	191	202
5	1	0	475	496	12	3	0	116	100	8	6	0	205	193	9	9	0	229	220	1	0	1	1392	1368
6	1	0	1363	1415	13	3	0	95	80	9	6	0	212	224	0	10	0	322	325	2	0	1	357	363
7	1	0	435	440	0	4	0	2333	2356	10	6	0	872	873	1	10	0	202	206	3	0	1	1496	1463
8	1	0	266	283	1	4	0	1355	1260	11	6	0	94	96	2	10	0	102	80	4	0	1	255	245
9	1	0	365	373	2	4	0	1310	1261	12	6	0	479	482	3	10	0	147	135	5	0	1	148	153
10	1	0	333	330	3	4	0	574	555	1	7	0	313	321	4	10	0	518	511	6	0	1	53	21
11	1	0	383	380	4	4	0	347	318	2	7	0	434	426	5	10	0	414	408	7	0	1	55	37
12	1	0	321	308	5	4	0	101	119	3	7	0	1035	1035	6	10	0	279	300	8	0	1	136	118
13	1	0	242	239	6	4	0	766	763	4	7	0	1072	1108	7	10	0	117	124	9	0	1	634	661
14	1	0	137	150	7	4	0	255	265	5	7	0	627	660	8	10	0	292	297	10	0	1	83	91
0	2	0	1259	1293	8	4	0	390	400	6	7	0	805	804	9	10	0	269	253	11	0	1	164	171
1	2	0	181	157	9	4	0	73	58	7	7	0	95	98	10	10	0	512	483	12	0	1	314	309
2	2	0	555	489	10	4	0	365	363	8	7	0	159	149	3	11	0	739	744	13	0	1	537	511
3	2	0	137	91	12	4	0	89	92	9	7	0	320	314	4	11	0	342	335	14	0	1	238	242
4	2	0	1348	1331	1	5	0	1408	1375	10	7	0	282	276	5	11	0	223	219	0	1	1	284	264
5	2	0	94	77	2	5	0	72	65	11	7	0	353	356	6	11	0	342	340	1	1	1	100	101
6	2	0	506	516	3	5	0	750	744	0	8	0	1066	1093	7	11	0	118	109	2	1	1	505	483
8	2	0	626	632	4	5	0	1136	1138	1	8	0	230	217	9	11	0	174	181	3	1	1	1678	1652
9	2	0	108	121	5	5	0	341	318	2	8	0	842	841	0	12	0	896	911	4	1	1	503	439
10	2	0	1116	1138	6	5	0	1019	1020	4	8	0	144	134	1	12	0	169	172	5	1	1	250	269
11	2	0	96	95	7	5	0	821	830	5	8	0	379	397	2	12	0	574	569	6	1	1	291	299
12	2	0	628	629	8	5	0	133	134	6	8	0	453	461	3	12	0	145	147	7	1	1	1071	1105
13	2	0	139	125	9	5	0	231	222	7	8	0	67	10	4	12	0	169	176	8	1	1	295	292

OBSERVED AND CALCULATED STRUCTURE FACTORS FOR EUCHROITE

H	K	L	10FO	10FC	H	K	L	10FO	10FC	H	K	L	10FO	10FC	H	K	L	10FO	10FC	H	K	L	10FO	10FC
9	1	1	211	217	2	4	1	471	438	8	6	1	225	212	4	9	1	248	242	5	12	1	174	171
10	1	1	107	168	3	4	1	951	931	9	6	1	463	462	5	9	1	180	183	6	12	1	305	279
11	1	1	162	150	4	4	1	484	477	10	6	1	219	238	6	9	1	283	329	7	12	1	150	148
13	1	1	315	305	5	4	1	197	245	11	6	1	219	218	7	9	1	398	418	8	12	1	210	211
14	1	1	100	109	6	4	1	129	138	12	6	1	112	93	8	9	1	413	391	1	13	1	151	151
0	2	1	122	109	7	4	1	359	363	0	7	1	511	515	9	9	1	234	229	2	13	1	392	394
1	2	1	1140	1175	8	4	1	251	252	1	7	1	192	174	10	9	1	245	217	3	13	1	288	277
2	2	1	606	566	9	4	1	583	588	2	7	1	686	717	11	9	1	131	110	4	13	1	129	137
3	2	1	949	979	10	4	1	76	110	3	7	1	777	855	0	10	1	268	259	5	13	1	189	193
4	2	1	593	537	11	4	1	188	201	4	7	1	488	452	1	10	1	382	392	6	13	1	283	285
5	2	1	252	206	12	4	1	262	245	5	7	1	198	213	2	10	1	221	223	0	14	1	256	259
6	2	1	428	443	13	4	1	350	351	6	7	1	275	270	3	10	1	449	455	1	14	1	256	240
7	2	1	470	492	0	5	1	81	74	7	7	1	672	684	4	10	1	468	475	2	14	1	125	108
8	2	1	475	507	1	5	1	404	381	8	7	1	198	197	5	10	1	167	151	3	14	1	225	225
9	2	1	621	613	2	5	1	536	525	9	7	1	371	387	6	10	1	182	191	4	14	1	317	295
10	2	1	213	208	3	5	1	1208	1190	10	7	1	151	134	7	10	1	222	219	0	0	2	1286	1229
11	2	1	207	222	4	5	1	284	282	11	7	1	141	131	8	10	1	244	251	1	0	2	924	856
13	2	1	478	470	5	5	1	171	131	12	7	1	141	156	9	10	1	259	266	2	0	2	1384	1259
0	3	1	157	170	6	5	1	417	411	0	8	1	309	321	10	10	1	218	198	3	0	2	46	26
1	3	1	152	105	7	5	1	724	748	1	8	1	563	601	0	11	1	431	434	4	0	2	1612	1588
2	3	1	417	430	8	5	1	424	436	2	8	1	235	216	1	11	1	205	198	5	0	2	401	415
3	3	1	854	859	9	5	1	232	232	3	8	1	595	615	2	11	1	529	568	6	0	2	61	47
4	3	1	338	351	10	5	1	212	193	4	8	1	213	215	3	11	1	324	325	7	0	2	116	112
5	3	1	330	326	11	5	1	168	148	5	8	1	220	228	4	11	1	314	299	8	0	2	198	209
6	3	1	161	150	12	5	1	242	243	6	8	1	218	229	5	11	1	58	53	9	0	2	498	508
7	3	1	870	866	13	5	1	256	257	7	8	1	375	383	6	11	1	285	284	10	0	2	694	708
8	3	1	272	276	0	6	1	471	472	8	8	1	228	225	7	11	1	305	324	11	0	2	521	529
9	3	1	425	429	1	6	1	786	823	9	8	1	471	461	8	11	1	133	126	12	0	2	452	451
10	3	1	85	68	2	6	1	467	502	10	8	1	155	177	9	11	1	184	181	13	0	2	154	150
11	3	1	139	169	3	6	1	829	886	11	8	1	184	178	0	12	1	394	406	0	1	2	300	296
12	3	1	88	89	4	6	1	487	494	0	9	1	61	53	1	12	1	336	333	1	1	2	969	965
13	3	1	237	237	5	6	1	276	276	1	9	1	124	132	2	12	1	91	109	2	1	2	771	624
0	4	1	369	380	6	6	1	296	313	2	9	1	318	319	3	12	1	415	400	3	1	2	1121	1073
1	4	1	796	735	7	6	1	216	231	3	9	1	544	551	4	12	1	300	301	4	1	2	852	846

OBSERVED AND CALCULATED STRUCTURE FACTORS FOR EUCHROITE

H	K	L	10FO	10FC	H	K	L	10FO	10FC	H	K	L	10FO	10FC	H	K	L	10FO	10FC	H	K	L	10FO	10FC
5	1	2	1125	1117	11	3	2	107	109	5	6	2	410	417	3	9	2	567	582	1	13	2	94	73
6	1	2	1156	1170	12	3	2	146	159	6	6	2	478	480	4	9	2	372	377	2	13	2	138	125
7	1	2	537	522	13	3	2	221	223	8	6	2	422	430	5	9	2	598	606	3	13	2	464	481
8	1	2	372	388	0	4	2	365	359	9	6	2	312	315	6	9	2	286	292	4	13	2	278	267
9	1	2	342	351	1	4	2	838	838	10	6	2	222	224	7	9	2	334	299	5	13	2	326	321
10	1	2	363	378	2	4	2	484	495	11	6	2	193	197	8	9	2	81	85	0	14	2	340	344
11	1	2	227	207	3	4	2	264	278	12	6	2	83	67	9	9	2	256	263	1	14	2	310	301
12	1	2	268	274	4	4	2	1022	1046	0	7	2	447	435	10	9	2	238	205	2	14	2	176	179
13	1	2	186	175	5	4	2	654	665	1	7	2	842	819	0	10	2	763	785	3	14	2	193	188
0	2	2	1885	1856	6	4	2	334	338	2	7	2	722	701	1	10	2	610	597	1	0	3	506	508
1	2	2	1040	1040	7	4	2	258	248	3	7	2	196	204	2	10	2	501	514	2	0	3	989	972
2	2	2	748	783	8	4	2	306	309	4	7	2	462	485	3	10	2	340	356	3	0	3	411	401
3	2	2	699	651	9	4	2	452	480	5	7	2	598	597	4	10	2	132	128	4	0	3	640	613
4	2	2	249	228	10	4	2	680	709	6	7	2	523	511	5	10	2	181	196	5	0	3	638	645
5	2	2	181	177	11	4	2	460	429	7	7	2	610	618	6	10	2	294	278	6	0	3	66	35
6	2	2	940	973	12	4	2	366	362	8	7	2	177	177	8	10	2	209	208	7	0	3	228	234
7	2	2	237	252	13	4	2	126	92	9	7	2	248	237	9	10	2	246	255	8	0	3	451	438
8	2	2	595	617	1	5	2	679	650	10	7	2	59	88	0	11	2	304	295	9	0	3	473	486
9	2	2	225	230	2	5	2	545	512	11	7	2	95	73	1	11	2	635	637	10	0	3	158	163
10	2	2	190	186	3	5	2	817	869	12	7	2	210	183	2	11	2	160	190	12	0	3	215	221
11	2	2	330	320	4	5	2	449	435	0	8	2	168	169	3	11	2	243	249	13	0	3	283	266
12	2	2	102	85	5	5	2	908	892	1	8	2	414	403	4	11	2	270	268	0	1	3	405	390
13	2	2	61	58	6	5	2	543	526	2	8	2	174	199	5	11	2	369	384	1	1	3	514	510
0	3	2	503	480	7	5	2	290	323	3	8	2	199	211	6	11	2	300	298	2	1	3	998	976
1	3	2	401	441	8	5	2	225	227	4	8	2	679	665	7	11	2	405	403	3	1	3	795	791
2	3	2	548	537	9	5	2	300	306	5	8	2	321	330	8	11	2	151	144	4	1	3	673	666
3	3	2	918	914	10	5	2	266	260	6	8	2	293	310	0	12	2	68	53	5	1	3	160	182
4	3	2	724	679	11	5	2	424	428	7	8	2	237	228	1	12	2	299	281	6	1	3	388	369
5	3	2	1058	1066	12	5	2	244	251	8	8	2	120	114	2	12	2	175	174	7	1	3	610	622
6	3	2	893	893	0	6	2	1842	1834	9	8	2	348	366	3	12	2	176	167	8	1	3	559	552
7	3	2	855	891	1	6	2	1290	1236	10	8	2	629	620	4	12	2	292	285	9	1	3	138	146
8	3	2	187	217	2	6	2	951	945	11	8	2	360	356	5	12	2	286	287	10	1	3	190	198
9	3	2	405	389	3	6	2	320	298	1	9	2	147	147	6	12	2	136	152	11	1	3	318	334
10	3	2	151	175	4	6	2	52	56	2	9	2	349	360	7	12	2	106	127	12	1	3	122	128

OBSERVED AND CALCULATED STRUCTURE FACTORS FOR EUCHROITE

H	K	L	10FO	10FC	H	K	L	10FO	10FC	H	K	L	10FO	10FC	H	K	L	10FO	10FC	H	K	L	10FO	10FC
13	1	3	147	138	8	4	3	576	557	5	7	3	336	362	6	10	3	195	229	1	1	4	781	777
0	2	3	229	230	9	4	3	254	274	6	7	3	411	396	8	10	3	246	233	2	1	4	805	819
1	2	3	476	474	10	4	3	262	254	7	7	3	237	246	9	10	3	171	165	3	1	4	541	526
2	2	3	796	829	11	4	3	149	129	8	7	3	514	500	1	11	3	130	101	4	1	4	358	335
3	2	3	180	186	12	4	3	218	207	9	7	3	87	96	2	11	3	328	338	5	1	4	906	911
4	2	3	329	317	0	5	3	539	538	10	7	3	154	155	3	11	3	219	229	6	1	4	345	338
5	2	3	550	537	1	5	3	519	526	11	7	3	276	283	4	11	3	75	49	7	1	4	354	354
6	2	3	129	148	2	5	3	791	823	0	8	3	76	102	5	11	3	218	181	8	1	4	362	363
7	2	3	129	110	3	5	3	357	352	1	8	3	464	458	6	11	3	294	301	9	1	4	249	220
8	2	3	399	400	4	5	3	601	640	2	8	3	569	566	7	11	3	93	95	10	1	4	273	279
9	2	3	458	458	5	5	3	159	132	3	8	3	124	124	8	11	3	347	328	11	1	4	178	176
11	2	3	77	37	6	5	3	367	365	4	8	3	443	454	0	12	3	206	207	12	1	4	389	380
12	2	3	395	380	7	5	3	385	390	5	8	3	399	409	1	12	3	297	292	0	2	4	174	170
13	2	3	177	154	8	5	3	409	421	6	8	3	348	370	2	12	3	343	332	1	2	4	289	287
1	3	3	297	280	9	5	3	143	125	7	8	3	296	274	4	12	3	422	405	2	2	4	625	633
2	3	3	405	444	11	5	3	195	197	8	8	3	396	409	5	12	3	213	184	3	2	4	423	417
3	3	3	563	543	12	5	3	150	155	9	8	3	206	202	6	12	3	184	166	4	2	4	749	781
4	3	3	475	505	0	6	3	438	431	10	8	3	264	234	0	13	3	298	287	5	2	4	600	581
5	3	3	397	399	1	6	3	528	500	0	9	3	266	263	1	13	3	221	222	6	2	4	121	151
6	3	3	378	387	2	6	3	632	640	1	9	3	304	302	2	13	3	445	433	7	2	4	122	123
7	3	3	314	333	3	6	3	537	561	2	9	3	478	473	3	13	3	170	177	8	2	4	114	95
8	3	3	658	662	4	6	3	314	325	3	9	3	176	177	4	13	3	292	283	9	2	4	514	516
9	3	3	115	108	5	6	3	359	352	4	9	3	431	420	0	0	4	1085	1095	10	2	4	291	278
10	3	3	232	202	6	6	3	278	289	5	9	3	135	134	1	0	4	1491	1532	11	2	4	609	612
11	3	3	241	241	7	6	3	105	105	6	9	3	143	141	3	0	4	362	362	12	2	4	203	175
12	3	3	123	138	8	6	3	288	265	7	9	3	277	256	4	0	4	307	320	0	3	4	90	95
0	4	3	88	93	9	6	3	363	357	8	9	3	242	224	6	0	4	627	629	1	3	4	485	483
1	4	3	353	356	10	6	3	123	122	9	9	3	247	238	7	0	4	444	450	2	3	4	805	826
2	4	3	804	813	11	6	3	111	111	0	10	3	467	462	8	0	4	547	539	3	3	4	337	358
3	4	3	227	224	0	7	3	117	122	1	10	3	147	132	9	0	4	96	79	4	3	4	476	512
4	4	3	555	546	1	7	3	312	311	2	10	3	403	390	10	0	4	96	82	5	3	4	950	932
5	4	3	455	487	2	7	3	428	414	3	10	3	406	375	11	0	4	234	231	6	3	4	261	286
6	4	3	340	342	3	7	3	434	449	4	10	3	343	321	12	0	4	151	153	7	3	4	414	396
7	4	3	227	238	4	7	3	248	246	5	10	3	212	231	0	1	4	786	763	8	3	4	434	410

OBSERVED AND CALCULATED STRUCTURE FACTORS FOR EUCHROITE

H	K	L	10FO	10FC	H	K	L	10FO	10FC	H	K	L	10FO	10FC	H	K	L	10FO	10FC	H	K	L	10FO	10FC
9	3	4	243	270	7	6	4	125	126	9	9	4	139	129	11	0	5	70	77	9	3	5	222	227
10	3	4	233	228	8	6	4	195	205	0	10	4	209	200	0	1	5	380	381	10	3	5	131	153
11	3	4	249	233	9	6	4	409	386	1	10	4	262	243	1	1	5	739	758	11	3	5	243	229
12	3	4	225	242	10	6	4	169	171	2	10	4	422	413	2	1	5	244	259	0	4	5	268	265
0	4	4	491	498	11	6	4	459	448	3	10	4	243	249	3	1	5	141	159	1	4	5	166	175
1	4	4	1101	1155	0	7	4	60	23	4	10	4	372	360	4	1	5	427	426	2	4	5	565	547
2	4	4	290	294	1	7	4	58	82	5	10	4	308	313	5	1	5	96	86	3	4	5	248	226
3	4	4	296	301	2	7	4	584	610	6	10	4	147	156	6	1	5	283	295	5	4	5	486	511
4	4	4	129	154	3	7	4	405	434	7	10	4	172	185	7	1	5	146	140	6	4	5	193	176
5	4	4	284	293	4	7	4	493	484	8	10	4	96	82	8	1	5	328	306	7	4	5	192	191
6	4	4	574	589	5	7	4	613	628	1	11	4	81	93	9	1	5	285	292	8	4	5	274	255
7	4	4	407	418	6	7	4	168	161	2	11	4	243	224	10	1	5	129	137	9	4	5	168	151
8	4	4	535	535	7	7	4	233	236	3	11	4	438	434	11	1	5	318	314	10	4	5	102	106
9	4	4	53	75	8	7	4	281	265	4	11	4	343	343	0	2	5	92	104	0	5	5	217	220
10	4	4	120	130	9	7	4	284	275	5	11	4	319	315	1	2	5	93	97	1	5	5	388	393
11	4	4	246	255	10	7	4	233	222	6	11	4	75	51	2	2	5	635	644	2	5	5	347	343
0	5	4	725	726	0	8	4	233	211	0	12	4	103	98	3	2	5	190	201	3	5	5	102	111
1	5	4	536	501	1	8	4	693	700	1	12	4	483	464	4	2	5	103	91	4	5	5	323	327
2	5	4	445	475	2	8	4	181	191	2	12	4	168	181	5	2	5	629	636	5	5	5	157	158
3	5	4	282	269	3	8	4	190	176	3	12	4	214	198	6	2	5	125	93	6	5	5	334	340
4	5	4	201	198	4	8	4	173	152	4	12	4	132	117	7	2	5	332	335	8	5	5	363	368
5	5	4	719	721	5	8	4	251	285	5	12	4	201	185	8	2	5	477	477	9	5	5	286	281
6	5	4	406	398	6	8	4	420	422	0	13	4	319	314	9	2	5	111	80	10	5	5	124	120
7	5	4	467	463	7	8	4	247	256	1	13	4	276	268	10	2	5	202	199	0	6	5	67	58
8	5	4	311	312	8	8	4	507	506	1	0	5	147	140	11	2	5	64	97	1	6	5	244	245
9	5	4	286	290	9	8	4	178	176	2	0	5	693	702	0	3	5	243	231	2	6	5	502	517
10	5	4	116	123	0	9	4	321	321	3	0	5	75	87	1	3	5	544	552	3	6	5	225	234
0	6	4	304	319	1	9	4	261	234	4	0	5	145	150	2	3	5	307	305	4	6	5	247	249
1	6	4	392	396	2	9	4	357	366	5	0	5	465	465	3	3	5	104	101	5	6	5	520	531
2	6	4	682	679	3	9	4	115	128	6	0	5	249	240	4	3	5	565	566	6	6	5	88	78
3	6	4	487	493	5	9	4	470	496	7	0	5	231	220	5	3	5	78	73	7	6	5	298	296
4	6	4	692	733	6	9	4	313	307	8	0	5	300	297	6	3	5	94	131	8	6	5	247	232
5	6	4	318	320	7	9	4	427	410	9	0	5	274	287	7	3	5	146	115	9	6	5	124	98
6	6	4	219	226	8	9	4	317	326	10	0	5	111	117	8	3	5	331	312	10	6	5	257	259

OBSERVED AND CALCULATED STRUCTURE FACTORS FOR EUCHROITE

H	K	L	10FO	10FC	H	K	L	10FO	10FC	H	K	L	10FO	10FC	H	K	L	10FO	10FC	H	K	L	10FO	10FC
1	7	5	533	543	3	11	5	219	231	9	2	6	181	180	5	6	6	161	151	8	0	7	181	166
2	7	5	281	286	4	11	5	219	199	0	3	6	453	457	6	6	6	255	252	0	1	7	465	464
3	7	5	234	240	0	12	5	300	291	1	3	6	427	447	7	6	6	385	374	1	1	7	277	280
4	7	5	438	452	0	0	6	395	386	2	3	6	387	404	8	6	6	315	309	2	1	7	73	72
5	7	5	82	121	1	0	6	153	141	3	3	6	253	258	0	7	6	605	618	4	1	7	275	299
6	7	5	196	197	2	0	6	526	548	4	3	6	336	359	1	7	6	270	254	6	1	7	154	159
7	7	5	179	181	3	0	6	744	771	5	3	6	365	376	2	7	6	392	411	8	1	7	155	153
8	7	5	261	240	4	0	6	474	480	6	3	6	442	437	3	7	6	177	187	0	2	7	84	59
9	7	5	198	198	5	0	6	476	487	7	3	6	104	110	4	7	6	210	214	1	2	7	90	90
0	8	5	144	140	6	0	6	119	117	8	3	6	335	323	5	7	6	265	264	2	2	7	247	237
1	8	5	124	108	7	0	6	142	144	9	3	6	256	225	6	7	6	299	301	3	2	7	190	188
2	8	5	280	293	8	0	6	235	236	0	4	6	349	350	7	7	6	184	169	4	2	7	380	376
3	8	5	339	340	9	0	6	210	195	1	4	6	66	59	0	8	6	175	180	5	2	7	212	207
4	8	5	103	97	10	0	6	59	32	2	4	6	439	426	1	8	6	72	87	6	2	7	388	391
5	8	5	431	431	0	1	6	189	194	3	4	6	608	627	2	8	6	363	363	7	2	7	138	124
6	8	5	174	183	1	1	6	404	418	4	4	6	293	293	3	8	6	413	414	8	2	7	149	130
7	8	5	157	149	2	1	6	542	532	5	4	6	353	391	4	8	6	227	232	0	3	7	454	455
8	8	5	213	196	3	1	6	163	185	6	4	6	189	206	5	8	6	208	198	1	3	7	168	185
0	9	5	160	137	4	1	6	408	403	7	4	6	103	67	6	8	6	152	137	3	3	7	88	84
1	9	5	214	209	5	1	6	429	439	8	4	6	154	150	1	9	6	163	170	4	3	7	318	334
2	9	5	107	128	6	1	6	241	254	9	4	6	214	211	2	9	6	299	307	5	3	7	158	141
3	9	5	118	109	7	1	6	134	112	0	5	6	181	164	3	9	6	204	180	6	3	7	92	106
4	9	5	222	226	8	1	6	290	286	1	5	6	245	264	4	9	6	423	439	7	3	7	127	120
5	9	5	310	315	9	1	6	277	274	2	5	6	525	509	5	9	6	183	147	0	4	7	140	145
6	9	5	192	184	10	1	6	171	173	3	5	6	315	328	0	10	6	78	57	1	4	7	97	121
7	9	5	97	99	0	2	6	126	114	4	5	6	478	497	1	10	6	337	320	2	4	7	252	254
1	10	5	225	232	1	2	6	597	586	5	5	6	292	281	2	10	6	291	288	3	4	7	212	195
2	10	5	271	283	2	2	6	180	157	6	5	6	172	187	1	0	7	120	105	4	4	7	229	228
3	10	5	218	202	3	2	6	102	86	7	5	6	73	59	2	0	7	313	317	5	4	7	227	238
4	10	5	209	186	4	2	6	105	101	8	5	6	246	231	3	0	7	191	201	6	4	7	288	295
5	10	5	278	279	5	2	6	213	220	1	6	6	560	555	4	0	7	235	234	7	4	7	234	228
0	11	5	100	67	6	2	6	276	286	2	6	6	213	194	5	0	7	350	357	0	5	7	469	455
1	11	5	405	414	7	2	6	652	661	3	6	6	110	99	6	0	7	384	374	1	5	7	342	346
2	11	5	246	249	8	2	6	422	391	4	6	6	110	107	7	0	7	234	236	3	5	7	171	178

A.4 LIROCONITE

OBSERVED AND CALCULATED STRUCTURE FACTORS FOR LIROCONITE

H	K	L	10FO	10FC	H	K	L	10FO	10FC	H	K	L	10FO	10FC	H	K	L	10FO	10FC	H	K	L	10FO	10FC
2	4	10	324	332	-4	1	11	364	365	6	3	11	312	312	2	0	12	756	794	5	3	12	628	642
4	4	10	358	341	-2	1	11	300	302	8	3	11	166	148	4	0	12	557	564	7	3	12	556	551
6	4	10	547	545	0	1	11	909	922	-7	4	11	276	252	6	0	12	432	475	-6	4	12	432	439
8	4	10	127	128	4	1	11	346	349	-5	4	11	813	830	8	0	12	202	182	-4	4	12	229	228
10	4	10	263	262	6	1	11	116	113	-3	4	11	570	584	-7	1	12	470	510	-2	4	12	404	453
-9	5	10	375	368	8	1	11	631	641	-1	4	11	123	104	-5	1	12	519	535	0	4	12	217	192
-7	5	10	100	23	10	1	11	203	180	1	4	11	70	25	-3	1	12	454	484	2	4	12	449	440
-5	5	10	386	375	-9	2	11	379	365	3	4	11	786	782	-1	1	12	449	476	4	4	12	277	278
-3	5	10	812	789	-7	2	11	117	134	5	4	11	761	764	1	1	12	551	576	-1	5	12	130	99
-1	5	10	429	436	-5	2	11	96	58	7	4	11	184	163	3	1	12	413	423	1	5	12	638	637
1	5	10	134	108	-3	2	11	167	153	-6	5	11	262	278	5	1	12	150	146	3	5	12	510	487
3	5	10	285	291	-1	2	11	301	305	-4	5	11	303	326	7	1	12	504	526	-6	1	13	185	158
5	5	10	789	787	1	2	11	304	305	-2	5	11	123	115	-8	2	12	219	192	-4	1	13	528	513
7	5	10	567	558	3	2	11	81	75	0	5	11	461	477	-6	2	12	376	405	-2	1	13	221	189
-4	6	10	133	124	5	2	11	114	92	2	5	11	92	93	-4	2	12	581	594	0	1	13	475	475
-2	6	10	557	573	7	2	11	179	152	4	5	11	320	319	-2	2	12	859	867	2	1	13	190	188
0	6	10	122	117	9	2	11	259	250	-3	6	11	112	83	0	2	12	393	387	4	1	13	406	397
2	6	10	69	87	-10	3	11	107	50	-1	6	11	578	564	2	2	12	314	334	-5	2	13	347	355
6	6	10	431	439	-8	3	11	211	189	1	6	11	636	606	4	2	12	446	451	-3	2	13	416	441
-1	7	10	193	161	-6	3	11	258	235	3	6	11	111	130	6	2	12	662	649	1	2	13	121	117
1	7	10	425	407	-4	3	11	682	681	-8	0	12	594	582	8	2	12	572	572	3	2	13	242	227
3	7	10	200	169	-2	3	11	295	286	-6	0	12	516	526	-5	3	12	106	92	5	2	13	452	449
-10	1	11	310	277	0	3	11	187	190	-4	0	12	547	546	-3	3	12	750	765	0	3	13	570	591
-8	1	11	601	611	2	3	11	172	188	-2	0	12	585	621	-1	3	12	512	499	2	3	13	219	187
-6	1	11	87	55	4	3	11	826	826	0	0	12	732	752	1	3	12	152	155					

OBSERVED AND CALCULATED STRUCTURE FACTORS FOR LIROCONITE

H	K	L	10FO	10FC	H	K	L	10FO	10FC	H	K	L	10FO	10FC	H	K	L	10FO	10FC	H	K	L	10FO	10FC
2	0	0	721	884	17	3	0	152	174	6	8	0	420	426	-3	2	1	1145	1016	-3	4	1	1655	1675
4	0	0	314	267	0	4	0	1588	1615	8	8	0	152	106	-1	2	1	108	117	-1	4	1	760	852
6	0	0	134	60	2	4	0	305	260	10	8	0	440	444	1	2	1	1397	1362	1	4	1	71	34
8	0	0	2683	2796	4	4	0	681	672	1	9	0	223	190	3	2	1	804	857	3	4	1	285	263
10	0	0	1097	1200	6	4	0	140	166	3	9	0	91	91	5	2	1	898	872	5	4	1	1093	1133
12	0	0	195	204	8	4	0	1225	1263	5	9	0	65	53	7	2	1	401	336	7	4	1	1064	1115
14	0	0	195	171	10	4	0	206	222	7	9	0	207	205	9	2	1	608	623	9	4	1	59	52
16	0	0	981	977	12	4	0	328	344	9	9	0	127	116	11	2	1	646	689	11	4	1	153	167
1	1	0	2053	2113	14	4	0	121	139	2	10	0	405	395	13	2	1	477	479	13	4	1	351	365
3	1	0	1031	994	16	4	0	518	518	4	10	0	265	244	15	2	1	173	171	15	4	1	639	642
5	1	0	157	85	1	5	0	1107	1216	6	10	0	416	397	17	2	1	147	133	-14	5	1	438	425
7	1	0	1029	1019	3	5	0	67	43	-16	1	1	530	508	-16	3	1	207	191	-12	5	1	141	118
9	1	0	1725	1799	5	5	0	159	186	-14	1	1	244	188	-14	3	1	308	317	-10	5	1	544	538
11	1	0	234	227	7	5	0	621	618	-12	1	1	702	737	-12	3	1	542	557	-8	5	1	76	75
13	1	0	474	476	9	5	0	783	817	-10	1	1	515	545	-10	3	1	590	597	-6	5	1	888	895
15	1	0	385	391	11	5	0	96	73	-8	1	1	1452	1514	-8	3	1	425	444	-4	5	1	554	563
17	1	0	601	592	15	5	0	447	425	-6	1	1	123	137	-6	3	1	894	836	-2	5	1	700	703
0	2	0	371	339	0	6	0	502	518	-4	1	1	1391	1409	-4	3	1	948	940	0	5	1	127	121
2	2	0	255	333	2	6	0	68	35	-2	1	1	202	289	-2	3	1	1603	1600	2	5	1	536	548
4	2	0	1818	1939	4	6	0	603	611	0	1	1	1825	1949	0	3	1	457	498	4	5	1	1030	1071
6	2	0	453	506	6	6	0	161	156	2	1	1	881	960	2	3	1	1021	894	6	5	1	856	890
8	2	0	140	69	8	6	0	147	136	4	1	1	1996	1930	4	3	1	296	357	8	5	1	86	80
10	2	0	359	341	10	6	0	405	422	6	1	1	500	586	6	3	1	574	641	10	5	1	363	355
12	2	0	1318	1353	12	6	0	460	471	8	1	1	800	845	8	3	1	601	611	12	5	1	662	695
14	2	0	431	399	14	6	0	72	44	10	1	1	877	911	10	3	1	413	416	14	5	1	274	273
16	2	0	91	87	1	7	0	487	505	12	1	1	722	739	12	3	1	324	326	-13	6	1	443	427
1	3	0	1110	1030	3	7	0	771	795	14	1	1	127	133	14	3	1	201	197	-9	6	1	222	213
3	3	0	1596	1666	5	7	0	518	528	16	1	1	285	281	16	3	1	473	464	-7	6	1	983	989
5	3	0	1947	2013	7	7	0	431	436	-17	2	1	206	182	-15	4	1	76	88	-5	6	1	1151	1179
7	3	0	152	151	9	7	0	162	155	-15	2	1	505	498	-13	4	1	321	316	-3	6	1	240	238
9	3	0	454	462	11	7	0	527	525	-13	2	1	480	490	-11	4	1	723	730	-1	6	1	77	11
11	3	0	497	515	13	7	0	416	406	-11	2	1	191	183	-9	4	1	649	660	1	6	1	934	980
13	3	0	1095	1113	2	8	0	520	531	-7	2	1	799	824	-7	4	1	102	22	3	6	1	1429	1493
15	3	0	107	66	4	8	0	285	279	-5	2	1	1476	1486	-5	4	1	83	27	5	6	1	420	413

OBSERVED AND CALCULATED STRUCTURE FACTORS FOR LIROCONITE

H	K	L	10FO	10FC	H	K	L	10FO	10FC	H	K	L	10FO	10FC	H	K	L	10FO	10FC	H	K	L	10FO	10FC
7	6	1	171	165	-5	10	1	294	278	7	1	2	381	376	9	3	2	879	873	-10	6	2	348	355
9	6	1	651	676	-3	10	1	287	289	9	1	2	995	988	11	3	2	308	340	-8	6	2	319	325
11	6	1	843	868	-1	10	1	123	127	11	1	2	96	102	13	3	2	382	392	-6	6	2	182	135
13	6	1	250	243	1	10	1	289	263	13	1	2	985	1005	15	3	2	445	442	-4	6	2	192	187
-12	7	1	187	215	3	10	1	306	310	15	1	2	227	230	-16	4	2	171	167	-2	6	2	665	675
-10	7	1	172	186	5	10	1	160	189	17	1	2	456	469	-14	4	2	317	300	0	6	2	429	418
-8	7	1	143	138	-16	0	2	133	140	-16	2	2	871	867	-12	4	2	897	904	2	6	2	100	116
-6	7	1	1006	1020	-14	0	2	183	176	-14	2	2	60	39	-8	4	2	671	661	4	6	2	215	164
-4	7	1	76	58	-12	0	2	1622	1589	-12	2	2	62	49	-6	4	2	273	290	6	6	2	460	475
-2	7	1	478	481	-10	0	2	215	233	-10	2	2	225	222	-4	4	2	1481	1498	8	6	2	449	467
0	7	1	260	294	-8	0	2	535	499	-8	2	2	2269	2332	-2	4	2	293	232	10	6	2	195	194
2	7	1	1029	1073	-6	0	2	849	904	-6	2	2	336	367	0	4	2	168	165	12	6	2	110	106
4	7	1	106	80	-4	0	2	3026	3083	-4	2	2	402	296	2	4	2	197	169	14	6	2	246	254
6	7	1	396	421	-2	0	2	846	935	-2	2	2	156	46	4	4	2	2062	2099	-13	7	2	132	101
8	7	1	186	166	0	0	2	313	194	0	2	2	2955	2976	6	4	2	79	93	-11	7	2	86	91
10	7	1	839	884	2	0	2	82	60	2	2	2	2170	2026	10	4	2	492	495	-9	7	2	506	487
12	7	1	138	130	4	0	2	2155	2170	4	2	2	1300	1181	12	4	2	662	679	-7	7	2	458	444
-11	8	1	652	640	6	0	2	798	853	6	2	2	279	221	14	4	2	373	369	-5	7	2	330	309
-9	8	1	593	559	8	0	2	192	205	8	2	2	1849	1903	-15	5	2	224	206	-3	7	2	217	203
-5	8	1	233	245	10	0	2	294	325	10	2	2	985	1040	-13	5	2	685	651	-1	7	2	642	648
-3	8	1	780	798	12	0	2	1181	1227	12	2	2	83	80	-11	5	2	734	733	1	7	2	604	629
-1	8	1	870	902	14	0	2	817	808	14	2	2	433	447	-7	5	2	194	212	3	7	2	252	255
3	8	1	79	94	-17	1	2	507	517	16	2	2	840	846	-5	5	2	1411	1429	5	7	2	98	49
5	8	1	404	382	-15	1	2	113	96	-15	3	2	521	508	-3	5	2	1243	1279	7	7	2	526	533
7	8	1	903	916	-13	1	2	733	717	-11	3	2	105	81	-1	5	2	226	265	9	7	2	576	575
9	8	1	84	58	-11	1	2	836	851	-9	3	2	883	915	1	5	2	184	164	11	7	2	263	254
-8	9	1	123	111	-9	1	2	1024	1034	-7	3	2	1497	1531	3	5	2	975	1022	13	7	2	136	116
-4	9	1	180	151	-7	1	2	938	948	-5	3	2	555	522	5	5	2	1238	1322	-10	8	2	358	338
-2	9	1	1032	1028	-5	1	2	1325	1326	-3	3	2	156	144	7	5	2	315	332	-8	8	2	254	222
0	9	1	264	250	-3	1	2	1306	1382	-1	3	2	391	503	11	5	2	438	448	-6	8	2	211	189
2	9	1	90	87	-1	1	2	901	851	1	3	2	2430	2420	13	5	2	753	774	-4	8	2	104	108
4	9	1	93	97	1	1	2	1690	1562	3	3	2	213	296	15	5	2	317	301	-2	8	2	476	487
6	9	1	797	818	3	1	2	1581	1417	5	3	2	268	235	-14	6	2	83	81	0	8	2	291	288
8	9	1	394	396	5	1	2	2365	2300	7	3	2	979	1005	-12	6	2	211	212	2	8	2	430	445

OBSERVED AND CALCULATED STRUCTURE FACTORS FOR LIROCONITE

H	K	L	10FO	10FC	H	K	L	10FO	10FC	H	K	L	10FO	10FC	H	K	L	10FO	10FC	H	K	L	10FO	10FC
6	8	2	406	423	-15	2	3	78	59	-11	4	3	76	68	1	6	3	208	236	0	9	3	101	116
8	8	2	199	183	-13	2	3	138	137	-9	4	3	57	28	3	6	3	164	157	2	9	3	793	795
10	8	2	295	279	-11	2	3	506	495	-7	4	3	1303	1320	5	6	3	635	639	4	9	3	302	289
-9	9	2	208	216	-9	2	3	272	243	-5	4	3	1550	1565	7	6	3	972	982	8	9	3	139	185
-7	9	2	131	88	-7	2	3	370	370	-3	4	3	702	759	9	6	3	396	402	-3	10	3	222	205
-5	9	2	157	137	-5	2	3	62	44	-1	4	3	262	219	11	6	3	274	277	-1	10	3	589	571
-3	9	2	102	54	-3	2	3	504	533	1	4	3	1010	1105	13	6	3	378	358	3	10	3	259	270
-1	9	2	270	284	-1	2	3	263	342	3	4	3	1758	1773	-12	7	3	140	104	-16	0	4	966	923
1	9	2	261	257	1	2	3	988	812	5	4	3	763	785	-10	7	3	930	930	-14	0	4	72	77
3	9	2	180	191	3	2	3	105	48	7	4	3	156	163	-6	7	3	190	159	-12	0	4	257	251
5	9	2	99	42	5	2	3	480	468	9	4	3	263	278	-4	7	3	297	283	-10	0	4	620	654
7	9	2	103	84	7	2	3	1041	1059	11	4	3	1066	1099	-2	7	3	1146	1139	-8	0	4	1650	1689
9	9	2	252	234	9	2	3	71	60	13	4	3	449	453	0	7	3	323	304	-6	0	4	847	893
-4	10	2	121	78	13	2	3	129	137	15	4	3	107	100	2	7	3	175	177	-4	0	4	1552	1454
-2	10	2	354	329	15	2	3	404	399	-14	5	3	458	476	4	7	3	292	308	-2	0	4	278	138
0	10	2	245	222	17	2	3	114	100	-10	5	3	344	343	6	7	3	658	686	0	0	4	1998	2020
2	10	2	354	323	-16	3	3	469	439	-8	5	3	306	303	8	7	3	554	579	2	0	4	1358	1365
4	10	2	193	161	-14	3	3	559	535	-6	5	3	811	833	12	7	3	285	308	4	0	4	82	107
-16	1	3	487	456	-12	3	3	483	478	-4	5	3	63	66	-11	8	3	219	238	6	0	4	1313	1192
-12	1	3	545	548	-10	3	3	232	187	-2	5	3	428	426	-9	8	3	97	7	8	0	4	2096	2068
-10	1	3	580	624	-8	3	3	1150	1168	0	5	3	621	606	-7	8	3	465	448	10	0	4	941	912
-8	1	3	913	936	-6	3	3	912	951	2	5	3	1557	1590	-5	8	3	590	582	12	0	4	139	155
-6	1	3	238	143	-4	3	3	1228	1206	4	5	3	97	104	-3	8	3	93	57	14	0	4	706	738
-4	1	3	132	69	-2	3	3	308	264	6	5	3	419	438	-1	8	3	285	313	16	0	4	591	588
-2	1	3	1875	1747	0	3	3	1007	959	8	5	3	722	745	1	8	3	654	642	-17	1	4	424	408
0	1	3	2094	2013	2	3	3	815	851	10	5	3	669	702	3	8	3	661	650	-15	1	4	607	591
2	1	3	302	367	4	3	3	1295	1298	12	5	3	210	221	5	8	3	142	138	-13	1	4	601	605
4	1	3	272	339	6	3	3	211	241	14	5	3	293	277	7	8	3	307	336	-11	1	4	572	590
6	1	3	627	652	8	3	3	428	459	-11	6	3	732	708	9	8	3	238	240	-9	1	4	323	317
8	1	3	1006	1045	10	3	3	533	536	-9	6	3	769	741	11	8	3	594	595	-7	1	4	1204	1228
10	1	3	111	108	12	3	3	859	870	-7	6	3	57	50	-8	9	3	161	108	-5	1	4	406	402
12	1	3	548	553	16	3	3	125	105	-5	6	3	142	133	-6	9	3	680	661	-3	1	4	1737	1592
14	1	3	238	208	-15	4	3	749	725	-3	6	3	786	799	-4	9	3	382	336	-1	1	4	1115	1043
16	1	3	525	528	-13	4	3	773	765	-1	6	3	1518	1572	-2	9	3	228	244	1	1	4	921	932

OBSERVED AND CALCULATED STRUCTURE FACTORS FOR LIROCONITE

H	K	L	10FO	10FC	H	K	L	10FO	10FC	H	K	L	10FO	10FC	H	K	L	10FO	10FC	H	K	L	10FO	10FC
3	1	4	242	192	5	3	4	1703	1691	-12	6	4	322	338	-5	9	4	109	90	1	2	5	111	179
5	1	4	2073	1867	7	3	4	464	472	-10	6	4	366	375	-3	9	4	253	256	3	2	5	1416	1383
7	1	4	70	36	9	3	4	685	658	-8	6	4	362	346	-1	9	4	269	258	5	2	5	607	591
9	1	4	1002	1009	11	3	4	412	422	-6	6	4	586	584	1	9	4	270	249	7	2	5	137	130
11	1	4	92	69	13	3	4	893	917	-4	6	4	776	784	3	9	4	109	57	9	2	5	68	28
13	1	4	501	505	15	3	4	506	489	-2	6	4	415	440	5	9	4	160	140	11	2	5	260	258
15	1	4	159	194	-14	4	4	69	73	0	6	4	588	604	7	9	4	189	173	13	2	5	414	427
-16	2	4	227	229	-12	4	4	91	85	2	6	4	553	556	-2	10	4	384	356	15	2	5	99	70
-14	2	4	194	197	-10	4	4	165	166	4	6	4	475	483	0	10	4	195	149	-16	3	5	249	245
-12	2	4	1370	1359	-8	4	4	993	984	8	6	4	547	564	2	10	4	265	245	-14	3	5	110	109
-10	2	4	660	669	-6	4	4	298	316	10	6	4	402	407	-16	1	5	306	298	-12	3	5	383	375
-8	2	4	202	193	-4	4	4	109	87	12	6	4	143	152	-14	1	5	394	348	-10	3	5	498	488
-6	2	4	245	182	-2	4	4	103	72	-11	7	4	354	328	-12	1	5	546	534	-8	3	5	809	821
-4	2	4	2906	2865	0	4	4	1321	1315	-9	7	4	266	250	-10	1	5	192	191	-6	3	5	314	305
-2	2	4	1102	1161	2	4	4	550	566	-7	7	4	125	91	-8	1	5	779	813	-4	3	5	323	321
0	2	4	327	172	4	4	4	72	62	-5	7	4	338	321	-6	1	5	808	850	-2	3	5	547	544
2	2	4	157	81	6	4	4	688	672	-3	7	4	555	554	-4	1	5	966	1008	0	3	5	1717	1674
4	2	4	2357	2250	8	4	4	853	866	-1	7	4	64	47	-2	1	5	147	187	2	3	5	66	66
6	2	4	1298	1303	10	4	4	527	534	1	7	4	215	222	0	1	5	1677	1585	4	3	5	197	192
8	2	4	181	30	14	4	4	202	210	3	7	4	305	292	2	1	5	365	420	6	3	5	716	693
10	2	4	123	109	-15	5	4	610	575	5	7	4	580	588	4	1	5	851	829	8	3	5	1064	1078
12	2	4	1052	1077	-13	5	4	123	96	7	7	4	154	153	6	1	5	227	146	10	3	5	82	55
14	2	4	605	597	-11	5	4	238	228	9	7	4	133	117	8	1	5	1113	1116	12	3	5	82	13
16	2	4	245	244	-9	5	4	701	706	11	7	4	267	249	10	1	5	385	394	14	3	5	320	285
-15	3	4	120	51	-7	5	4	1111	1128	-10	8	4	227	217	12	1	5	711	703	-15	4	5	137	96
-13	3	4	766	785	-5	5	4	426	431	-6	8	4	243	247	14	1	5	113	86	-13	4	5	124	104
-11	3	4	768	755	-1	5	4	953	970	-4	8	4	87	96	16	1	5	300	283	-11	4	5	501	482
-9	3	4	164	147	1	5	4	1156	1174	-2	8	4	377	385	-15	2	5	413	390	-9	4	5	973	987
-7	3	4	518	503	3	5	4	852	888	0	8	4	110	113	-13	2	5	543	546	-7	4	5	162	191
-5	3	4	1507	1510	5	5	4	140	158	2	8	4	294	297	-9	2	5	68	63	-5	4	5	293	308
-3	3	4	1977	1978	7	5	4	675	689	4	8	4	68	48	-7	2	5	341	337	-3	4	5	642	660
-1	3	4	158	211	9	5	4	983	997	6	8	4	282	273	-5	2	5	1011	1013	-1	4	5	1316	1333
1	3	4	776	730	11	5	4	377	368	10	8	4	245	239	-3	2	5	168	121	1	4	5	590	593
3	3	4	1026	1031	13	5	4	149	120	-7	9	4	144	125	-1	2	5	166	108	5	4	5	827	840

OBSERVED AND CALCULATED STRUCTURE FACTORS FOR LIROCONITE

H	K	L	10FO	10FC	H	K	L	10FO	10FC	H	K	L	10FO	10FC	H	K	L	10FO	10FC	H	K	L	10FO	10FC
7	4	5	1102	1108	-8	7	5	194	212	4	0	6	1967	1933	10	2	6	1077	1048	-9	5	6	106	60
9	4	5	618	614	-6	7	5	742	723	6	0	6	1354	1328	12	2	6	175	165	-5	5	6	554	542
11	4	5	73	64	-4	7	5	194	175	8	0	6	410	423	14	2	6	308	314	-3	5	6	1144	1150
13	4	5	308	301	0	7	5	360	361	10	0	6	552	522	-15	3	6	658	623	-1	5	6	382	415
15	4	5	641	634	2	7	5	813	815	12	0	6	937	936	-13	3	6	120	93	1	5	6	166	155
-14	5	5	322	310	4	7	5	507	531	14	0	6	757	755	-11	3	6	500	517	3	5	6	628	619
-12	5	5	423	415	6	7	5	185	184	-15	1	6	386	379	-9	3	6	781	789	5	5	6	985	980
-10	5	5	810	827	8	7	5	301	323	-13	1	6	575	568	-7	3	6	1105	1122	7	5	6	459	449
-6	5	5	644	652	10	7	5	438	424	-11	1	6	898	917	-5	3	6	744	744	9	5	6	164	168
-4	5	5	428	423	-9	8	5	625	619	-9	1	6	185	141	-3	3	6	610	572	11	5	6	240	226
-2	5	5	879	873	-7	8	5	68	17	-7	1	6	590	538	-1	3	6	309	332	13	5	6	649	645
0	5	5	471	479	-5	8	5	284	315	-5	1	6	619	621	1	3	6	1525	1502	-12	6	6	224	206
2	5	5	680	682	-3	8	5	462	436	-3	1	6	1845	1817	3	3	6	331	343	-10	6	6	221	204
4	5	5	741	734	-1	8	5	803	799	-1	1	6	58	16	7	3	6	69	45	-8	6	6	374	369
6	5	5	436	437	1	8	5	402	407	1	1	6	1454	1383	9	3	6	1180	1173	-6	6	6	105	70
8	5	5	348	358	3	8	5	467	464	3	1	6	312	314	11	3	6	441	447	-4	6	6	88	91
10	5	5	65	53	5	8	5	207	188	5	1	6	1561	1519	13	3	6	87	91	-2	6	6	308	286
12	5	5	485	489	7	8	5	668	668	7	1	6	600	600	15	3	6	90	75	0	6	6	314	310
14	5	5	164	161	9	8	5	308	306	9	1	6	717	699	-14	4	6	184	212	2	6	6	104	42
-13	6	5	561	544	-6	9	5	172	172	11	1	6	192	190	-12	4	6	695	693	6	6	6	274	278
-11	6	5	166	114	-2	9	5	683	680	13	1	6	803	814	-10	4	6	197	187	8	6	6	156	169
-9	6	5	278	286	0	9	5	417	408	15	1	6	290	284	-8	4	6	151	142	-11	7	6	247	210
-7	6	5	840	825	2	9	5	89	5	-14	2	6	316	276	-6	4	6	230	229	-9	7	6	424	415
-5	6	5	1062	1098	4	9	5	177	183	-12	2	6	340	356	-4	4	6	911	923	-7	7	6	504	488
-3	6	5	429	417	6	9	5	673	657	-10	2	6	143	110	-2	4	6	819	804	-5	7	6	196	207
-1	6	5	275	260	-16	0	6	64	17	-8	2	6	1533	1573	0	4	6	691	700	-3	7	6	208	200
1	6	5	452	433	-12	0	6	1456	1502	-6	2	6	403	423	2	4	6	647	640	-1	7	6	588	578
3	6	5	1161	1170	-10	0	6	820	838	-4	2	6	132	114	4	4	6	911	930	1	7	6	702	684
5	6	5	365	365	-8	0	6	153	187	-2	2	6	593	555	6	4	6	728	737	3	7	6	374	366
7	6	5	135	124	-6	0	6	678	679	0	2	6	2298	2226	10	4	6	568	598	5	7	6	160	130
9	6	5	236	215	-4	0	6	2061	2074	2	2	6	795	800	12	4	6	593	601	7	7	6	375	362
11	6	5	745	742	-2	0	6	2090	2092	4	2	6	238	202	14	4	6	311	292	9	7	6	401	400
13	6	5	470	455	0	0	6	614	682	6	2	6	555	484	-13	5	6	449	436	-8	8	6	213	206
-10	7	5	86	82	2	0	6	571	523	8	2	6	1022	1001	-11	5	6	599	584	-6	8	6	408	390

OBSERVED AND CALCULATED STRUCTURE FACTORS FOR LIROCONITE

H	K	L	10FO	10FC	H	K	L	10FO	10FC	H	K	L	10FO	10FC	H	K	L	10FO	10FC	H	K	L	10FO	10FC
-4	8	6	90	35	-1	2	7	729	726	-8	5	7	388	393	5	8	7	354	341	-12	2	8	801	803
-2	8	6	317	288	1	2	7	834	824	-6	5	7	318	299	7	8	7	130	150	-10	2	8	609	627
0	8	6	276	254	5	2	7	434	433	-2	5	7	463	458	-2	9	7	163	135	-8	2	8	70	61
2	8	6	403	400	7	2	7	555	556	0	5	7	685	675	2	9	7	549	514	-6	2	8	377	373
4	8	6	94	88	9	2	7	415	420	2	5	7	159	168	-14	0	8	376	354	-4	2	8	1041	1011
6	8	6	308	300	11	2	7	130	132	4	5	7	166	170	-12	0	8	136	80	-2	2	8	1061	1076
8	8	6	233	231	13	2	7	212	197	6	5	7	63	36	-10	0	8	292	304	0	2	8	466	460
-5	9	6	85	53	-14	3	7	290	269	8	5	7	717	750	-8	0	8	1754	1773	2	2	8	874	822
-3	9	6	138	99	-12	3	7	413	399	10	5	7	254	258	-6	0	8	1018	1070	4	2	8	905	878
-1	9	6	193	158	-10	3	7	253	291	-11	6	7	479	468	-4	0	8	99	110	6	2	8	956	960
1	9	6	144	131	-8	3	7	116	110	-9	6	7	807	817	-2	0	8	93	24	8	2	8	403	396
3	9	6	231	214	-6	3	7	478	472	-7	6	7	411	400	0	0	8	1713	1695	10	2	8	459	475
5	9	6	97	61	-4	3	7	985	1011	-5	6	7	177	213	2	0	8	1763	1746	12	2	8	366	348
-12	1	7	739	719	-2	3	7	446	415	-3	6	7	443	424	4	0	8	166	155	-13	3	8	331	317
-10	1	7	489	492	2	3	7	322	307	-1	6	7	1002	989	6	0	8	237	184	-11	3	8	859	854
-8	1	7	1018	1026	4	3	7	959	947	1	6	7	532	541	8	0	8	1068	1067	-9	3	8	95	82
-6	1	7	102	136	6	3	7	353	358	5	6	7	147	152	10	0	8	1219	1214	-7	3	8	264	265
-4	1	7	925	931	10	3	7	203	171	7	6	7	994	999	12	0	8	551	539	-5	3	8	409	405
-2	1	7	410	423	12	3	7	584	576	9	6	7	486	495	14	0	8	311	352	-3	3	8	1147	1155
0	1	7	1266	1239	-13	4	7	598	576	11	6	7	84	13	-13	1	8	110	98	-1	3	8	380	394
2	1	7	599	648	-11	4	7	90	77	-10	7	7	539	517	-11	1	8	530	528	1	3	8	479	441
4	1	7	647	658	-9	4	7	245	251	-8	7	7	451	430	-9	1	8	162	176	3	3	8	286	273
6	1	7	512	504	-7	4	7	297	308	-6	7	7	253	268	-7	1	8	1313	1305	5	3	8	1300	1306
8	1	7	1026	1001	-5	4	7	1102	1078	-4	7	7	449	449	-5	1	8	95	81	7	3	8	619	588
10	1	7	554	542	-3	4	7	434	435	-2	7	7	810	827	-3	1	8	555	569	9	3	8	325	342
12	1	7	301	298	-1	4	7	424	442	0	7	7	513	510	-1	1	8	251	222	11	3	8	74	72
14	1	7	168	146	1	4	7	283	308	4	7	7	664	703	1	1	8	1559	1555	13	3	8	585	580
-15	2	7	141	150	3	4	7	961	959	6	7	7	516	504	3	1	8	766	788	-12	4	8	121	118
-13	2	7	178	161	5	4	7	801	807	8	7	7	457	456	5	1	8	576	569	-10	4	8	357	365
-11	2	7	255	258	7	4	7	298	293	-7	8	7	255	211	7	1	8	72	29	-8	4	8	826	838
-9	2	7	493	478	11	4	7	522	516	-5	8	7	828	804	9	1	8	650	632	-6	4	8	368	357
-7	2	7	452	467	13	4	7	482	475	-3	8	7	173	161	11	1	8	663	673	-4	4	8	185	185
-5	2	7	171	160	-12	5	7	79	68	1	8	7	162	149	13	1	8	297	304	-2	4	8	607	615
-3	2	7	842	883	-10	5	7	282	268	3	8	7	752	732	-14	2	8	79	119	0	4	8	839	857

OBSERVED AND CALCULATED STRUCTURE FACTORS FOR LIROCONITE

H	K	L	10FO	10FC	H	K	L	10FO	10FC	H	K	L	10FO	10FC	H	K	L	10FO	10FC	H	K	L	10FO	10FC
2	4	8	603	616	-6	8	8	243	231	-8	3	9	699	707	-3	6	9	617	612	3	1	10	390	407
4	4	8	111	122	-4	8	8	222	193	-6	3	9	123	93	-1	6	9	155	149	5	1	10	657	650
6	4	8	461	465	-2	8	8	390	366	-4	3	9	187	194	1	6	9	265	254	7	1	10	542	537
8	4	8	524	512	0	8	8	92	66	-2	3	9	353	352	3	6	9	831	807	9	1	10	470	477
10	4	8	245	239	2	8	8	352	352	0	3	9	883	860	5	6	9	685	673	11	1	10	272	294
12	4	8	200	191	4	8	8	281	270	2	3	9	150	126	-6	7	9	457	461	-10	2	10	140	185
-11	5	8	95	131	-12	1	9	530	523	4	3	9	235	245	-4	7	9	374	358	-8	2	10	745	754
-9	5	8	325	310	-10	1	9	337	316	6	3	9	122	102	-2	7	9	72	59	-6	2	10	1039	1058
-7	5	8	873	895	-8	1	9	409	380	8	3	9	768	761	0	7	9	358	387	-4	2	10	144	146
-5	5	8	367	377	-6	1	9	201	185	10	3	9	140	118	2	7	9	490	484	-2	2	10	418	431
-1	5	8	248	230	-4	1	9	720	724	12	3	9	83	48	4	7	9	328	313	0	2	10	942	957
1	5	8	856	848	-2	1	9	556	581	-11	4	9	342	315	6	7	9	226	243	2	2	10	1021	1026
3	5	8	516	496	0	1	9	554	546	-9	4	9	588	595	-1	8	9	690	665	4	2	10	485	486
5	5	8	68	89	2	1	9	465	495	-7	4	9	535	518	1	8	9	376	357	6	2	10	612	633
7	5	8	308	287	4	1	9	817	824	-5	4	9	110	62	-12	0	10	703	697	8	2	10	718	725
9	5	8	505	506	6	1	9	306	277	-3	4	9	253	248	-10	0	10	760	744	10	2	10	699	683
11	5	8	475	461	8	1	9	442	437	-1	4	9	898	925	-8	0	10	87	73	-11	3	10	161	204
-10	6	8	81	7	10	1	9	261	244	1	4	9	486	480	-6	0	10	475	507	-9	3	10	85	48
-8	6	8	117	116	12	1	9	592	596	3	4	9	149	156	-4	0	10	863	852	-7	3	10	864	857
-6	6	8	168	172	-13	2	9	278	271	5	4	9	103	71	-2	0	10	901	881	-5	3	10	692	689
-4	6	8	368	383	-11	2	9	173	158	7	4	9	652	645	0	0	10	439	444	-3	3	10	386	404
-2	6	8	114	82	-9	2	9	142	140	9	4	9	491	488	2	0	10	548	544	-1	3	10	249	244
2	6	8	547	558	-7	2	9	357	343	11	4	9	79	55	4	0	10	561	565	1	3	10	734	726
4	6	8	530	531	-5	2	9	629	642	-10	5	9	419	431	6	0	10	939	943	3	3	10	942	940
6	6	8	142	112	-3	2	9	480	461	-8	5	9	70	87	8	0	10	665	677	5	3	10	239	247
10	6	8	390	405	-1	2	9	192	205	-6	5	9	65	76	10	0	10	334	389	7	3	10	98	86
-7	7	8	121	93	1	2	9	87	75	-4	5	9	946	955	12	0	10	292	270	9	3	10	548	539
-5	7	8	505	481	3	2	9	684	675	-2	5	9	411	423	-11	1	10	460	464	11	3	10	482	472
-3	7	8	499	473	5	2	9	458	465	0	5	9	394	400	-9	1	10	154	136	-10	4	10	159	144
-1	7	8	520	501	7	2	9	226	216	4	5	9	825	834	-7	1	10	714	751	-8	4	10	98	69
1	7	8	170	156	9	2	9	95	100	6	5	9	96	29	-5	1	10	92	96	-6	4	10	390	393
3	7	8	355	327	11	2	9	455	439	8	5	9	333	349	-3	1	10	880	888	-4	4	10	792	798
5	7	8	517	503	-12	3	9	160	135	-7	6	9	212	179	-1	1	10	365	380	-2	4	10	398	408
7	7	8	318	297	-10	3	9	458	454	-5	6	9	772	765	1	1	10	619	647	0	4	10	222	221

Appendix B

DLS PROGRAM OUTPUT

The program output is listed in full for only the first refinement (idealized olivenite). The rest of the output is abbreviated to include: starting and final atomic parameters; starting and final cell dimensions; number of l.s. cycles; the final R-index; and interatomic distances within the asymmetric unit.

B.1 THE OLIVENITE GROUP

```
***   OLIVENITE, IDEALIZED   ***

 0   6   0   0

 8   7              0.0       0.0       0.0

45  21  24

  2.0840    2.8470    1.6800    2.7430    2.0200    2.8800    3.4000    3.2500
  0.0       0.0       0.0       0.0       0.0       0.0       0.0       0.0

  0.8000    0.3000    1.0000    0.3000    0.0800    0.0400    0.0400    0.0400
  0.0       0.0       0.0       0.0       0.0       0.0       0.0       0.0

  0.0       0.0       0.0       0.0       0.0       0.0       0.0       0.0
  0.0       0.0       0.0       0.0       0.0       0.0       0.0       0.0

      0         0         0         0         0         0         0         0
      0         0         0         0         0         0         0         0

  8.6150    8.2400    5.9530              0.0       0.0       0.0

     22        23        24                   0         0         0

ORIGINAL COORDINATES,INDEX OF ATOM AND INDICES OF VARIABLES

CU 1                  0.118000 0.637600-0.017200         1         1   0     2   0     3
CU 2                  0.500000 0.500000 0.250000         2         0   0     0   0     0
AS                    0.248800 0.252800-0.010300         3         4   0     5   0     6
O(1)                  0.105000 0.388000-0.080000         4         7   0     8   0     9
O(2)                  0.420000 0.368000 0.006000         5        10   0    11   0    12
O(3)                  0.803000 0.634000 0.475000         6        13   0    14   0    15
O(4)                  0.271000 0.652000 0.260000         7        16   0    17   0    18
O(5)                  0.746000 0.364000 0.243000         8        19   0    20   0    21
01A                  -0.105000 0.602000 0.080000         9        -7   0    -8   0    -9
02A                   0.580000 0.632000-0.006000        10       -10   0   -11   0   -12
03A                   0.397000 0.368000 0.525000        11       -13   0   -14   0   -15
03B                   0.103000 0.868000-0.025000        12        13   0   -14   0    15
04A                   0.223000 0 156000 0.240000        13       -16   0    17   0   -18
05A                   0.246000 0 136000-0.217000        14        19   0   -20   0    21


05B                   0.254000 0.636000-0.283000        15       -19   0   -20   0   -21

IDENTIFICATIONS AND INDICES OF ATOMS, PRESCRIBED DISTANCE AND WEIGHT

CU 1      03B          1        12          2.0200    0.0800
CU 1      05B          1        15          2.0200    0.0800
CU 1      01A          1         9          2.0200    0.0800
CU 1      O(1)         1         4          2.0200    0.0800
CU 1      O(4)         1         7          2.0200    0.0800
CU 2      O(2)         2         5          2.0840    0.8000
CU 2      O(3)         2         6          2.0840    0.8000
CU 2      02A          2        10          2.0840    0.8000
CU 2      O(4)         2         7          2.0840    0.8000
CU 2      O(5)         2         8          2.0840    0.8000
CU 2      03A          2        11          2.0840    0.8000
AS        05A          3        14          1.6800    1.0000
AS        O(1)         3         4          1.6800    1.0000
AS        O(2)         3         5          1.6800    1.0000
AS        04A          3        13          1.6800    1.0000
05A       O(1)        14         4          2.7430    0.3000
05A       O(2)        14         5          2.7430    0.3000
05A       04A         14        13          2.7430    0.3000
O(1)      04A          4        13          2.7430    0.3000
O(1)      O(2)         4         5          2.7430    0.3000
04A       O(2)        13         5          2.7430    0.3000
03B       05B         12        15          2.8800    0.0400
03B       01A         12         9          2.8800    0.0400
CU 1      AS           1         3          3.2500    0.0400
03B       O(4)        12         7          2.7430    0.3000
05B       01A         15         9          2.8800    0.0400
05B       O(1)        15         4          2.8800    0.0400
05B       O(4)        15         7          2.8800    0.0400
01A       O(1)         9         4          2.7430    0.3000
01A       O(4)         9         7          2.8800    0.0400
O(1)      O(4)         4         7          2.8800    0.0400
O(2)      02A          5        10          2.9470    0.3000
O(2)      03A          5        11          2.8470    0.3000
O(2)      O(4)         5         7          2.9470    0.3000
O(2)      O(5)         5         8          2.9470    0.3000
O(3)      02A          6        10          2.9470    0.3000
O(3)      O(4)         6         7          2.8470    0.3000
O(3)      O(5)         6         8          2.8470    0.3000
02A       O(4)        10         7          2.9470    0.3000
02A       O(5)        10         8          2.8470    0.3000
O(3)      03A          6        11          2.9470    0.3000
O(4)      03A          7        11          2.8470    0.3000
O(5)      03A          8        11          2.8470    0.3000
CU 1      CU 2         1         2          3.4000    0.0400
CU 2      AS           2         3          3.2500    0.0400

 AGREEMENT FACTORS BEFORE CYCLE    1

 SQRT(SUM((W*(BL-D))**2)/(NEREQ-NU))                              0.1087E+00
 ESTIMATED SQRT(SUM((W*(BL-D))**2)/(NEREQ-NU)) AFTER INVERSION    0.1510E-01

 AGREEMENT FACTORS BEFORE CYCLE    2
```

AGREEMENT FACTORS BEFORE CYCLE 3

SQRT[SUM[(W*(BL-D))**2]/(NEREQ-NU)] 0.1384E-01

ESTIMATED SQRT[SUM[(W*(BL-D))**2]/(NEREQ-NU)] AFTER INVERSION 0.1354E-01

AGREEMENT FACTORS BEFORE CYCLE 4

SQRT[SUM[(W*(BL-D))**2]/(NEREQ-NU)] 0.1364E-01

ESTIMATED SQRT[SUM[(W*(BL-D))**2]/(NEREQ-NU)] AFTER INVERSION 0.1353E-01

AGREEMENT FACTORS BEFORE CYCLE 5

SQRT[SUM[(W*(BL-D))**2]/(NEREQ-NU)] 0.1353E-01

ESTIMATED SQRT[SUM[(W*(BL-D))**2]/(NEREQ-NU)] AFTER INVERSION 0.1353E-01

INTERATOMIC DISTANCES AND RESIDUALS BEFORE CYCLE 6

CU 1	O3B	2.0235	-0.0003
CU 1	O6B	1.8301	0.0152
CU 1	O1A	1.7882	0.0178
CU 1	O(1)	1.9719	0.0038
CU 1	O(4)	1.8408	0.0143
CU 2	O(2)	2.0782	0.0052
CU 2	O(3)	2.0876	-0.0032
CU 2	O2A	2.0788	0.0047
CU 2	O(4)	2.0874	-0.0031
CU 2	O(5)	2.0846	-0.0005
CU 2	O3A	2.0841	-0.0001
AS	O5A	1.6808	-0.0008
AS	O(1)	1.6808	-0.0008
AS	O(2)	1.6807	-0.0007
AS	O4A	1.6807	-0.0007
O5A	O(1)	2.7262	0.0050
O5A	O(2)	2.7428	0.0000
O5A	O4A	2.8045	-0.0184
O(1)	O4A	2.7248	0.0048
O(1)	O(2)	2.7168	0.0072
O4A	O(2)	2.7450	-0.0006
O3B	O5B	2.8067	0.0021
O3B	O1A	1.8819	0.0347
CU 1	AS	3.1186	0.0053
O3B	O(4)	2.7824	-0.0116
O5B	O1A	3.1676	-0.0123
O5B	O(1)	2.8377	-0.0031
O5B	O(4)	3.0438	-0.0074
O1A	O(1)	2.7276	0.0046

O1A	O(4)	3.1557	-0.0116
O(1)	O(4)	2.8426	-0.0033
O(2)	O2A	2.8546	-0.0023
O(2)	O3A	2.8213	0.0077
O(2)	O(4)	2.8803	-0.0100
O(2)	O(5)	2.8765	-0.0088
O(3)	O2A	2.8271	0.0060
O(3)	O(4)	2.8312	0.0047
O(3)	O(5)	2.8026	0.0133
O2A	O(4)	2.8580	-0.0026
O2A	O(5)	2.8615	-0.0103
O(3)	O3A	2.8753	-0.0085
O(4)	O3A	2.8224	0.0074
O(5)	O3A	2.8241	0.0058
CU 1	CU 2	3.3447	0.0022
CU 2	AS	3.3621	-0.0046

AGREEMENT FACTORS BEFORE CYCLE 6

SQRT[SUM[(W*(BL-D))**2]/(NEREQ-NU)] 0.1353E-01

ESTIMATED SQRT[SUM[(W*(BL-D))**2]/(NEREQ-NU)] AFTER INVERSION 0.1353E-01

COORDINATES AFTER CYCLE 6

*** OLIVENITE, IDEALIZED ***

ATOM	X(OLD)	DX	X(NEW)	Y(OLD)	DY	Y(NEW)	Z(OLD)	DZ	Z(NEW)
CU 1	0.1350	0.0000	0.1350	0.5805	-0.0000	0.5805	-0.0027	0.0000	-0.0027
CU 2	0.5000	0.0	0.5000	0.5000	0.0	0.5000	0.2500	0.0	0.2500
AS	0.2462	-0.0000	0.2462	0.2218	0.0000	0.2218	0.0010	0.0000	0.0010
O(1)	0.0828	-0.0000	0.0828	0.3528	-0.0000	0.3528	-0.0005	0.0000	-0.0005
O(2)	0.4234	-0.0000	0.4234	0.3241	0.0000	0.3241	0.0001	-0.0000	0.0001
O(3)	0.5785	0.0000	0.5785	0.6880	-0.0000	0.6880	0.5004	-0.0000	0.5004
O(4)	0.2628	0.0000	0.2628	0.6088	0.0000	0.6088	0.2583	-0.0000	0.2583
O(5)	0.7377	-0.0000	0.7377	0.3832	-0.0000	0.3832	0.2622	-0.0000	0.2622

CELL PARAMETERS AFTER CYCLE 6

1 = OLD, 2 = CHANGE, 3 = NEW

	A	B	C	COSA	COSB	COSC
1	7.8713	8.1087	5.8483	0.0	0.0	0.0
2	-0.0002	0.0002	0.0000	0.0	0.0	0.0
3	7.8711	8.1089	5.8483	0.0	0.0	0.0

BETA # 89.881 DEGREES

CU 1	05B	1.8301	0.0152
CU 1	01A	1.7962	0.0178
CU 1	O[1]	1.8718	0.0038
CU 1	O[4]	1.8409	0.0143
CU 2	O[2]	2.0782	0.0052
CU 2	O[3]	2.0876	-0.0032
CU 2	02A	2.0786	0.0047
CU 2	O[4]	2.0874	-0.0030
CU 2	O[5]	2.0848	-0.0005
CU 2	03A	2.0841	-0.0001
AS	05A	1.6406	-0.0008
AS	O[1]	1.6808	-0.0008
AS	O[2]	1.6807	-0.0007
AS	04A	1.6807	-0.0007
05A	O[1]	2.7262	0.0050
05A	O[2]	2.7429	0.0000
05A	04A	2.6045	-0.0184
O[1]	04A	2.7255	0.0049
O[1]	O[2]	2.7189	0.0072
04A	O[2]	2.7450	-0.0006
03B	05B	2.8067	0.0021
03B	01A	1.8816	0.0347
CU 1	AS	3.1184	0.0053
03B	O[4]	2.7824	-0.0118
05B	01A	3.1674	-0.0123
05B	O[1]	2.9379	-0.0031
05B	O[4]	3.0439	-0.0074
01A	O[1]	2.7275	0.0046
01A	O[4]	3.1556	-0.0118
O[1]	O[4]	2.9428	-0.0033
O[2]	02A	2.8546	-0.0023
O[2]	03A	2.8213	0.0077
O[2]	O[4]	2.8803	-0.0100
O[2]	O[5]	2.9765	-0.0088
O[3]	02A	2.8271	0.0060
O[3]	O[4]	2.9312	0.0047
O[3]	O[5]	2.9028	0.0133
02A	O[4]	2.9580	-0.0035
02A	O[5]	2.9815	-0.0103
O[3]	03A	2.8753	-0.0085
O[4]	03A	2.8224	0.0074
O[5]	03A	2.8241	0.0088
CU 1	CU 2	3.3446	0.0022
CU 2	AS	3.3621	-0.0045

AGREEMENT FACTORS BEFORE CYCLE 7

SORT(SUM((W*(BL-D))**2)/(NEREQ-NU)) 0.1353E-01

ESTIMATED SORT(SUM((W*(BL-D))**2)/(NEREQ-NU)) AFTER INVERSION 0.0

Libethonite Idealized

	Starting Atomic Parameters			Final Atomic Parameters		
	x	y	z	x	y	z
Cu(1)	0.5000	0.5000	0.2507	0.5000	0.5000	0.2449
Cu(2)	0.8617	0.3753	0.0000	0.8945	0.3496	0.0000
P	0.7673	0.7516	0.0000	0.7432	0.7369	0.0000
O(1)	0.3406	0.2607	0.2112	0.3614	0.2766	0.2241
O(2)	0.8671	0.9111	0.0000	0.8393	0.9057	0.0000
O(3)	0.8979	0.6162	0.0000	0.8789	0.5963	0.0000
OH	0.3762	0.6029	0.0000	0.3333	0.5987	0.0000

Unit Cell Data

Starting Cell(Å)	a: 8.062	b: 8.384	c: 5.881
Final Cell (Å)	a: 7.774	b: 7.974	c: 5.815

Final Interatomic Distances
Within the Asymmetric Unit

CU 2	O(3)	1.9710	0.0026
CU 2	O1D	1.8074	0.0076
CU 2	O1A	1.8113	0.0073
CU 2	O3A	1.8140	0.0151
CU 2	O4A	1.8181	0.0148
P	O(2)	1.5384	-0.0030
P	O(3)	1.5385	-0.0031
P	O1B	1.5389	-0.0036
P	O1C	1.5389	-0.0036
CU 1	O(1)	2.0853	-0.0011
CU 1	O(4)	2.0801	0.0035
CU 1	O1B	2.0852	-0.0011
CU 1	O2A	2.0803	0.0034
CU 1	O2B	2.0803	0.0034
CU 1	O4A	2.0801	0.0035
CU 1	CU 2	3.5678	-0.0035
CU 1	P	3.0284	0.0088
CU 2	P	3.3048	-0.0022
O1A	O1D	3.2046	-0.0182
O1A	O3A	2.9525	-0.0061
O1A	O4A	2.8228	0.0071
O(3)	O1D	3.3782	-0.0232
O(3)	O3A	2.4288	0.0148
O(3)	O4A	2.2666	0.0213
O1D	O3A	2.9500	-0.0060
O1D	O4A	2.8189	0.0072
O3A	O4A	3.5326	-0.0283
O(1)	O2A	3.0037	-0.0170
O(1)	O2B	3.0078	-0.0183
O(1)	O(4)	2.8882	0.0176
O(1)	O4A	2.8844	0.0188
O1B	O2A	3.0079	-0.0183
O2B	O1B	3.0037	-0.0170
O1B	O(4)	2.8844	0.0188
O1B	O4A	2.8882	0.0176
O(4)	O2A	2.9082	0.0116
O(4)	O4A	3.0327	-0.0257
O2A	O2B	2.8162	0.0082
O2B	O4A	2.9082	0.0116
O(3)	O(2)	2.4864	0.0074
O(2)	O1B	2.4993	0.0035
O(2)	O1C	2.4883	0.0035
O(3)	O1B	2.4932	0.0053
O(3)	O1C	2.4932	0.0053

Number of L.S. Cycles = 9
Final R-index = 1.67%

Atom Conversions for
Tables in Chapter 6

Cu(1)=Cu(2) Cu(2)=Cu(1)
O(1) = O(4) O(2) = O(2)
O(3) = O(1)

Adamite Idealized

	Starting Atomic Parameters			Final Atomic Parameters		
	x	y	z	x	y	z
Zn(1)	0.3653	0.3642	0.5000	0.3511	0.3985	0.5000
Zn(2)	0.5000	0.0000	0.2526	0.5000	0.0000	0.2531
As	0.2498	0.2438	0.0000	0.2363	0.2636	0.0000
O(1)	0.104	0.104	0.000	0.0798	0.1295	0.0000
O(2)	0.424	0.148	0.000	0.4132	0.1575	0.0000
O(3)	0.231	0.360	0.223	0.2255	0.3766	0.2336
OH	0.393	0.127	0.500	0.4099	0.1608	0.5000

Unit Cell Data

Starting Cell(Å) a: 8.304 b: 8.530 c: 6.047
Final Cell (Å) a: 8.135 b: 8.200 c: 5.872

Final Interatomic Distances
Within the Asymmetric Unit

ZN 1	01B	1.8747	0.0118
ZN 1	03B	1.8774	0.0117
ZN 1	O(3)	1.8774	0.0117
ZN 1	01A	1.9752	0.0038
ZN 1	OH	2.0074	0.0013
AS	O(2)	1.6817	-0.0017
AS	O(3)	1.6579	0.0221
AS	03D	1.7068	-0.0268
AS	O(1)	1.6818	-0.0018
ZN 2	O(2)	2.0821	0.0025
ZN 2	03A	2.0862	-0.0010
ZN 2	03C	2.0862	-0.0010
ZN 2	02A	2.0821	0.0025
ZN 2	OH	2.0820	0.0026
ZN 2	OHA	2.0820	0.0026
ZN 1	ZN 2	3.7745	-0.0030
ZN 1	AS	3.2740	0.0002
ZN 2	AS	3.3688	-0.0044
01A	01B	2.4883	0.0148
01A	O(3)	3.0420	-0.0073
01A	03B	3.0420	-0.0073
01B	03B	3.2803	-0.0168
01B	OH	2.2085	0.0261
OH	03B	2.7886	0.0025
OH	O(3)	2.7886	0.0025
03B	O(3)	3.1280	-0.0108
01B	O(3)	3.2803	-0.0168
03A	O(2)	2.8868	-0.0104
03A	OH	2.8268	0.0108
03A	OHA	2.8183	0.0128
03A	02A	3.0042	-0.0126
03C	O(2)	3.0042	-0.0126
03C	OH	2.8183	0.0128
03C	OHA	2.8268	0.0108
03C	02A	2.8868	-0.0104
OH	OHA	3.0164	-0.0163
OH	O(2)	2.8365	0.0077
02A	O(2)	2.8442	0.0053
O(3)	03D	2.8021	-0.0177
O(3)	O(2)	2.7279	0.0045
O(3)	O(1)	2.7169	0.0072
03D	O(1)	2.7490	-0.0018
03D	O(2)	2.7579	-0.0045
02A	OHA	2.8365	0.0077
O(1)	O(2)	2.7217	0.0064

Number of L.S. Cycles = 9
Final R-index = 1.38%

Atom Conversion for
Tables in Chapter 6

O(3) = O(4)

Andalusite Idealized

	Starting Atomic Parameters			Final Atomic Parameters		
	x	y	z	x	y	z
Al(1)	0.0000	0.0000	0.2419	0.0000	0.0000	0.2498
Al(2)	0.3705	0.1391	0.5000	0.3607	0.1109	0.5000
Si	0.2460	0.2520	0.0000	0.2353	0.2374	0.0000
O(1)	-0.0754	0.1371	0.5000	-0.0805	0.1575	0.5000
O(2)	0.603	0.0997	0.5000	0.5778	0.1199	0.5000
O(3)	0.423	0.3629	0.5000	0.4181	0.3428	0.5000
O(4)	0.2305	0.1339	0.2394	0.2204	0.1155	0.2474

Unit Cell Data

Starting Cell(Å)	a: 7.798	b: 7.903	c: 5.557
Final Cell (Å)	a: 7.694	b: 7.626	c: 5.386

Final Interatomic Distances
Within the Asymmetric Unit

AL 1	O[4]	1.9105	-0.0012
AL 1	O[1]	1.9044	0.0005
AL 1	O3A	1.9083	0.0005
AL 1	O3B	1.9083	0.0005
AL 1	O1A	1.9044	0.0005
AL 1	O4B	1.9105	-0.0012
SI	O[4]	1.6286	-0.0006
SI	O4C	1.6286	-0.0006
SI	O2B	1.6285	-0.0005
SI	O1B	1.6284	-0.0004
AL 2	O[3]	1.8222	0.0006
AL 2	O[2]	1.8722	0.0126
AL 2	O2A	1.8228	0.0006
AL 2	O[4]	1.7372	0.0074
AL 2	O4A	1.7372	0.0074
O[4]	O4C	2.6649	-0.0015
O[4]	O1B	2.6664	-0.0025
O[4]	O2B	2.6548	0.0015
O4C	O1B	2.6634	-0.0025
O4C	O2B	2.6548	0.0015
O1B	O2B	2.6445	0.0046
O[3]	O[2]	2.0874	0.0232
O[3]	O[4]	2.6775	0.0000
O[3]	O4A	2.6775	0.0000
O[2]	O2A	2.1863	0.0197
O[2]	O[4]	3.0188	-0.0156
O[2]	O4A	3.0688	-0.0156
O[4]	O4A	2.7211	-0.0017
O[4]	O2A	2.7357	-0.0023
O2A	O4A	2.7357	-0.0023
AL 1	AL 2	3.1368	0.0080
AL 1	SI	2.8920	0.0083
AL 2	SI	3.0188	0.0013
O[1]	O[4]	2.7037	-0.0011
O3A	O[4]	2.6805	0.0028
O3B	O[4]	2.6872	0.0008
O[4]	O1A	2.7088	-0.0028
O[1]	O4B	2.7088	-0.0028
O3A	O4B	2.6872	0.0008
O3B	O4B	2.6805	0.0028
O1A	O4B	2.7037	-0.0011
O1A	O[1]	2.7024	-0.0007
O3B	O[1]	2.6930	0.0021
O1A	O3A	2.6830	0.0021
O3B	O3A	2.7088	-0.0021

Number of L.S. Cycles = 7
Final R-index = 0.82%

Atom Conversions for
Tables in Chapter 6

Al(1)=Al(2)	Al(2)=Al(1)
O(1) = O(2)	O(2) = O(1)

Olivenite Idealized Towards Libethenite

Starting Olivenite Parameters				Final Libethenite Parameters (x- and y-axes reversed)			
	x	y	z		x	y	z
Cu(1)	0.1180	0.6376	-0.0172	Cu(2)	0.6316	0.1126	0.0005
Cu(2)	0.5000	0.5000	0.2500	Cu(1)	0.5000	0.5000	0.2500
As	0.2496	0.2626	-0.0103	P	0.2571	0.2614	-0.0004
O(1)	0.105	0.398	-0.060	O(3)	0.3839	0.1209	-0.0002
O(2)	0.420	0.368	0.006	O(2)	0.3626	0.4183	0.0000
OH	0.603	0.634	0.475	OH	0.6351	0.5893	0.5000
O(4)	0.277	0.658	0.260	O(1)	0.6554	0.2551	0.2837
O(5)	0.746	0.364	0.283	O(1)	0.3443	0.7449	0.2827

Unit Cell Data

Olivenite Cell (Å) a: 8.615 b: 8.240 c: 5.953
Libethenite Cell (Å) a: 8.194 b: 8.254 c: 5.852
(x- and y-axes reversed)

Final Interatomic Distances
Within the Asymmetric Unit

CU 1	O3B	1.8208	0.0053
CU 1	O5B	2.0418	0.0013
CU 1	O1A	1.8315	0.0010
CU 1	O(1)	2.0308	0.0057
CU 1	O(4)	2.0416	0.0013
CU 2	O(2)	1.9554	-0.0018
CU 2	O(3)	1.8771	0.0014
CU 2	O2A	1.9553	-0.0017
CU 2	O(4)	2.3976	-0.0038
CU 2	O(5)	2.3877	-0.0037
CU 2	O3A	1.9773	0.0013
AS	O5A	1.6233	-0.0028
AS	O(1)	1.6586	-0.0024
AS	O(2)	1.6573	-0.0028
AS	O4A	1.6234	-0.0029
O5A	O(1)	2.4816	0.0077
O5A	O(2)	2.5576	-0.0075
O5A	O4A	2.5376	-0.0035
O(1)	O4A	2.4814	0.0077
O(1)	O(2)	2.4611	0.0095
O4A	O(2)	2.6567	-0.0071
O3B	O5B	2.7473	0.0066
O3B	O1A	2.6768	0.0123
CU 1	AS	3.3055	-0.0022
O3B	O(4)	2.7521	0.0045
O5B	O1A	3.5328	0.0047
O5B	O(1)	2.8463	-0.0125
O5B	O(4)	3.3143	-0.0026
O1A	O(1)	2.7578	0.0058
O1A	O(4)	3.5338	0.0046
O(1)	O(4)	2.8493	-0.0127
O(2)	O2A	2.6248	0.0000
O(2)	O3A	2.5269	0.0056
O(2)	O(4)	3.2143	-0.0126
O(2)	O(5)	3.1658	-0.0054
O(3)	O2A	2.8265	0.0059
O(3)	O(4)	3.0395	0.0136
O(3)	O(5)	2.9808	0.0209
O2A	O(4)	3.1693	-0.0058
O2A	O(5)	3.2124	-0.0124
O(3)	O3A	2.8601	-0.0070
O(4)	O3A	2.8471	0.0214
O(5)	O3A	3.0418	0.0122
CU 1	CU 2	3.6772	-0.0011
CU 2	AS	3.1603	0.0036

Number of L.S. Cycles = 7
Final R-index = 1.16%

Libethenite Idealized Towards Olivenite

Starting Libethenite Parameters				Final Olivenite Parameters (x- and y-axes reversed)			
	x	y	z		x	y	z
Cu(1)	0.5000	0.5000	0.2507	Cu(2)	0.5000	0.5000	0.2488
Cu(2)	0.8617	0.3753	0.0000	Cu(1)	0.3916	0.8731	0.0000
P	0.7673	0.7516	0.0000	As	0.7569	0.7548	0.0000
O(1)	0.3406	0.2607	0.2112	O(4)	0.2603	0.3609	0.2319
O(2)	0.8671	0.9111	0.0000	O(2)	0.9256	0.8575	0.0000
OH	0.3762	0.6029	0.0000	OH	0.5780	0.3575	0.0000
O(3)	0.8979	0.6162	0.0000	O(1)	0.6151	0.8942	0.0000

Unit Cell Data

Libethenite Cell (Å) a: 8.062 b: 8.384 c: 5.881
Olivenite Cell (Å) a: 8.614 b: 8.263 c: 5.916
(x- and y-axes reversed)

Final Interatomic Distances
Within the Asymmetric Unit

Number of L.S. Cycles = 9
Final R-index = 2.23%

CU 2	O(3)	1.8336	0.0107
CU 2	O1D	2.0548	0.0101
CU 2	O1A	2.0585	0.0083
CU 2	O2A	1.8239	0.0155
CU 2	O4A	1.9233	0.0158
P[AS	O[2]	1.6828	-0.0017
P[AS	O[3]	1.6786	0.0009
P[AS	O1B	1.6786	0.0008
P[AS	O1C	1.6786	0.0008
CU 1	O[1]	2.3851	-0.0001
CU 1	O[4]	2.0008	-0.0040
CU 1	O1B	2.3851	-0.0001
CU 1	O2A	2.0015	-0.0046
CU 1	O2B	2.0015	-0.0046
CU 1	O4A	2.0006	-0.0040
CU 1	CU 2	3.5411	0.0024
CU 1	P[AS	3.3802	-0.0140
CU 2	P[AS	3.2848	-0.0045
O1A	O1D	3.1867	0.0083
O1A	O3A	2.8581	-0.0047
O1A	O4A	2.8703	-0.0056
O[3]	O1D	3.6107	-0.0849
O[3]	O3A	2.6441	0.0125
O[3]	O4A	2.6635	0.0109
O1D	O3A	2.8585	-0.0045
O1D	O4A	2.8677	-0.0054
O3A	O4A	3.8417	-0.0833
O[1]	O2A	3.1363	-0.0061
O[1]	O2B	3.1553	-0.0114
O[1]	O[4]	3.0612	0.0050
O[1]	O4A	3.0390	0.0085
O1B	O2A	3.1553	-0.0114
O2B	O1B	3.1363	-0.0061
O1B	O[4]	3.0390	0.0085
O1B	O4A	3.0612	0.0050
O[4]	O2A	2.9560	-0.0102
O[4]	O4A	2.7105	0.0065
O2A	O2B	2.6817	0.0123
O2B	O4A	2.9580	-0.0102
O[3]	O[2]	2.6911	0.0104
O[2]	O1B	2.7752	-0.0064
O[2]	O1C	2.7752	-0.0064
O[3]	O1B	2.7340	0.0018
O[3]	O1C	2.7340	0.0018
O1B	O1C	2.7443	-0.0003

B.2 THE KEISERITE GROUP

Keiserite Idealized

	Starting Atomic Parameters			Final Atomic Parameters		
	x	y	z	x	y	z
Mg	0.0000	0.5000	0.0000	0.0000	0.5000	0.0000
S	0.0000	0.1549	0.2500	0.0000	0.1749	0.2500
O(1)	0.1761	0.0447	0.3943	0.1684	0.0707	0.4028
O(2)	0.0916	0.2676	0.1491	0.1061	0.2791	0.1585
O(3)	0.0000	0.6353	0.2500	0.0000	0.6126	0.2500

Unit Cell Data

Starting Cell(Å) a: 6.912 b: 7.624 c: 7.462 ß= 117.7°
Final Cell (Å) a: 6.756 b: 8.138 c: 7.550 ß= 116.9°

Final Interatomic Distances
Within the Asymmetric Unit

MG 1	O(2)	2.0880	0.0000
MG 1	O(3)	2.0880	0.0000
MG 1	O1A	2.0880	0.0000
MG 1	O1C	2.0880	0.0000
MG 1	O2A	2.0880	0.0000
MG 1	O3A	2.0880	0.0000
O1A	O(2)	2.8670	-0.0000
O1A	O(3)	2.8670	-0.0000
O1A	O2A	2.8670	-0.0000
O1A	O3A	2.8670	-0.0000
O1C	O(2)	2.8670	-0.0000
O1C	O(3)	2.8670	-0.0000
O1C	O2A	2.8670	-0.0000
O1C	O3A	2.8670	-0.0000
O3A	O(2)	2.8670	-0.0000
O3A	O2A	2.8670	-0.0000
O(3)	O(2)	2.8670	-0.0000
O(3)	O2A	2.8670	-0.0000
S	O(1)	1.4690	-0.0000
S	O(2)	1.4690	-0.0000
S	O1B	1.4690	-0.0000
S	O2B	1.4690	-0.0000
O(1)	O(2)	2.3889	0.0000
O(1)	O1B	2.3889	0.0000
O(1)	O2B	2.3889	0.0000
O(2)	O1B	2.3889	0.0000
O(2)	O2B	2.3889	0.0000
O1B	O2B	2.3881	0.0000
MG 1	S	3.2500	0.0

Number of L.S. Cycles = 9
Final R-index = 0.001%

Keiserite Idealized Towards Poitenvenite: A Simple Model

	Starting Atomic Parameters				Final Atomic Parameters		
	x	y	z		x	y	z
Mg	0.0000	0.5000	0.0000	Cu	0.0000	0.5000	0.0000
S	0.0000	0.1549	0.2500		0.0000	0.1672	0.2500
O(1)	0.1761	0.0447	0.3943		0.1845	0.0509	0.3846
O(2)	0.0916	0.2676	0.1491		0.0727	0.2788	0.1502
O(3)	0.0000	0.6353	0.2500		0.0000	0.6708	0.2500

Unit Cell Data

Starting Cell(Å) a: 6.912 b: 7.624 c: 7.462 ß= 117.7°
Final Cell (Å) a: 6.756 b: 8.138 c: 7.550 ß= 122.0°

Final Interatomic Distances
Within the Asymmetric Unit

MG 1	O[2]	1.9674	0.0001
MG 1	O[3]	2.4594	0.0003
MG 1	O1A	1.9676	0.0001
MG 1	O1C	1.9676	0.0001
MG 1	O2A	1.9676	0.0001
MG 1	O3A	2.4594	0.0003
O1A	O[2]	2.7626	0.0000
O1A	O[3]	3.1487	-0.0010
O1A	O2A	2.7626	0.0000
O1A	O3A	3.1487	-0.0010
O1C	O[2]	2.7626	0.0000
O1C	O[3]	3.1487	-0.0010
O1C	O2A	2.7626	0.0000
O1C	O3A	3.1487	-0.0010
O3A	O[2]	3.1487	-0.0010
O3A	O2A	3.1487	-0.0010
O[3]	O[2]	3.1487	-0.0010
O[3]	O2A	3.1487	-0.0010
S	O[1]	1.4801	-0.0001
S	O[2]	1.4801	-0.0001
S	O2B	1.4801	-0.0001
O[1]	O[2]	2.3842	0.0002
O[1]	O1B	2.4036	0.0002
O[1]	O2B	2.4038	0.0002
O[2]	O1B	2.4038	0.0002
O[2]	O2B	2.4037	0.0003
O1B	O2B	2.3842	0.0002
MG 1	S	3.2480	0.0

Number of L.S. Cycles = 9
Final R-index = 0.07%

Keiserite Idealized Towards Poitenvenite: A Complex Model

	Starting Atomic Parameters				Final Atomic Parameters		
	x	y	z		x	y	z
Mg	0.0000	0.5000	0.0000	Cu	0.0000	0.5000	0.0000
S	0.0000	0.1549	0.2500		0.0000	0.1694	0.2500
O(1)	0.1761	0.0447	0.3943		0.1710	0.0577	0.4032
O(2)	0.0916	0.2676	0.1491		0.1083	0.2871	0.1636
O(3)	0.0000	0.6353	0.2500		0.0000	0.6918	0.2500

Unit Cell Data

Starting Cell(Å)	a: 6.912	b: 7.624	c: 7.462	ß= 117.7°
Final Cell (Å)	a: 6.756	b: 8.138	c: 7.550	ß= 117.9°

Final Interatomic Distances
Within the Asymmetric Unit

Number of L.S. Cycles = 11
Final R-index = 0.37%

MG 1	O[2]	1.9339	0.0037
MG 1	O[3]	2.3619	0.0037
MG 1	O1A	2.0405	0.0032
MG 1	O1C	2.0405	0.0032
MG 1	O2A	1.9339	0.0037
MG 1	O3A	2.3619	0.0037
O1A	O[2]	2.6922	-0.0018
O1A	O[3]	3.1277	-0.0010
O1A	O2A	2.9257	-0.0053
O1A	O3A	3.1451	-0.0031
O1C	O[2]	2.9257	-0.0053
O1C	O[3]	3.1451	-0.0031
O1C	O2A	2.6922	-0.0018
O1C	O3A	3.1277	-0.0010
O3A	O[2]	2.8939	0.0033
O3A	O2A	3.2330	-0.0050
O[3]	O[2]	3.2330	-0.0050
O[3]	O2A	2.8939	0.0033
S	O[1]	1.4602	-0.0002
S	O[2]	1.4803	-0.0003
S	O1B	1.4602	-0.0002
S	O2B	1.4803	-0.0003
O[1]	O[2]	2.3875	0.0005
O[1]	O1B	2.4033	0.0004
O[1]	O2B	2.4175	0.0005
O[2]	O1B	2.4175	0.0005
O[2]	O2B	2.3910	0.0035
O1B	O2B	2.3875	0.0005
MG 1	S	3.1092	0.0042
MG 1	MG2	3.6196	-0.0020
O[2]	O1D	3.1440	0.0015
O1C	O2B	3.1440	0.0015

B.3 THE CHALCOMENITE/TEINITE STRUCTURE

Chalcomenite Idealized

	Starting Atomic Parameters			Final Atomic Parameters		
	x	y	z	x	y	z
Cu	0.9809	0.8458	0.7140	1.0000	0.8815	0.7500
Se	0.7713	0.6089	0.9573	0.7695	0.6315	0.9477
O(1)	0.756	0.719	0.772	0.7711	0.7981	0.8165
O(2)	0.529	0.614	0.0295	0.5735	0.6315	0.0084
O(3)	0.234	0.941	0.644	0.2289	0.9650	0.6835
O(4)	0.949	0.7845	0.356	0.9265	0.8946	0.5084
O(5)	0.792	0.0585	0.690	0.9274	0.1315	0.7849

Unit Cell Data

Starting Cell(Å) a: 6.664 b: 9.156 c: 7.369
Final Cell (Å) a: 8.299 b: 7.897 c: 8.236

Final Interatomic Distances
Within the Asymmetric Unit

CU 1	O(1)	2.0840	0.0000
CU 1	O(3)	2.0838	0.0000
CU 1	O4	2.0838	0.0000
CU 1	O5	2.0838	0.0000
CU 1	O2A	2.0838	0.0000
CU 1	O5A	2.0838	0.0000
O4	O(1)	2.8472	-0.0000
O4	O(3)	2.8472	-0.0000
O4	O5	2.8471	-0.0000
O4	O5A	2.8471	-0.0000
O2A	O(1)	2.8470	0.0000
O2A	O(3)	2.8472	-0.0000
O2A	O5	2.8471	-0.0000
O2A	O5A	2.8470	-0.0000
O(1)	O5A	2.8470	0.0000
O(1)	O5	2.8472	-0.0000
O(3)	O5A	2.8472	-0.0000
O(3)	O5	2.8471	-0.0000
SE	O(1)	1.7020	-0.0000
SE	O(2)	1.7020	0.0000
SE	O3A	1.7020	0.0
O(2)	O3A	2.6300	0.0000
O(1)	O(2)	2.6300	0.0000
O(1)	O3A	2.6300	0.0
CU 1	SE	3.1951	0.0002
SE	O2A	3.1614	-0.0002
SE	O5A	3.1614	-0.0002
SE	O3B	3.1500	0.0000

Number of L.S. Cycles = 9
Final R-index = 0.02%

Teinite Idealized

	Starting Atomic Parameters			Final Atomic Parameters		
	x	y	z	x	y	z
Cu	1.0307	0.8440	0.7011	0.9975	0.8652	0.7400
Te	0.7894	0.6105	0.9738	0.7804	0.6243	0.9642
O(1)	0.740	0.713	0.742	0.7699	0.7872	0.8092
O(2)	0.521	0.619	0.043	0.5670	0.6245	0.0205
O(3)	0.224	0.935	0.633	0.2251	0.9431	0.6708
O(4)	0.935	0.787	0.449	0.9280	0.8548	0.5005
O(5)	0.787	0.052	0.670	0.9227	0.1119	0.7518

Unit Cell Data

Starting Cell(Å)	a: 6.634	b: 9.597	c: 7.428
Final Cell (Å)	a: 8.354	b: 8.047	c: 8.350

Final Interatomic Distances
Within the Asymmetric Unit

CU 1	O(1)	2.0838	0.0000
CU 1	O(3)	2.0838	0.0000
CU 1	O4	2.0838	0.0000
CU 1	O5	2.0838	0.0000
CU 1	O2A	2.0838	0.0000
CU 1	O5A	2.0838	0.0000
O4	O(1)	2.9471	-0.0000
O4	O(3)	2.9471	-0.0000
O4	O5	2.9471	-0.0000
O4	O5A	2.9471	-0.0000
O2A	O(1)	2.9470	-0.0000
O2A	O(3)	2.9471	-0.0000
O2A	O5	2.9471	-0.0000
O2A	O5A	2.9471	-0.0000
O(1)	O5A	2.8470	-0.0000
O(1)	O5	2.9471	-0.0000
O(3)	O5A	2.9471	-0.0000
O(3)	O5	2.8471	-0.0000
TE	O(1)	1.8440	-0.0000
TE	O(2)	1.8440	0.0
TE	O3A	1.8440	0.0
O(2)	O3A	2.7750	0.0000
O(1)	O(2)	2.7750	0.0000
O(1)	O3A	2.7750	0.0
CU 1	TE	3.2478	0.0001
TE	O2A	3.1353	-0.0001
TE	O5A	3.1353	-0.0001
TE	O3B	3.1300	0.0000

Number of L.S. Cycles = 9
Final R-index = 0.01%

B.4 THE KRÖHNKITE GROUP

Kröhnkite Idealized: Without Restraints

	Starting Atomic Parameters			Final Atomic Parameters		
	x	y	z	x	y	z
Cu	0.0000	0.0000	0.0000	0.0000	0.0000	0.0000
Na	0.5714	0.1247	0.2099	0.5932	0.1354	0.2337
S	0.2375	0.1179	0.5445	0.2695	0.1167	0.6002
O(1)	0.0038	0.1725	0.4874	0.0324	0.1840	0.5604
O(2)	0.2911	0.0573	0.7844	0.2858	0.0438	0.8166
O(3)	0.2319	0.0425	0.3322	0.2458	0.0590	0.3561
O(4)	0.4385	0.1923	0.5617	0.5155	0.1802	0.6643
OW	-0.1685	0.1343	-0.0487	-0.1880	0.1439	-0.0909

Unit Cell Data

Starting Cell(Å) a: 5.807 b: 12.656 c: 5.517 ß=108.3°
Final Cell (Å) a: 5.194 b: 12.888 c: 5.314 ß=107.5°

Final Interatomic Distances
Within the Asymmetric Unit

CU 1	O(3)	2.0814	0.0011
CU 1	OW	2.0840	0.0000
CU 1	O2A	2.0844	-0.0002
CU 1	O2B	2.0844	-0.0002
CU 1	O3A	2.0814	0.0011
CU 1	OWB	2.0840	0.0000
O2A	O(3)	2.9430	0.0008
O2A	OW	2.9488	-0.0004
O2A	O3A	2.9483	-0.0003
O2A	OWB	2.9461	0.0002
O2B	O(3)	2.9483	-0.0003
O2B	OW	2.9461	0.0002
O2B	O3A	2.9430	0.0008
O2B	OWB	2.9488	-0.0004
O(3)	OW	2.9478	-0.0002
O(3)	OWB	2.9428	0.0008
O3A	OW	2.9428	0.0008
O3A	OWB	2.9478	-0.0002
NA 1	O(3)	2.3149	0.0105
NA 1	O(4)	2.5076	-0.0048
NA 1	O1A	2.4843	-0.0037
NA 1	O2C	2.4283	0.0015
NA 1	O4A	2.4195	0.0023
NA 1	OWA	2.3264	0.0048
O4A	O(3)	3.8837	-0.0148
O4A	O(4)	3.2085	0.0057
O4A	O1A	3.3608	0.0012
O4A	OWA	3.2568	0.0043
O2C	O(3)	3.1404	0.0078
O2C	O(4)	4.1855	-0.0236
O2C	O1A	3.5556	-0.0077
O2C	OWA	2.9461	0.0002
O1A	OWA	3.3411	0.0018
O(3)	OWA	4.4387	-0.0312
O1A	O(4)	2.8003	0.0150
NA 1	S 1	2.8418	0.0082
S 1	O(1)	1.4680	0.0000
S 1	O(2)	1.4680	0.0001
S 1	O(3)	1.4680	-0.0000
S 1	O(4)	1.4680	-0.0000
O(1)	O(2)	2.4021	-0.0006
O(1)	O(3)	2.3932	0.0018
O(1)	O(4)	2.4015	-0.0004
O(2)	O(3)	2.4002	-0.0001
O(2)	O(4)	2.3868	0.0004
O(3)	O(4)	2.3878	0.0034
CU 1	NA 1	3.4315	-0.0009
CU 1	S 1	3.4209	-0.0006
NA 1	O2A	2.5928	-0.0116

Number of L.S. Cycles = 13
Final R-index = 1.04%

Roselite Idealized Towards Kröhnkite

	Starting Atomic Parameters				Final Atomic Parameters		
	x	y	z		x	y	z
Mg	0.0000	0.0000	0.0000	Cu	0.0000	0.0000	0.0000
Ca	0.5618	0.1216	0.2307	Na	0.5867	0.1354	0.2291
As	0.2161	0.1204	0.5669	S	0.2672	0.1159	0.5982
O(1)	-0.0578	0.1739	0.4974		0.0279	0.1821	0.5545
O(2)	0.2810	0.0531	0.8384		0.2850	0.0434	0.8158
O(3)	0.2368	0.0352	0.3423		0.2479	0.0577	0.3560
O(4)	0.4382	0.2060	0.5719		0.5114	0.1802	0.6607
OW	-0.1846	0.1386	-0.0353		-0.1852	0.1445	-0.0877

Unit Cell Data

Starting Cell(Å) a: 5.801 b: 12.898 c: 5.617 ß=107.4°
Final Cell (Å) a: 5.199 b: 12.887 c: 5.320 ß=107.5°

Final Interatomic Distances
Within the Asymmetric Unit

MG 1	O[3]	2.0805	0.0012
MG 1	OW	2.0841	-0.0000
MG 1	O2A	2.0846	-0.0002
MG 1	O2B	2.0846	-0.0002
MG 1	O3A	2.0805	0.0012
MG 1	OWB	2.0841	-0.0000
O2A	O[3]	2.9433	0.0007
O2A	OW	2.8450	-0.0004
O2A	O3A	2.8471	-0.0000
O2A	OWB	2.8464	0.0001
O2B	O[3]	2.8471	-0.0000
O2B	OW	2.8464	0.0001
O2B	O3A	2.9433	0.0007
O2B	OWB	2.8450	-0.0004
O[3]	OW	2.9476	-0.0001
O[3]	OWB	2.9421	0.0010
O3A	OW	2.9421	0.0010
O3A	OWB	2.8476	-0.0001
CA 1	O[3]	2.2873	0.0121
CA 1	O[4]	2.5102	-0.0050
CA 1	O1A	2.4848	-0.0038
CA 1	O2C	2.4312	0.0013
CA 1	O4A	2.4177	0.0024
CA 1	OWA	2.3377	0.0088
O4A	O[3]	3.8011	-0.0150
O4A	O[4]	3.2113	0.0057
O4A	O1A	3.3703	0.0059
O4A	OWA	3.2548	0.0044
O2C	O[3]	3.1256	0.0082
O2C	O[4]	4.1787	-0.0234
O2C	O1A	3.5107	-0.0063
O2C	OWA	2.8464	0.0001
O1A	OWA	3.2837	0.0032
O[3]	OWA	4.4267	-0.0312
O1A	O[4]	2.9067	0.0148
CA 1	AS 1	2.9407	0.0052
AS 1	O[1]	1.4678	0.0002
AS 1	O[2]	1.4678	0.0002
AS 1	O[3]	1.4678	0.0002
AS 1	O[4]	1.4678	0.0001
O[1]	O[2]	2.4061	-0.0012
O[1]	O[3]	2.3816	0.0017
O[1]	O[4]	2.4044	-0.0008
O[2]	O[3]	2.4022	-0.0004
O[2]	O[4]	2.3894	0.0001
O[3]	O[4]	2.3761	0.0044
MG 1	CA 1	3.4060	-0.0050
MG 1	AS 1	3.4088	-0.0052
CA 1	O2A	2.5728	-0.0100

Number of L.S. Cycles = 9
Final R-index = 1.05%

Roselite Idealized: Without Restraints

	Starting Atomic Parameters			Final Atomic Parameters		
	x	y	z	x	y	z
Mg	0.0000	0.0000	0.0000	0.0000	0.0000	0.0000
Ca	0.5618	0.1216	0.2307	0.5189	0.1313	0.1667
As	0.2161	0.1204	0.5669	0.2174	0.0957	0.5481
O(1)	-0.0578	0.1739	0.4974	-0.0876	0.1346	0.4898
O(2)	0.2810	0.0531	0.8384	0.2887	0.0380	0.8179
O(3)	0.2368	0.0352	0.3423	0.2622	0.0148	0.3335
O(4)	0.4382	0.2060	0.5719	0.4102	0.1960	0.5509
OW	-0.1846	0.1386	-0.0353	-0.0969	0.1541	0.0124

Unit Cell Data

Starting Cell(Å) a: 5.801 b: 12.898 c: 5.617 ß=107.4°
Final Cell (Å) a: 5.375 b: 13.220 c: 5.685 ß=102.8°

Final Interatomic Distances
Within the Asymmetric Unit

MG 1	O[3]	2.1065	0.0006
MG 1	OW	2.1078	0.0000
MG 1	O2A	2.1080	-0.0000
MG 1	O2B	2.1080	-0.0000
MG 1	O3A	2.1065	0.0006
MG 1	OWB	2.1078	0.0000
O2A	O[3]	2.9813	-0.0002
O2A	OW	2.9814	-0.0001
O2A	O3A	2.9783	0.0006
O2A	OWB	2.9808	0.0000
O2B	O[3]	2.9783	0.0006
O2B	OW	2.9809	0.0000
O2B	O3A	2.9813	-0.0002
O2B	OWB	2.9814	-0.0001
O[3]	OW	2.9820	-0.0002
O[3]	OWB	2.8781	0.0006
O3A	OW	2.8781	0.0006
O3A	OWB	2.9820	-0.0002
CA 1	O[3]	2.3980	0.0055
CA 1	O[4]	2.5320	-0.0051
CA 1	O1A	2.4761	-0.0006
CA 1	O2C	2.4591	0.0007
CA 1	O4A	2.4116	0.0045
CA 1	OWA	2.4242	0.0027
O4A	O[3]	4.2882	-0.0186
O4A	O[4]	3.1811	0.0056
O4A	O1A	3.8428	-0.0088
O4A	OWA	3.3542	0.0018
O2C	O[3]	2.8236	0.0126
O2C	O[4]	4.2632	-0.0161
O2C	O1A	2.8328	0.0103
O2C	OWA	2.8808	0.0000
O1A	OWA	2.7165	0.0147
O[3]	OWA	4.8231	-0.0235
O1A	O[4]	2.8125	0.0106
CA 1	AS 1	3.0172	0.0116
AS 1	O[1]	1.6786	0.0002
AS 1	O[2]	1.6801	-0.0001
AS 1	O[3]	1.6788	0.0002
AS 1	O[4]	1.6803	-0.0004
O[1]	O[2]	2.7448	0.0001
O[1]	O[3]	2.7822	-0.0018
O[1]	O[4]	2.7435	0.0004
O[2]	O[3]	2.7435	0.0004
O[2]	O[4]	2.7442	0.0002
O[3]	O[4]	2.7325	0.0031
MG 1	CA 1	3.2428	-0.0122
MG 1	AS 1	3.3285	-0.0183
CA 1	O2A	2.4267	0.0031

Number of L.S. Cycles = 13
Final R-index = 1.02%

Kröhnkite Idealized: With Restraints

	Starting Atomic Parameters			Final Atomic Parameters		
	x	y	z	x	y	z
Cu	0.0000	0.0000	0.0000	0.0000	0.0000	0.0000
Na	0.5714	0.1247	0.2099	0.5698	0.1343	0.2056
S	0.2375	0.1179	0.5445	0.2215	0.1081	0.5850
O(1)	0.0038	0.1725	0.4874	-0.0352	0.1524	0.5568
O(2)	0.2911	0.0573	0.7844	0.2888	0.0429	0.8187
O(3)	0.2319	0.0425	0.3322	0.2297	0.0448	0.3562
O(4)	0.4385	0.1923	0.5617	0.4089	0.1930	0.6027
OW	-0.1685	0.1343	-0.0487	-0.1500	0.1509	-0.0546

Unit Cell Data

Starting Cell(Å)	a: 5.807	b: 12.656	c: 5.517	ß=108.3°
Final Cell (Å)	a: 5.381	b: 12.768	c: 5.314	ß=103.6°

Final Interatomic Distances
Within the Asymmetric Unit

CU 1	O(3)	2.0632	0.0002
CU 1	OW	2.0630	0.0004
CU 1	O2A	2.0646	-0.0002
CU 1	O2B	2.0646	-0.0002
CU 1	O3A	2.0632	0.0003
CU 1	OWB	2.0630	0.0004
O2A	O(3)	2.9470	-0.0000
O2A	OW	2.9484	0.0003
O2A	O2A	2.9468	0.0000
O2A	OWB	2.9483	-0.0003
O2B	O(3)	2.9488	0.0000
O2B	OW	2.9483	-0.0003
O2B	O2A	2.9470	-0.0000
O2B	OWB	2.9484	0.0003
O(3)	OW	2.9482	0.0002
O(3)	OWB	2.9487	0.0003
O3A	OW	2.9487	0.0003
O3A	OWB	2.9482	0.0002
NA 1	O(3)	2.4487	0.0002
NA 1	O(4)	2.5731	-0.0100
NA 1	O1A	2.4884	-0.0032
NA 1	O2C	2.4000	0.0038
NA 1	O4A	2.3285	0.0050
NA 1	OWA	2.2422	0.0133
O4A	O(3)	3.8180	-0.0125
O4A	O(4)	3.0296	0.0111
O4A	O1A	3.8084	-0.0152
O4A	OWA	3.2617	0.0014
O2C	O(3)	3.1568	0.0073
O2C	O(4)	4.2945	-0.0284
O2C	O1A	3.2644	0.0036
O2C	OWA	2.9483	-0.0003
O1A	OWA	3.1812	0.0092
O(3)	OWA	4.6002	-0.0280
O1A	O(4)	3.1011	0.0090
NA 1	S 1	3.0758	0.0174
S 1	O(1)	1.4678	0.0002
S 1	O(2)	1.4678	0.0002
S 1	O(3)	1.4886	-0.0008
S 1	O(4)	1.4886	-0.0008
O(1)	O(2)	2.4084	-0.0018
O(1)	O(3)	2.4018	-0.0006
O(1)	O(4)	2.4008	-0.0003
O(2)	O(3)	2.4031	-0.0008
O(2)	O(4)	2.3892	0.0002
O(3)	O(4)	2.3730	0.0076
CU 1	NA 1	3.4583	-0.0017
CU 1	S 1	3.3538	0.0016
NA 1	O2A	2.6325	-0.0086
OWA	O4B	2.6649	0.0022
OWA	O1B	2.6188	0.0000

Number of L.S. Cycles = 13
Final R-index = 1.16%

Roselite Idealized: With Restraints

	Starting Atomic Parameters			Final Atomic Parameters		
	x	y	z	x	y	z
Mg	0.0000	0.0000	0.0000	0.0000	0.0000	0.0000
Ca	0.5618	0.1216	0.2307	0.5105	0.1395	0.1487
As	0.2161	0.1204	0.5669	0.2545	0.0925	0.5590
O(1)	-0.0578	0.1739	0.4974	-0.0548	0.1442	0.4692
O(2)	0.2810	0.0531	0.8384	0.2951	0.0296	0.8217
O(3)	0.2368	0.0352	0.3423	0.2952	0.0146	0.3424
O(4)	0.4382	0.2060	0.5719	0.4898	0.1824	0.6007
OW	-0.1846	0.1386	-0.0353	-0.0865	0.1535	0.0008

Unit Cell Data

Starting Cell(Å) a: 5.801 b: 12.898 c: 5.617 ß=107.4°
Final Cell (Å) a: 5.174 b: 13.417 c: 5.712 ß=107.2°

Final Interatomic Distances
Within the Asymmetric Unit

MG 1	O[3]	2.1050	0.0012
MG 1	OW	2.1085	-0.0002
MG 1	O2A	2.1080	-0.0000
MG 1	O2B	2.1080	-0.0000
MG 1	O3A	2.1050	0.0012
MG 1	OWB	2.1085	-0.0002
O2A	O[3]	2.9805	0.0001
O2A	OW	2.8834	-0.0005
O2A	O3A	2.8777	0.0007
O2A	OWB	2.8786	0.0003
O2B	O[3]	2.8777	0.0007
O2B	OW	2.8786	0.0003
O2B	O3A	2.8805	0.0001
O2B	OWB	2.8834	-0.0005
O[3]	OW	2.8842	-0.0005
O[3]	OWB	2.9746	0.0013
O3A	OW	2.8746	0.0013
O3A	OWB	2.8842	-0.0006
CA 1	O[3]	2.4484	0.0015
CA 1	O[4]	2.6788	-0.0158
CA 1	O1A	2.4460	0.0018
CA 1	O2C	2.4678	0.0001
CA 1	O4A	2.4037	0.0061
CA 1	OWA	2.4771	-0.0007
O4A	O[3]	4.5011	-0.0210
O4A	O[4]	3.3828	0.0013
O4A	O1A	3.5307	-0.0016
O4A	OWA	2.2728	0.0025
O2C	O[3]	2.6288	0.0165
O2C	O[4]	4.0821	-0.0128
O2C	O1A	2.8186	0.0108
O2C	OWA	2.8786	0.0003
O1A	OWA	2.6351	0.0163
O[3]	OWA	4.5046	-0.0231
O1A	O[4]	2.7248	0.0146
CA 1	AS 1	3.0791	0.0171
AS 1	O[1]	1.6786	0.0007
AS 1	O[2]	1.6798	0.0005
AS 1	O[3]	1.6787	0.0004
AS 1	O[4]	1.6805	-0.0008
O[1]	O[2]	2.7458	-0.0002
O[1]	O[3]	2.7870	-0.0030
O[1]	O[4]	2.7418	0.0008
O[2]	O[3]	2.7660	-0.0002
O[2]	O[4]	2.7804	-0.0014
O[3]	O[4]	2.7173	0.0068
MG 1	CA 1	3.1425	-0.0221
MG 1	AS 1	3.3147	-0.0307
CA 1	O2A	2.3815	0.0068
OWA	O4B	2.6872	-0.0014
OWA	O1B	2.7281	-0.0014

Number of L.S. Cycles = 13
Final R-index = 1.27%

B.5 LINDGRENITE & CHALCOCYANITE

Lindgrenite Idealized

	Starting Atomic Parameters			Final Atomic Parameters		
	x	y	z	x	y	z
Cu(1)	0.0000	0.0000	0.0000	0.0000	0.0000	0.0000
Cu(2)	0.8638	0.0939	0.4870	0.8848	0.0929	0.4731
Mo	0.4559	0.1546	0.8772	0.4592	0.1507	0.8497
O(1)	0.980	0.2234	0.436	1.0031	0.2288	0.4138
O(2)	0.651	0.0918	0.101	0.6772	0.0752	0.0743
O(3)	0.553	0.1299	0.594	0.5203	0.1394	0.5343
O(4)	0.145	0.1130	0.873	0.1264	0.1213	0.8545
O(5)	0.132	0.0306	0.341	0.2239	0.0339	0.3871

Unit Cell Data

Starting Cell(Å) a: 5.394 b: 14.023 c: 5.608 ß= 98.5°
Final Cell (Å) a: 5.112 b: 14.303 c: 5.209 ß=105.2°

Final Interatomic Distances
Within the Asymmetric Unit

CU 1	O(5)	2.0871	-0.0044
CU 1	O2A	2.0888	-0.0016
CU 1	O2B	2.0888	-0.0016
CU 1	O4A	2.0838	0.0067
CU 1	O4B	2.0838	0.0067
CU 1	O5B	2.0871	-0.0044
O(5)	O2A	2.9015	0.0080
O(5)	O2B	3.0173	-0.0123
O(5)	O4A	2.9635	-0.0029
O(5)	O4B	2.8210	0.0045
O5B	O2A	3.0173	-0.0123
O5B	O2B	2.9015	0.0080
O5B	O4A	2.8210	0.0045
O5B	O4B	2.9635	-0.0029
O2A	O4A	2.8884	0.0035
O2A	O4B	2.9740	-0.0047
O2B	O4A	2.9740	-0.0047
O2B	O4B	2.8884	0.0065
CU 2	O[1]	2.0822	0.0006
CU 2	O[2]	2.0848	-0.0003
CU 2	O[3]	2.0798	0.0014
CU 2	O4A	2.0852	-0.0004
CU 2	O5A	2.0798	0.0014
CU 2	O5B	2.0831	0.0003
O4A	O[1]	2.6862	0.0438
O4A	O[3]	3.1186	-0.0302
O4A	O5A	2.8844	0.0092
O[2]	O[1]	3.0288	-0.0145
O[2]	O[3]	2.8700	0.0135
O[2]	O5A	2.9015	0.0080
O[2]	O5B	3.1326	-0.0325
O[1]	O[3]	2.8886	-0.0073
O[1]	O5A	3.0243	-0.0135
O[3]	O5B	2.7810	0.0251
O5B	O5A	2.8851	-0.0088
MO	O[3]	1.7584	0.0002
MO	O[4]	1.7589	0.0002
MO	O1A	1.7585	0.0002
MO	O2A	1.7586	0.0003
O[3]	O[4]	2.9445	-0.0176
O[3]	O1A	2.7508	0.0304
O[3]	O2A	2.4661	0.0020
O[4]	O1A	2.8438	0.0075
O[4]	O2A	2.8246	0.0123
O1A	O2A	2.8838	-0.0300
CU 1	CU 2	2.8658	0.0025
CU 2	MO	3.3824	-0.0004
CU 1	MO	3.4288	-0.0016

Chalcocyanite Idealized

	Starting Atomic Parameters			Final Atomic Parameters		
	x	y	z	x	y	z
Cu	0.000	0.500	0.000	0.0000	0.5000	0.0000
S	0.185	0.250	0.445	0.1613	0.2500	0.5364
O(1)	0.141	0.250	0.755	0.1587	0.2500	0.8572
O(2)	0.375	0.250	0.439	0.3269	0.250	0.4340
O(3)	0.129	0.069	0.307	0.0798	0.0450	0.4273

Unit Cell Data

Starting Cell(Å)	a: 8.390	b: 6.690	c: 4.830
Final Cell (Å)	a: 8.401	b: 5.847	c: 4.576

Final Interatomic Distances
Within the Asymmetric Unit

CU 1	01A	2.0838	0.0000
CU 1	01B	2.0838	0.0000
CU 1	02A	2.0838	0.0000
CU 1	02B	2.0838	0.0000
CU 1	03A	2.0838	0.0000
CU 1	03B	2.0838	0.0000
01A	02A	2.9470	-0.0000
01A	02B	2.9472	-0.0000
01A	03A	2.9469	0.0000
01A	03B	2.9472	-0.0000
01B	02A	2.9472	-0.0000
01B	02B	2.9470	-0.0000
01B	03A	2.9472	-0.0000
01B	03B	2.9469	0.0000
02A	02A	2.9472	-0.0000
02A	03B	2.9470	-0.0000
02B	03A	2.9470	-0.0000
02B	03B	2.9472	-0.0000
S	O(1)	1.4881	-0.0002
S	O(2)	1.4881	-0.0002
S	O(3)	1.4881	-0.0002
S	03A	1.4881	-0.0002
O(1)	O(2)	2.3872	0.0006
O(1)	O(3)	2.3873	0.0005
O(1)	03A	2.3873	0.0005
O(2)	O(3)	2.3875	0.0005
O(2)	03A	2.3875	0.0005
O(3)	03A	2.3877	0.0005
CU 1	S	3.1621	-0.0004

Number of L.S. Cycles = 8
Final R-index = 0.03%